ISSN 0289-842X

RIKEN Accelerator Progress Report

1989

vol. 23

理化学研究所
the Institute of Physical and Chemical Research

RIKEN Accelerator Progress Report 1989
January-December

理化学研究所
the Institute of Physical and Chemical Research
Wako-shi, Saitama, 351-01 JAPAN

CONTENTS

I. INTRODUCTION

H. Kamitsubo

The long range project to construct a heavy-ion accelerator complex at the Institute of Physical and Chemical Physics (RIKEN) was started in 1974 and completed in 1989. The accelerator complex consists of two injectors, that is, a variable-frequency heavy-ion linac and an AVF cyclotron, and of an energy booster or a separated sector cyclotron. The project in its first phase was devoted to the construction of the linac (RILAC), which was completed in 1980. The construction of a separated sector cyclotron (RIKEN Ring Cyclotron, RRC) was started successively. The RRC was put into operation in December, 1986. The second injector, an AVF cyclotron (AVF) was completed in 1988. Construction of experimental devices was continued from 1986 to 1988 and the major devices were completed by the end of FY 1988. The first beam from AVF was extracted in April and ^{14}N ions was successfully accelerated at RRC at the highest energy of 135MeV/u in July, 1989. The celebration of the project completion was held on October 13, 1989.

During the past one year collaborative research work using ion accelerators at RIKEN has been carried out in the fields of nuclear and atomic physics, condensed matter physics, nuclear and radiation chemistry, and radiation biology. The main facilities dedicated to this collaborative research work are the heavy-ion accelerator complex, a 160 cm cyclotron, and a 1MV electrostatic accelerator (TANDETRON). The 160cm cyclotron will be shut down at the end of March, 1990.

RILAC has been operated as an injector to RRC as well as an independent heavy-ion accelerator for its own users. The beam time for the injection to RRC was nearly a half of the total beam time of RILAC. On the other hand, AVF is used only as an injector to RRC, although it has one beam line for its own users. RRC has been in routine operation this year except June and July, when test operation in combination with AVF was pursued. Now the basic operation schedule of RRC is as follows: it is used for experiments for three successive weeks and then for machine study and maintenance for one week.

This year experiments were carried out by inside and outside users on ten and eleven subjects in nuclear and non-nuclear physics fields, respectively. Large spin polarization was observed for the first time in projectile fragments from intermediate-energy heavy-ion collision. Subthreshold pion production and hard photon production were extensively studied in heavy ion reactions. The interaction radii of the neutron-rich nuiclei were systematically studied at Berkeley and their anomalous behavior was found. Search for new isotopes has also been continued.

Theoretical studies were pursued on the production of hypernuclei and mesic atoms in high-energy nuclear collisions. Low and intermediate-energy heavy-ion collisions were analyzed by applying the transport formalism.

Muon-catalyzed fusion reactions were studied by measuring muonic X-rays arising from μ^- sticking on a helium atom in liquid d-t mixture. The theoretical analysis of muonic molecules and $d\mu+t$ collisions were performed.

Experimental studies were carried out on atomic collision processes and on beam foil spectroscopy by measuring the energy spectra of photons and electrons, charge-state distributions of colliding ions, and angular distributions of X rays and electrons as well as scattered ions. High-energy and highly-ionized ions were used for these studies. Laser spectroscopy of highly-excited atoms were investigated for atomic and nuclear structure studies.

Mössbauer spectroscopy, a perturbed angular correlation technique, Rutherford scattering methods, and a nuclear reaction method have been applied to the studies of internal structure of condensed matter and impurity distribution and chemical states of ions in solid and liquid. Charged-particle activation analysis and PIXE analysis have been applied to the analysis of light-element impurities in high-purity materials, and to the composition analysis of medical, environmental, and geological samples, and to the analysis of light-element impurities inhigh-purity materials.

RIKEN and Japan Atomic Energy Research Institute (JAERI) has a plan to built an 8 GeV synchrotron radiation source (SPring-8). The design studies of the storage ring and R&D work on accelerator engineering needed for a high-brilliance synchrotoron radiation source have been pursued. The site for the SPring-8 was decided to be at Harima Science Garden City, Hyougo Prefecture. Construction is scheduled to start in April, 1990.

RIKEN Accel. Prog. Rep. 23 (1989)

II. OPERATION OF ACCELERATORS

1. RRC Operation

Y. Yano, K. Hatanaka, M. Kase, A. Goto, H. Isshiki,*
R. Abe,* S. Otsuka,* H. Akagi,* T. Ishikawa,* and R. Ichikawa*

Ten themes of RRC experiments with a one-week machine time per each were carrid out by using RILAC-injected beams from January through June. In this period, the final extension of beam distribution lines was made to new experiment areas of E4, E5, and E6 together with the installation of a large experimental setup of RIPS; thus all the experiments were carried out at E1 room isolated from this work.

A new injector, K70 AVF cyclotron, was installed in the ring cyclotron building last December, and its assembling and tuning were finished this April. The first beam of 7 MeV/u $^{14}N^{5+}$ was successfully extracted immediately after that.

On July 20 we succeeded in extrating a 135 MeV/u $^{14}N^{7+}$ beam from RRC in the AVF cyclotron injection. This beam has the largest magnetic rigidity that K540 RRC can produce, and the world-highest energy among nitrogen CW beams. On July 26 fully completed radiation-controlled areas underwent the inspection by the authorities for this top-energy beam.

After the summer regular machine overhaul in August-mid September the RRC experiment programs started again by using both RILAC and AVF injected beams. New beams used for experiments are listed in Table 1.

Table 1. New RRC beams in January-November 1989.

		RILAC			RRC			
	F (MHz)	Q_1	E_1 (MeV/u)	T_N	Q_2	h_2	E_2 (MeV/u)	I (enA)
^{20}Ne	33	3	2.2	6	9	9	37	150
^{22}Ne	28	3	1.25	5	8	10	21	40
^{40}Ar	20	3	0.65	5	11	10	10	1500
^{84}Kr	20	5	0.65	5	18	10	10	70
		AVF			RRC			
	F (MHz)	Q_1	E_1(MeV/u)	h_1	Q_2	h_2	E_2 (MeV/u)	I (enA)
^{14}N	32.6	5	7	2	7	5	135	500
^{18}O	29	6	5.5	2	8	5	100	30

F, RF frequency of RRC (RILAC works at the same frequency as RRC, while AVF at half RRC frequency); Q_1, Q_2, Charge state; E_1, E_2, Beam Energy; T_N, Number of tanks; h_1, h_2, Harmonic number; I, Maximum beam intensity during the experimental run.

The beam transmission efficiency through RRC has been improved stepwise, finding a better tuning method. At present it is over 50% and typically 100% for a full injected beam. For the extraction, nearly 100% transmission can be achieved.

* Sumijyu Accelerator Service, Ltd.

RIKEN Accel. Prog. Rep. 23 (1989)

II-2. RILAC Operation

Y. Miyazawa, M. Hemmi, T. Inoue, M. Yanokura, M. Kase, E. Ikezawa, T. Aihara,* T. Ohki,* H. Hasebe,* and Y. Chiba

RILAC has supplied various kinds of ion beams for many research fields and also been operated as an injector to RIKEN Ring Cyclotron (RRC). Table 1 gives the statistics of operation for Jan. 1-Dec. 31, 1989. The total beam-time decreased by two days compared with that of the last year. Table 2 gives the beam time for individual research groups. Total beam-time for atomic and solid-state physics shows a 30% increase compared with that of the last year.

A private company used three days. The beam time for the injection to RRC decreased from 80 to 67 days, because a new AVF cyclotron was completed as another injector. Table 3 shows the statistics of ions used this year.

To test the possibility of acceleration in a frequency region near the upper limit, a C^{4+} beam (44 MeV) was accelerated at a frequency of 44 MHz without problems. Nb^{6+}, Dy^{7+}, and Hf^{7+} were produced for the first time by using a sputter PIG source, but they were not yet accelerated in RILAC. Best beam transmission (from the ion source to a Faraday cup installed just behind the switching magnet) achieved after carefull beam tunning is 13%.

Table 1. Statistics of the operation for Jan.1-Dec.31, 1989.

	Day	%
Beam time	174	47.7
Frequency change	15	4.1
Overhaul and improvement	45	12.3
Periodic inspection and repair	15	4.1
Machine trouble	1	0.3
Scheduled shut down	115	31.5
Total	365	100

Table 2. Beam time for individual research groups.

	Day	%
Atomic physics	41	23.6
Solid-state physics	22	12.6
Nuclear physics	21	12.1
Radiation chemistry	15	8.6
Accelerator research	5	2.9
Beam irradiation	3	1.7
Beam transportation to RRC	67	38.5
Total	174	100

Table 3. List of ions used this year.

Ion	Mass	Charge state	Day
C	12	2	6
C	12	4	2
N	14	2	8
N	14	3	18
Ne	20	2	13
Ne	20	3	6
Ne	20	4	1
Ne	22	3	5
Al	27	3	2
Ar	40	3	19
Ar	40	4	55
Ar	40	6	2
Ti	48	3	4
Ti	48	4	2
Cr	52	4	2
Cu	63	4	3
Kr	84	5	10
Xe	132	7	1
Xe	132	9	15

This year we had maintenance items as listed follows:

1) Because of the deteriorated surface insulation of a cylindrical insulator housing, a 500 kV injector power supply (made in USA) used for the past twelve years was replaced with a new one (made by Nichikon). We had been worried about occational flashings along the surface.

2) We experienced two incidents with an optical fiber link controlling the ion source on a 500kV voltage terminal: one was the disconnection of a fiber core by electrostatic stress, and the other was flashings caused by fine dust laid for years on the cable surface.

We developed and tested a new optical link transmitting light signals directly through space without a fiber cable.

3) An rf feeder for a No. 6 resonator had a vacuum leak at the cone-shaped alumina feed-through insulator. The insulator was replaced with a new one.

4) Thin copper sheets (10 cm wide, 7 cm long, and 0.3 mm thick), which formed an rf path between the upper and the lower structure of the

* Sumijyu Accelerator Service, Ltd.

resonator, melted over one meter with an anomalous rf current.

5) A sliding transformer (14 kVA) in the final tube filament power supply of a No. 1 rf power amplifier was worn out for twelve year operation; replaced by a new one.

6) Electronics of beam current monitor system with beam slits and Faraday cups were replaced by a new-designed system which uses an intelligent interface circuit DIM (Device Interface Module), as a sequenser.[1)]

References

1) M. Kase, T. Aihara, and I. Yokoyama: This report, p. 112.

RIKEN Accel. Prog. Rep. 23 (1989)

II-3. Status of the RIKEN-ECRIS for the AVF Cyclotron

K. Hatanaka and E. Ikezawa

The RIKEN-ECRIS was successfully operated in 1989; the preliminary performance of the source was reported elsewhere.[1-3] The beam line downstream the charge analyzing system[3] to the injector AVF-cyclotron was installed at the end of last March. The schematic drawing of the beam injection line is shown in Fig. 1. The system consisting of two 45°bending magnets and three quadrupole singlets constitutes an achromatic one and bends the beam vertically down to the cyclotron. A beam emittance is shaped by use of the quadrupole quartet to match the acceptance of the cyclotron. Two Glazer lenses and a steering magnet are set inside the hole of the upper yoke. The injected beam is bent into the median plane of the cyclotron with a spiral inflector installed at the center of the cyclotron.

The AVF cyclotron was also completed last March. The first operation was acheived in April to inject ions to the cyclotron, and the first beam of $^{14}N^{5+}$ with 7 MeV/u, the designed maximum energy, was successfully extracted after two-day operation. The beam was injected into RIKEN Ring Cyclotron (RRC) and a $^{14}N^{7+}$ beam of 135 MeV/u corresponding to the maximum magnetic rigidity of RRC was extracted on July 20. So far two kinds of ion species, $^{14}N^{5+}$ and $^{18}O^{6+}$, were injected to the AVF cyclotron from ECRIS.

An operational test with solid elements have been performed to increase ion species from the source. Multi chaged ions were obtained for three kinds of elements, Mg, Al and Ni. For each element, ions were produced by sputtering ceramics containing MgO, Al_2O_3 and NiO. Cramics were inserted into the plasma region through the space between poles of an open hexapole magnet in the main stage, and sputtered by ^{16}O ions in the plasma. Following results have been obtained from the preliminary test: $^{24}Mg^{7+}$ 3.5 eμA, $^{27}Al^{8+}$ 15 eμA, $^{58}Ni^{10+}$ 8.5 eμA, $^{58}Ni^{12+}$ 12 eμA, $^{58}Ni^{13+}$ 9 eμA, $^{58}Ni^{14+}$ 8.5 eμA, $^{58}Ni^{15+}$ 7 eμA, $^{58}Ni^{16+}$ 8 eμA, and $^{58}Ni^{17+}$ 4 eμA. Figure 2 shows a typical spectrum oftained with Ni. The cross section of the sample is 4 mmϕ for MgO and Al_2O_3, and 4 mm□ for NiO, respectively. The consumption rate of the sample was less than 0.5 mm/hour for all materials. With the AVF cyclotron, $^{24}Mg^{7+}$ and $^{27}Al^{8+}$ ions can be accelerated up to 7 MeV/u, and $^{58}Ni^{16+}$ up to 5 MeV/u.

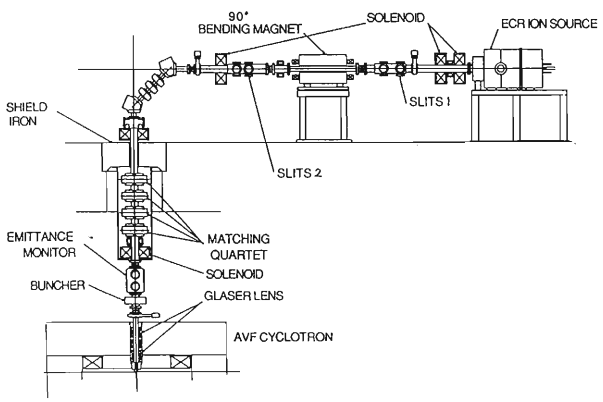

Fig. 1. Schematic drawing of the beam injection line.

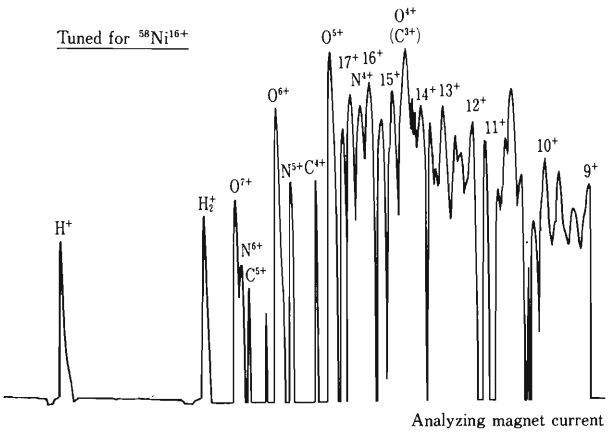

Fig. 2. Charge state spectrum with Ni.

References

1) K. Hatanaka, H. Nonaka, and H. Kamitsubo: Proc. Int. Conf. ECR Ion Sources and Their Applications, p. 353 (1987).
2) K. Hatanaka and H. Nonaka: Proc. Int. Conf. the Physics of Multiply Charged Ions and Int. Workshop E.C.R. Ion Sources (1989).
3) K. Hatanaka, H. Nonaka, E. Ikezawa, and W. Yokota: *RIKEN Accel. Prog. Rep.*, **22**, 219 (1988).

RIKEN Accel. Prog. Rep. 23 (1989)

II-4. Cyclotron Operation

K. Ogiwara, T. Kageyama, and S. Kohara

The 160 cm cyclotron was operated on a 24 hours-a-day basis during the period XXIV from Jan. 1 to Dec. 31, 1989.

The statistics of the machine operation time is shown in Table 1.

Table 2 shows the beam-time allotment to various activities during this period. Table 3 shows the distribution of the scheduled beam-time among various particles.

The 160 cm cyclotron was decided to be shut down in March 1990.

Table 1. Cyclotron Operation in the period XXIV.

	Oscillator	Ion source	Beam
Reading of the time meter on Jan. 06 1989(h)	97,380.8	103,421.5	61,45.39
Reading of the time meter on Jan. 06 1990(h)	99,107.6	105,423.5	62,797.0
Defference(h)	1,726.8	2,002.0	13,413.1

Schedule in this period:	
Beam-time	134 d
Overhaul and installation	79
Periodical inspection and repair	42
Schedule shutdown	107
Machine trouble	3

Table 2. Scheduled beam-time and research subjects in period XXIV.

Subject	Heavy ion	Light ion	Total
RI production for nuclear and solid physics	87 h	149 h	236 h
Nuclear chemistry	0	513	513
Radiation biology	63	50	113
Radiation chemistry	290	46	336
Radiation damage of polymer	8	41	49
Radiation damage of semiconductor	0	28	28
Test of radiation detector	0	2	2
Outside users			
Radiochemical analyses	0	310	310
Radiation damage of device for sattelite	0	18	18
Test of single event upset	38	8	46
Proton irradiation on thyristor	0	298	298
Total	486 h	1,463 h	1,949 h
Percentage in total	24.9%	75.1%	100%

Table 3. Distribution of beam-time among particles accelerated.

Particle	(h)	(%)
p	636	32.6
$^{3}He^{2+}$	358	18.4
$^{4}He^{2+}$	469	24.1
$^{12}C^{4+}$	31	1.6
$^{14}N^{4+,5+}$	414	21.2
$^{16}O^{5+}$	41	2.1
Total	1,949	100.0

RIKEN Accel. Prog. Rep. 23 (1989)

II-5. Tandetron Operation

T. Kobayashi, H. Sakairi, E. Yagi, and T. Urai

The Tandetron was operated for 97 days during the 10 months from Jan.1 to Oct.31,1989. Accelerated ions were ^{1}H, ^{4}He, and ^{11}B.

An accelerating tube sparked on Jan.23,1989, and the machine was shut down until Mar.12, 1989, to repair damaged parts in an SF_6 tank. Other major failures include the cracking of a cesium-ion gun and the dislocating of a duoplasmatron housing caused by the overheating of synthetic-resin glue.

Experimental studies were carried out on the following subjects.

(1) Rutherford backscattering spectroscopy
- a) Behavior of Kr atoms in Al (Metal Physics Lab.)
- b) RBS analysis of Ti-Al-N thin films (Metal Physics Lab.)
- c) Characterization of AlN_x (Surface Characterization Center)
- d) Crystallographic polarity of ideomorphic faces on c-BN single crystal (Surface Characterization Center and Surface and Interface Lab.)
- e) Ion irradiation effect on a Bi-Sr-Ca-Cu-O oxide superconductor (Surface Characterization Center and Surface and Interface Lab.)
- f) Analysis of damage and Cu distribution in Cu-implanted CaF_2 (Semiconductor Lab. and Surface Characterization Center)

(2) Nuclear reaction analysis
- a) State of hydrogen in Nb-Mo alloys (Metal Physics Lab.)
- b) Lattice location of B atoms in Ni_3Al intermetallic compounds (Metal Physics Lab.)

(3) Particle induced X-ray emission (PIXE)
- a) Behavior of Si and P atoms in Fe and Ni (Metal Physics Lab.)
- b) Basic study of PIXE and its application to medical, environmental, archaeological, and materials science (Inorganic Chemical Physics Lab.)

RIKEN Accel. Prog. Rep. 23 (1989)

III. RESEARCH ACTIVITIES

1. Nuclear Physics

1. ^{1}H(d,2p)n Reaction at 200 MeV

T. Motobayashi, C. Perrin,*1 J. Carbonell,*1 C. Wilkin,*2 S. Kox,*1 F. Merchez, *1 Nguyen van Sen,*1 D. Rebreyend,*1 G. Guillaume,*3 J. Arvieux,*4 J. Yonnet, *4 B. Bonin,*5 A. Boudard,*5 M. Garcon,*5 J. Guillot,*6 and G. Gaillard*7

{NUCLEAR REACTIONS ^{1}H(d,2p), $E=200$ MeV; measured $\sigma(\theta)$, $A_y(\theta)$, $A_{yy}(\theta)$, $A_{xx}(\theta)$, CsI(Tl) scintillator array. PWIA analysis.}

The cross section, vector A_y and two tensor analyzing powers A_{xx} and A_{yy} have been measured for the ^{1}H(d,2p)n reaction at $E_d=200$ MeV by using a tensor polarized deuteron beam from the synchrotron Saturne II at Saclay. Two protons emitted from the (d,2p) reaction were detected in coincidence by the EMRIC device,[1] an array of 24 detection modules composed of $4\times 4\times 10$ cm^3 CsI(Tl) crystals (Fig. 1). The experimental results are shown in Fig. 2. The agreement with the prediction of a plane wave impulse approximation calculation[2] is, in general, very good up to a momentum transfer of $q=200$ MeV/c in the region of low p-p excitation energies. The large cross section and significant tensor analyzing powers measured confirm that the reaction may be used as a basis of an efficient and convenient deuteron tensor polarimeter at intermediate energies.

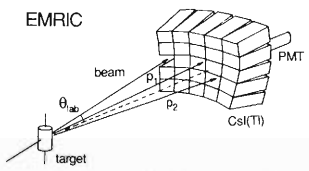

Fig. 1. Schematic view of the experimental setup.

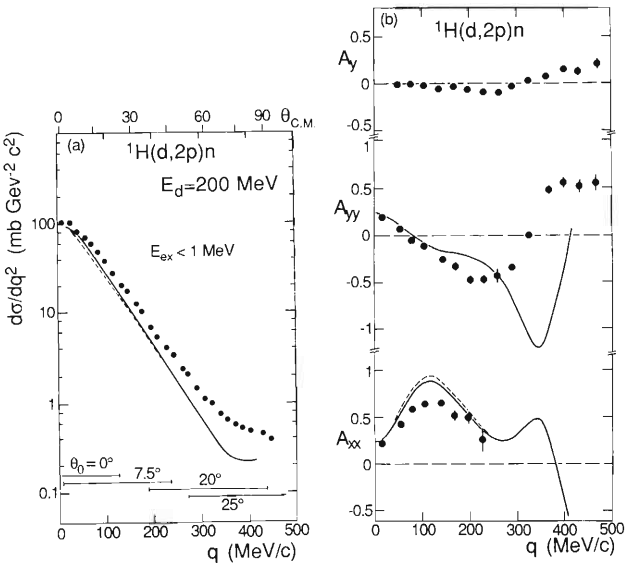

Fig. 2. Differential cross section (a), vector analyzing power A_y and tensor analyzing powers A_{yy} and A_{xx} (b). The solid curves represent the results calculated by the PWIA model.

*1 Institut des Science Nucleaires, 38026 Grenoble Cedex, France.
*2 University College London, London WC1E 6BT, U.K.
*3 Centre de Recherches Nucleaires, 67037 Strasbourg Cedex, France.
*4 Laboratoire National Saturne, 91191 Gif-sur-Yvette Cedex, Fracne.
*5 DPhN/ME-Saclay, 91191 Gif-sur-Yvette Cedex, France.
*6 Institute de Physique Nucleaire, 91406 Orsay Cedex, France.
*7 DPNC Universite de Geneve, 1211 Geneve 4, Switzerland.

References

1) F. Merchez, S. Kox, C. Perrin, J. Mistretta, J.C. Gondrand, L.N. Imouk, P. Gretillat, and E. Schwarz: *Nucl. Instrum. Methods*, **A275**, 133 (1989).
2) D.V. Bugg and C. Wilkin: *Nucl. Phys.*, **A467**, 575 (1987).

RIKEN Accel. Prog. Rep. 23 (1989)

III-1-2. The 7^+ States in ^{26}Al Observed in the ^{24}Mg(α, d) and ^{25}Mg(^{3}He, d) Reactions

M. Yasue, H. Sato, M.H. Tanaka,*1 T. Tanabe,*1 T. Hasegawa,*2 K. Nisimura,*3 H. Ohnuma, H. Toyokawa,*4 H. Shimizu, K. Ieki, K. Ogawa,*5 S.I. Hayakawa, and R.J. Peterson*6

[NUCLEAR REACTION ^{24}Mg(α, d)^{26}Al, E_α=63.7 MeV and ^{25}Mg(^{3}He, d)^{26}Al, E_h=55.2 MeV, DWBA analyses, enhancement factors for 7^+ states.]

The 7^+ states in ^{26}Al were studied by the ^{24}Mg (α, d)^{26}Al reaction at E_α=63.7 MeV and by the ^{25}Mg (^{3}He, d)^{26}Al reaction at E_h=55.2 MeV by using the INS-SF cyclotron, the University of Tokyo.

Five 7^+ states were newly indentified, in addition to the known 8.14 MeV 7^+ state, from the (α, d) angular distributions. Comparisons of the (α, d) and (^{3}He, d) cross sections showed that the 11.81 MeV state was excited through the $(d_{5/2}g_{9/2})$ component and the other 7^+ states through the $(f_{7/2})^2$ component. The results obtained are listed in Table 1. Details will be published elsewhere.[1]

Table 1. Spectroscopic strengths for the 7^+ states in ^{26}Al observed via (α, d) and (^{3}He, d) reactions. Spectroscopic information on the 6.88-MeV 6^- state cited from Ref. 1 is shown for comparison. Integrated (α, d) cross sections σ_{INT} are also given. Abbreviated notations for the two-nucleon configurations are used: for instance, f7f7 means $(f_{7/2})^2$.

E_x (MeV)	J^π	Conf.	NLJ	σ_{INT} in (α, d) (mb)	Enhancement factor in (α, d)	Spectroscopic factor in (^{3}He, d)
6.88	6^-	d5f7	056	1.67	0.33	0.13
7.89	7^+	f7f7	067	0.31	0.05	—
8.14	7^+	f7f7	067	1.10	0.17	—
8.98	7^+	f7f7	067	0.12	0.02	—
10.61	7^+	f7f7	067	0.09	0.01	—
11.81	7^+	d5g9	067	0.70	0.11	0.047
12.00	7^+	f7f7	067	0.11	0.03	—

References

1) R.J. Peterson *et al.*: *Phys. Rev.*, **C38**, 1130 (1988).

*1 Institute for Nuclear Study, University of Tokyo.
*2 Faculty of Engineering, Miyazaki University.
*3 Miyagi University of Education.
*4 Department of Physics, Tokyo Institute of Technology.
*5 Laboratory of Physics, Kanto Gakuin University.
*6 Nuclear Physics Laboratory, University of Colorado.

RIKEN Accel. Prog. Rep. 23 (1989)

III-1-3. Fragmentation of the 6^- and 5^- States in ^{26}Al from the (α,d) Reaction

M. Yasue, H. Sato, M.H. Tanaka,*1 T. Tanabe,*1 T. Hasegawa,*2 K. Nisimura,*3 H. Ohnuma, H. Toyokawa,*4 H. Shimizu, K. Ieki, S.I. Hayakawa, and R.J. Peterson*5

[NUCLEAR REACTION ^{24}Mg(α,d)^{26}Al, E_α = 63.7 MeV, DWBA analyses, enhancement factors for 6^- and 5^- states.]

The 6^- and 5^- states in ^{26}Al were studied in the region of excitation energy E_x=5-15 MeV with the ^{24}Mg(α,d)^{26}Al reaction at E_α=63.7 MeV by using the INS-SF cyclotron, the University of Tokyo. The data were analyzed within the framework of the zero-range DWBA theory for a macroscopic deuteron-cluster transfer as well as for a microscopic two-nucleon transfer, and compared with our previous results[1] on the ^{25}Mg-(^{3}He,d)^{26}Al reaction at E_h=55.2 MeV. Two 6^- and four 5 states are newly proposed, the lowest 5^-, T=0 state at E_x=6.88 MeV in particular. Possible configurations of the 6^- and 5^- states are discussed from comparisons of the (α,d) and (^{3}He,d) cross sections. Mixtures of the $(d_{5/2}f_{5/2})$ and $(d_{3/2}f_{7/2})$ components are suggested for the 5^- states above E_x=8 MeV. Five 6^- states previously assigned as T=1 were observed in the present (α,d) reaction. The isospin impurity amplitudes of the 6^- wave functions estimated from the measured (α,d) cross sections under simplified assumptions were consistent with those deduced from the comparison of the (α,^{3}He) and (α,t) data, and were at least partially explained by a density-dependent Hartree-Fock calculation.[2] A possible admixture of the $3\hbar\omega$ $(0d_{5/2}1f_{7/2})$ configuration is also suggested for the high-lying 6^- states. Results obtained are displayed in Fig. 1.

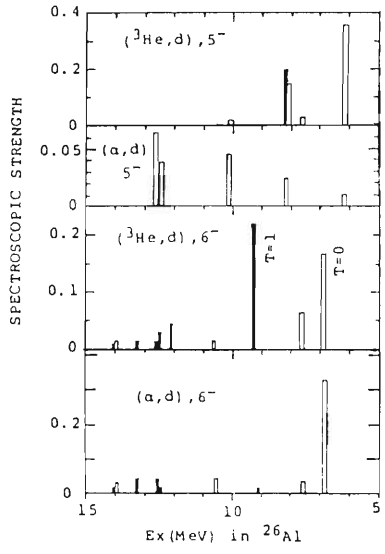

Fig. 1. Enhancement factors ε for the ^{24}Mg(α,d)^{26}Al reaction leading to the 6^- and 5^- states are compared with spectroscopic factors S for the $0f_{7/2}$ single proton transfer obtained in Refs. 1 and 3. The white and black bars represent the strengths for T=0 and 1 states, respectively.

References

1) R.J. Peterson, M. Yasue, M.H. Tanaka, T. Hasegawa, K. Nisimura, H. Ohnuma, H. Shimizu, K. Ieki, H. Toyokawa, and S.I. Hayakawa: *Phys. Rev.*, **C38**, 1130 (1988).
2) H. Sato and Y. Okuhara: *Phys. Rev.*, **C34**, 2171 (1986).
3) M. Yasue, H. Sato, T. Hasegawa, J. Takamatsu, A. Terasawa, T. Nakagawa, and R.J. Peterson: *Phys. Rev.*, **C39**, 2159 (1989).

*1 Institute for Nuclear Study, the University of Tokyo.
*2 Faculty of Engineering, Miyazaki University.
*3 Miyagi University of Education.
*4 Department of Physics, Tokyo Institute of Technology.
*5 Nuclear Physics Laboratory, University of Colorado.

RIKEN Accel. Prog. Rep. **23** (1989)

III-1-4. Deformed Nature of the 6^- States in ^{26}Al Observed by the (α,t) Reaction

M. Yasue, H. Sato, T. Hasegawa,* T. Nakagawa,**
J. Takamatsu,** A. Terakawa,** and R.J. Peterson***

[NUCLEAR REACTION ^{25}Mg(α, t)^{26}Al, E_α = 50 MeV, E_x = 5.0-9.3 MeV, DWBA analyses, spectroscopic factors.]

The ^{25}Mg(α, t)^{26}Al reaction has been studied at E_α=50 MeV in the region of excitation energy from 5 to 10 MeV with an energy resolution of 20 keV by using the INS-SF cyclotron, the University of Tokyo. The fragmentation of the strengths for the stretched 6^- states is found to be consistent with the calculation for an oblately deformed nucleus, in contrast to the prolate shape of the ground-state band. Results obtained are listed in Table 1. Details were published elsewhere.[6]

Table 1. Spectroscopic information for $0f_{7/2}$ stripping to the high spin states in ^{26}Al studied by the ^{25}Mg(α,t)^{26}Al reaction at E_α=50 MeV.

Previous work[a]		Present work			Spectroscopic factors		
						Previous works	
E_x (MeV)	J^π; T	E_x (MeV)	NL2J	σ_{INT} (mb)	Present work (α,t)	(^{3}He,d)[b]	(α,t)[c]
6.892	6^-;0	6.892	0F7	0.16	0.17	0.13	0.16
7.529	6^-;0	7.527	0F7	0.06	0.09	0.11	0.15
9.264[c]	6^-;1	9.267	0F7	0.10	0.22	0.17	0.20
6.083	5^-;0[d]	6.084	0F7	0.33	0.38	0.31	0.32
7.548	5^-;0	7.550	0F7	0.02	0.03		
8.011	5^-;0	8.008	0F7	0.08	0.15	0.10	0.14
8.067	5^-;1	8.065	0F7	0.10	0.20	0.18	0.19
5.394	4^-;0	5.394	0F7	0.10	0.10	0.10	0.10
5.676	4^-;0	5.676	0F7	0.21	0.26	0.31[e]	0.35[e]
5.692	3^-;0	5.692	0F7	0.08	0.12		
6.724	4^-;0	6.726	0F7	0.01	0.02		
7.109	4^-;0	7.107	0F7	0.02	0.03		
7.168	4^-;0	7.163	0F7	0.03	0.04		
7.348	4^-;1 +(0)	7.350	0F7	0.09	0.16		
7.410	4^-;0[d]+(1)	7.413	0F7	0.07	0.12		

Errors in excitation energy is ± 5 keV.

a) (p,γ) in Ref. 1 and (d,α) in Ref. 2.
b) (^{3}He,d) at 55 MeV in Ref. 3.
c) (α,t) at 81 MeV in Ref. 4.
d) Isospin assignment from (α,d) at 64.7 MeV in Ref. 5.
e) The doublet at 5.676 MeV and 5.692 is not separated.
These values are given by assuming the doublet to be a 4^- state.
σ_{INT} means the integrated cross section over the range of angles θ_{cm}=5°-40° $\sigma_{INT}=2\pi\int d\sigma/d\Omega \sin\theta d\theta$.

References

1) P.M. Endt, P. Dewit, and C. Alderliesten: *Nucl. Phys.*, **A459**, 61 (1986).
2) D.O. Boerma, A.R. Arends, P.M. Endt, W. Gruebler, V. Konig, P.A. Schmelzbach, and R. Risler: *Nucl. Phys.*, **A449**, 187 (1986).
3) R.J. Peterson *et al.*: *Phys. Rev.*, **C38**, 1130 (1988).
4) R.J. Peterson *et al.*: *ibid.*, **C33**, 31 (1986).
5) M. Yasue *et al.*: unpublished.
6) M. Yasue *et al.*: *Phys. Rev.*, **C39**, 2159 (1989).

* Faculty of Engineering, Miyazaki University.
** Department of Physics, Tohoku University.
*** Nuclear Physics Laboratory, University of Colorado.

RIKEN Accel. Prog. Rep. 23 (1989)

III-1-5. Emission of Complex Fragments for $^{84}Kr+^{27}Al$ at 10.6 MeV/u

T. Nakagawa, K. Yuasa-Nakagawa, S.C. Jeong, H. Fujiwara, Y.H. Pu,
T. Mizota, H. Kugoh, K. Ieki, I. Tanihata, B. Heusch, T. Sugimitsu, and S.M. Lee

[NUCLEAR REACTION $^{84}Kr+^{27}Al$ $E_L=10.6$ MeV/u; energy spectrum and charge distrution of intermediate mass fragments.]

In recent years the observation of intermediate mass fragments (IMF) and its theoretical interpretation have become one of the most puzzling topics in intermediate energy heavy ion reactions.[1] In order to study the mechanism of IMF emission, it must be worthwhile to see the energy dependence of IMF mass distribution experimentally. A $^{84}Kr+^{27}Al$ system has already been investigated at 35 MeV/u;[2] however, its quantitative interpretation is very difficult since incomplete fusion is dominant at an entrance channel. We have chosen the same system, $^{84}Kr+^{27}Al$, but at lower energy, 10.6 MeV/u, where complete fusion is still dominant (~90%). In this experiment IMF and fission-like products were measured simultaneously. The fission parts are reported separately,[3] and the experimental procedure is discussed therein.

The source velocity extracted from IMF emission is found to be equal to the velocity of the complete fusion products. Energy spectra ($3 \leq Z \leq 10$) in the center of mass system are shown in Fig. 1. The energy of the maximum point of the spectrum seems to be governed by the coulomb energy of the excit channel and increases as the atomic number Z of an emitted particle increases. Energy spectra changes in shape from maxwellian to the gaussian as Z of an emitted particle increases, showing the typical characteristics of complex fragment evaporation.[4] Figure 2 shows the Z distribution of the angle-integrated cross section for IMF. At this energy,

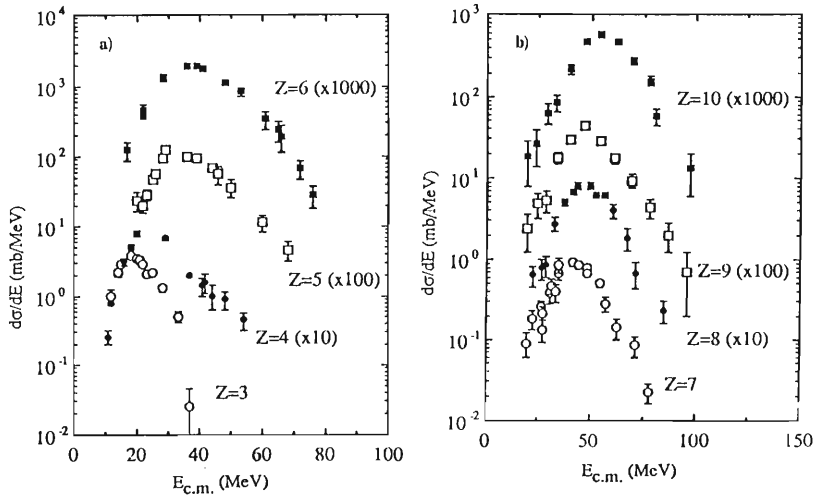

Fig. 1. Energy spectrum of complex fragments ($3 \leq Z \leq 6$) in a c.m. sytsem a) $3 \leq Z \leq 6$; b) $7 \leq Z \leq 10$.

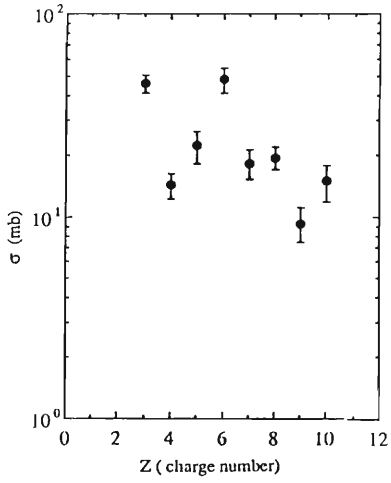

Fig. 2. Angle-integrated charge distributions of complex fragments.

the Z-distribution does not exhibit smooth $Z^{-\tau}$ behavior, but some structures. This result may indicate that a Q-value effect might be large in reproducing Z-distribution. A statistical model analysis is now in progress.

References

1) T. Matsuse, M. Ogihara, and S.M. Lee: Proc. of RIKEN-IN2P3 Symp. on Heavy-ion Collision, Shimoda, Oct., p. 288 (1987).
2) F. Auger *et al.*: *Phys. Rev.*, **C35,** 190 (1987).
3) Y.H. Pu *et al.*: This report, p.13.
4) L.G. Moretto: *Nucl. Phys.*, **A249,** 271 (1975).

RIKEN Accel. Prog. Rep. 23 (1989)

III-1-6. Experimental Study of the Damped Nuclear Reactions of a $^{84}Kr+^{27}Al$ System at 10.6 MeV/u

Y.H. Pu, T. Nakagawa, B. Heusch, K. Ieki, T. Sugimitsu, H. Fujiwara, S.C. Jeong, T. Mizota, K. Yuasa-Nakagawa, H. Kugoh, I. Tanihata, and S.M. Lee

[NUCLEAR REACTIONS, fission-like fragments, Z-distribution.]

A large difference between the element distributions of binary reaction products at $E_{lab}=5.9$ MeV/u[1] and $E_{lab}=35$ MeV/u[2] for the $^{84}Kr+^{27}Al$ system was observed. We have performed an experiment for the system at an incident energy of 10.6 MeV/u intending to investigate the evolution of the reaction mechanisms. A self-supporting ^{27}Al target of 610 $\mu g/cm^2$ in thickness was bombarded with ^{84}Kr beams of 10.6 MeV/u delivered by the RIKEN Ring Cyclotron. Inclusive measurements were made to get element and angular distribution by using two small counter telescopes, each consisting of a gridded ionization chamber and a solid state detector. The solid angles of these two telescopes were 0.41 msr and 0.83 msr, respectively. Exclusive measurements of the two reaction products were also performed by introducing another gas counter telescope which is position sensitive and has a large entrance window[3] ($\Delta\theta\simeq 8°$). Elements up to about $Z=16$ were clearly identified. From simple kinematical considerations, the source velocities of the observed fragments were extracted. Figure 1 shows the independence of the extracted source velocities on the detection angle for $Z=25$. We carried out the same things for other elements and observed that the average values for all elements are exactly equal to the recoil velocity of complete fusion products, indicating that they are all due to binary decays of the same compound nucleus. The measured angular distributions are essentially of $(\sin\theta)^{-1}$ shapes in the reference frame of the emitter. The cross section for each element is obtained by integrating the angular distribution with a $(\sin\theta)^{-1}$ fit, the preliminary result is given in Fig. 2. Further data analysis including the exclusive data and theoretical analyses based on scission point model[4] and saddle point model [2,5] are under way. A more complete experiment on the same system and at the same energy including mass measurement is now being prepared.

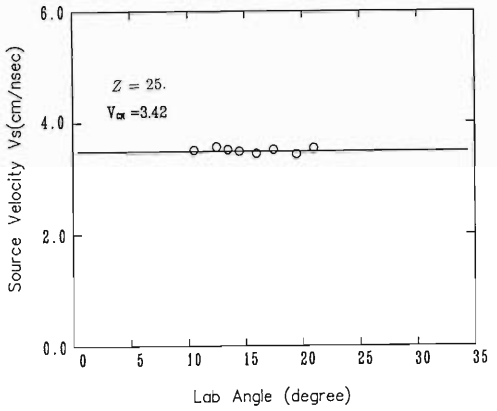

Fig. 1. Source velocities extracted from the energy spectra as a function of detection angles.

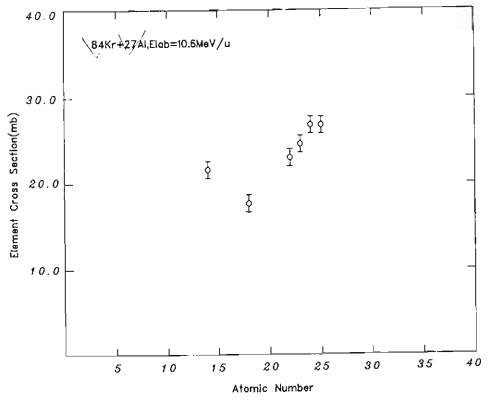

Fig. 2. Preliminary result of the Z-distribution of the measured fission-like fragments.

References

1) B. Heusch *et al.*: *Z. Phys.*, **A322**, 309 (1985).
2) F. Auger *et al.*: *Phys. Rev.*, **C35**, 190 (1987).
3) Y.H. Pu *et al.*: *UTTAC Annu. Rep.*, p. 13 (1988).
4) S.M. Lee and T. Matsuse: Proc. of Int. Symp. on Heavy-Ion Physics. Mt. Fuji, p. 272 (1984).
5) L.G. Moretto: *Nucl. Phys.*, **A247**, 271 (1975).

RIKEN Accel. Prog. Rep. 23 (1989)

III-1-7. Electromagnetic Transition Probabilities in the Natural-Parity Rotational Band of ^{173}Yb

M. Oshima, M. Matsuzaki,* S. Ichikawa,* H. Iimura,* H. Kusakari, T. Inamura, A. Hashizume, and M. Sugawara

[NUCLEAR REACTIONS ^{173}Yb(^{58}Ni, ^{58}Ni′γ), $E=250$ MeV; measured E_γ, nuclear lifetimes; recoil distance method; B(M1) signature dependence and calculation.]

In the natural-parity rotatioanal band of ^{163}Dy we have found that the phase of the signature dependence of B (M1) values is opposite to the one which is expected for the dominant $j=9/2$ configuration,[1,2] while the quasiparticle energy splitting and the absolute value of B (M1) are in agreement with the dominant $j=9/2$ character for this band. This "inverted" signature dependence was shown in terms of a rotating shell model to originate from the characteristic coherence between the orbital and spin contributions in the spin-down ($\Omega=\Lambda-1/2$) dominant one-quasiparticle states.[2,3] In order to confirm such a mechanism, the counterpart, *i.e.*, the spin-up ($\Omega=\Lambda+1/2$) dominant configurations should be studied. Therefore, we performed a Coulomb-excitation experiment on ^{173}Yb whose ground-state rotational band is based on the natural-parity Nilsson state $\nu 5/2[512]$. We have assigned levels up to $J^\pi=(27/2^-)$ and measured γ-ray branchings, E2/M1 mixing rations and nuclear lifetimes, and determined the absolute intraband transition probabilities up to the $25/2^-$ state.[4]

All observed quantities show almost no signature dependence as is generally expected for the spin-up one quasiparticle bands with natural parity. Our rotating shell-model calculations well reproduce both the absolute values and the signature dependence of these quantities. Here we adopted geometrical factors proposed by Donau[5] to make a correction for the deviation between the direction of the total angular momentum and the cranking axis, which is not incorporated in the rotating shell model. (This deviation becomes larger for lower spin states in odd nuclei.) Figure 1 shows the experimental and theoretical B (M1) values for $I \rightarrow I-1$ transitions.

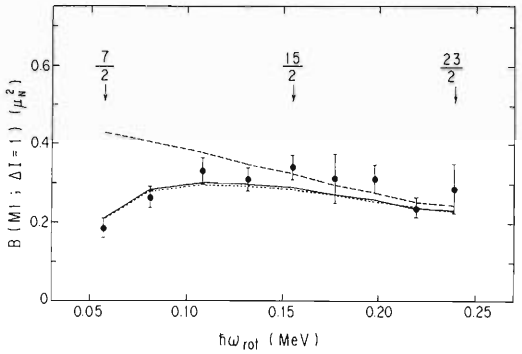

Fig. 1. B(M1; $I \rightarrow I-1$) values for the ground-state rotational band of ^{173}Yb. The solid (broken) line shows the calculation with (without) the geometrical factor. The dotted line includes the γ vibration besides the geometrical factor.

We conclude that the signature dependence of the spin-down and the spin-up configurations with natural parity is reproduced in a consistent manner in terms of the rotating shell model.

References

1) E. Minehara, M. Oshima, S. Kikuchi, T. Inamura, A. Hashizume, and H. Kumahora: *Phys. Rev.*, **C35**, 858 (1987).
2) M. Oshima, E. Minehara, S. Kikuchi, T. Inamura, A. Hashizume, H. Kusakari, and M. Matsuzaki: *ibid.*, **C39**, 645 (1989).
3) M. Matsuzaki: *ibid.*, p. 691 (1989).
4) M. Oshima, M. Matsuzaki, S. Ichikawa, H. Iimura, H. Kusakari, T. Inamura, A. Hashizume, and M. Sugawara: *Phys. Rev.*, **C40**, 2084 (1989).
5) F. Donau: *Nucl. Phys.*, **A471**, 469 (1987).

* Japan Atomic Energy Research Institute, Tokai.

RIKEN Accel. Prog. Rep. 23 (1989)

III-1-8. Angular Momentum Transfer in a Fusion-Like Process

T. Takei, K. Ieki, N. Iwasa, K. Yoshida, J. Kasagi, H. Hama, M. Sakurai, M. Kodama, K. Furutaka, T. Kubo, W. Galster, and A. Galonsky

[NUCLEAR REACTION ^{92}Mo+^{40}Ar, $E(^{40}\mathrm{Ar})/A=26$ MeV/u; measured angular correlation between two evaporative neutrons, angular momentum transfer.]

We studied the angular correlation between two neutrons emitted in the ^{92}Mo+^{40}Ar reaction at 26 MeV/nucleon. The experimental setup is the same as reported elsewhere.[1] The neutrons are detected with a 2π BaF_2 ball and discriminated from γ rays by measuring the fast and slow components of light output from the BaF_2 detectors. Residual nuclei were measured in coincidence with a PPAC to deduce excitation energy.

Figure 1(a) shows an angular correlation analyzed as a function of θ for a complete fusion reaction. The angle θ is defined as

$$\cos\theta = |\boldsymbol{p}\cdot(\boldsymbol{v}_1\times\boldsymbol{v}_2)| / |\boldsymbol{v}_1\times\boldsymbol{v}_2|,$$

where $\boldsymbol{p}$, $\boldsymbol{v}_1$, and $\boldsymbol{v}_2$ denotes unit vectors of a beam direction and directions of two detected neutrons, respectively. When neutrons are emitted from a fully rotating compound nucleus, the neutrons should be emitted in the direction perpendicular to the angular momentum direction ("flywheel effect"). Thus the direction of $\boldsymbol{v}_1\times\boldsymbol{v}_2$ should be the spin axis of the residual nuclei which must be perpendicular to $\boldsymbol{p}$. therefore $\theta=90°$ is expected to evaporative neutrons from fully rotating systems and the deviation from that value implies angular momentum relaxation at the stage of the neutron emission.

Since the BaF_2 detectors do not cover a whole solid angle, we performed Monte Carlo simulation to compare with. In the calculation, following points are taken into account:

1) geometry of the detectors is fully considered;
2) spin axis of the compound nucleus is supposed to lie in the plane perpendicular to $\boldsymbol{p}$;
3) the angular distribution of the neutrons is expressed as

$$W(\phi)\propto\exp(-\beta\cos^2\phi),$$

where ϕ is the angle between the emission direction and the spin axis and β is the anisotropy parameter. A larger β corresponds to larger angular momentum transfer; and
4) the energy distribution of the neutron is given by

$$N(E_n)\propto\sqrt{E_n}\exp(-E_n/T),$$

where T is nuclear temperature of the residual nuclei and is determined emprically.

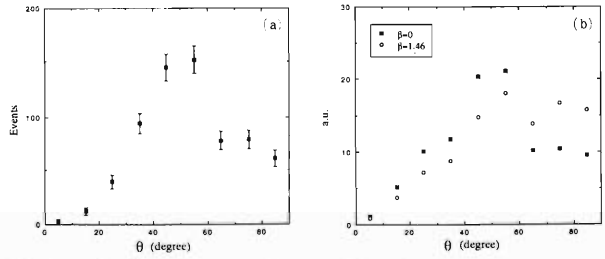

Fig. 1. (a) Experimental correlation between two neutrons. For explanation of θ, see text. (b) Results of the Monte Carlo simulation for the cases of $\beta=0$ (solid square) and $\beta=1.46$ (open circle). A value of 5 MeV is taken as the parameter T for the complete fusion reaction.

The results of the simulation are shown in Fig. 1(b) for $\beta=0$ and $\beta=1.46$. The latter value was selected from the calculation using a sharp cut off model for the complete fusion reaction. Owing to the insufficient solid angle of the detectors, the maximum angle of the correlation shifted from $\phi=90°$ to 50°. The difference in the correlation between two β values is mainly seen for large θ values. The experimental result (Fig. 1(a)) is found to be rather similar to the case of $\beta=0$, suggesting that the transferred angular momentum is fully relaxed or fairly small at the stage of neutron evaporation.

Further analyses are now in progress.

References

1) K.Yoshida *et al.*: to be published.

RIKEN Accel. Prog. Rep. 23 (1989)

III-1-9. Angular Momentum Transfer and Spin Alignment in the Reaction of $^{40}Ar+^{209}Bi$ at 26 MeV/Nucleon

N. Iwasa, K. Ieki, J. Ruan (Gen), S. Shirato,H. Murakami,
Y. Ando, M. Ogiwara, S. Shibuya, K. Hata, S.M. Lee,
Y. Nagashima, M. Ogihara, S.C. Jeong,H. Fujiwara, Y.H. Pu,
T. Mizota,S. Okumura, M. Ishihara, and T. Murayama

Nuclear Reaction $^{209}Bi+^{40}Ar$, $E(^{40}Ar)/A=26$ MeV/nucleon; projectile-like fragment, fission-fragment angular distribution, deduced angular momentum transfer

In a previous report,[1] we showed that the emission of projectile-like fragments (PLF's) was accompanied partly with an angular momentum transfer process in the $^{40}Ar+^{209}Bi$ reaction at $E/A=26$ MeV/nucleon. An angular momentum l_{tr} transferred to residual fissile nuclei was deduced from the angular distribution of coincident fission fragments by using a statistical theory of fission.[2] In the present paper, the angular distribution of the fission fragments is re-analyzed in detail and the dependence of l_{tr} on the atomic number Z of PLF's is studied.

Since the fission fragments were detected with thin Si solid state detectors, the discrimination of fission fragments from evaporative light particles was incomplete at low energies ($E\leq 30$ MeV). In the present analysis, the yields of low-energy fission fragments are estimated by fitting fission-fragment energy spectra. The momentum distribution of fission fragments is assumed to be of a Gaussian shape in the rest frame of fissile nuclei. The energy loss of the fission fragments in a target and the pulse height defect in the detectors are taken into account. In the determination of the rest frame of the fissile nuclei, some missing momentum is required to fulfill kinematical requirement.

The experimental angular distribution of fission fragments is compared with calculation based on the statistical theory of fission.[2] In the calculation, the spin orientation of fissile nuclei is assumed to be axially symmetric with respect to the normal of the reaction plane defined by the beam axis and the detection of PLF's. The size of l_{tr} and the degree of spin depolarization are treated as parameters. Figure 1 shows an example of the out-of-plane angular distribution of the fission fragments for six in-plane angles in the laboratory frame. Solid lines show the calculation that fits the data. The overall behavior of the distribution is well reproduced from the calculation.

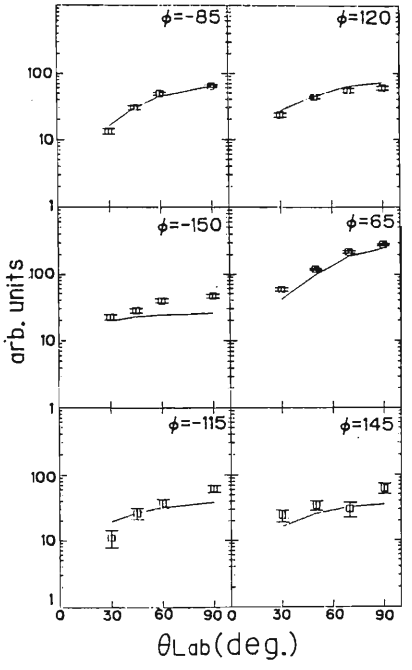

Fig. 1. Out-of-plane angular distribution of fission fragments in coincidence with PLF's of $5\leq Z\leq 10$. It is displayed for six in-plane angles(ϕ) in the laboratory frame. Solid lines show the calculation.

The deduced values of l_{tr} are $23.7\,\hbar\pm 0.4\,\hbar$ for $5\leq Z\leq 10$ and $31.6\,\hbar\pm 0.4\,\hbar$ for $11\leq Z\leq 15$. The large values of l_{tr} imply that a part of the projectile is emitted as PLF and the remnant of the projectile is transferred to residual fissile nuclei. However, as the dependence of l_{tr} on Z is opposite to expectation of such a naive massive transfer picture, more sophisticated explanation is needed for the present data.

References

1) N. Iwasa *et al.*: *RIKEN Accel. Prog. Rep.*, **22**, 18 (1988).
2) R. Vandenbosch and J.R. Huizenga: "Nuclear Fission," Academic Press, New York, p. 179 (1973); L.G. Morreto: *Nucl. Phys.*, **A364**, 125 (1981).

RIKEN Accel. Prog. Rep. 23 (1989)

III-1-10. Strong Inhibition of Gamma-ray Emission from Highly Excited Nuclei

K. Yoshida, J. Kasagi, H. Hama, M. Sakurai, K. Ieki,
W. Galster, M. Ishihara, and T. Kubo

[NUCLEAR REACTION ^{92}Mo+^{40}Ar, $E(^{40}\mathrm{Ar})=21$, 26 MeV/nucleon; measured γ-rays coincidence with residues.]

In order to investigate the evolution of Giant Dipole Resonance (GDR) as a function of excitation energy, we measured high energy γ rays in coincidence with fusion-like products from the reaction ^{92}Mo+^{40}Ar at 21 MeV/n and 26 MeV/n. Argon beams from the RIKEN Ring Cycrotron (RRC) bombarded an enriched ^{92}Mo foil of 2 mg/cm^2 in theckness. The high energy γ rays were detected in a BaF_2 high energy γ-ray detector placed at 90° with respect to the beam axis and 15 cm from the target. The detector consists of seven hexagonal BaF_2 crystal (37cm^2×20cm) separated optically. Events due to neutrons were completely rejected by a time-of-flight method together with a pulse shape analysis.[1] Fusion-like residues were detected in an annular Parallel Plate Avalanche Counter (PPAC, outer diameter is 12 cm) positioned 30 (40) cm from the target in the forward direction for $E_i=21$ (26) MeV/ nucleon.

In Fig. 1 are shown γ-ray spectra obtained in coincidence with the fusion residues. Data are plotted for different residue velocities represented by the ratio R of the observed velocity to the one for complete fusion residues. The excitation energy for each value of R was estimated on a simple assumption in which whole target nucleus merges with a part of the projectile and the remaining part of a projectile pass through with their initial velocity. Estimated excitation energies E_x and the masses of a fused system A_{fus} are summarized in Table 1.

In spite of a huge difference in excitation energies, observed spectra are essentially identical in shape except for a high energy region ($E_\gamma>25$ MeV). The observed spectrum shows three different slopes. In order of γ-ray energies, these components correspond to the γ-ray emissions after particle decays, from GDR decay competing with particle evaporations, and from nucleon-nucleon bremsstrahlung in the early stage of the reaction.[2] The fact that the slope of the γ-ray yield in the highest energy region depends only on the incident energy strongly supports this interpretation. The contributions of the bremsstrahlung emission have been estimated by assuming an exponential function as the shape and subtracted from the data. The extracted inverse slopes are 8.5 MeV and 10.3 MeV for incident energy 21 MeV/ n and 26 MeV/ n, respectively. All the subtracted spectra are almost identical in spite of a large difference in excitation energies. In simple consideration the GDR yields are expected to increase with excitation energies because of more chance for γ rays to compete with particle evaporations. Similar inhibition of γ decay in high excitation energies are also reported by Gaardhoje *et al.*[3] For characterization of the innibition, a statistical model calculation with using a code CASCADE is now in progess.

Table 1. Average excition energies and masses for various R value.

Beam energy	R	E_x(MeV)	A_{fus}
	1.0	508	132
21 MeV/n	0.7	360	120
	0.5	280	109
	1.0	616	132
26 MeV/n	0.7	480	120
	0.5	370	109

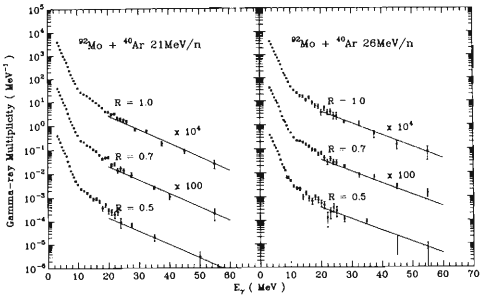

Fig. 1. Gamma-ray spectra for various R values. Solid lines show bremsstrahlung components.

References

1) T. Murakami *et al.*: *Nucl. Instrum. Methods*, **A253**, 163 (1986).
2) E. Grosse *et al.*: *Europhys. Lett.*, **2**, 9 (1986).
3) J.J. Gaardhoje *et al.*: *Phys. Rev. Lett.*, **59**, 1409 (1987).

RIKEN Accel. Prog. Rep. 23 (1989)

III-1-11. First Observation of Spin Polarization in Projectile Fragments from Intermediate Energy Heavy Ion Collision

K. Asahi, M. Ishihara, H. Takanashi, M. Kouguchi, M. Adachi, M. Fukuda, N. Inabe, D. Mikolas,* D. Morrissey,* D. Beaumel,** T. Ichihara, T. Kubo, T. Shimoda, H. Miyatake, and N. Takahashi

NUCLEAR REACTION ^{197}Au(^{14}N, ^{12}B), $E=40$ MeV/nucleon; measured β-ray asymmetry of ^{12}B nuclei; deduced spin polarization of ^{12}B. Comparison with predictions from a projectile fragmention model.

Spin polarization P of ejectiles ^{12}B was measured for a projectile fragmentation reaction induced by a 40 MeV/nucleon ^{14}N beam. The result shows stimulatingly large values of P (P ~5-20%) over a wide range of fragment momentum, implying a promising prospect of polarized radioactive isotopes to be applied to spectroscopic studies of nuclei far from stability.

The beam line used is schematically shown in Fig. 1. A ^{14}N beam from RIKEN Ring Cyclotron was used to bombard a 97 mg/cm^2 thick Au target. Fragments ^{12}B emitted from the target in the direction $\theta_L=5°$ were transmitted through a dipole magnet and implanted into a stopper placed at the focus F. Spin polarization P was deduced from the observed up/down asymmetry in the beta decay of ^{12}B$_{g.s.}$ ($I^\pi=1^+$, $T_{1/2}=20.2$ ms) to ^{12}C$_{g.s.}$ ($I^\pi=0^+$).

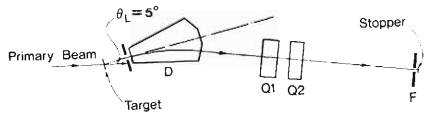

Fig. 1. Schematic view of the beam line used.

The experimental results are presented in Fig. 2. The momentum distribution of ^{12}B fragments shown in the lower part exhibits a single broad peak with a maximum located close to the momentum corresponding to the incident beam velocity. The observed spin polarization P of ^{12}B fragments is shown in the upper part of Fig. 2, as a function of the ^{12}B outgoing momentum. The polarization P shows positive values in the higher momentum side of the peak whereas it becomes negative for the lower momentum side. The sign changes at the peak momentum. This behavior well conforms to a simple picture[1,2] based on models[3,4] of projectile fragmentation.

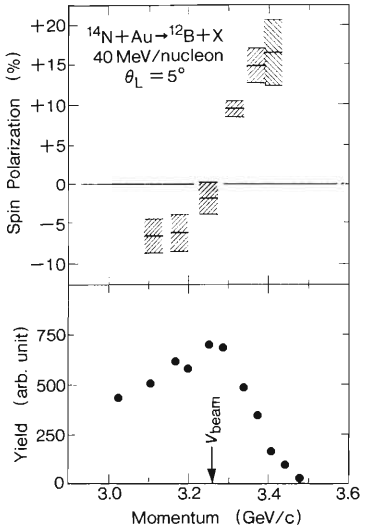

Fig. 2. Experimental result. The spin polarization (upper part) and the yield (lower part) for fragment ^{12}B are shown as a function of outgoing momentum.

References

1) K. Asahi *et al.*: *Nucl. Phys.*, **A488**, 83c (1988).
2) K. Asahi *et al.*: in preparation.
3) A.S. Goldhaber: *Phys. Lett.*, **53B**, 306 (1974).
4) J. Hüfner and M.C. Nemes: *Phys. Rev.*, **C23**, 2538 (1981).

* NSCL, Michigan State University, East Lansing, MI 48824, U.S.A.
** Institut de Physique Nucleaire, B.P. 1, 91406 Orsay, France.

RIKEN Accel. Prog. Rep. 23 (1989)

III-1-12. Energy Dependence of Interaction Cross Sections

S. Shimoura, I. Tanihata, T. Kobayashi, K. Matsuta,* K. Katori,*
K. Sugimoto,* D.L. Olson,** W.F.J. Müller,** and H.H. Wieman**

[Nuclear matter distribution, secondary nuclear beams, heavy-ion collisions.]

In past several years, we have been measuring interaction cross sections, σ_I (the total cross sections for change of proton and/or neutron numbers in a projectile) of various nuclei at 0.8 GeV/nucleon and deduced root-mean-square (rms) radii of unstable nuclei by fitting σ_I with a Glauber-type optical model.[1-3] To check the accuracy of the model, we have measured interaction cross sections of stable and exotic nuclei, ^{12}C and ^{11}Li (^{8}He, ^{14}Be), on Be, C and Al targets at 0.4 (0.6) GeV/nucleon, where nucleon-nucleon (N-N) cross sections are different from those at 0.8 GeV (*e.g.* σ_{NN} [0.4 GeV]$\approx$0.7 σ_{NN} [0.8 GeV]). Experiment was performed at the LBL Bevalac by using separated secondary nuclear beams from a B42 line and HISS detectors.

For a ^{12}C projectile, a Glauber model[4] using free N-N cross sections and nucleon distributions obtained from electron-scattering data[5] reproduces observed interaction cross sections at 0.4, 0.6 and 0.8 GeV/nucleon without any adjustable parameters (Fig. 1). In the model, interaction cross sections are calculated from a transparency function T(b) as

$$\sigma_I = 2\pi \int_0^\infty (1 - T(b))\, b\, db,$$

$$T(b) = \exp\left[-\sigma_{NN}\, \rho_{ov}(b)\right],$$

where b, σ_{NN} and $\rho_{ov}(b)$ are the impact parameter, N-N cross sections and density-overlap between a projectile and target nuclei, respectively. Since $1-T(b)$ behaves like Fermi-distribution ($T(0)\approx 0$ and $T(\infty)=1$), $\sigma_I \approx \pi b_0^2$, where $T(b_0) = \exp[-\sigma_{NN}\, \rho_{ov}(b_0)] = 1/2$. Thus smaller σ_{NN} gives larger $\rho_{ov}(b_0)$, *i.e.* b_0 corresponds to a larger density. In other words, by changing energy (σ_{NN}), the nuclear radius with different density can be obtained, which provides information about the diffuseness of nuclear density. If the radio of diffuseness and radius is small (large), the energy dependence of σ_I becomes weak (strong).

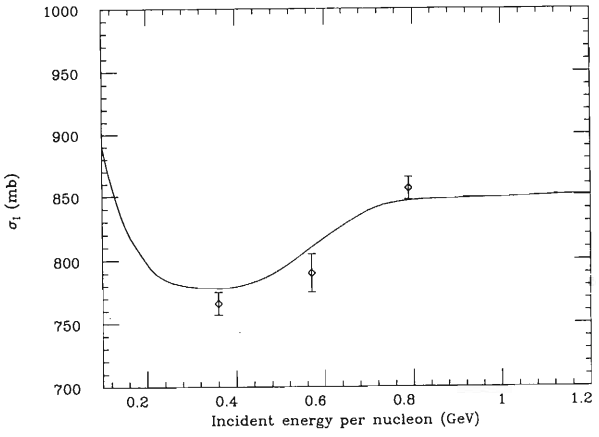

Fig. 1. Interaction cross sections of ^{12}C on a ^{12}C target at 0.4, 0.6 and 0.8 GeV/nucleon. The line shows the Glauber-model calculation with free N-N cross sections and nucleon density obtained from electron scattering data.

For a ^{11}Li projectile, the ratio σ_I [0.4 GeV] /σ_I [0.8 GeV] = 0.91±0.02, which is almost the same as the ^{12}C projectile case, was observed. Because of the large radius of a ^{11}Li nucleus ($R(^{11}\mathrm{Li})/R(^{12}\mathrm{C}) \approx 1.3$), the diffuseness is expected to be a value proportional to the radius, which is not of a usual (stable) nucleus with a constant diffuseness.

In summary, the energy dependence of interaction cross sections gives information on the density distributions of nuclei, especially for unstable nuclei, from which one can extract radii and diffuseness parameters.

References

1) I. Tanihata *et al.*: *Phys. Lett. B*, **206**, 592 (1988).
2) I. Tanihata *et al.*: *ibid.*, **160**, 380 (1985).
3) I. Tanihata *et al.*: *Phys. Rev. Lett.*, **55**, 2676 (1985).
4) P.J. Karol: *Phys. Rev.*, **C11**, 1203 (1975).
5) H. de Vries, C. W. de Jager, and C. de Vries: *At. Data Nucl. Data Tables*, **36**, 495 (1987).

* Faculty of Science, Osaka University.
** Lawrence Berkeley Laboratory, University of California, USA.

RIKEN Accel. Prog. Rep. 23 (1989)

III-1-13. Electromagnetic Dissociation and Soft Giant Dipole Resonance of Neutron Dripline Nuclei*

T. Kobayashi, S. Shimoura, I. Tanihata, K. Katori, K. Matsuta, T. Minamisono, K. Sugimoto, W.F.J. Müller,** D.L. Olson,** T.J.M. Symons,** and H.H. Wieman**

[NUCLEAR STRUCTURE, radioactive beam, heavy ion collisions, giant resonance, neutron halo.]

Electromagnetic dissociations (EMD) provide important information on nuclei with the giant neutron halo. For stable nuclear projectiles, observations of the EMD process at energies from 1 GeV to 200 GeV/nucleon have been reported, in which fragmentation due to the EMD process has clearly been seen, in particular in single-nucleon-removal channels on high-Z targets. This phenomenon at an energy of a few GeV/nucleon was interpreted as being the excitation and decay of a giant dipole resonance (GDR) of a projectile by virtual photons of the Coulomb field from a target.

The EMD cross sections for ^{11}Li fragmentation by a Pb target is determined to be 1.72 ± 0.65b at a beam energy of 800A MeV. For comparison of the obtained EMD cross sections of neutron-rich nuclei with a typical cross section for stable nuclei, the total EMD cross section, $\sigma_I^{EMD}(^{12}C+Pb)$, was estimated as 90 ± 35 mb. The value was obtained by adding the observed EMD parts of single-nucleon-removal cross sections at 1.05 GeV/nucleon, with $\sigma_{-n}^{EMD}(^{12}C+Pb)$ and $\sigma_{-p}^{EMD}(^{12}C+Pb)$ being the major contributions. The value of σ^{EMD} for ^{11}Li is about 20-times larger than that for ^{12}C. If the projectile charge dependence of σ^{EMD} is assumed to be Z_{proj}^2, the enhancement of $\sigma^{EMD}(^{11}Li)$ compared with $\sigma^{EMD}(^{12}C)$ is extremely large, by a factor of 80. Large EMD cross sections were also observed for ^{8}He and ^{14}Be. Therefore, it is considered that the observed large EMD cross sections are related to a specific nuclear property of extremely neutron-rich nuclei.

Concerning the GDR of extremely neutron-rich nuclei, Ikeda suggested the possibility that the GDR could split into two components for nuclei with a giant neutron halo. One component corresponds to the oscillation of the core protons against the core neutrons with a normal frequency, and the other to the oscillation of the core against the skin neutrons, as shown schematically in Fig. 1. Within the framework of this model, the energy of the soft GDR can be estimated. The GDR at a normal excitation energy ($E_{normal\ GDR}\approx22$ MeV estimated from the systematics) contributes to σ_I^{EMD} only by about 80 mb. Therefore, the main part of σ_I^{EMD} is from the excitation of the soft GDR. An integrated strength of the soft GDR was estimated as 10% of the total E1 strength, since the E1 strength is roughly proportional to the square of the number of neutrons involved in each mode. In order to reproduce the observed $\sigma_I^{EMD}(^{11}Li+Pb)$, the energy of the soft GDR had to be $E_{soft\ GDR}=0.9^{+0.5}_{-0.3}$MeV. Thus, the excitation energy of the soft GDR turned out to be really low. Qualitatively, the most essential conclusion drawn here is that the observed large EMD cross section, together with the rapidly-decreasing virtual-photon spectrum, requires an appreciable strength of the E1 mode to be located at a very low excitation energy.

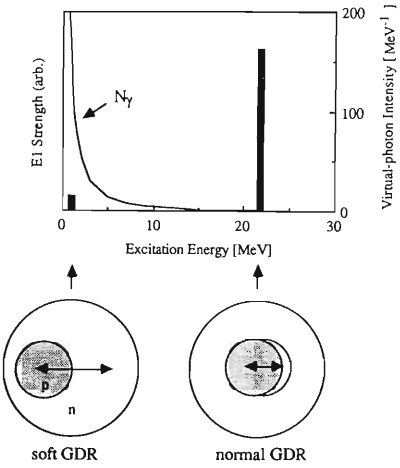

Fig. 1. Schematic pictures of the expected soft GDR and the normal GDR in the extremely neutron-rich nucleus with a neutron halo. The dipole oscillation between protons (shaded area) and neutrons (white area) is shown for each mode. The E1 strength of the soft and the normal GDR (black bar) is shown together with the virtual-photon spectrum (solid line) seen by the 0.8 GeV/nucleon ^{11}Li projectile on a Pb target.

* Condenced from RIKEN-AF-NP-76, *Phys. Lett.*, **B232**, 51 (1989).

** Lawrence Berkeley Laboratory, Berkeley, Ca 94720, USA.

RIKEN Accel. Prog. Rep. 23 (1989)

III-1-14. Electromagnetic Dissociation of ^{11}Be at 0.8 A GeV and the Giant Dipole Resonance of Neutron-Rich Nuclei

T. Kobayashi, S. Shimoura, I. Tanihata, T. Suzuki, K. Sugimoto, K. Matsuta, T. Minamisono, H.H. Wieman,* D. Olson,* and W.F.J. Müller*

[Nuclear structure, radioactive beam, heavy-ion collisions, giant resonance, neutron halo.]

The soft mode of Giant Dipole Resonance (GDR) in extremely-neutron-rich nuclei has been suggested[1] from the observed large electromagnetic dissociation (EMD) cross sections of neutron dripline nuclei such as ^{8}He, ^{11}Li, and ^{14}Be. In this report, we present a new observation of large EMD cross sections in the collisions of ^{11}Be on high-Z targets at 800A MeV incident energy.

The experiment was carried out using secondary beams from the Lawrence Berkeley Laboratory Bevalac. The interaction cross section σ_I and one-neutron removal cross section σ_{-n} of a ^{11}Be projectile on various targets were determined using a large acceptance spectrometer HISS. The target mass dependences of the measured cross sections are shown in Fig. 1, in which estimated nuclear cross sections are also shown; the solid curve for σ_I^{nucl} and the dotted line for σ_{-n}^{nucl}. Large EMD cross sections are seen as the difference between data points and the corresponding line. One neutron removal cross section of the ^{11}Be projectile on a Pb target is found to be about 40 times larger than that of ^{12}C projectile[2] after scaling the cross section by Z_{proj}.[2]

Because the EMD cross section is calculated by folding photonuclear cross sections by a virtual photon spectrum, the energy of GDR in ^{11}Be can be estimated if the Lorenzian shape of a photonuclear cross section and the Thomas-Reiche-Khoon sum rule are assumed.[1] The estimation gives $E_{GDR}=6.5\pm1.3$ MeV, which is much lower than that estimated from the systematics of stable nuclei. The available data of near neutron dripline nuclei, the small neutron separation energy (0.5 MeV for ^{11}Be), the neutron halo,

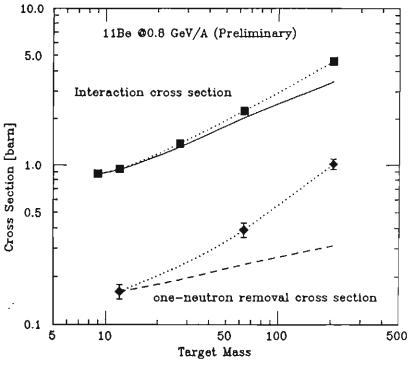

Fig. 1. Target mass dependence of the interaction cross section and the one neutron removal cross sections of the ^{11}Be+Creaction at 800A MeV.

the large EMD cross section, and the soft mode of GDR, are mutually correlated. In contrast, none of these properties are observed in stable nuclei. It is also interesting that a preliminary analysis shows narrow momentum distribution of a ^{10}Be fragment from the projectile fragmentation of ^{11}Be on a carbon target, presumably reflecting the long neutron tail of a weakly-bound neutron in ^{11}Be nucleus.

References

1) T. Kobayashi, O. Yamakawa, K. Omata, K. Sugimoto, T. Shimoda, N. Takahashi, and I. Tanihata: *Phys. Rev. Lett.*, **60**, 2599 (1988); T. Kobayashi, S. Shimoura, I. Tanihata, K. Katori, K. Matsuta, T. Minamisono, K. Sugimoto, W. Müller, D.L. Olson, T.J.M. Symons, and H. Wieman: *Phys. Lett.*, **B232**, 51 (1989).
2) H. Heckman and P. Lindstrom: *Phys. Rev. Lett.*, **37**, 56 (1976).

* Lawrence Berkeley Laboratory, Berkeley, CA 94720, USA.

RIKEN Accel. Prog. Rep. 23 (1989)

III-1-15. Inclusive Production of K^+ Mesons in 2.1 A GeV Nuclear Collisions*

S. Schnetzer,** R. M. Lombard,** M.-C. Lemaire,** E. Moeller,**
S. Nagamiya,** G. Shapiro,** H. Steiner,** and I. Tanihata

[Heavy ion collisions, K^+.]

Positively charged K meson production by 2.1-GeV/ nucleon Ne, d, and p projectiles on NaF and Pb targets has been measured. The cross sections depend exponentially upon the kaon energy in the nucleon-nucleon c.m. frame, with an inverse slope T_0 larger than the values obtained from comparable proton and π^- spectra. Figure 1 shows the K^+ spectrum from Ne+NaF collisions together with some model calculations.

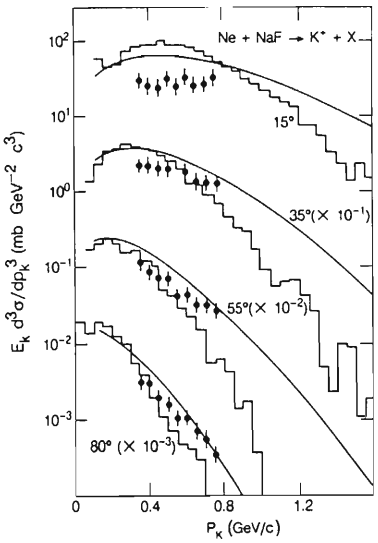

Fig. 1. Invariant spectrum of K^+ mesons from the Ne+NaF reaction at 2.1 GeV/ nucleon. The histogram corresponds to the results of a cascade calculation (Ref. 1) and the curves to calculations with the firestreak model (Ref. 2).

Our motivation for undertaking this experiment was to study hadronic interactions in heretofore unexplored territory. We hoped to exploit the unique properties of K^+ mesons -their strangeness and their relatively low-interaction cross sections- as a probe of nuclear interaction dynamics at high energies. We wanted to take advantage of their long mean free path to suppress secondary interactions and thereby to get more direct information about the early stages of the production process. Perhaps most of all we wanted to know whether or not kaon production in nucleus-nucleus collisions involved any interesting new phenomena, or if the measured cross sections could be explained on the basis of standard.

Our result produced no great surprises. The mechanism for the kaon production by nuclei seems to be quite similar to that in nucleon-nucleon collisions. To be sure there are kinematic differences. There is extra energy available when nuclei collide (as contrasted with the p-p case) some of which goes to the produced kaon, resulting in exponentially falling momentum distributions. The slope of the exponential is slighty less steep in the nucleus-nucleus case than for p nucleus. As in the p-p case the dominant reaction is $NN \rightarrow YNK$. Qualitative fits to data can be obtained with single scattering models, either by invoking exponentially falling Fermi momentum distributions or by colliding small clusters of nucleons. Much more sophisticated intranuclear cascade calculations and thermodynamic models have been published, which are in reasonable agreement with our measurements. Quarks, compressional effects, and/or other nonstandard mechanisms are not needed at this stage to explain the results.

Since the completion of the experimental part of this work, there have been further speculations about how kaons might signal new phenomena. Among the topics mentioned in these papers are (1) the role of quark cluster states, (2) compressional effects, (3) high Fermi momentum components, (4) the quark-gloun plasma, (5) the time evolution of high-energy nuclear reactions, (6) the nuclear equation of state, and (7) subthreshold reaction mechanisms. Although the results obtained here have shed little, if any, light on these issues, they seem to have at least stimulated considerable new theoretical and experimental activity.

References

1) K.K. Gudima and V.D. Toneev: Proc. of the 7th International Symp. on Problems of High Energy Physics Dubna, Joint Institute for Nuclear Research Rep., p. 567 (1985).
2) K.K. Gudima and V.D. Toneev: *Yad. Fiz.*, **42**, 645 (1985), (*Sov. J. Nucl. Phys.*, **42**, 409 (1985)).

* Condenced from *Phys. Rev.*, **C40**, 640 (1989).

** Lawrence Berkeley Laboratory, Berkeley, CA94720, USA.

RIKEN Accel. Prog. Rep. 23 (1989)

III-1-16. Evidence Against Condensed Matter Fusion Induced by Cosmic-Ray Muons

K. Nagamine, T. Matsuzaki, K. Ishida, S. Sakamoto,* Y. Watanabe,* M. Iwasaki,* Y. Miyake, K. Nishiyama,* H. Kurihara,* E. Torikai, T. Suzuki,** S. Isagawa,** and K. Kondo**

[NUCLEAR REACTION $D(D, n)^3He$, muon catalyzed fusion in Pd.]

It has recently been proposed that cosmic ray muons might catalyze d-d fusion in condensed matter,[1] offering a possible origin for claims of observations of fusion neutrons from deuterated Pd or Ti. In order to test this hypothesis, we have studied the behavior of accelerator-produced negative muons in Pd (D).

Experiment was carried out at the pulsed muon facility of UT-MSL/KEK by measuring the following muon-induced events: a) the timing of decay electrons to see the relative fraction of muons stopping in D versus Pd by a lifetime method; b) the energy and timing of neutrons with n-γ discrimination to see fusion neutrons; c) the energy and timing of X-rays to see (μ^3He) events associated with (ddμ) fusion as well as to see electronic X-ray in Pd associated with charged particle emission if it exists. All the experimental arrangements employed here were the same as those used for recent successful experiments on the direct observation of alpha-sticking phenomena in liquid and high T_2 concentration D_2/T_2 mixtures by an X-ray method.[2]

Pd (D) samples used were a) a Pd rod of 5 mm in diameter with 10 days D loading; b) a 3 mm thick Pd plate with 60% D loading; c) a 1 mm thick Pd plate in D_2O with electrolysis *in situ*. As a control, we used Pd samples without D.

So far, no differences were observed between Pd and Pd (D) in all the above observables for these 3 systems. In particular, the missing of a 2.2 μs lifetime component in a decay electron time spectrum, placed a limit on the atomic capture ratio (final capture ratio including D to Pd transfer reaction) for D to Pd (below 3%). Also, the missing of fusion neutrons placed a limit on (ddμ) fusion rates in Pd (D) (below 0.3/μ^-). The obtained result suggests that the fusion rate for ddμ in Pd (D) induced by cosmic-ray muons is below 10^{-6} (s^{-1}), which provides evidence against the extraordinarily enhanced fusion rates assumed in the proposal.[1]

References

1) N.W. Guinan *et al.*: UCPL Preprint, 10081 (1989).
2) K. Nagamine *et al.*: to be publishied (1989).

* Meson Science Laboratory, University of Tokyo (UT-MSL) Hongo, Bunkyo-ku, Tokyo, Japan.
** National Laboratory for High Energy Physics (KEK) Tsukuba, Ibaraki, Japan.

RIKEN Accel. Prog. Rep. 23 (1989)

III-1-17. X-Ray Observation of α-Sticking Phenomena in Muon Catalyzed Fusion for a High Density D-T Mixture of High T_2 Concentration

K. Nagamine, T. Matsuzaki, K. Ishida, Y. Watanabe,* S. Sakamoto,* M. Iwasaki,* Y. Miyake,* K. Nishiyama,* E. Torikai, H. Kurihara,* H. Kudo,** M. Tanase,** M. Kato,** K. Kurosawa,** H. Sugai,** M. Fujie,** and H. Umezawa**

[NUCLEAR REACTION T(D, n)α, muon catalyzed fusion, measured neutrons, muonic X-rays.]

The most important unknown parameter to be determined for muon catalyzed fusion is the α-sticking probability ω_s in a D_2/T_2 mixture of high density and high T_2 concentration C_T where 150 fusions per a single negative muon (μ^-) were observed. The ω_s strictly places an upper limit for energy production capability. A conventional neutron method[1,2] is an indirect method for the determination of ω_s; various additional corrections must be done for loss processes other than ω_s.

As a direct measurement of ω_s, two new methods have been proposed: the measurement of $(\mu\alpha)^+$ ions and the measurement of muonic X-ray from $(\mu\alpha)$.[3,4] The X-ray measurement, which is the only method to be applied to the direct ω_s measurement for a high density and high C_T D_2/T_2 mixture, can not be done by the conventional detection system; a huge bremsstrahlung background up to 18.7 keV due to tritium β-decay masks weak K_α X-ray (8.23 keV) from sticked $(\mu\alpha)$ atom. Pulsed muons available at the Meson Science Laboratory, University of Tokyo, located at KEK (UT-MSL/KEK), is particularly effective to overcome this difficulty.

Following the first test experiment performed in UTMSL-RIKEN-BYU-LANL collaboration,[4] a revised experiment was carried out in UTMSL-RIKEN-JAERI collaboration. The experiment was carried out by using a 60 MeV/c backward μ^- beam. In order to obtain the numbers of the μ^- stopping in a liquid D_2/T_2 target, we used plastic scintillation counters for μe detections from the D_2/T_2 target. A Si(Li) detector for low energy X-ray measurement as well as a liquid scintillation counter for 14 MeV fusion neutrons was used.

From our measurements, we obtained the following results: a) the central energy of the peak, 8.234(8) keV; b) the broadening, 0.53(10) keV; c) the mean-life of the X-ray intensity, 0.61(21) μs; and d) the relative intensity of K_β line compared to that of K_α line, 0.08(9). All these four numbers are consistent with theoretical predictions and support strongly the first successful observation of an X-ray associated with the α-sticking phenomena in μCF for the D_2/T_2 system of high ϕ and high C_T.

An X-ray yield for the earliest one third data in 13 days run, which should be the safest data as far as ^{3}He accumulation is concerned, was obtained as $Y_x=0.121(39)$ photon/μ^-. By using a cycling rate of $\lambda_c=112$ μs^{-1} for μCF obtained in reported experiments[1,2], we can obtain $\kappa\omega_s$ (Preliminary)$=0.00113(36)$. Our value of $\kappa\omega_s$ for $C_T=0.30$ should be compared to a value obtained at PSI for $C_T=2\times10^{-4}$ (0.0021(5)). An effective sticking probability is obtained by assuming theoretical values[5] of $\kappa=0.28$ (photon/initial sticking) and $R=0.34$ (regeneration probability); ω_s^{eff} (X) (Preliminary)$=0.0026(9)$ which should be compared to a value claimed in neutron measurements. The upper limit of an energy production capability was derived to be 5-10 GeV/μ^-.

References

1) S.E. Jones *et al.*: *Phys. Rev. Lett.*, **51**, 1757 (1983); *Phys. Rev. Lett.*, **56**, 588 (1986).
2) W.H. Breunlich *et al.*: *Phys. Rev. Lett.*, **58**, 329 (1987).
3) H. Bossy *et al.*: *Phys. Rev. Lett.*, **59**, 2864 (1987).
4) K. Nagamine *et al.*: *Muon Catalyzed Fusion*, **1**, 137 (1987).
5) J.S. Cohen: *Phys. Rev. Lett.*, **58**, 1407 (1987).

* Meson Science Laboratory, University of Tokyo, Bunkyo-ku, Tokyo, Japan.
** Japan Atomic Energy Research Institute, Tokai, Ibaraki, Japan (JAERI).

RIKEN Accel. Prog. Rep. **23** (1989)

III-1-18. Ultra-Slow μ^- Production *via* Muon Catalyzed Fusion

K. Nagamine

[NUCLEAR REACTION T(D, n)α, muon catalyzed fusion, negative muon beam.]

So far, various ideas have been proposed for the production of an intense slow positive muon (μ^+) beam. Here, we propose an entirely new idea for the source of slow μ^- which will be realized with the help of celebrated phenomena of muon catalyzed fusion.

As it is known in our present knowledge on muon catalyzed fusion at the process which takes place at the instant of the fusion reaction inside the muon molecule, most of the μ^- (more than 99%) which is once bound to a ^{5}He nucleus is liberated because of the disappearance of the corenucleus and then, in the process of each μCF cycle, the μ^- is liberated with an energy of around 10 keV. According to our knowledge, this μ^- liberation process could take place up to 150 times during the μ^- life time.

Then, let us consider the following situation; MeV μ^- is stopped in a thin layer of condensed D_2/T_2 layer. The one MeV μ^- which is without much difficulties obtained by the pion decay in flight is now stopped in a thin layer of condensed D_2/T_2 layer. Inside this thin layer, 10 keV μ^- is successively generated during the μCF processes up to 150 times on the average during the μ^- life-time. Let us define $l_{\rm eff}$ as a range of μ^- produced at each liberation process before it is captured to form (μd) or (μt) atoms. Also, let us introduce a multiplication factor α_c for the range which is determined by the successive μCF processes. When $\alpha_c l_{\rm eff}$ exceeds the thickness of the D_2/T_2 layer, the generated μ^- may have a chance to be released from the surface of the D_2/T_2 layer. Thus, ultra-slow μ^- is produced.

The value of α_c is determined from the number of μCF cycles (around 150) and from the kinetics involved in the (dtμ)-μCF such as the slowing-down mechanism of μ^- as well as the effective diffusion length ($l_{\mu d}$, $l_{\mu t}$) of (μd) and (μt) before the formation of a (dtμ) molecule. Admitting that (μd) or (μt) is formed at thermal energy of the μ^-, $l_{\mu d}$ and $l_{\mu t}$ could be determined by the transfer reaction from (μd) to (μt) and by the formation reaction to (dtμ), all of which should be considered as a central problem in the present μCF physics. Therefore, the proposed ultra-slow μ^- generation should also be considered as a tool to understand the μCF itself.

The conversion efficiency ε from one MeV to 10 keV can be estimated at $\varepsilon = \alpha_c l_{\rm eff} / R_\mu$ (1 MeV), where $R_\mu(E)$ represents the range of the initial μ with energy E in the condensed D_2/T_2 layer. In order to obtain a qualitative estimate of ε, let us assume that the range of a low energy charged-particle like μ^- has momentum (P) dependence like $(P)^{3.5}$; R_μ(1 MeV)=0.9 mm and $l_{\rm eff}$=0.3 μm. By using α_c obtained by Monte Carlo calculation, for the two limiting cases 1) $l_{\mu d}$, $l_{\mu t} \ll l_{\rm eff}$ and 2) $l_{\mu d}$, $l_{\mu t} \gg l_{\rm eff}$, ε becomes as follows; for Case 1, ε=0.04 and for Case 2, ε=0.225.

Following this 10 keV μ^- source, an electrostatic extraction system combined with electrostatic optics or a conventional magnetic optics system with large acceptance like an axial focussing split-coil can be placed to transport the produced μ^- efficiently onto an experimental target. Thus a very bright and intense keV μ^- source will be realized.

The slow μ^- will be applied to a variety of fields of scientific research. The μ^- nuclear or atomic capture can be easily studied in a very low pressure gas target. Moreover, the slow μ^- can be stopped at the atomic surface layers of material and precise element analysis can be done for the atomic layer on the surface and/or intersurfaces. One of the most important example might be the analysis of a hydrogen content on the uppermost atomic surface layer by detecting 2.0 keV muonic X-ray, where, combined with a well-known rapid transfer reaction from (μp) to high Z atoms, (μp) signal mainly comes from hydrogen on the uppermost layer.

Helpful discussions with Drs. K. Ishida, M. Leon, Y. Kuno and Prof. T. Yamazaki are greatly acknowledged.

RIKEN Accel. Prog. Rep. 23 (1989)

III-1-19. Muon Production from Heavy Ion Reactions Detected by "Large Ω" Secondary Beam Course

K. Ishida, T. Matsuzaki, K. Nagamine, H. Kitazawa,
Y. Miyake, and E. Torikai

[NUCLEAR REACTION $^{12}C(^{14}N, \pi^+)$, $E=135A$ MeV; measured muon yield.]

A new type of beam transport system for secondary light charged particles, called Large Ω, was used to transport positive muons from the decay of pions stopped at the surface skin of a production target (surface muons) produced in heavy ion reactions at RIKEN Ring Cyclotron (RRC). The design and the first test experiment of the transport system have already been reported.[1,2] The system is designed to accept charged particles emitted in a large solid angle by using the focusing property of axially symmetric magnetic field produced by three superconducting coils.

Here we report an experiment carried out by using a $^{14}N^{7+}$ beam of 135 MeV/u from RRC. A graphite target of 0.9 g/cm^2 in thickness was used. A detection system for muons was placed at the focus 2.5m apart from the target and consisted of a stack of 4 plastic scintillation counters with thicknesses of 0.2 mm, 2 mm, 2 mm and 120 mm, respectively. Muons are expected to stop at the second counter and decay by emitting positrons with a lifetime of 2.2 μs. Main background to the detection system are considered to be beam positrons produced around the production target, since charged particles heavier than muon are stopped before reaching the second counter. The muon event was confirmed from the positron background due to the larger energy deposit to the counters. Also, a measured time spectrum of the delayed positron after muon stop clearly showed a lifetime of 2.2 μs.

A number of muons were measured for various momenta as shown in Fig. 1. The result shows a peak at 29 MeV/c and a sharp cutoff at higher momenta. This momentum dependence is typical for surface muons. The sharpness of the cutoff

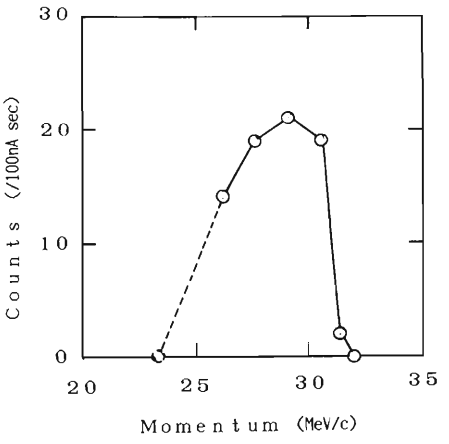

Fig. 1. Number of detected muons as a function of average momentum. The number is normalized by the integrated current of the primary beam. There is an artificial cutoff of intensity below 26 MeV/c due to the muons stopping at the first counter.

implies a good momentum selection by the system.

Next, we changed the production target to aluminum and copper which have an equivalent thickness for beam energy loss. The number of muons shows almost inverse dependence on the mass number of the target. Since the conversion efficiency from pions to muon is expected to be almost independent of target materials, the result means that the cross section for low energy pion production does not depend so much on target nuclei. A detailed analysis is now in progress.

References

1) K. Ishida, T. Matsuzaki, and K. Nagamine: *RIKEN Accel. Prog. Rep.*, **21**, 172 (1987).
2) K. Ishida, T. Matsuzaki, K. Nagamine, H. Kitazawa, Y. Miyake, and E. Torikai: *ibid.*, **22**, 153 (1988).

RIKEN Accel. Prog. Rep. 23 (1989)

III-1-20. Search for Neutron Emission from Cold Fusion

S. Nakabayashi, A. Kira, T. Ichihara, H. Kumagai, T. Suzuki,
K. Yoshida, and I. Tanihata

[Cold fusion, neutron detection, electrolysis.]

For testing the occurence of cold fusion in electrolysis, the emission of neutrons was measured under various electro-chemical conditions. A pair of 8″ diameter liquid scintillators (NE213) were used for the detection. A pulse shape discrimination was applied to identify neutrons and γ rays. Radiation shield consisted of polietylene, iron, and lead combined with veto counters made of plastic scintillators provided a very low backgorund condition. Figure 1 shows a two-dimensional scatter plot of liquid scintillator signals. Clear separation of neutrons and γ rays was seen. We found that the monitoring of the neutron signal in particular the separation between γ rays is extremely important for reproducibility of the data. Figure 2 shows an example of the neutron spectrum after subtraction of the background which was measured with the same system by turning off electrolysis. So far no sign of neutron emission associated with cold fusion has been obseved above $\sim 2 \times 10^{-3}$/s. More accumulation of data under different conditions is underway.

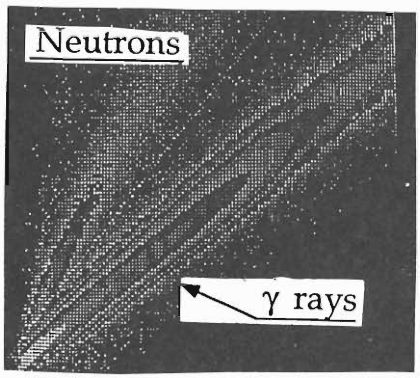

Fig. 1. A particle identification spectrum. Each signal is plotted according to its amplitudes of the fast component (abscissa) and the slow component (ordinate). Clear separation was obtained between γ rays and neutrons.

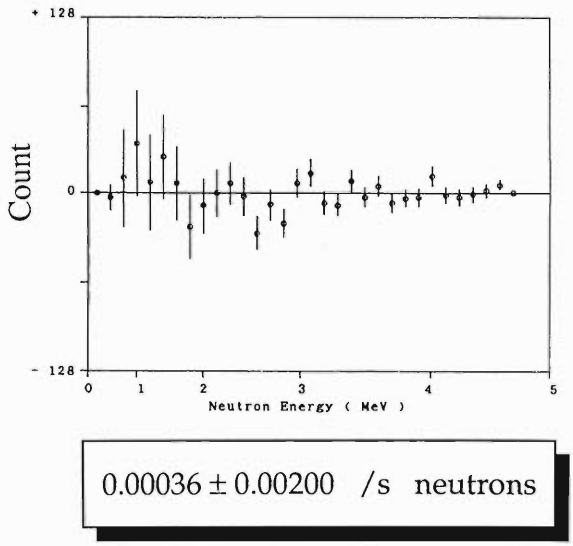

Fig. 2. A neutron spectrum after subtraction of background. No enhancement of neutron emission is seen.

RIKEN Accel. Prog. Rep. 23 (1989)

III-1-21. Coulomb Dissociation of ^{11}Li

K. Soutome, S. Yamaji, and M. Sano

[dissociation of ^{11}Li, interference, Glauber approximation.]

A recent measurement of the dissociation cross section of a neutron-rich nucleus ^{11}Li at 0.8 GeV/A incident energy,[1] ^{11}Li+target→^{9}Li+2n+X, indicates that the dissociation due to an electromagnetic (EM) force is enhanced for heavy target—0.21±0.04b for Cu and 0.89±0.10 b for Pb—compared with the EM dissociation of usual stable nuclei. Furthermore, the target-charge dependence of the EM dissociation cross section is quite different from Z_T^2: $\sigma_{EMD} \propto Z_T^{1.41\pm0.22}$. The aim of the present report is to examine the effect of interference between EM and nuclear forces: our interest is how much the interference affects the magnitude and Z_T-dependence of the cross section.

For describing the above process, we assumed that ^{11}Li consists of a ^{9}Li-core and two neutrons around it, and the two neutrons are in the 1p1/2 orbets of a harmonic oscillator (HO) potential $V = m\omega^2(r_1^2 + r_2^2)/2$. Thus the dissociation cross section can be written in a manner similar to the case of deuteron.[2] In deuteron dissociation, a Glauber approximation and a static Coulomb potential are used for targets of Gaussian-type distribution. These prescriptions were also used in our calculation.

Results are shown in Fig. 1. The HO parameter $a_0 = (m\omega)^{-1/2}$ is related to the root mean square (rms) distance between the origin and the c.m. of two neutrons by $a_0^2 = (4/5)\langle R^2\rangle$ with $\boldsymbol{R} = (\boldsymbol{r}_1 + \boldsymbol{r}_2)/2$. There are some ways of determining the value of a_0: if we adjust a_0 so that the weakly-bound nature of the two neutrons can be reproduced,[3] a_0 becomes 8.5 fm; if we use $R_{rms}^2(^{11}\mathrm{Li}) = (9/11)R_{rms}^2(^{9}\mathrm{Li}) + (2/11)R_{rms}^2(2n)$ with $R_{rms}^2(2n) = 2\langle R^2\rangle$ and put experimental values[4] to $R_{rms}(^{11}\mathrm{Li})$ and $R_{rms}(^{9}\mathrm{Li})$, a_0 is 3.6 fm. The magnitude of the cross section, $\sigma_C + \sigma_{CN}$, is fairly sensitive to a_0, but the Z_T-dependence is almost Z_T^2 insensitive to a_0: our model cannot reproduce the experimental Z_T-dependence. To solve this disagreement, we would need to include an excitation process of a "soft" giant dipole resonance mode of ^{11}Li suggested by Ikeda.[1]

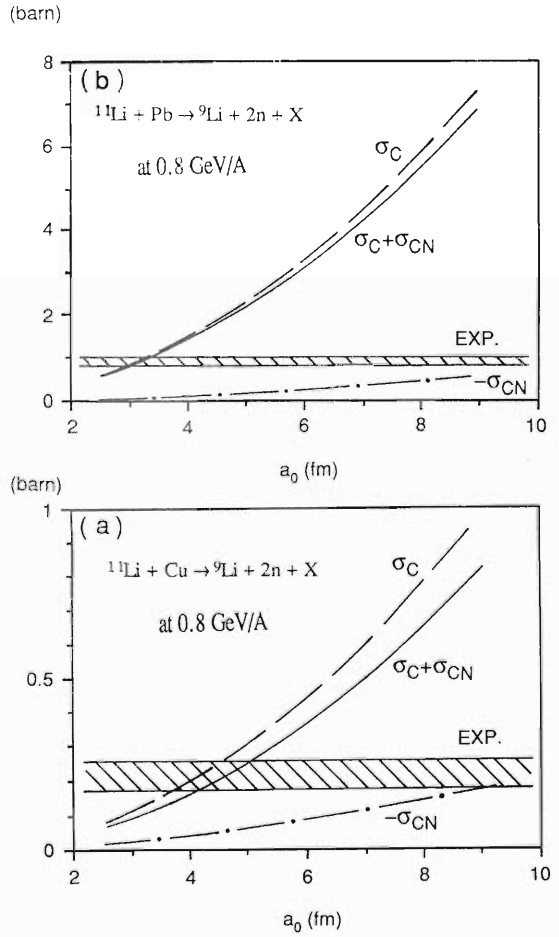

Fig. 1. Coulomb and interference contributions to the dissociation cross section, σ_C and σ_{CN}. Targets are Cu (a) and Pb (b). The oscillator parameter a_0 is defined in the text.

References

1) T. Kobayashi *et al.*: *Phys. Lett. B*, **232**, 51 (1989).
2) G. Fäldt: *Phys. Rev. D*, **2**, 846 (1970).
3) M. Sano and M. Wakai: This Report, p. 29.
4) I. Tanihata *et al.*: *Phys. Rev. Lett.*, **55**, 2676 (1985).

RIKEN Accel. Prog. Rep. 23 (1989)

III-1-22. Momentum Distributions of ^{9}Li Produced by Projectile Fragmentation of ^{11}Li

M. Sano and M. Wakai

[nuclear fragmentation, momentum distribution, nucleus-nucleus collision, Glauber scattering theory.]

Recent experimental results for the momentum distribution of ^{9}Li from the fragmentation of ^{11}Li at 800 MeV/nucleon show two Gaussian peak structures of different widths.[1] No simple gross theory can explain the two-component structure of the momentum distribution. The momentum spectrum of the fragment reflects the momentum distribution of removed nucleons. It may be considered that the narrow component is produced by reactions in which two weakly bound neutrons are removed from ^{11}Li. The small momentum fluctuation of the last two neutrons is also consistent with the large size of ^{11}Li, because it indicates a long tail in the wave function in the r space. The broader component may be due to the removal of normally bound neutrons. Since the nucleus becomes unstable upon the removal of deeply bound neutrons, one has to consider the reaction mechanism in more detail for fully understanding of the momentum spectrum.

The peripheral collision process may be divided into a direct fragmentation and a hard-scattering processes. In the direct fragmentation process the detected ^{9}Li comes out of the parent nucleus ^{11}Li as a spectator without scattering with nucleons in the target nucleus, while in the hard scattering process it suffers a simple collision with a constituent of the target nucleus. The cross sections for the fragment corresponding to the processes are described with Glauber's scattering formalism.

There is another possibility to produce the ^{9}Li fragment by the two-step process of ^{11}Li+target $\rightarrow ^{10}$Li+X$\rightarrow ^{9}$Li+n+X, since ^{10}Li produced by the removal of the last neutron is in an unbound state and automatically decays into the ground state of ^{9}Li. The first step process is described by the same formalism and the decay of ^{10}Li into ^{9}Li is assumed as to be spherical symmetric in the rest frame of ^{10}Li.

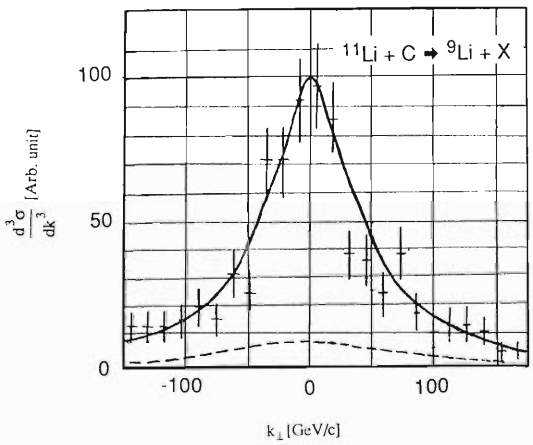

Fig. 1. Transverse-momentum distributions of the ^{9}Li fragment from the reaction ^{11}Li+C. The solid line shows calculated results corresponding to the direct fragmentation process and the dotted line represents contributions from the hard-scattering fragmentation and two-step fragmentation processes.

Figure 1 represents the momentum distribution of ^{9}Li for two-neutron removal in the $p_{1/2}$ shell. In numerical calculations, we take a Wood-Saxon potential so as to fit the separation energy of the last neutrons in the $p_{1/2}$ shell. The momentum distribution is well reproduced by the calcuation corresponding to the direct fragmentation process (solid line). The calculated cross sections for other processes (dotted line) are considerably small compared with that of the direct fragmentation process.

References

1) T. Kobayashi, O. Yamakawa, K. Omata, K. Sugimoto, T. Shimoda, N. Takahashi, and I. Tanahata: *Phys. Rev. Lett.*, **60**, 2599 (1988).

RIKEN Accel. Prog. Rep. 23 (1989)

III-1-23. Production of Energetic Particles in Heavy-Ion Collisions[1)]

W. Cassing,* V. Metag,** U. Mosel,* and K. Niita

[Production of Energetic Particles]

We have discussed the production of particles, photons, dileptons, and mesons, in heavy-ion collisions at bombarding energies ranging from roughly 20 MeV/u up to 2 GeV/u. We have shown that presently available data are all compatible with a picture in which observed particle yields are ascribed to the incoherent summation of particle-production from individual nucleon-nucleon collisions. This is a quite important conclusion since it becomes now possible to use particles produced in heavy-ion collisions as sensitive probes for specific regions of single-particle phase space. This conclusion is based on two essential ingredients: one is a transport theory that can describe the time-evolution of a one-body density matrix throughout the heavy-ion reaction for a wide energy range. Here we used a so-called VUU (Vlasov-Uehling-Uhlenbeck) method. The other is the description of in-medium particle production rates by individual nucleon-nucleon collisions.

For the production of photons we argued that the data in the energy-regime from about 15 MeV/u up to 125 MeV/u seem indeed to reflect a transition from a ground state interaction to a free interaction and thus an in-medium correction to the free $NN^{635}\gamma$ cross section. We also discussed that at bombarding energies roughly above 200-300 MeV/u the observation of direct photons will not be possible because these are swamped by π^{648} decay photons. However, at higher energies there is a possibility to use dileptons as an alternative electromagnetic probe. We showed that the data, obtained recently at the BEVALAC, can be understood in terms of NN bremsstrahlung for a light system p+Be. For heavier systems, like Ca+Ca, there is a clear deficiency of the bremsstrahlung cross section at higher invariant masses of dileptons which can probably be attributed to pion annihilation radiation. This is in itself an exciting question, as dileptons originating from this process could contain information about the pion self-energy at high density.

For the production of mesons we have shown that a few pion data can be described quite well in the same theoretical framework of independent NN collisions above bombarding energies of roughly 60 MeV/u. Below this energy theoretical cross sections are clearly too low; this points to more cooperative effects or may require a quantummechanical treatment. In any case, pions experience strong final state interactions and this necessitates, after the quite involved and sophisticated theories to describe the primordial yield, the application of rather crude models with free parameters to describe this reabsorption and rescattering. We discussed that a similar problem appears also for η's that can be strongly absorbed by the N* (1535) resonance.

To a large extent K^+-mesons are free of such final state interactions. Due to their high threshold they are at most SIS energies produced after many collisions of the colliding, K^+-producing nucleons. These kaons thus come predominantly from an equilibrated, hot unclear medium and represent optimal probes for possible studies of the nuclear equation of state. Preliminary estimates show a sensitivity of about a factor of 2 when varying nuclear compressibility. However, we have not yet included K^+-production from such reactions as $\pi N \rightarrow \Lambda K^+$. This obviously necessitates a nonperturbative treatment in which pions are actually followed in their time-development in the dense baryonic environment.

References

1) *Phys. Rep.*, (1990) in press.

* Institut für Theoretische Physik, Universität Gießen D-6300 Gießen, West Germany.
** II. Physikalisches Institut, Universität Gießen D-6300 Gießen, West Germany.

RIKEN Accel. Prog. Rep. 23 (1989)

III-1-24. Hard Photon Production within a Selfconsistent Transport Approach to Heavy-Ion Collisions[1)]

K. Niita, W. Cassing,* and U. Mosel*

〔Hard Photon Production.〕

We have studied heavy-ion reaction dynamics on the basis of a transport equation of the Vlasov-Uehling-Uhlenbeck type with a consistent treatment of the time-dependent mean field and the in-medium nucleon-nucleon cross section which are both derived from the same G-matrix.[2)] For numerical applications we have employed a density-dependent effective parametrization for G appropriate for nuclear configurations not too far from the groundstate where Re{G} and Im {G} approximately fulfill the unitary relation for G. One of the novel features of this choice of parametrization is that at normal density $\rho=\rho_0$ the effective interaction can be interpreted as being generated by scalar meson exchange only. We can thus easily evaluate the radiative corrections to the G-matrix as well as the in-medium NN cross section at $\rho=\rho_0$ in a selfconsistent way.

Within this approach the stationary solutions of the VUU equation for spherical nuclei are found to yield quite reliable shapes of the nuclear density distribution as well as for the momentum distribution except in the very high momentum region due to the classical limits adopted. Furthermore, binding energies for spherical nuclei are as accurately reproduced as for HF calculations with the same effective interaction and are very close to the experimental data. The time evolution of heavy-ion collisions in phase space in the mean field(Vlasov) limit is found to be very close to the results from TDHF and thus indicates a reliable reproduction of mean field properties in the energy regime from 15 MeV/u to 150 MeV/u. In addition, the treatment of nucleon-nucleon collisions in the simulation could be shown to give quite satisfying results in the opposite case, *i.e.* colliding nuclei in the infinite nuclear matter limit. We thus are convinced that our numerical simulation of the VUU equation, based on time-dependent G-matrix theory, allows for quite realistic simulations of heavy-ion reactions at nonrelativistic bombarding energies.

The yield of hard photons from heavy-ion collisions has been calculated in this consistent and parameter free approach, which involves an approximation to the G-matrix. Up to 20 MeV/u bombarding energy the experimental hard photon yields are well reproduced with a G-matrix paramatrization for the ground state configuration. With increasing bombarding energy, however, these results underestimate the experimental photon spectra systematically. We thus applied a different parametrization of the effective interaction for the evaluation of photon-probabilities which is fitted to free high energy p-nucleus data. The photon yields with this NN interaction are in good agreement with the data above 30 MeV/u, but overestimate those for lower bombarding energies. This may indicate that the G-matrix changes significantly in heavy-ion collisions from 20 MeV/u to 80 MeV/u.

At bombarding energies below 20 MeV/u we have, furthermore, observed two sources of hard photons, *i.e.* from first-chance NN collisions and from an excited thermal source. The yields and the energy spectra of hard photons from the two different sources for nearly symmetric systems, contrary to very asymmetric systems, are almost equivalent due to the high temperature achieved. Therefore, we need a more exclusive analysis, *e.g.* photon angular distributions in coincidence with heavy fragments, and their total-kinetic-energy-loss(TKEL) to disentangle these two sources in the experimental spectra.

References

1) K. Niita, W. Cassing, and U. Mosel: *Nucl. Phys.*, **A504**, 391(1989).
2) W. Cassing, K. Niita, and S.J. Wang: *Z. Phys.*, **A331**, 439(1988).

* Institut für Theoretische Physik, Universität Giessen 6300 Giessen, West Germany

RIKEN Accel. Prog. Rep. 23 (1989)

III-1-25. Production of Hypernuclei in Relativistic Ion Beams

H. Bandō,* M. Sano, M. Wakai, and J. Žofka**

{hypernucleus, nuclear collision, nuclear fragmentation, pion, kaon, lambda, coalescence model.}

Hypernuclear physics in the last few years is characterized by application of new hypernucleus producing reactions and their detailed studies. Since various reactions reveal various properties to a different extent, they all constitute complementary parts which then, put together, reveal a rich variety of hypernuclear world. It is thus very important, since experiments are difficult, to make use of all data as fully as possible and to optimize the experiments theoretically in advance. One such example is hypernuclear production by relativistic ion collisions. Theoretical studies[1] concentrated on introducing a reliable model and exploring kinematics for single and double Λ-hypernuclei on targets which are theoretically interesting.

There appeared, however, new measurments[2] producing ${}^{4}_{\Lambda}$H and ${}^{7}_{\Lambda}$Li on a ^{12}C target. Under analysis are further data on ${}^{12}_{\Lambda}$C and ${}^{19}_{\Lambda}$F hypernuclei.[3] A new calculation in the coalescence scheme is performed to pertinently describe the above cases for the projectile (incident energy) ^{4}He (3.7 GeV/nucl.), ^{7}Li (3.0 GeV/nucl.), ^{12}C (3.7 GeV/nucl.), and ^{19}F (3.7 GeV/nucl.). It makes possible to verify the model of relativistic ion hypernuclear production itself and to limit the parameters entering it by using the values for cross sections already measured. It further allows one to predict the production rates of species now under experimental study and even more importantly, it points at hypernuclei produced abundantly in the process employed, but not analyzed.

The production of K- and especially of π-mesons in high-energy nuclear collisions is large. The latter is more abundant by a factor of $\sim 10^3$. Thus the secondary yields of hypernuclei through (Kπ) and (πK) reactions may be quite appreciable and reach values comparable with the primary direct process.

The comparison of corresponding calculated values with available experimental ones reveals good agreement: For ^{4}He beam, Ref. 2 gave 0.2 μb of ${}^{4}_{\Lambda}$H whereas our theoretical value is 0.29 μb. For ^{7}Li beam, Ref. 2 suggested an upper limit only, which has been put there at 1μb. For the experimental data under investigation,[3] the present model gives 0.18 μb and 0.13 μb cross sections for ^{12}C(${}^{12}_{\Lambda}$C) and ^{19}F(${}^{19}_{\Lambda}$F) beams(resulting fragments), respectively. Where available, the experimental and theoretical values agree very well and are well below 1μb. Theoretical values have however revealed that not optimal hypernuclei (the largest production cross-sections combined with still appreciable π^- mesonic weak decay) have been necessarily used. It has been suggested that the best optimal tuning should etect ${}^{4}_{\Lambda}$H and ${}^{3}_{\Lambda}$H and, after π^- decay, ^{4}He and ^{3}He nuclei.

In contrast to the secondary ($K^-\pi$) hypernuclear production, the model for (πK) production [(π^+K^+) and (π^-K^0)][4] here yielded rather appreciable contribution, constituting some 20% (and often more) of the primary production, and should be taken into account. It further improves the agreement with the experiment.

References

1) F. Asai, H. Bandō, and M. Sano: *Phys. Lett.*, **B145**, 19 (1984); M. Wakai, H. Bandō, and M. Sano: *Phys. Rev.*, **C38**, 748 (1988).
2) S. Avramenko *et al.*: JINR E1-87-337, Dubna (1987).
3) S. Avramenko *et al.*: *JETP*, **48**, 477 (1988).
4) H. Bandō, M. Sano, M. Wakai, and J. Žofka: *Nucl. Phys.*, **A501**, 900 (1989).

* Division of Mathematical Physics, Fukui University.
** Nuclear Physics Institute, Rez/Prague, Czechoslovakia.

RIKEN Accel. Prog. Rep. **23** (1989)

III-1-26. Strangeness Production in High-Energy Nuclear Collisions

M. Sano

[Strangeness, hypernucleus, H-particle, quark, gluon, QCD, nuclear collision, lambda, sigma, kusi, coalescence model.]

We have known, from experiments, that the production cross sections of kaons and Λ particles are considerably large in high-energy heavy-ion collisions even at 2.1 GeV/nucleon. We can expect, therefore, that high-energy heavy-ion collisions become a possible tool for the formation of a hypernucleus and moreover for the formation of exotic nuclear species such as a H-particle and hypernucleus with multi-Λ particles.

Asai *et al.*[1] have tried to apply a coalescence model[2] to the description of hypernucleus formation and to estimate the formation cross section at 2.1 GeV/nucleon by incorporating various experimental and theoretical information on high-energy heavy-ion collisions. The calculation has further been extended up to an energy range of about 5 GeV/nucleon by Wakai *et al.*[3] and estimated the formation cross section of double Λ-hypernucleus in addition to single Λ-hypernucleus. In this report,[7] calculation methods for strange particles, H-particles, and hypernuclei are reviewed and calculated results are discussed.

Calculations for the hypernucleus formation were performed for projectile ^{3}He, ^{4}He, ^{6}Li, ^{7}Li, ^{12}C, and ^{19}F on a ^{12}C target, which are pertinent to recent Dubna experiments. Table 1 shows calculated[4] and experimental results.[5,6] Where available for hypernucleus production, the experimental and theoretical values agree very well.

The H-particle with spin-parity $J^{\pi}=0^{+}$, isospin $I=0$, and strangeness $S=-2$ is a six-quark state consisting of two u, d, and s quarks coupled to a flavor SU (3) singlet. In the traditional hadron physics, one can not predict a bound state for the H dibaryon. The H-particle is a very interesting particle, because it becomes a good example for demonstrating the validity of the quark model and the QCD. Table 2 shows the cross sections of H-particle production. An abrupt increase of the H-particle may be expected, if the quark-gluon plasma phase is realized. Thus, the enhancements of the H-particle production cross section may become a signature of a quark-gluon plasma.

Table 1. Hypernucleus production cross sections.

Reaction	Beam energy (GeV/nucl.)	Cross section (μb) Th.	Exp.
^{3}He+C $\rightarrow{}^{3}_{\Lambda}$H+X	5.14	0.03	$0.05^{+0.05}_{-0.03}$ [6]
^{4}He+C $\rightarrow{}^{3}_{\Lambda}$H+X	3.7	0.06	<0.1 [5]
$\rightarrow{}^{4}_{\Lambda}$H+X		0.29	$0.4^{+0.4}_{-0.2}$ [5]
^{6}Li+C $\rightarrow{}^{3}_{\Lambda}$H+X	3.67	0.09	$0.2^{+0.2}_{-0.15}$ [6]
$\rightarrow{}^{4}_{\Lambda}$H+X		0.20	$0.3^{+0.3}_{-0.15}$ [6]
^{7}Li+C $\rightarrow{}^{7}_{\Lambda}$Li+X	3.0	0.11	<1 [5]
^{12}C+C $\rightarrow{}^{12}_{\Lambda}$C+X	3.7	0.18	—
^{19}F+C $\rightarrow{}^{19}_{\Lambda}$F+X	3.7	0.13	—

Table 2. H-particle production cross sections.

Collision	Beam energy (GeV/nucl.)	Cross section
Ne+Ne	5	2.6 μb
O+Au	200	0.09mb
S+Au	200	0.17mb

References

1) F. Asai, H. Bandō, and M. Sano : *Phys, Lett.*, **145B**, 19 (1984).
2) H. Sato and K. Yazaki : *ibid.*, **98B**, 153 (1981).
3) M. Wakai, H. Bandō, and M. Sano : *Phys. Rev.*, **C38**, 748 (1988).
4) H. Bandō, M. Sano, M. Wakai, and J. Zofka: *Nucl. Phys.*, **A501**, 900 (1989).
5) S. Avramenko *et al.*: *JETP*, **48**, 477 (1988).
6) J. Lukstins : Talk at the XXIII Yamada Conf. on Nucl. Weak Proc. and Nucl. Structure, Osaka (1989).
7) M. Sano : RIKEN-AF-NP-77 and Proc. of the NATO Advanced Studies Institute on "Nuclear Equation of State", Peniscola, Spain, May 21-June 3 (1989).

RIKEN Accel. Prog. Rep. 23 (1989)

III-1-27. Mesonic Atom Production in High-Energy Nuclear Collisions

M. Wakai, H. Bandō,* and M. Sano

[mesonic atom, nuclear collision, muclear fragment, pion, kaon, coalescence model.]

In high-energy nuclear collisions, many kinds of particles and nuclei are produced. Previously we used a coalescence model[1,2] to estimate the hypernucleus production probability in high-energy nuclear collisions and get a conclusion that hypernuclei could be produced with fairly large cross sections, of the order of magnitude of μb in p+Ne and Ne+Ne collisions at 2-5 GeV/nucleon.

As for the branching ratios of possible elementary processes, those of pion-production q_π are much larger than that of Λ-particle, q_Λ, that is, $q_\pi/q_\Lambda \approx 10^2$ at 5 GeV/nucleon. This result suggests us an unnegligible production probability of π-mesonic atoms in high-energy collisions. The purpose of this paper is to estimate a π-mesonic atom production probability in nuclear collisions by using the coalescence model. Numerical calculations are performed for p+Ne, Ne+Ne at 2.1 GeV and 5 GeV/nucleon. The model is also extended to the case of K-mesonic atom production.

In a π-mesonic atom, a negative pion is bound to a fragment nucleus F through Coulomb interaction. The Inclusive cross section of negative pions are evaluated by a statistical phase space model. The calculated π^- cross sections for Ne+Ne collision at 2.1 GeV/nucleon can reproduce the slope of an experimental curve, but the absolute values of the cross section are three-times larger than the experimental values. We then use theoretical values of cross sections multiplied by a factor of 1/3 as the π^- production cross section. Calculated results of π-mesonic atom production cross sections are displayed in Fig. 1(a) and (b) for Ne+Ne collisions at 2.1 GeV and 5 GeV/nucleon.

We found that the cross section of mesonic atom production at 5 GeV/nucleon is about a few factor smaller than at 2.1 GeV/nucleon, since the overlap between momentum distributions of pions and nuclear fragments becomes poor although the pion production increases with increasing beam energy. The production cross sections of K^--atoms are about $10^3 \sim 10^4$ factor smaller than the π^--atom production cross sections, reflecting the difference between the magnitude of the π^- and K^- production cross sections.

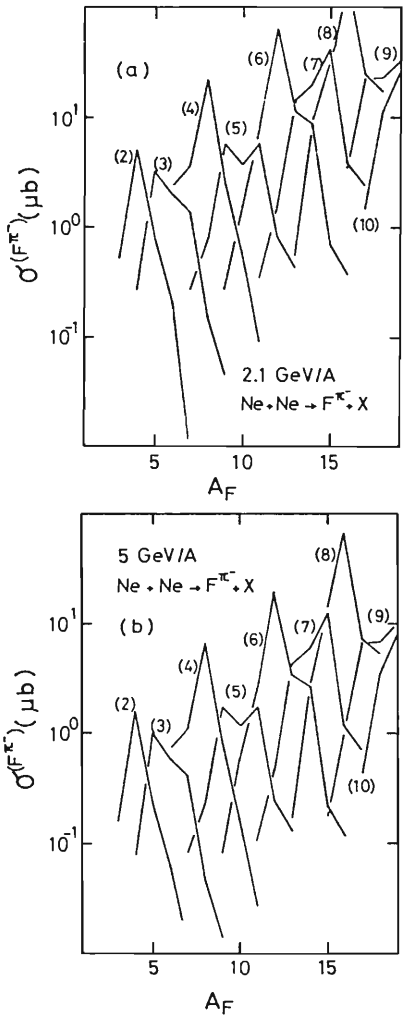

Fig. 1. The production cross sections of π^--mesonic atoms in Ne + Ne collisions at 2.1 and 5.0 GeV/A.

References

1) H. Sato and K. Yazaki: *Phys. Lett.*, **98B**, 153 (1981).
2) F. Asai, H. Bandō, and M. Sano: *Phys. Lett.*, **145B**, 19 (1984); M. Wakai, H. Bandō, and M. Sano: *Phys. Rev.*, **C38**, 748 (1988).

* Division of Mathematical Physics, Fukui University.

RIKEN Accel. Prog. Rep. 23 (1989)

III-1-28. Possibility of H-Particle Production in High-Energy Nuclear Collisions

M. Sano, M. Wakai, and H. Bandō*

[H-particle, quark, gluon, QCD, strangeness, nuclear collision, lambda, sigma, kusi, coalescence model.]

A bound dibaryon state with spin-parity $J^{\pi}=0^{+}$, isospin $I=0$, and strangeness $S=-2$ was predicted in 1977 by Jaffe[1] using the MIT bag model. The predicted binding energy was about -80 MeV below the energy of two lambda particles. This so-called H-particle is a six-quark state consisting of two u, d, and s quarks coupled to a flavor SU(3) singlet.

Since then, many studies have been performed using relativistic quark bag models, Skyrme models, quark cluster models, and lattice QCD. The estimated binding energy of the H particle is quite model dependent, ranging from positive (unbound) to -650 MeV (strongly bound). The H particle is a very interesting particle, because it is a very good example for demonstrating the validity of the quark model and QCD.

We study the production of the H particle in high-energy nuclear collisions by employing the coalescence model as a formation mechanism of the H particle. In previous work[2] we studied hypernucleus production in high-energy nuclear collisions. We find a reasonable agreement between predicted values and recent experimental data obtained at Dubna.[3] This success motivated us to extend the calculation to H-particle production, since the H particle consisting of six quarks is expressed in terms of two baryon configurations as

$$|\mathrm{H}\rangle=\sqrt{\frac{1}{8}}\,|\Lambda\Lambda\rangle+\sqrt{\frac{4}{8}}\,|\mathrm{N}\Xi\rangle-\sqrt{\frac{3}{8}}\,|\Sigma\Sigma\rangle. \quad (1)$$

The baryon production cross sections in Ne+Ne collisions at 5 GeV/nucleon are calculated by the statistical phase-space model and are shown in Fig. 1. Figure 2 shows the calculated H-particle production cross sections and three channel contributions (without statistical weights) at $\theta=0^{\circ}$ in Ne+Ne collisions. It should be noticed that the cross sections extend up to quite high momenta. This is due to the similar momentum distributions of two baryons, which

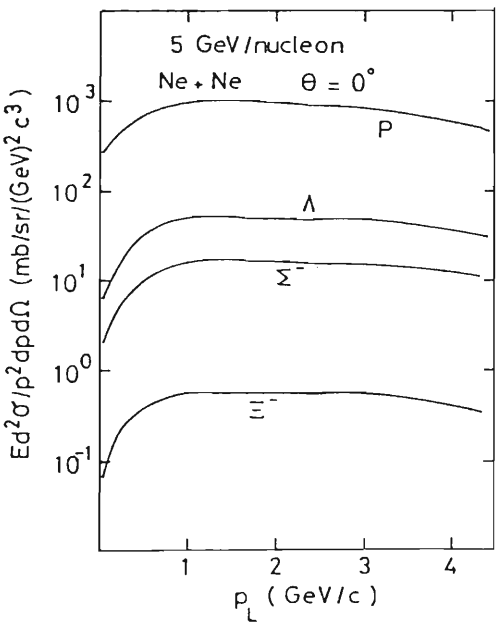

Fig. 1. p, Λ, Σ^{-}, and Ξ^{-} momentum spectra at $\theta=0^{\circ}$.

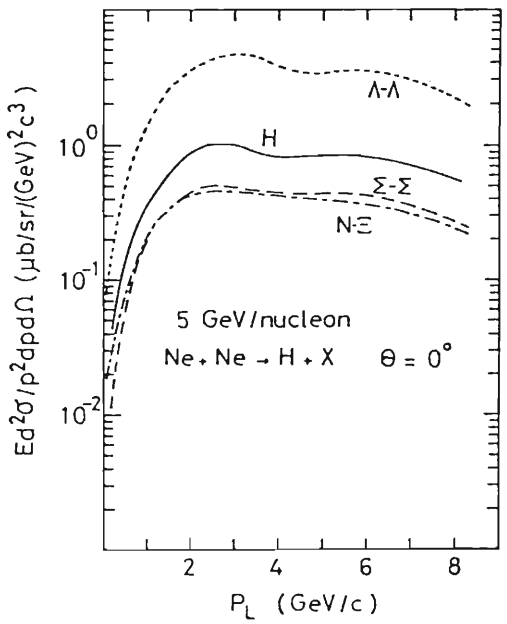

Fig. 2. The H-particle momentum spectra at $\theta=0^{\circ}$.

* Division of Mathematical Physics, Fukui University.

in turn make the integrated cross section large. The obtained total cross section is~2.6 μb, which is surprisingly one order of magnitude larger than hypernuclear production cross sections. The magnitude of the cross section is insensitive to the binding energy of the H particle. It is expected that the production cross sections increase with incident beam energy since hyperon productions increase.

References

1) R.L. Jaffe: *Phys. Rev. Lett.*, **38**, 195 (1977).
2) F. Asai, H. Bandō, and M. Sano: *Phys. Lett.*, **B145**, 19 (1984); M. Wakai, H. Bandō, and M. Sano: *Phys. Rev.*, **C38**, 748 (1988); H. Bandō, M. Sano, M. Wakai, and J. Zofka: *Nucl. Phys.* **A501**, 900 (1989).
3) S. Avramenko *et al.*: *JETP*, **48**, 477 (1988); J. Lukstins: Talks at the XXIII Yamada Conference on Nucl. Weak Proc. and Nucl. Structure, Osaka (1989).

RIKEN Accel. Prog. Rep. 23 (1989)

III-1-29. Hadronic Matter at Finite Temperature

K. Soutome, T. Maruyama,* and K. Saito**

[Equation of state, σ-ω model, relativistic Hartree-Fock, finite temperature.]

The study of the equation of state (EOS) for hadronic matter is an important subject in the context of heavy-ion reactions or astrophysical phenomena. To study hadronic matter, Walecka proposed a simple model—a relativistic σ-ω model[1]—on the basis of quantum field theory. The extension of the model to the one at finite temperature was done within the mean-field (MF) approximation by using the imaginary-time formalism of a finite-temperature field theory.[2] In this formalism, however, summation over discrete frequencies must be carried out in evaluating Feynman diagrams, and the calculation of exchange-term contributions seems to be difficult because of the divergence problem. We have thus used Thermo Field Dynamics (TFD) formalism[3] to perform the relativistic Hartree-Fock (HF) calculation at finite temperature.[4]

TFD has many advantageous features: it is closely related to the conventional zero-temperature field theory; the Feynman diagram technique is available, but we need no sum over discrete frequencies; free propagators split into temperature-dependent and temperature-independent parts from the outset, which means that the divergence can be eliminated by the counterterms set up at zero temperature.

In Fig. 1 we show the resulting EOS for neutron matter at low temperature and low density. The liquid-gas phase transition seen in the MF approximation disappears in the HF approximation. This shows the importance of exchange-term contributions in the neutron matter calculation at finite temperature.

The Lagrangian density we used containes neither the self-interactions of σ-mesons nor the contribution of pions. These terms are important for more realistic descriptions of hot and/or dense hadronic matter. In particular, the self-interactions of σ-mesons can soften the nuclear matter EOS.[5] Self-consistent treatment of such models may be easier in the TFD formalism than in the imaginary-time formalism. These points will be studied in the future.

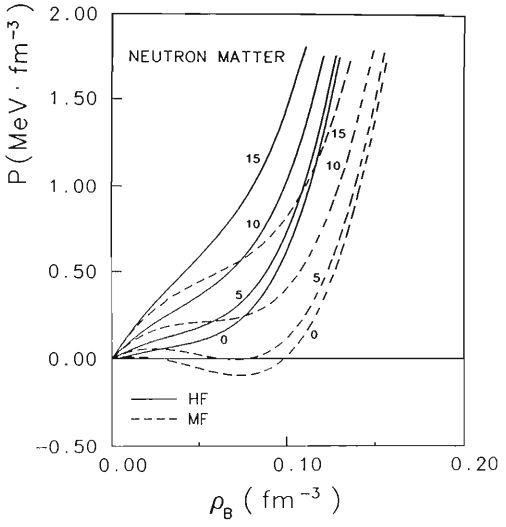

Fig. 1. EOS (pressure *vs.* baryon density) for neutron matter at temperatures $T=0$, 5, 10, and 15 MeV.

References

1) J.D. Walecka: *Ann. Phys.*, **80**, 361 (1974); B.D. Serot and J.D. Walecka: *Adv. Nucl. Phys.*, **16**, 1 (1986).
2) J.D. Walecka: *Phys., Lett. B*, **59**, 109 (1975).
3) H. Umezawa, H. Matsumoto, and M. Tachiki: "Thermo field dynamics and condensed states", North-Holland, Amsterdam (1982); N.P. Landsman and Ch. G. van Weert: *Phys. Rep.*, **145**, 141 (1987), and references therein.
4) K. Soutome, T. Maruyama, and K. Saito: RIKEN-AF-NP-74 (to be published in *Nucl. Phys. A*).
5) N.K. Glendenning: *Phys. Lett. B*, **208**, 335 (1988).

* Institut für Theoretische Physik, Universität Tübingen, D-7400 Tübingen, F.R.G.
** Physics Division, Tohoku College of Pharmacy.

RIKEN Accel. Prog. Rep. 23 (1989)

III-1-30. Self-Consistent Transport Tensors for Collective Motion in Several Dimensions

S. Yamaji, R. Samhammer,* and H. Hofmann*

[Large Scale Collective Motion, Linear Response Theory, Fission.]

At finite intrinsic excitations nuclear collective motion can be viewed as a diffusion process in collective phase space. This picture was introduced by Kramers.[1] However, Markovian behavior in his treatment is questionable since the time scales for collective and intrinsic degrees of freedom are not separated widely enough. In Ref. 2, it was argued that Kramers' picture can nevertheless be retained in its essential features if the transport coefficients are calculated at a finite local frequency within the framework of a locally harmonic approximation.

In the present study, we generalized the one dimensional teatment of Ref. 2 to two (and more) degrees of freedom (Q_μ: $\mu=1,\cdots,n$). We reported details elsewhere,[3] and present only results and remarks. We choose two collective variables to specify the shape of fissioning nucleus ^{212}Po. The first one, $Q_1=z$, measures the distance between the centers of the two fragments, and the second parameter, $Q_2=\varepsilon$, has the meaning of a neck parameter.[3] In Table 1 we present values for the tensors of inertia $M_{\mu\nu}$ and friction $\gamma_{\mu\nu}$ calculated at a temperature of 2MeV along the path of minimal potential energy. We introduce a new coordinate system $\begin{pmatrix} Q_\parallel \\ Q_\perp \end{pmatrix}$, where $Q_\parallel$ and $Q_\perp$ are the collective coordinates parallel and perpendicular to the fission path, respectively. We compare the "true" result with that of the Markov limit.[4]

Table 1. Inertial tensor in units of $\left[(10^{-23}\,\mathrm{sec})^2\,\frac{\mathrm{MeV}}{\mathrm{fm}}\right]$ and friction tensor in units of $\left[(10^{-23}\,\mathrm{sec})\,\frac{\mathrm{MeV}}{\mathrm{fm}}\right]$ along fission path for $T=2$ MeV.

z	$M_\parallel(0)$	$M_\parallel$	$M_\perp(0)$	$M_\perp$	$\gamma_\parallel(0)$	$\gamma_\parallel$	$\gamma_\perp(0)$	$\gamma_\perp$
6.0	0.418	0.673	0.592	0.924	1.83	1.47	1.43	2.77
7.0	0.738	0.723	1.08	0.912	2.04	2.34	2.09	2.92
8.0	1.23	1.86	1.32	1.99	2.65	2.84	2.93	4.17
13.0	6.55	7.90	3.71	4.23	14.6	16.0	6.86	7.11
15.8	8.30	9.49	4.43	4.67	12.7	13.9	11.9	12.2
17.0	14.5	14.6	0.631	0.144	21.7	21.3	9.92	12.8
18.5	9.91	16.1	5.56	7.89	20.0	46.4	7.63	18.0

In general, we can say that these results confirm the findings of Ref. 2: a) The coordinate dependence is generally weaker than that expected from "cranking"-type calculations; b) at $T=$ 2MeV the zero-frequency limit seems to be a fair approximation up to the barrier region, but becomes bad behind the barrier.

We observed a new feature that along the "fission path" both tesors $M_{\mu\nu}$ and $\gamma_{\mu\nu}$ are far from being diagonal.

Finally we want to give some numbers to the local collective equilibration time $\gamma_{\mathrm{kin}}^{\mathrm{rel}}=\mathrm{M}/\gamma$ and the dissipation strength $\eta_\mathrm{f}=\gamma_\mathrm{f}/2\sqrt{M_\mathrm{f}\,|\,C_\mathrm{f}\,|}$. Physically $\gamma_{\mathrm{kin}}^{\mathrm{rel}}$ defines the time relevant for relaxation to a Maxwell distribution. Along the fission path we find: $\gamma_{\mathrm{kin}}^{\mathrm{rel}}\simeq 3.5,\ 2.1\times10^{-22}$ sec for $T=2,3,4$ MeV. With increasing temperature, η_f itself increases linearly, reaching values around 4 for $T\simeq 4\cdots5$ MeV. Again, this behavior is very similar to the results discussed in Ref. 2.

References

1) H.A. Kramers: *Physica*, **7**, 284 (1940).
2) S. Yamaji, H. Hofmann, and R. Samhammer: *Nucl. Phys.*, **A475**, 487 (1988).
3) R. Samhammer, H. Hofmann, and S. Yamaji: *ibid.*, **A503**, 404 (1989).
4) H. Hofmann: *Phys. Lett.*, **61B**, 423 (1976).

* Department of Physics, Tech. Univ. Munich.

RIKEN Accel. Prog. Rep. 23 (1989)

III-1-31. Nuclear Collective Motion: Markovian or Not?

S. Yamaji, H. Hofmann,* and R. Samhammer*

〔Large Scale Collective Motion, Linear Response Theory.〕

In nuclei collective motion exhibits itself in various forms, ranging from vibrations around stable configurations to processes of large scale as encountered in fission and heavy-ion collisions. It was only shortly after the discovery of fission that Kramers[1] suggested that the nuclear collective motion at finite intrinsic excitation can be viewed as a diffusion process in the collective phase space. This picture, as well as the equation itself, is manifestly Markovian, requiring conditions on time scales for intrinsic and collective degrees of freedom being widely separated enough.

Here, we report the study of this question. Details are given in Ref. 2. First, we study the vibration at zero temperature. We choose a description in terms of shape-variable Q. With $q=Q-Q_m$ defined as the deviation of Q from its equilibrium value $Q_m=Q_0$, the equation of motion can be written as:

$$\kappa q(t) = -\int_{-\infty}^{\infty} ds \tilde{\chi}(s)\, q(t-s) \tag{1}$$

Here, κ is the coupling constant given by $\kappa=-C(0)-\chi(\omega=0)$ with the first term representing the static stiffness coefficient and the second one the static response. The $\tilde{\chi}(t)$ stands for the response function. Equation 1 has typical non-Markovian features. If, as compared to $\tilde{\chi}(s)$, $q(t-s)$ changes slowly with s, we approximate the integral by expanding $q(t-s)$. A short calculation shows that the collective frequency is given by $\omega^2_{\text{zero}}=C(0)/M(0)$, with $M(0)$ being the cranking inertia.[3] This approximation applies to low frequency vibrations, but will geneally fail for giant resonances, since the characteristic frequency of $\chi(\omega)$ is not large compared to the frequency of a giant resonance. Thus the latter has to be calculated from the full dispersion relation:

$$\kappa+\chi(\omega)=0 \tag{2}$$

For the generalization to large scale motion at finite temperature,[4,5] Q_0 can be any fixed value of the coordinate which the system may reach. The basic assumption consists in the hypothesis that for a small time interval, δt, actual $Q(t)$ can be approximately described by a harmonic motion.

By comparing Eq. 2 with the one obtained by expanding it to the second order in ω, we find the conditions for the zero-frequency limit: namely $|C(0)/\chi(0)| \ll 1$ and $4\eta^2=\gamma^2/|MC| \ll 1$. The first condition implies $-\kappa \simeq \chi(0)$. For larger friction the second condition becomes important. It implies a violation of the Markov-limit even for comparatively small values of η. Clearly, in the strongly overdamped case, *i.e.* for $\eta \gg 1$, it will become possible to entirely neglect this term, which means to neglect any influence of the inertia. In this case it will only be the first condition that is to be obeyed.

To summarize we believe that the approximate answer to the question raised in the title could be: Yes, nuclear collective motion is largely non-Markovian, indeed. Nevertheless, we may use differential equations with selfconsistent transport coefficients to describe this motion adequately in most cases.

References

1) H.A. Kramers: *Physica,* **7**, 284 (1940).
2) H. Hofmann, R. Samhammer, and S. Yamaji: *Phys. Lett.*, **B229**, 309 (1989).
3) H. Hofmann: *ibid.*, **B61,** 423 (1976).
4) S. Yamaji, H. Hofmann, and R. Samhammer: *Nucl. Phys.*, **A475**, 487 (1988).
5) R. Samhammer, H. Hofmann, and S. Yamaji: *ibid.*, **A503**, 404 (1989).

* Department of Physics, Tech. Univ. Munich.

RIKEN Accel. Prog. 23 (1989)

III-2. Atomic and Solid-State Physics

1. Note on Symmetric Charge Exchange Cross Sections at Low Velocity Ion Impact

L. Végh, T. Watanabe, and S. Sakabe*

The cross section of the symmetric charge exchange processes $X^+ + X \rightarrow X + X^+$ at low energies as a function of the projectile velocity can be described as

$$\sigma^{1/2}(v) = A - B \ln v$$

where A and B are constants determined from the ionization potential of atom X involved in the collision.[1] The cross section σ, a function of the ionization potential, taken at a given projectile velocity decreases exponentially.[2] All available $X^+ + X \rightarrow X + X^+$ data show this trend except for unexpectedly large cross sections for $U^+ + U \rightarrow U + U^+$ (by a factor of 8)[3] and for $Gd^+ + Gd \rightarrow Gd + Gd^+$ (by a factor of 5).[4]

Mizushima[5] pointed out that the large $U^+ + U \rightarrow U + U^+$ cross section can be explained on the basis of the structure of U atom. The outer-shell configuration of uranium atom is given as $5f_{5/2}7s^26d^1$. Since the $5f_{5/2}$ core can be excited very easily, the inclusion of the contribution of the final states of the projectile and target with excited $5f_{5/2}$ core gives an increase in the cross section by a factor of about 4. The transfer of one of the 7s-electrons contributes to the cross section of charge transfer to about the same extent as that of the 6d-electron and this produces a further enhancement by a factor of about 2; a theoretical value agrees with the measured cross section.

We note that the enhanced charge exchange cross section for $Gd^+ + Gd \rightarrow Gd + Gd^+$ can be explained similarly to the anomaly for the uranium symmetric collision. Gadolinium having the outer-shell configuration $4f_{5/2}4f_{7/2}6s^25d^1$ shows a similiar structure to the uranium. Considering very similar characters of the $7s^26d^1$ and $6s^25d^1$ configurations, the contribution of 6s electrons to the exchange $Gd^+ + Gd \rightarrow Gd + Gd^+$ may have the same importance as that for the uranium case, and this can explain the observed enhancement.

Similar behavior can be predicted for the symmetric charge exchange for ytterbium and scandium atoms since their outer-shell configurations, $5s^24d^1$ for the ytterbium and $4s^23d^1$ for the scandium, are similar to that of the uranium and gadolinium.

References

1) D. Rapp and W. E. Francis: *J. Chem. Phys.*, **37**, 2631 (1962).
2) S. Sakabe: unpublished.
3) H. Niki, Y. Izawa, H. Ohtani, and C. Yamanaka: *Trans. Inst. Electr. Eng. Jpn.*, **102C**, 45 (1982).
4) T. Naka: dissertation, Osaka University (1987) (unpublished).
5) M. Mizushima: *Jpn. J. Appl. Phys.*, **27**, 449 (1988).

* Osaka University, Institute of Laser Engineering.

RIKEN Accel. Prog. Rep. 23 (1989)

III-2-2. Recoil Ion Velocities at Very Small Scattering Angles

H. Fukuda, L. Végh, and T. Watanabe

Dörner *et al.* have recently reported[1] double differential cross sections for 0.5 MeV singly ionizing p-He collisions. They measured the deflection angle θ of protons in a regime between 0.1 and 2 mrad in coincidence with the transverse momentum $q_{R\perp}$ of the recoiled He^+ ions and performed a complete three-body transverse-momentum measurement.

The kinematical limit of a scattering angle for proton-electron scattering is, since the electron is at rest before the collision, $\theta \approx \sin\theta = m/M_p = 0.545$ mrad, where m and M_p are the masses of an electron and a proton, respectively. Therefore, the momentum exchanges in the region investigated are determined by the interplay of proton-electron and proton-alpha particle interactions.

The minimum value of momentum q, transferred by a proton projectile to He atom is determined by energy conservation and is given as $q_{//} = \Delta E/v$, where $q_{//}$ is the parallel component of momentum transfer, ΔE is the excitation energy of the atom and v is the velocity of the projectile. The scattering angle is given by $q_\perp = M_p v\theta$, where $q_\perp$ is the transverse component of the momentum transfer.

If $q_\perp$ is very large, a recoil velocity can be calculated from $q_\perp + q_{R\perp} = 0$, that is, the proton-alpha collision is responsible for the measured scattering angle and the recoil velocity. In the region around 0.5 mrad both proton-electron and proton-alpha collisions play an important role. At very small scattering angles of 0.1 mrad the recoil due to the electron ejection by proton-electron interaction becomes significant.

If we take the relationship between the recoil energy E_R and proton deflection angle θ, E_R decreases with decreasing θ at large deflection angles. However, there is saturation value of E_R at very small deflection angles. Using the special experimental equipment,[1] the saturation value is found to be about 15 meV. At very small θ, the sum of the momentum of He^+ and that of the ejected electron is considered to be zero. Then the saturation value should be equal to the average momentum of ejected electrons.

To describe the behavior of the $E_{R\perp}(\theta)$ function in a wide range we apply a model based on an eikonal distorted wave method.[2] In this approximation the deflection of a charged projectile in the average field of a target atom is represented by the eikonal distortion factor. Neglecting the longitudinal component of the momentum transfer in projectile-target nucleus collision, we expand the eikonal distortion factor into a plane-wave series. By using this expansion, where the Fourier components can easily be calculated, the integration over the projectile coordinate is performed making use of the Bethe integral. The calculations are in progress.

References

1) R. Dörner, J. Ullrich, H. Schmidt-Böcking, and R.E. Olson: *Phys. Rev. Lett.*, **63**, 147 (1989).
2) F.W. Byron, Jr. and C.J. Joachain: *Phys. Rep.*, **34c**, 233 (1977).

RIKEN Accel. Prog. Rep. 23 (1989)

III-2-3. Theoretical Calculation of the Charge Transfer in Highly Charged Ions

K. Fujima, F. Koike,* and T. Kato**

Recent plasma diagnostics has pointed out growing importance of the charge transfer process between highly charge ions in tokamak.[1] We have calculated the following charge transfer cross sections as examples:

$$Ne^{+6}(2s^2)+Ti^{21+}(1s)\rightarrow Ne^{7+}(2s)+Ti^{20+}(1snl)$$
$$O+^{6}(1s2s)+Ti^{21+}(1s)\rightarrow O^{+7}(1s)+Ti^{+20}(1snl).$$

Since a detailed calculation method is stated elsewhere,[2] we summarize it briefly. The potential curves of the system and radial coupling matrices for charger transfer are calculated by using a Discrete Variational Xa (DV-Xa) method.[3] On the basis of perturbed stationary state (PSS) scheme, obtained time-dependent coupled equations are integrated along the relative motion of ions.[4] We neglect rotational coupling because radial coupling is the dominant mechanism in relatively low energy collisions.

Figure 1(a) shows potential curves obtained with a $Ne^{+6}+Ti^{21+}$ system. The initial channel for the present collision is channel 10, as indicated in Fig. 1. This state undergoes an avoided crossing with a bunch of the orbitals correlated to $5l$ of Ti^{21+} ($l=0,1,\cdots,5$) at about 5 a.u. Figure 1(b) shows partial and total charge transfer cross sections against collision energy. The total cross section has a sharp threshold at about 1.0 keV. With regard to the partial cross sections, the higher l state has the larger probability to get an electron.

In Fig. 2(a) and (b), preliminary potential curves and charge transfer cross sections through radial coupling are indicated for $Ti^{+23}+O^{+6}$ collision.

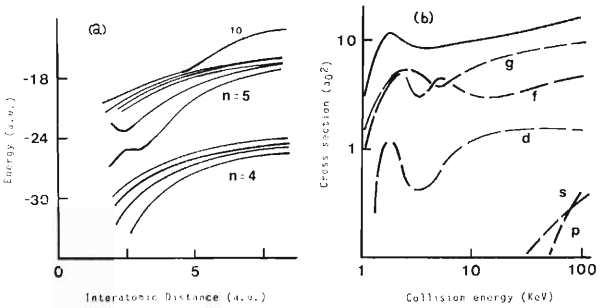

Fig. 1. (a) Potential curves of Ne^{6+} $(2s^2)+Ti^{21+}$ (1s) system. (b) Solid curve indicates the total charge transfer cross section. Dashed curves marked with s, p, ···, g are partial cross sections for charge transfer to 5s, 5p,···, 5g of the Ti ion, respectively.

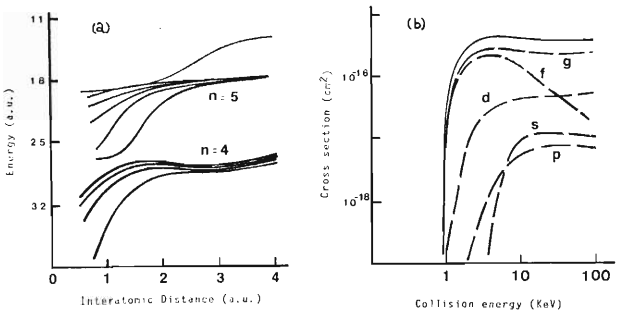

Fig. 2. Potential (a) and charge transfer cross sections (b) for O^{6+} (1s2s)+Ti^{21+}(1s), respectively. Probabilities of getting an electron into $5l$ (l=s, p, ···,g) of the Ti ion are also indicated.

References

1) T. Kato *et al.*: *Phys. Rev.*, **A36**, 795 (1987).
2) For example, M.R.C. McDowell, and J.P. Coleman: Introduction to the Theory of Ion-Atom Collisions, North-Holland, Amsterdam (1970).
3) K. Fujima *et al.*: *Phys. Rev.*, **A32**, 3585 (1985).
4) F. Koike *et al.*: *J. Phys.*, **B11**, 4193 (1978).

* School of Medicine, Kitasato University.
** National Institute of Fusion Sciense.

RIKEN Accel. Prog. Rep. 23 (1989)

III-2-4. Hyper-radial Adiabatic Treatment of $d\mu+t$ Collisions at Low Energies

H. Fukuda, S. Hara, and T. Ishihara*

An adiabatic expansion method in hyper-radius R has been applied to atomic three-body systems such as the doubly-excited states of H^- and He.[1] Having no constant spurious couplings, this method has an advantage over a conventional Born-Oppenheimer (BO) representation for molecular systems. In fact, hyper-radial calculations have given better results for energies of HD^+ ion[2] and $(dt\mu)^{+3}$[3] than the BO representation using the same number of expansion terms. The hyper-radial expansion is also expected to be useful for collision processes. At present, however, there is no practical application except for a simple e+H elastic collision. The present study aims to examine the applicability of the hyper-radial method to collision processes, taking a $d\mu+t$ system at thermal energy as an example. This process is important in muon catalyzed fusion research.

We have carried out numerical calculations for the process

$$\begin{aligned}(d\mu)_{1s}+t &\rightarrow (d\mu)_{1s}+t \\ &\rightarrow (t\mu)_{1s}+d+48\,\mathrm{eV} \qquad (1)\end{aligned}$$

at a center-of-mass incident energy $E_i=10^{-3}$eV in two-state approximation. In Table 1, our results are compared with those of a perturbed stationary state (PSS) method[4] and of a distorted atomic orbital (DAO) method.[4] Both PSS and DAO results are in a two-state approximation. In the DAO method, basis functions for each channel are defined by eigenfunctions of the total Hamiltonian with a relative Jacobi coordinate fixed. Thus, they satisfy the exact boundary conditions for both channels and, therefore, there appears no spurious coupling. In the PSS method,[4] the reduced mass of an adiabatic Hamiltonian is defined as that of a $d\mu$ atom. Therefore, the dissociation energy of the incident channel is given correctly.

Table 1. Elastic and μ-transfer cross sections (in units of 10^{-20} cm^2) for $d\mu+t$ collisions at a center-of-mass incident energy $E_i=10^{-3}$eV.

	Present	DAO[4]	PSS[4]
Elastic	1.7	2.0	2.2
Transfer	9.1	16.	3.9

For a μ-transfer process, the DAO results are in good agreement with variational calcudations and with the experimental results deduced from muon catalyzed fusion data. On the other hand, the PSS cross sections are much smaller than the DAO cross sections. This descrepancy is attributed to the poor description of the final channel wave function in the PSS method.[4] In the present formalism, the basis functions satisfy the correct boundary conditions as $R\rightarrow\infty$. However, there exist long range couplings of order $1/R$ with the states neglected in our two-state approximation. Because of these couplings, improvement over the PSS results is not sufficient. For further improvement, more states are necessary to be included in the expansion.

For an elastic process, there is no experimental results to be compared with. The present results agree very well with the DAO results. The PSS results are also in good agreement with these two, because the incident channel wave function is not very bad for such low energies.

References

1) J. H. Macek: *J. Phys.*, **B1,** 831 (1968).
2) S. Hara, H. Fukuda, and T. Ishihara: *Phys. Rev.*, **A39,** 35 (1989).
3) S. Hara, H. Fukuda, T. Ishihara, and A.V. Matveenko: *Phys. Lett.*, **A130,** 22 (1988).
4) K. Kobayashi, T. Ishihara, and N. Toshima: *Muon Catalyzed Fusion,* **2**, 191 (1988).

* Institute of Applied Physics, University of Tsukuba.

RIKEN Accel. Prog. Rep. 23 (1989)

III-2-5. Series of Resonances in Muonic Molecules

I. Shimamura

The d-t and d-d fusion catalyzed by muons without the need of high-temperature plasmas has been the subject of increasing experimental and theoretical interest in these years. It has been established experimentally that a single muon can catalyze d-t fusion about 150 times on the average during its lifetime in a dense mixture of deuterium and tritium under certain conditions. In each of these 150 events an energy of 16.7 MeV is emitted as fusion energy. In pure deuterium, less efficient muon-catalyzed d-d fusion occurs. The clue to the mechanism of the catalysis is the formation of muonic molecular ions $(dt\mu)^+$ or $(dd\mu)^+$.

Particular attention has been paid to *weakly* bound states, since they are considered to be formed efficiently in thermal collisions $d+t\mu(1s) \rightarrow (dt\mu)^+ + \Delta E$ or similar collisions between d and $d\mu(1s)$. This is because the excess energy ΔE is small for weakly bound states of the muonic molecule, and is efficiently absorbed by the vibrational-rotational motion of a hydrogen-like electronic molecule $d^+(dt\mu)^+e^-e^-$, in which the muonic molecule $(dt\mu)^+$ has a much smaller size than the electron orbitals and plays a role of a pseudonucleus in the electronic molecule.

The purpose of the present work is to study what happens if a deuteron collides with a $t\mu$ or a $d\mu$ atom in an excited state, say, in the state $n=2$. Just as in collisions involving the ground-state atoms, the $dt\mu$ or $dd\mu$ molecules are expected to be formed efficiently, if they have states just below the $n=2$ level of the muonic atom. These levels are not really bound states but are resonance states, because their energies are in the continuum. Therefore, our concern is in the possibility of existence of resonance states close to the level $n=2$ of the muonic atom.

In fact, it is possible to prove that there exist infinite series of resonances converging from below to the threshold for excitation of the $n=2$ level of the target atom, if the total angular momentum J is less than 7.[1] For homonuclear systems like $dd\mu$, there is one infinite series with the gerade property, and one with the ungerade property. For heteronuclear systems like $dt\mu$, there is one infinite series below $d+t\mu(n=2)$ and another series below $t+d\mu(n=2)$.[1] These resonances are similar to the infinite series of resonances known in electron scattering by hydrogen atoms.

Reference 1 also derives a simple formula $A\alpha^v$ for the position of the vth resonance for high v, where α and A are constants. In other words, the knowledge of several high-lying members of the series gives us information on the energy positions of all high-lying members of the infinite series. Furthermore, the size of the muonic molecule in a resonance state lying at ε_v(eV) relative to the $n=2$ dissociation limit is estimated to be $[4\sqrt{|\varepsilon_v|}]^{-1}$ in angstroms. Therefore, the resonance states of our interest can be of a size comparable to the electronic molecule.

These results have been derived from the nonrelativistic Schrödinger equation. A peculiar property of these high-lying resonances, however, is the strong influence by the relativistic and quantum electrodynamic corrections, which change all the infinite series of resonances into finite series. In spite of this change, there still exist weakly bound resonances with ΔE as small as a fraction of an electron volt according to a preliminary calculation.

The resonances in muonic molecules studied here may play some role as intermediate states in muon-transfer processes such as $d\mu(n=2)+t \rightarrow d+t\mu(n=2)$ or in the fusion process.

References

1) I. Shimamura: *Phys. Rev.*, **A40**, 4863 (1989).

RIKEN Accel. Prog. Rep. 23 (1989)

III-2-6. Bound and Resonance Levels of Muonic Molecules and Their Fusion Rates

S. Hara and T. Ishihara*

We calculate, by a variational procedure, the bound state energies of the even-parity muonic molecules with total angular momentum $J=1$ and the energies of the $(dd\mu)^+$ and $(dt\mu)^+$ resonant states below the $n=2$ energy level of muonic atoms.[1] We have found 11 resonant states with $J=0$ and 12 with $J=1$ for $(dd\mu)^+$ and 9 states with $J=0$ and 10 with $J=1$ for $(dt\mu)^+$. Some of the resonant energies, relative to the $n=2$ level of the muonic atoms, are less than the dissociation energy of H_2 and, therefore, these states may play some role in muon catalyzed fusion.

Figure 1 gives a schematic diagram for the adiabatic potential curves, bound (solid curve) and resonant (dashed curves) energy levels of the muonic molecule $(dd\mu)^+$ below the $n=2$ muon atomic levels.

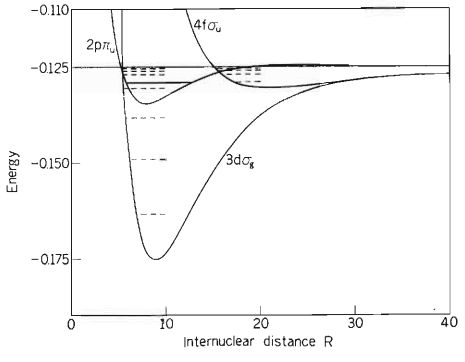

Fig. 1. Schematic diagram for the adiabatic potential curves, bound (solid curve) and resonant (dashed curve) states of the muonic molecules in the units of $e=\hbar=m_\mu$ (muon mass)=1.

Table 1. Energies (ineV) of the even-parity bound states with $J=1$.

Isotopes	Energy (eV)
$(pp\mu)^+$	−13.542
$(dd\mu)^+$	−22.595
$(tt\mu)^+$	−27.413
$(pd\mu)^+$	−3.684
$(pt\mu)^+$	−1.566
$(dt\mu)^+$	−19.124

Table 2. Resonant energies (ineV) of the g-type $(dd\mu)^+$, relative to the $n=2$ level of $d\mu$.

v	$J=0$	$J=1$
0	−218.113	−211.926
1	−135.278	−130.348
2	−72.962	−69.225
3	−31.884	−29.504
4	−12.606	−11.478
5	−5.304	−4.758
6	−2.210	−1.913

Table 3. Resonant energies (ineV) of $(dt\mu)^+$, relative to the $n=2$ level of $t\mu$.

v	$J=0$	v	$J=1$
0	−217.892	0	−212.547
1	−139.724	1	−135.375
2	−79.095	2	−75.674
3	−36.567	3	−34.233
0[a]	−19.124[a]	4	−19.161
4	−17.443	5	−16.351
5	−11.414	6	−10.505
6	−7.225	7	−6.485
7	−3.565	8	−3.185
8	−1.600	9	−1.346

[a] Even parity bound state with $J=1$.

Table 1 is the results for the $J=1$ even-parity bound states, and Tables 2 and 3, the results for the resonant states.

Fusion rates of $(dt\mu)^+$ resonance states are about 10^{-3} smaller than the fusion rates of the states related to the $n=1$ levels of muonic atoms.

References

1) S. Hara and T. Ishihara: *Phys. Rev.*, **A40**, 4232 (1989).

* Institute of Applied Physics, University of Tsukuba, Ibaraki 305, Japan.

RIKEN Accel. Prog. Rep. 23 (1989)

III-2-7. Radiative Electron Capture Cross Section for 26-MeV/u Ar^{18+} Ions on a Carbon Target

Y. Awaya, A. Hitachi, T. Kambara, Y. Kanai,
K. Kuroki, and T. Mizogawa

We have obtained the total radiative electron capture (REC) cross section, σ_{REC}, for the collision system of 26-MeV/u Ar^{18+} ions on a carbon target by measuring the yield of REC X rays. The REC cross section was found in fair agreement with a theoretical value.

Ar^{13+} ions accelerated by RIKEN Ring Cyclotron up to 26 MeV/u were passed through an aluminum foil and Ar^{18+} ions were selected, momentum analyzed, and then led to a carbon target; measurements for Ar^{13+} ions were also carried out for comparison. Since Ar^{18+} ions have two K holes whereas Ar^{13+} ions have no K holes before collision, we can obtain information about the probability of double collision concerning the K electron. X rays were measured with two Si (Li) detectors placed at 90° and 270° with respect to the beam. The angular dependence of an REC X-ray yield is assumed to be $\sin^2\theta$ on the basis of previous results.[1] X-ray spectra obtained for both ions are shown in Fig. 1. The X-ray background due mainly to secondary electron bremsstrahlung is subtracted by normalizing the calculated curve to the experimental data for energies higher than about 23 keV.

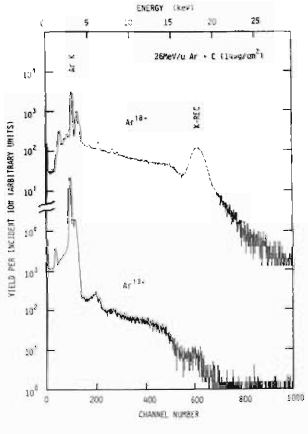

Fig. 1. X-ray spectra obtained for Ar^{18+} and Ar^{13+} ions on a C target.

Single collision seems to be realized under the present collision conditions for thin carbon targets. We confirmed this by studying the dependence of the REC X-ray yield on the thickness of the target (11.8-67.7 $\mu g/cm^2$). The number of incident Ar ions were estimated from the amount of charge collected by a Faraday cup. The mean charge of Ar ions as a function of C foil thickness was estimated from the results of previous work.[2]

Finally, we obtained the σ_{REC} value of $(1.7\pm 0.5)\times 10^{-22}$ cm^2.

According to the theory of Bethe-Salpeter,[3] the REC cross section for a projectile with a K hole on a target atom with a valence electron, σ_{BS}, is represented as

$$\sigma_{BS}=\frac{2^8\pi^2 r_0^2}{3\alpha}\nu^6(1+\nu^2)^{-2}\frac{\exp\{-4\nu\tan^{-1}(1/\nu)\}}{1-\exp(-2\pi\nu)}, \quad (1)$$

where r_0 is the classical electron radius, α is the fine structure constant, ν is the Coulomb parameter of a projectile in natural unit. In the present case, an Ar^{18+} ion has two electron holes and a target atom has N_{eff} quasi-free target electrons; therefore the theoretical total REC cross section $\sigma_{REC,Th}$, becomes

$$\sigma_{REC,Th}=2N_{eff}\sigma_{BS}. \quad (2)$$

By taking the value of N_{eff} as the nuclear charge of the target,[4] 6, the value of 1.82×10^{-22} cm^2 was obtained for the $\sigma_{REC,Th}$. This value agrees well with the experimental one, σ_{REC}.

References

1) Y. Awaya *et al.*: High-Energy Ion-Atom Collisions (ed. D. Berenyi and G. Hock), Springer-Verlag, Berlin Heidelberg p. 185 (1988).
2) Y. Kanai *et al.*: *RIKEN Accel. Prog. Rep.*, **22**, 54 (1988).
3) H. A. Bethe and E. E. Salpeter: Quantum Mechanics of One- and Two-Electron Atoms, Plenum Publishing Corp., New York (1977).
4) K. Hino and T. Watanabe: *Phys. Rev.* **A39**, 3373 (1989).

RIKEN Accel. Prog. Rep. 23 (1989)

III-2-8. Scaling Law of MO X Rays

K. Ishii, K. Maeda, Y. Sasa, M. Takami, M. Uda, and S. Morita*

In order to investigate the contributions of atomic bremsstrahlung (AB)[1] and molecular orbital X ray (MO)[2] to continuum X-ray spectra, we have measured continuum X rays from the targets of atomic numbers Z_T=6-29 bombarded with Si^{3+} ions accelerated at 1.4 MeV/amu by the RIKEN RILAC.

The production cross sections of continuum X rays can not be compared straightforward with each other by the Anholt's scaling law because of plural parameters. Hence, we have studied a more simple formula as expressed by

$$\frac{d\sigma^{MO}}{d\hbar\omega} \propto f(\omega a_0/(v_P(Z_P+Z_T)))$$

where a_0 is the Bohr radius and v_P is the projectile velocity. Our scaling law includes only one parameter $\omega a_0/(v_P(Z_P+Z_T))$. Figure 1 shows a scaling representation of continuum X rays where the ordinate represents the production cross section of continuum X rays expressed by

$$\frac{d\sigma^{B}}{d\hbar\omega d\Omega} = N \times S(E_P) \times \frac{1}{E_P},$$

where N is the intensity of continuum X rays in units of photons/(keV·sr) and $S(E_P)$ is the stopping power for the projectile with an energy E_P. As seen in this figure, the experimental results are quite well scaled by this method. This fact implies that the continuum X rays are emitted from united atoms. Figure 2 shows the intensity of continuum X rays as a function of the target-atomic number. Here, we can recognize a dip at symmetric collision. We will try to interpret these dips which are expected to result from interference between the AB and MO processes.

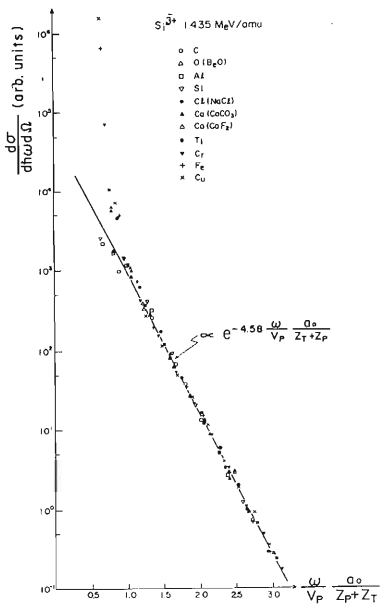

Fig. 1. Scaling representation of continuum X rays.

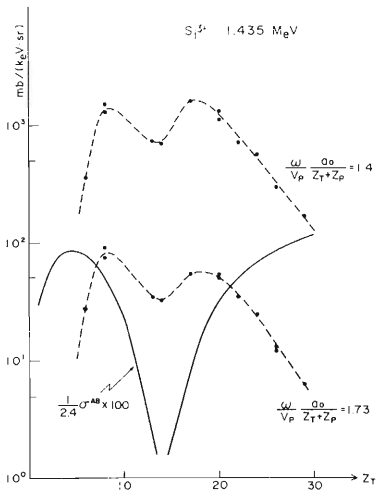

Fig. 2. Intensity of continuum X rays as a function of the target-atomic number.

References

1) K. Ishii and S. Morita: *Phys. Rev. A*, **30**, 2278 (1984).
2) R. Anholt: *Rev. Mod. Phys.*, **57**, 995 (1985).

* Laboratory for Materials Science and Technology, Waseda University.

RIKEN Accel. Prog. Rep. 23 (1989)

III-2-9. Measurements of Anisotropic K X-Ray Emission with Respect to the Scattering Plane in 10 and 26 MeV Ne-Ne Collision Systems

T.Kambara, Y.Awaya, Y.Kanai, T.Mizogawa, M.Terasawa,
H.Schmidt-Böcking, R.Dörner, and H.Vogt

We have measured angular correlations between a K X-ray and scattered particle in Ne-Ne collisions. The purpose was to get information of the magnetic substate population of K-shell excited states after the collisions for the investigation of the excitation mechanism. We obtained the probability of K X-ray production as a function of the charge state of the scattered ions q, scattering angle θ and the angle between the scattering plane and the X-ray emission direction ϕ. The geometrical relation is shown in Fig. 1.

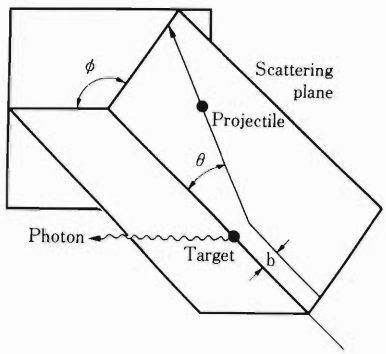

Fig. 1. Geometry of the measurement. b is the impact parameter, θ is the scattering angle, and ϕ is the angle between the scattering plane and the emitted photon.

Measurements were performed at RILAC with Ne^{7+}-ions (Li-like) of 10.5 and 26 MeV. The experimental setup was almost the same as that reported previously.[1] A collimated Ne-beam was led to a gas target of Ne. Scattered ions were charge-state analyzed and detected by a position-sensitive detector. The analyzed charge states of the scattered ions were from 4+ to 8+ at 10.5 MeV and from 5+ to 9+ at 26 MeV. Coincidence events between the scattered particles and Ne K-X rays from the target region were recorded. The analyzed scattering angle θ ranged up to 4×10^{-3} rad with angular resolution of 8×10^{-5} rad.

In each θ and ϕ region, the number of the coincidence events was normalized by the total number of scattered particles to get the probability of X-ray emission. The efficiency and the solid angle of an X-ray detector were corrected. An impact parameter b was calculated from θ with a screened Coulomb potential after correction for focusing with the charge-state analyzing magnet.

The ϕ-dependence of X-ray emission probabilities in the different b regions were fitted to a function $A\sin^2\phi+B$ by the least-squares method. From obtained values of A and B, an anisotropy parameter $R=A/2B$ was calculated. In Fig. 2, examples of the b-dependence of R are shown. The value of R is positive at $b<6000$ fm at an incident energy of 26 MeV. However, the value is smaller at 10.5 MeV. At a larger b, the value of R approaches zero. Further investigation is in progress.

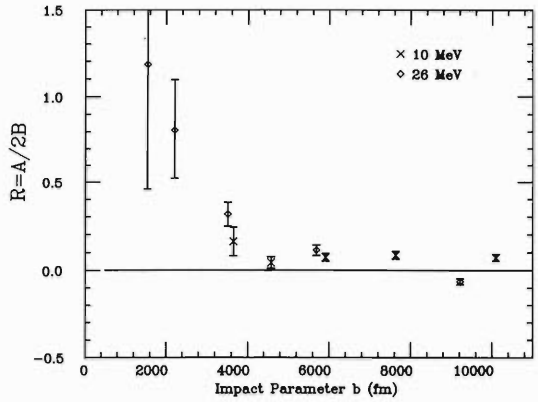

Fig. 2. Impact parameter (b) dependence of the anisotropy parameter $R=A/2B$ averaged over the charge states of scattererd projectiles.

References

1) T. Kambara, Y. Awaya, Y. Kanai, H. Schmidt-Böching, and H. Vogt: *RIKEN Accel. Prog. Rep.*, **22**, 72 (1988).

RIKEN Accel. Prog. Rep. 23 (1989)

III-2-10. Coincidence Measurements of Recoil Ions with Projectile Ions in 1.05 MeV/amu Ar^{q+}-Ar Collisions

T. Matsuo, T. Tonuma, H. Kumagai, and H. Tawara

We measured the partial ionization cross sections of recoil Ar^{i+} ions in follwing collisions of 1.05 MeV/amu Ar^{q+}:

$$Ar^{q+}(q=4,6,8,10,12,\text{and } 14)+Ar \rightarrow Ar^{q'+}+Ar^{i+}+(q'-q+i)\,e \qquad (1)$$

Projectile Ar^{q+} beams were provided by RILAC. Cross-sections were measured using a projectile ion-recoil ion coincidence technique which enables us to distinguish pure ionization, electron loss, and electron transfer ionization of projectiles from each other.

Figure 1 shows cross sections $\sigma^i_{q,q'}$ for pure ionization $q'=q$ $(k=q'-q=0)$, loss $q'>q$ $(k>0)$ and transfer $q'<q$ $(k<0)$ ionization for Ar^{12+} projectiles. The cross section for pure ionization $(k=0)$ decrease rapidly with increasing recoil-ion charge i, indicating that low charge state recoil ions are mainly produced through collisions at large impact parameters. The production cross sections of recoil ions in collisions where projectiles change their charge are found to be strongly correlated with the projectile final charge q' and show quite different features compared with those due to pure ionization. Similar results were obtained for other projectile charge states.

In analyzing pure ionization processes, we applied the independent electron approximation and found that this model to be a good description of the present data, $\sigma^i_{q,q'}$ in low-charge recoil ions from $i=1$ up to $i=5$-6 in all $Ar^{q+}+Ar$ collisions investigated.

In order to see the general trends on the target ionization, we introduce the average charge, $\langle i\rangle_{q,q'}$, which is obtained from the measured cross sections through

$$\langle i\rangle_{q,q'}=\sum_i i\sigma^i_{q,q'}/\sum_i \sigma^i_{q,q'} \qquad (2)$$

Figure 2 shows average charges $\langle i\rangle$ as a function of the incident projectile q with the number of $k=q'-q$ as a parameter. The average charges for pure ionization $(k=0)$ increase only slightly

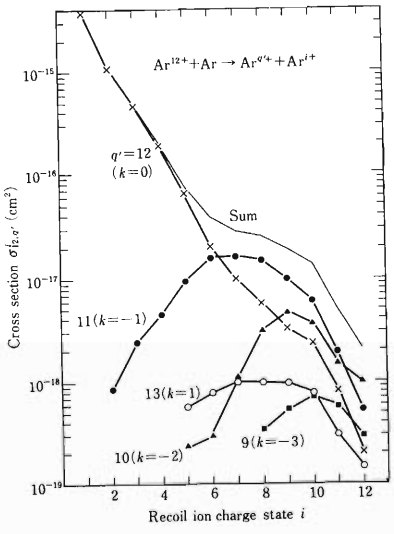

Fig. 1. Cross sections, $\sigma^i_{q,q'}$, for the production of recoil ions in 1.05 MeV/amu $Ar^{12+}+Ar$ collisions.

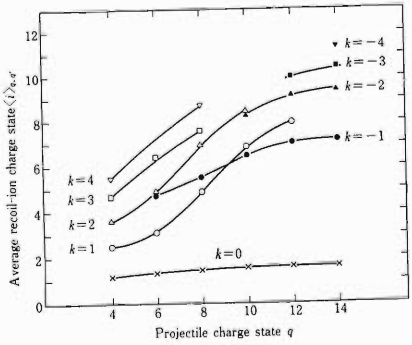

Fig. 2. Average recoil ion charge $\langle i\rangle$ versus the projectile charge in $Ar^{q+}+Ar \rightarrow Ar^{q'}+Ar^{i+}$ collisions.

from 1.19 to 1.62 with increasing projectile charge from 4 to 14, indicating that the recoil ions of low charge states are produced most dominantly in the pure ionization process. On the other hand, in electron loss and capture processes, the values of $\langle i\rangle$ are considerably larger than those in pure ionization processes and they increase significantly with projectile charge.

RIKEN Accel. Prog. Rep. 23 (1989)

III-2-11. Multiply Charged Carbon Ions Produced in MeV/amu $Ar^{q+}(q=4-14)$ + CH_4 Collisions

H. Tawara, T. Tonuma, H. Kumagai, and T. Matsuo

Collisions between 1.05 MeV/amu Ar^{q+} ion and CH_4 molecule have been investigated using a final charge-selected projectile-recoil ion time-of-flight technique.[1] A typical charge spectrum of Ar^{14+} ions after collisions with CH_4 molecules and mass/charge spectra of recoil ions are shown in Fig.1. In pure ionization (Fig.1(b)), undissociated CH_4^+ ions are the most intense and an enhancement in the production of CH_m^+ (m = 0-2) is observed. It should be noted that C^+ ions become more intense than CH_m^+(m=1,2) ions. On the other hand, electron capture processes are found to result in significant enhancement of the production of multiply charged carbon ions (Fig. 1(c) and (d)) and C^{3+} and C^{4+} ions become most intense, with a trace of C^{6+} ions, suggesting that collisions involving electron capture or loss of projectiles are violent, followed by complete dissociation of all molecular ions produced in collisions.

After normalizing the present observed spectra to total ionization cross sections determined by Mahli *et al.*,[2] the final cross sections have been obtained for the recoil ion production. Furthermore, by summing up these cross sections over recoil ions with various charges, total cross sections for pure ionization, electron capture, and electron loss processes of Ar^{q+} ions are determined and are found to be in reasonable agreement with previously observed results using a different technique in $F^{q+}+CH_4$ collisions.[3]

In all other collision system investigated in the present work, pure ionization processes are found to be far dominant over other processes including electron capture or loss of projectiles. This can be understood from the fact that the velocity of a 1 MeV/amu projectile is equivalent to that of electrons of a kinetic energy of 572 eV which is well above the binding energy of carbon L-shell as well as K-shell electrons. Thus, in the present collision energy, the most important role in electron transfer is played by K-shell electrons, whereas in ionization processes the distant collisions play a role and the outer-shell electron ionization still dominates the innershell ionization, which is estimated to be more than two orders of magnitude smaller than the outershell ionization.

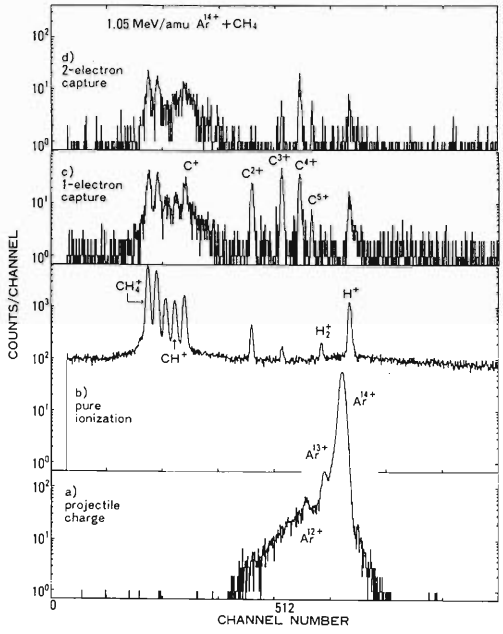

Fig. 1. a) Projectile charge spectrum, b) recoil ion charge spectrum in pure ionization, c) that in one-electron capture, and d) that in two-electron capture processes in 1.05 MeV/amu $Ar^{14+}+CH_4$ collisions.

References

1) T.Tonuma *et al.*: *RIKEN Accel. Prog. Rep.*, **21**, 84 (1987).
2) N.B.Mahli *et al.*: *J. Chem. Phys.*, **87**, 6502 (1987).
3) T.R.Dillingham *et al.*: *Nucl. Instrum. Methods Phys. Res.*, **B40/41**, 40 (1989).

RIKEN Accel. Prog. Rep. 23 (1989)

III-2-12. Excitation of Convoy-like Electrons by Impact of Glancing-Angle Incident Fast Xe Ions

H. Ishikawa, A. Koyama, and Y. Sasa

In a previous report,[1] we showed the energy spectra of convoy-like electrons emitted at angles less than 20° to the surface of an Al target by impacts of fast heavy ions, N^{2+}, N^{7+}, Ar^{4+}, and Ar^{12+} at the glancing-angle to the surface of the Al target; we named these convoy-like electrons "Surface-Stimulated-Convoy (SSC) electrons." The peak energies of the SSC electrons induced by these ions are higher than those of usual convoy electrons emitted from a thin foil in the forward direction by fast ion bombarding and are maximum at emission angles of 4-6°. In the present report, we show the energy spectra of electrons emitted from an solid Al surface by impact of glancing-angle incident 0.98 MeV/amu Xe^{9+} and Xe^{27+} ions.

Figure 1 shows the energy spectra of electrons emitted at small angles (a) $Q_e=1.5°$, b) $Q_e=2.0°$, and c) $Q_e=2.5°$) to the beam direction on the impact of Xe^{9+} incident at an angle of 0.8° to the target surface. These spectra have double peaks. A sharp peak (peak I) in the low energy range has almost the same value (533 eV) as that for usual convoy electrons. The intensity of peak I markedly decreases with increasing of emission angle (Q_e). These results suggest that the electrons of peak I correspond to usual convoy electrons induced by fast highly charged Xe ions from the microscopic projections of the target surface. On the other hand, a broad peak (peak II) in the high energy range shows a large value compared with that for usual convoy electrons, and is considered to be the peak of SSC electrons. Figure 2 shows the emission angle dependence of peak II energy for Xe^{9+} and Xe^{27+} impact at an incidence angle of 1°. An energy difference between SSC electrons and usual convoy electrons is large for Xe ions compared with for N or Ar ions. This result suggests that the SSC electrons are electrons in the continuum states of incident ions accelerated by image potential induced by the projectile on the target surface.

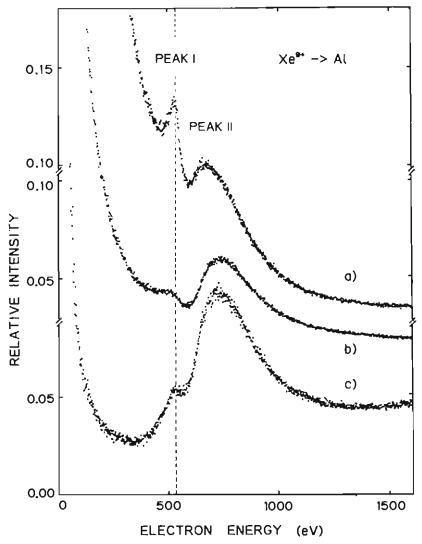

Fig. 1. Energy spectrum of electrons emitted at angle a) 1.5°, b) 2.0°, and c) 2.5°, to the beam direction. Xe^{9+} ions 0.98MeV/amu impact on the Al target surface at an incidint angle of 0.8°. The dashed line shows the energy of usual convoy electrons, 533eV.

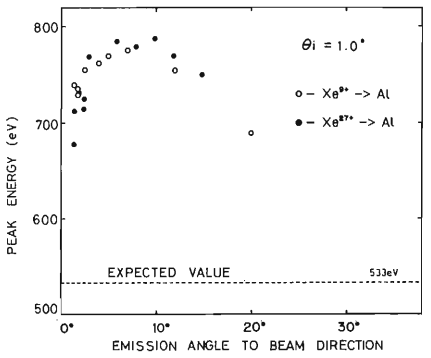

Fig. 2. Emission angle dependence of the maximum energy for peak II induced by Xe^{9+} and Xe^{27+} ions incidence at an angle of 1.0°. The dashed line shows a value expected for usual convoy electrons.

References

1) A. Koyama, H. Ishikawa, and Y. Sasa: *RIKEN Accel. Prog. Rep.*, **22**, 88 (1988).

RIKEN Accel. Prog. Rep. 23 (1989)

III-2-13. Incident-Angle Dependence of Peak Energies of Al- and Si-LVV Auger Electrons for Ar^{12+} Ion Impact

A. Koyama, H. Ishikawa, K. Maeda, Y. Sasa,
O. Benka,* and M. Uda**

Energy spectra were measured for Al- and Si-LVV Auger electrons emitted by the impact of 1.3 MeV/amu Ar^{12+} ions at incident angles of 39° and 4° with respect to the surface of a target. The energy spectra measured at 4° show a decrease in peak energy and a broadening in line width compared with those for the 39° incidence. These spectral changes at 4° may be caused by electron holes in a valence band induced by projectiles. We analyzed the data to get the lifetime of these holes, τ_h, on the assumptions that the peak energy decreases in proportion to the number of the holes produced by secondary electron emission, and that the number of the holes decreases exponentially with time. Thus, the change in the energy decrease with time evolution is given by $\Delta E(t)=\Delta E_0 e^{-t/\tau_h}$, where ΔE_0 is the energy decrease just at the time of hole creation and is considered to be proportional to the yield of SE emission. The number of Auger electrons emitted per unit time interval changes according to e^{-t/τ_A}, where τ_A is the relaxation-time of an L-shell hole. From a simple algebra, an energy spectrum of the Auger electrons influenced by the holes concerned, $I(E)$, is given by

$$I(E)=A\int_{E}^{E+\Delta E_0} I_0(E') \times\{(E'-E_0)/\Delta E_0\}^{\alpha-1}dE', \quad (1)$$

where A is the normalization factor, $I_0(E')$ is the energy spectrum of the Auger electrons without holes, and $\alpha=\tau_h/\tau_A \cdot I_0(E')$ is approximated by the spectrum for 39 incidence because of a very small energy decrease for this incident angle.

Figures 1 and 2 show the results of calculation. The solid curves show the experimental spectra. The spectra for 39° incidence are approximated by the dotted curves in Figs. 1(a) for Al and 2(a) for Si. The spectra for 4° incidence are calculated by a parameter fitting method. The dotted curves in Figs. 1(b) and 2(b) are spectra calculated with parameters; $\Delta E_0=4.8$ eV, $\alpha=0.33$ for Al, and $\Delta E_0=7.0$ eV, $\alpha=0.3$ for Si. For Al, τ_A is approximated to be 1.6×10^{-14} s, and $\tau_h\simeq5\times10^{-15}$ s is obtained. This is the first experimental deduction of the life-time of holes in the valence band of a nearly free electron metal such as Al.

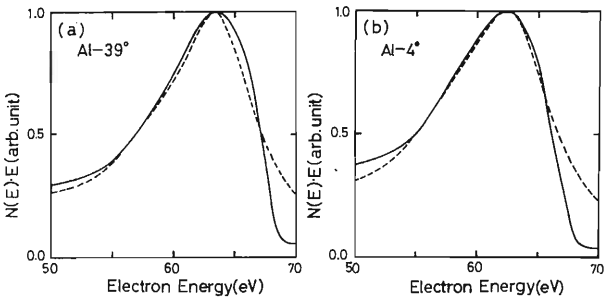

Fig. 1. Energy spectra for Al-LVV Auger electrons induced by fast Ar^{12+} ions incident at 4° relative to the surface of the target. Solid curves represent experimental spectra and dotted ones those calculated. (a) for 39° incidence and (b) for 4° incidence.

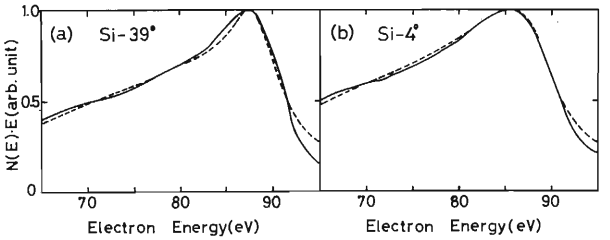

Fig. 2. Energy spectra of Si-LVV Auger electrons induced by Ar^{12+} ions incident at 4°. Solid curves represent exprimental spectra and dotted ones those calculated. (a) for 39° incidence, and (b) for 4° incidence.

* University Linz, A-4040 Linz-Auhof, Austria.
** Waseda University, Kiku-icho, Shinjuku, Tokyo, 162, Japan.

RIKEN Accel. Prog. Rep. 23 (1989)

III-2-14. High Resolution L-Auger Spectroscopy of Na-Like Sulfur Excited in 63-MeV S^{5+}+He Collisions

N. Stolterfoht,* K. Kawatsura, M. Sataka,** Y. Nakai,** H. Naramoto,**
Y. Yamazaki, K. Komaki, Y. Kanai, T. Kambara, and Y. Awaya

The method of zero-degree Auger spectroscopy[1] was used to measure high-resolution L-Auger spectra of S^{5+} excited in collisions with He of an incident energy of 63 MeV. This method is well suited to avoid Doppler broadening effects normally causing problems in fast ion spectroscopy. The light target atom He and the relatively high projectile energy were chosen to establish the conditions for 'needle excitation',[1] *i.e.*, the excitation of the inner shell without disturbing the outer shell. Previous studies of Ar ion[2] show that rather high resolution is needed to resolve individual lines in L-Auger spectra. Since, in the present Auger spectroscopy, resolution is primarily limited by counting statistics, a high-quality ion beam is indispensable. An intense beam of sulfur ions was provided by the Tandem accelerator at JAERI in Tokai. A typical high-resolution Auger spectrum shown in Fig. 1 shows line groups attributed to the configuration $1s^22s^22p^53snl$ where $n=3, 4, 5,\cdots$.

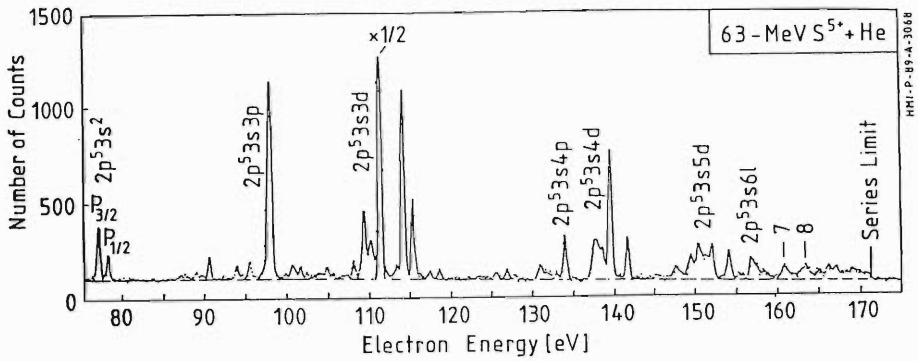

Fig. 1. L-Auger spectrum of S^{5+} produced in 63-MeV S^{5+}+He collisions. Electron energies are transformed to the projectile rest frame.

As expected the most intense group is attributed to the configuration $1s^22s^22p^53s3d$ due to dipole transition 2p→3d. However, the group due to quadrupole transition 2p→3p was also found significant. Identification of line requires further theoretical work including atomic structure calculations.

References

1) A. Itoh, T. Schneider, G. Schiwietz, Z. Roller, H. Platten, G. Nolte, D. Schneider, and N. Stolterfoht: *J. Phys. B*, **16**, 3965 (1983).
2) Th. Schneider, P. Focke, I. Kadar, D. Schneider, G. Schiwietz, H. Platten, A. Itoh, J. E. Hansen, and N. Stolterfoht: Abst. of 16th Int. Conf. on the Phys. of Elec. and Atom. Collisions, New York, p. 506 (1989).

* Hahn-Meitner-Institut, Berlin, F.R.G.
** Japan Atomic Energy Research Institute, Tokai.

RIKEN Accel. Prog. Rep. 23 (1989)

III-2-15. Angular Momentum Distribution of Autoionizing Rydberg States Produced by 64-MeV S Ions in Collisions with Carbon Foils

K. Kawatsura, M. Sataka,* H. Naramoto,* Y. Nakai,*
Y. Yamazaki, K. Komaki, K. Kuroki, Y. Kanai,
T. Kambara, Y. Awaya, and N. Stolterfoht**

We have measured the spectra of electrons ejected from the autoionizing Rydberg state at an observation angle of zero degree with respect to the incident beam direction. The electrons due to the Coster-Kronig transition $1s^22pnl \rightarrow 1s^22s + \varepsilon l'$ ($n \geq 9$) in S^{12+} ions were produced in the 64-MeV S^{q+}+C foil collisions ($q = 5$-15) as well as in the S^{12+}+He collisions under similar experimental conditions. The experiments were performed at the Tandem accelerator facility at JAERI in Tokai by using high-resolution zero-degree electron spectroscopy. The thickness of target carbon foils ranged from 2 to 30 $\mu g/cm^2$. Figure 1(b) shows the electron spectra associated with the configuration $1s^22p9l$ produced in the collisions of 64 MeV S^{12+} on a carbon foil. The Coster-Kronig electron energies ($1s^22p9l \rightarrow 1s^22s + \varepsilon l$) calculated for $l = 0$, 1, 2, 3, and higher are indicated respectively as s, p, d, f, and g in Fig. 1. The energies were transformed to the projectile rest frame. The prominent peak seems to be associated with higher angular momenta ($l = 2$, 3, and higher). Comparing the spectra for the carbon foil with those for a He target shown in Fig. 1(a), we may say that higher angular momentum states of the autoionizing Rydberg state are selectively enhanced in the case of S^{12+} on a carbon foil collisions. This enhancement is more prominent than that for carbon projectiles obtained experimentally[1] and theoretically.[2] Further study is in progress.

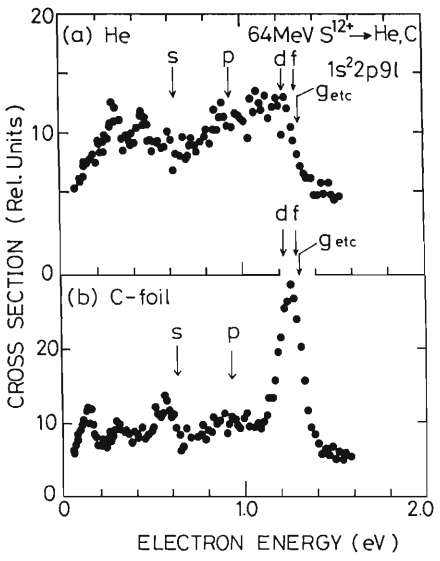

Fig. 1. Spectrum of the electrons associated with the configuration $1s^22p9l$ produced in the collisions of 64-MeV S^{12+} ions (a) on He, and (b) on C foil. Electron energies are transformed to the projectile rest frame.

References

1) Y. Yamazaki, N. Stolterfoht, P. D. Miller, H. F. Krause, P. L. Pepmiller, S. Datz, I. A. Sellin, J. N. Scheurer, S. Andriamonje, D. Bertault, and J. F. Chemin: *Phys. Rev. Lett.*, **61**, 2913 (1988).
2) J. Burgdörfer and C. Bottcher: *ibid.*, **61**, 2917 (1988).

* Japan Atomic Energy Research Institute, Tokai.
** Hahn-Meitner-Institut, Berlin, F.R.G.

RIKEN Accel. Prog. Rep. 23 (1989)

III-2-16. High-Resolution Measurement of Ejected Electrons from Helium-Like Carbon Ions ($2l3l'$)

H. Sakaue, Y. Kanai, T. Inaba, M. Kushima, K. Ohta,*
S. Ohtani, K. Wakiya, H. Suzuki, T. Takayanagi,*
T. Kambara, A. Danjo, M. Yoshino, and Y. Awaya

We carried out high-resolution measurements of electrons ejected from the autoionizing state of doubly-excited He-like carbon ions. Projectiles, 67-keV $^{13}C^{6+}$, made by the RIKEN ECRIS were analyzed with a 90° analyzing magnet and then allowed to collide with a target He in a gas cell. Doubly-excited He-like states were produced by double-electron eapture from the target He atoms. Emitted electrons were measured by zero-degree electron spectroscopy.[1]

High resolution spectra of the ejected electron from the ($2l3l'$) states are shown in Fig. 1. Few calculations of these peaks have been reported.[2-4] Considering these calculations, we identified each peak as denoted in Fig. 1.

Our experiment results are listed in Table 1, in which each state is designated using a correlated classification scheme. Since our measured values are shifted by a post-collision interaction (PCI) effect, they are corrected for the energy shift using theoretical lifetimes[6] as shown in parentheses in Table 1. The absolute values of ejected electron energies from ^1S and ^1P states in our measurements are in good agreement with theoretical values.[3,4] More accurate calculations of ^1D and ^1F states are needed to ascertain our results.

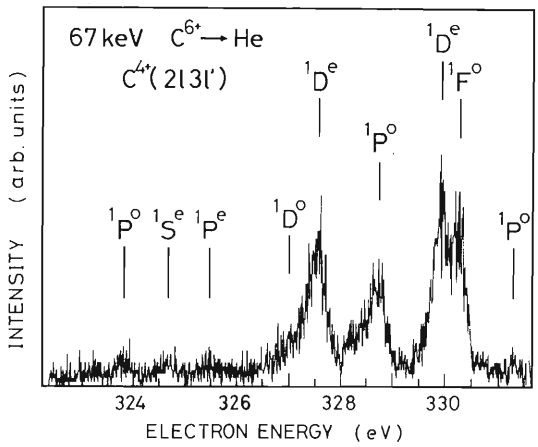

Fig. 1. Ejected electron spectra of the ($2l3l'$) states. Peaks are identified as shown.

Table. 1 Energies of electrons ejected from the C^{4+} ($2l3l'$) . The uncertainty of the absolute energy values is ±0.2 eV. Energy values corrected for the PCI effect are given in parentheses.

Our result (eV)	$^{2S+1}L^{\pi}$	$(K,T)^A$	Theory (eV)		
			Refs. 2 & 5	Ref. 3	Ref. 4
323.7(323.7)	$^1P^o$	$(1, 0)^-$	323.91	323.88	
324.7(324.9)	$^1S^e$	$(1, 0)^+$	325.16	324.96	
325.5(325.5)	$^1P^e$	$(0, 1)^-$	325.71		325.65
327 (327)	$^1D^o$	$(0, 1)^0$	327.56		
327.5(327.7)	$^1D^e$	$(1, 0)^+$	328.17		
328.7(328.8)	$^1P^o$	$(0, 1)^+$	329.41	328.90	
329.9(329.9)	$^1D^e$	$(0, 1)^0$	330.34		
330.2(330.2)	$^1F^o$	$(1, 0)^0$	330.71		
331.2(331.2)	$^1P^o$	$(-1, 0)^0$	331.70	331.36	

References

1) H. Sakaue, K. Ohta, T. Inaba, Y. Kanai, S. Ohtani, K. Wakiya, H. Suzuki, T. Takayanagi, T. Kambara, and Y. Awaya: *RIKEN Accel. Prog. Rep.*, **22**, 74 (1988).
2) L. Lipsky, R. Anania, and M.J. Conneely: *At. Data Nucl. Data Tables*, **20**, 127 (1977).
3) Y.K. Ho: *Phys. Rev. A*, **23**, 2137 (1981).
4) E. Holøien and J. Midtdal: *J. Phys. B*, **4**, 1243 (1971).
5) C.D. Lin: *Phys. Rev. A*, **39**, 4355 (1989).
6) U. I. Safronova: *Phys. Scr.*, **T26**, 59 (1989).

* Department of Physics, Sophia University.

RIKEN Accel. Prog. Rep. 23 (1989)

III-2-17. Spectrum of Highly Ionized Titanium Atoms in Beam-Foil Experiment

K. Ando, S. Kohmoto, Y. Awaya, T. Tonuma, and S. Tsurubuchi*

Ne-like ions are important in the X-ray laser experiment, because the intensity of their 3s-3p transitions is amplified in a laser-produced plasma. Although many theoretical calculations predict this amplification on the basis of theoretical transition probabilities, the levels of the predicted transition which showed laser amplification differ in total angular momenta from observed one. Thus, the transition probabilities should be determined experimentally.

Using the LINAC, we plan to measure the 3s-3p transition probabilities of Ne-like Ti ion. To this end the spectral lines of these transitions must be identified. Spectra were measured of titanium ions of 21, 29, and 38 MeV. The wavelengths of spectral lines were determined by referring to known spectral lines. A part of the spectrum is shown in Fig. 1 with identified spectral lines.

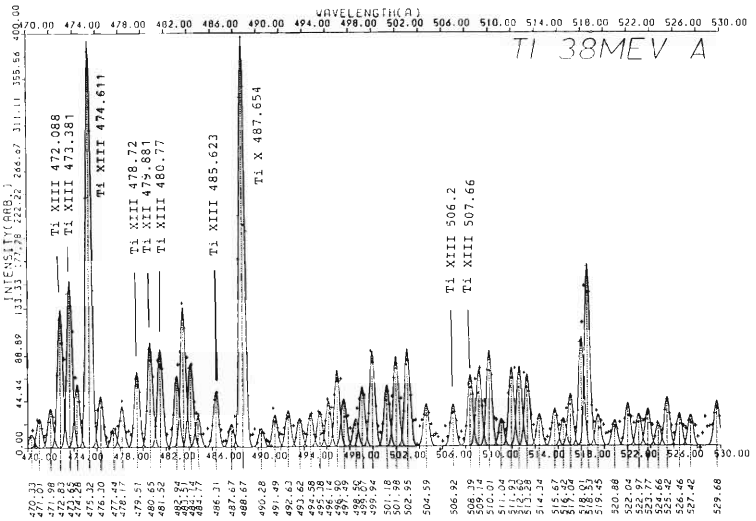

Fig. 1. Spectrum of highly ionized titanium atoms obtained in a beam-foil experiment. The numbers shown under the abscissa are shifted from the true wavelengths by about 0.1A.

* Tokyo University of Agriculture and Technology, Koganei-shi, Tokyo 184, Japan.

RIKEN Accel. Prog. Rep. 23 (1989)

III-2-18. Efficient Resonance Ionization of Lu I BY Two Step Laser Excitation

H. Maeda,* Y. Matsumoto, A. Suzuki,* and M. Takami

For applying resonance ionization spectroscopy (RIS) to the study of sh rt-lived nuclei, efficient ionization of the relev nt atoms is of crucial importance since the num ber of available atoms is usually very small. In the present work we studied the ionization characteristics of highly excited Lu I atoms by two different methods, electric field ionization of highly excited Rydberg atoms and direct ionization by excitation of autoionizing states.

The field ionization threshold for highly excited Rydberg atoms decreases as the principal quantum number n increases. However, the laser excitation cross section also decreases as n increases. As a compromise for efficient ionization, therefore, one has to excite the levels around $n=15$ and to field-ionize with rather strong electric field of the order of a few kV/cm. We found, however, that a previously reported weakly perturbing state[1] was an excellent candidate as the final state for field ionization. This $J=3/2$ doubly excited state, located 45 cm^{-1} below the first ionization limit among dense highly-excited Rydberg states, can be easily ionized with the field strength over 100 V/cm owing to a small fraction of the mixed character of Rydberg states.[2] Furthermore, the perturbing state has a large excitation cross section since it still retains the character of valence states. A preliminary measurement on the ionization characteristics from this state shows that the excited atoms are completely ionized before spontaneous emission under an electric field of the order of 100 V/cm. This ionization scheme has advantages that an atom is excited with a moderate laser fluence and subsequently field-ionized with a weak electric field.

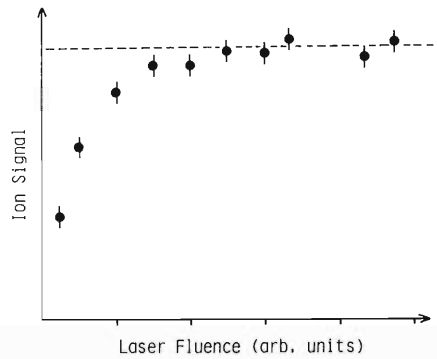

Fig. 1. Laser power dependence of ionization signal when an autoionization level 70 cm^{-1} above the first ionization limit is excited. The laser beam diameter is approximately 1 mm. The maximum laser power is about 1 mJ. Note that the ion signal is completely saturated at a moderate laser fluence.

As a second ionization scheme, we examined an autoionizing level approximately 70 cm^{-1} above the ionization limit. Figure 1 shows the laser power dependence of the ionization signal where the maximum laser power was around 1 mJ/pulse. The result indicates strong saturation of the ion signal intensity, *i.e.*, almost 100% ionization with the laser power well below 1 mJ. Because autoionizing states are frequently found in heavy transition metal elements like lanthanides, efficient ionization will be easily realized with a moderate laser power.

References

1) H. Maeda, Y. Mizugai, Y. Matsumoto, A. Suzuki, and M. Takami: *RIKEN Accel. Prog. Rep.*, **22**, 77 (1988).
2) H. Maeda, Y. Mizugai, Y. Matsumoto, A. Suzuki, and M. Takami: *J. Phys.*, **B22**, L511 (1989).

* Department of Nuclear Engineering, Faculty of Engineering, University of Tokyo.

RIKEN Accel. Prog. Rep. 23 (1989)

III-2-19. Resonance Ionization Spectroscopy of Organic Molecules

T. Mionowa, H. Katsuragawa, and T. Inamura

1, 4-Dioxane, methanol, ethanol, and acetone added into argon considerably improved the multiplication gain of a proportional counter.[1] However, the addition of these organic molecules produces extra spectra in the near UV region, where we carried out resonance ionization spectroscopy (RIS) of Al and Fe.[2] Since the spectra obscure atomic spectra, we carried out a study to make clear what molecules are responsible for the spectra.

We carried out RIS on the organic molecules listed above. The experimental setup was similar to that described in Ref. 2. The filling gases for the proportional counter were as follows (total pressure 1000 mmHg): Ar + 1, 4-dioxane (60 mmHg), Ar + methanol (40 mmHg), Ar + ethanol (20 mmHg), and Ar + acetone (50 mmHg).

A typical spectrum observed is shown in Fig. 1. The most puzzling is the spectrum observed for all the filling gases. This result suggests that the spectrum is attributed to an impurity molecule contained in the organic compounds in common, or to a reaction product produced by irradiation of a pulsed dye laser, or to an unstable transient molecule appearing during chemical reactions. Chemical reactions in a gas phase proceed by collisions between transient molecules, or transient molecules and stable molecules. Therefore RIS under the collisionless condition is helpful to see the origin of the spectrum.

We carried out RIS of molecular beams of the organic molecules in a vacuum chamber evacuated to lower than 10^{-4} Torr, where collisions between molecules were ruled out. The experimental setup was similar to that described in Ref. 3. Ion-electron pairs produced by irradiation of a pulsed dye laser were detected by two CERATRON detectors and the differences in the time of flight (TOF) between the ions and elec-

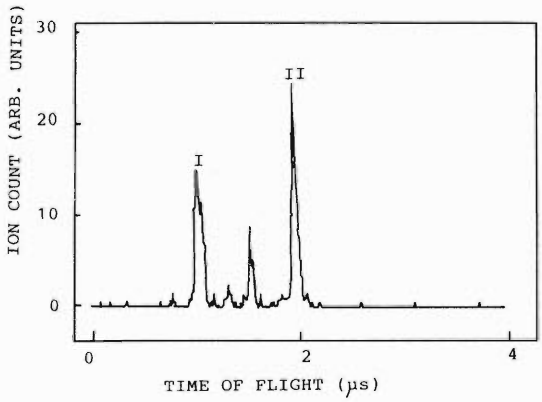

Fig. 2. Observed time-of-flight spectrum.

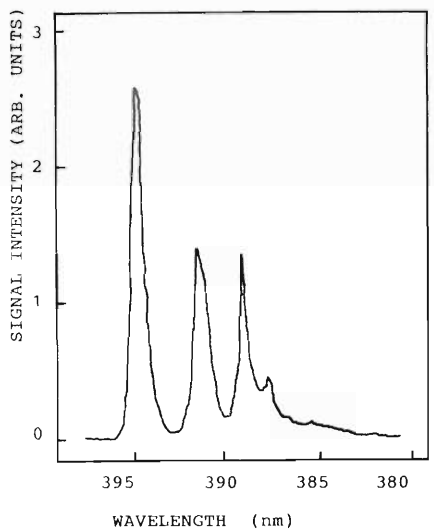

Fig. 1. Observed resonance ionization spectrum for argon containing 1, 4 dioxane, methanol, ethanol, and acetone.

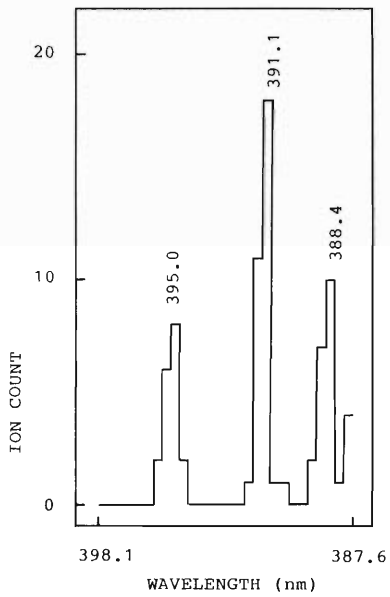

Fig. 3. Ion counting rate against the wavelength of a pulsed dye laser. The ions were counted whose TOF coincided with C_2 ion.

trons were recorded in a TOF spectrum (Fig. 2). Peak I and II seem to be due to C_2 and C_4 ions, respectively. These peaks were seen for all organic molecular beams (it is not clear how C_4 ions were produced by photoionization of methanol (CH_3OH) and ethanol (C_2H_5OH)).

The counting rate of ions whose TOF coincide with that of C_2 ion was recorded against the wavelength of the pulsed dye laser (Fig. 3). This is a kind of resonance ionization spectrum if the C_2 ion is the dissociation product following resonance ionization of any molecule. The spectrum shown in Fig. 3 coincides with that shown in Fig. 1. Thus, we conclude that the molecule resonantly ionized is not a reaction product due to a laser beam.

Sharp lines were observed in resonance ionization spectroscopy of organic molecules. The lines seem to be due to photoionization of impurity commonly containing in the samples, or due to that of transient molecules produced by photodissociation.

References

1) H. Katsuragawa, T. Minowa, and T. Inamura: This Report, p.94.
2) H. Katsuragawa, T. Minowa, and T. Inamura: *Nucl. Instrum. Methods B*, **43**, 259 (1989).
3) H. Katsuragawa, T. Minowa, M. Shimazu, and T. Inamura: *ibid.*, **26**, 440 (1987).

RIKEN Accel. Prog. Rep. 23 (1989)

III-2-20. ^{61}Ni Mössbauer Studies of a New Ferromagnetic Heusler Alloy, $RuFe_{1.5}Ni_{0.5}Si$

T. Okada, Y. Kobayashi, M. Katada,* H. Sano,*
M. Iwamoto, and F. Ambe

For clarification of the magnetism of intermetallic systems, Mössbauer studies of the hyperfine magnetic fields at the nuclei of constituent atoms is very useful. Heusler alloys are a class of ferromagnetic ones having a general composition of X_2YZ; its structure is designated as $L2_1$, with X atoms forming a simple cubic matrix and Y and Z occupying alternate body centers in the cubic structure.

We have already performed ^{99}Ru Mössbauer studies on a magnetically ordered Heusler alloy system with a chemical formula $Ru_xFe_{3-x}Si$.[1-3] Recently, a progressive study has been carried out on a new system $RuFe_{2-x}Ni_xSi$ by ^{61}Ni-Mössbauer spectroscopy. In a Heusler alloy system containing Ni, the magnetic moment and the electronic state of Ni atoms have not been thoroughly determined yet because of the experimental difficulty in ^{61}Ni Mössbauer measurement. In spite of many experimentally undesirable nuclear properties, ^{61}Ni can be a powerful probe in solid-state physics and chemistry as a sole Mössabuer nuclide other than ^{57}Fe in the iron group transition elements.

A source nuclide ^{61}Cu ($T_{1/2}$=3.5 h) was produced by an (α, p) reaction in the cyclotron. The experimental procedures of the source production and Mössbauer measurements were reported previously.[4] It is nessesary to maintain both a source and an absorber at low temperatures because the Mössbauer γ-ray energy (67.5 keV) is rather high and the Debye-Waller factor is low.

In Fig. 1 is shown a ^{61}Ni Mössbauer spectrum of a $RuFe_{1.5}Ni_{0.5}Si$ specimen below the Curie temperature. This is the first Mössbauer observation of magnetic Ni atoms in the Heusler matrix. The computer analysis shows that the spectrum consists of two components with different hyperfine magnetic fields and that Ni atoms are substituted for Fe atoms in the [A,C] and [B] sites, respectively, at a ratio of 2 to 1. This assignment of the two components is based on the magnetic moment of Ni itself and the magnetic contribution from the first-near-neighbor shells of Fe atoms. More detailed discussion will be described elsewhere along with the results of ^{57}Fe Mössbauer spectroscopy and magnetization measurements.

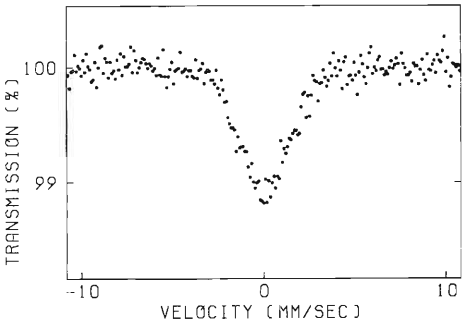

Fig. 1. ^{61}Ni Mössbauer spectrum of $RuFe_{1.5}Ni_{0.5}Si$ at liquid-helium temperature.

References

1) Y. Kobayashi, M. Katada, H. Sano, T. Okada, K. Asai, and F. Ambe: *J. Radioanal. Nucl. Chem. Lett.*, **136**, 387 (1989).
2) Y. Kobayashi, M. Katada, H. Sano, T. Okada, K. Asai, M. Iwamoto, and F. Ambe: *Hyperfine Interact.*, in press.
3) Y. Kobayashi, M. Katada, H. Sano, T. Okada, K. Asai, M. Iwamoto, and F. Ambe: This Report, p.73.
4) T. Okada, Y. Kobayashi, M. Katada, H. Sano, M. Iwamoto, and F. Ambe: *ibid.*, **22**, 122 (1988).

* Tokyo Metropolitan University

RIKEN Accel. Prog. Rep. 23 (1989)

III-2-21. ^{57}Fe Mössbauer Study on $Bi_2Sr_4Fe_3O_{12}$

T. Okada, N. Sakai, K. Asai, and T. Yamadaya*

The mechanism of superconductivity in high-T_c copper oxides still remains undetermined, and the study of related materials may contribute to the development of a viable theory. A superconductor $Bi_2Sr_2Ca_2Cu_3O_{12}$ (a so-called "2223" superconductor) is well known to have a high T_c of 108 K. Recently, iron oxide $Bi_2Sr_4Fe_3O_{12}$ was synthesized and analyzed to be isostructural with "2223".[1] One main difference between the iron and the copper oxides is the higher oxygen content of the iron oxide, resulting in the formation of mainly trivalent iron with an octahedral oxygen coordination. This iron oxide is semiconductive at low temperatures. We report the Mössbauer spectroscopic properties of $Bi_2Sr_4Fe_3O_{12}$ oxide measured at various temperatures to elucidate the electronic and magnetic states of the iron ions. ^{57}Fe Mössbauer spectra were taken with a conventional driving system, and analyzed with a FACOM780 computer. The X-ray powder analysis was performed using a RIGAKU powder diffractometer with a Cu-Kα radiation.

For the preparation of the samples, Bi_2O_3, $SrCO_3$, and Fe_2O_3 were mixed, heated in a corundum boat in air at 850°C and quenched at room temperature. The reaction was interrupted several times for regrindings. Although $Bi_2Sr_4Fe_3O_{12}$ is hard to be prepared in a perfect single phase, we are succeeded in perparing a nearly single phase at 850°C after a total firing time 96 h. The presence of a small amount of a perovskite of $SrFeO_3$ type was just detectable in an X-ray diagram in addition to the diffraction pattern of $Bi_2Sr_4Fe_3O_{12}$. The average structure of $Bi_2Sr_4Fe_3O_{12}$ is tetragonal with $a=5.475$ Å, $c=37.02$ Å. Figure 1 shows the Mössbauer spectra of a $Bi_2Sr_4Fe_3O_{12}$ specimen at various temperatures. The spectra at 298 K and 80 K are composed of an asymmetric doublet arising from the pure electrical quadrupolar interactions and a small amount of sixtet arising from magnetic hyperfine interaction. The computer analysis of the spectra shows that the doublet consists of two doublets having different quadrupole splittings, and positive and negative isomer shifts relative to iron metal. The positive isomer shift value (IS=0.20 mm/s) leads to the presence of the trivalent iron ions. The negative one (IS=−0.12 mm/s) suggests the presence of tetravalent or pentavalent iron ions. The spectrum measured at 5 K shown in Fig. 1 consists of a broadened sixtet and a small amount of a narrow sixtet. The value of the hyperfine magnetic field (H_{hf}) of broadened sixtet is about 480 kOe, which is similar to the value for trivalent iron ion in covalent sites. The value of H_{hf} of the narrow one is roughly 290 kOe. This value is as large as one of pentavalent iron ions observed in a perovskite-type (Sr,Ca) FeO_{3-x}.[2] This result clearly demonstrates the presence of two states of iron ions in $Bi_2Sr_4Fe_3O_{12}$ which is magnetically ordered at low temperatures.

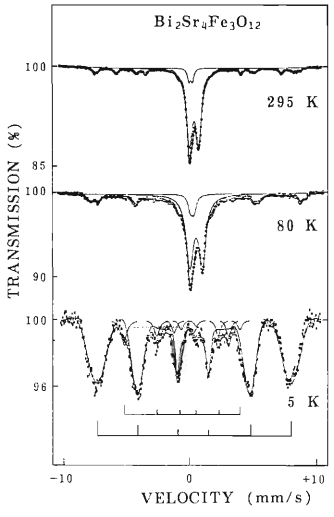

Fig. 1. Mössbauer spectra of $Bi_2Sr_4Fe_3O_{12}$ at 5, 80, and 295 K.

References

1) R. Retoux, C. Michel, M. Hervieu, N. Nguyen, and B. Raveau: *Solid State Commun.*, **69**, 599 (1989).
2) M. Takano, N. Nakanishi, Y. Takeda, S. Naka, and T. Takada: *Mater. Res. Bull.*, **12**, 923 (1977).

* Faculty of Literature and Science, Yokohama City University.

RIKEN Accel. Prog. Rep. 23 (1989)

III-2-22. Evolution of Krypton Precipitates in Kr-Implanted Aluminium

E. Yagi

It has been demonstrated that heavy inert gas atoms (Ar, Kr, and Xe) implanted into metals at ambient temperature precipitate into a solid phase (solid bubbles).[1,2] The evolution of such bubbles has been investigated mainly by transmission electron microscopy (TEM) and by X-ray diffraction.

The channelling analysis is a very useful method to study the phenomena inaccessible by TEM or X-ray diffraction, such as bubble nucleation in the early stage of implantation, *i.e.*, in the range of a low implantation dose. In the present study the behaviour of Kr atoms implanted in Al at room temperature was investigated by an ion-channelling method with a 1 MeV He^+ beam. Experiments extended to a lower Kr concentration, 1×10^{14} Kr/cm^2, than that covered in previous studies[3-5] demonstrated that Kr atoms are distributed over substitutional (S) sites, random (R) sites (in the form of precipitates), tetrahedral (T) and octahedral (O) sites. The T- and O-site occupancies can be interpreted as a result of the multiple trapping of implantation-introduced vacancies (V) by a Kr atom; the Kr atoms trap multiple vacancies and, accordingly, are displaced to the T- and O-sites to form KrV_4 and KrV_6 complexes, respectively. The fraction of the T-site occupancy decreases with increasing implantation dose, whereas that of the O-site occupancy once increases between 1×10^{14} and 4×10^{14}/cm^2 and then decreases above 4×10^{14}/cm^2 (Fig. 1). In accordance with the decrease in the T- and O-site occupancies, the fraction of the R-site occupancy (precipitates) increases. This result indicates the growth of KrV_4 to KrV_6 complexes by trapping still more vacancies during implantation, and that the complexes such as KrV_4 and KrV_6 are formed in the early stage of Kr implantation and act as trapping centres for Kr atoms and vacancies, *i.e.*, nucleation centres for Kr precipitation.

The effect of annealing was investigated on a

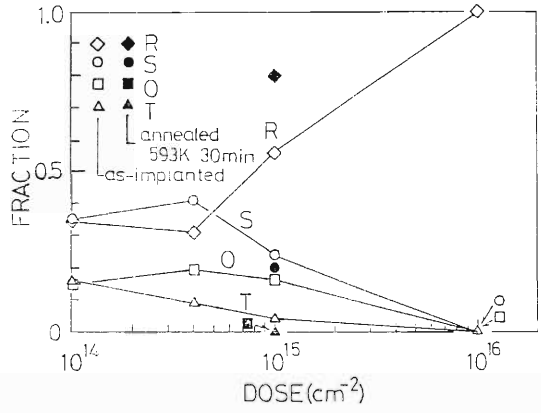

Fig. 1. Dose dependence of the fractions of Kr atoms located at various kinds of sites.

1×10^{15} Kr/cm^2 implanted specimen. After annealing at 683 K for 30 min, a channelling Kr-dip about 1.5 times as broad as the Al-dip came to be observed for the ⟨110⟩ channel, indicating the formation of an epitaxially aligned solid Kr phase on annealing. This change was not observed in electron diffraction. In some case, the channelling method is more sensitive than the electron diffraction method for the detection of the epitaxially grown Kr solid phase. More detailed descriptions are given in Ref. 6.

References

1) A. vom Felde, J. Fink, Th. Müller-Heinzerling, J. Plüger, B. Scheerer, G. Linker, and D. Kaletta: *Phys. Rev. Lett.*, **53**, 922 (1984).
2) C. Templier, C. Jaouen, J. -P. Rivière, J. Delafond, and J. Grilhé: *C.R. Acad. Sci. Paris*, **299**, 613 (1984).
3) E. Yagi: *Phys. Stat. Solidi*, **A104**, K13 (1987).
4) E. Yagi, M. Iwaki, K. Tanaka, I. Hashimoto, and H. Yamaguchi: *Nucl. Instrum. Methods*, **B33**, 724 (1988).
5) E. Yagi: *ibid.*, **B39**, 68 (1989).
6) E. Yagi, I. Hashimoto, and H. Yamaguchi: *J. Nucl. Mater.*, **169**, 158 (1989).

RIKEN Accel. Prog. Rep. 23 (1989)

III-2-23. Lattice Location of B Atoms in $Ni_{0.75}Al_{0.15}Ti_{0.10}$ Intermetallic Compounds as Observed by a Channeling Method

K. Tanaka and E. Yagi

It has been observed that the ductility of polycrystalline $L1_2$-type Ni_3Al intermetallic compounds is improved even at room temperature by doping a small amount of B atoms. For theoretical studies on the mechanism of this phenomenon, the lattice location of B atoms is indispensably determined. In the present study, the location of B atoms in 0.5 at%B-doped $Ni_{0.75}Al_{0.15}Ti_{0.10}$ was investigated by a channeling method. To overcome the difficulty in preparing a just-stoichiometric Ni_3Al single crystal, Ti was selected as a ternary addition. Channeling experiments were carried out at room temperature with a 720 keV H^+ beam accelerated with a TANDETRON. The B atoms were detected by measuring α-particles generated by a reaction $^{11}B(p, \alpha)^8Be$. Proton-induced characteristic X-rays from Ni, Al, and Ti atoms and backscattered protons were measured simultaneously. α-Angular profiles shown in Fig. 1 indicate that the B atoms occupy octahedral (O) sites. Figure 2 shows the <100> and <111> angular profiles for Ni $K_{\alpha,\beta}$ and Al K_α X-rays. The angular full-widths ($2\psi_{1/2}$) of the <100> and <111> channeling dips are summarized in Table 1. The agreement of the values of $2\psi_{1/2}$ between Ti $K_{\alpha,\beta}$ and Al K_α X-rays directly demonstrates that the Ti atoms substitute the Al atoms in Ni_3Al. The values of $2\psi_{1/2}$ for the <111> α-particle dip is approximately the same as that for the Al X-ray dip, and smaller than that for the Ni X-ray dip, indicating that the B atoms are not shadowed by Ni atomic rows, but Al atomic rows in the <111> channel. There are two types of O-sites in the Ni_3Al structure: the sites surrounded by six nearest neighbor Ni atoms (type-I) and those surrounded by four Ni atoms and two Al atoms (type-II). From the present results we concluded that in $Ni_{0.75}Al_{0.15}Ti_{0.10}$ most of the B atoms occupy O-sites of type-I. More detailed descriptions are given in Ref. 1.

Table 1. Summary of full angular width (deg.) of channeling dips ($2\psi_{1/2}$) for α-particles, X-rays and backscattering protons.

Channel	B ($^{11}B(p,\alpha)^8Be$)	Al (X-rays)	Ti (X-rays)	Ni (X-rays)	Ni (backscattered protons)
<100>	1.18	1.09	1.12	1.29	1.60
<111>	0.81	0.80	0.80	0.91	1.05

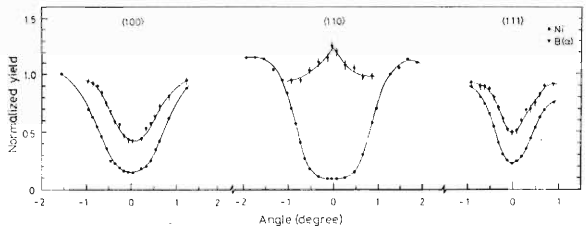

Fig. 1. Channeling angular profiles of backscattered protons (●) and emitted α-particles (▼) across <100>, <110>, and <111> axes for the $Ni_{0.75}Al_{0.15}Ti_{0.10}$ crystal.

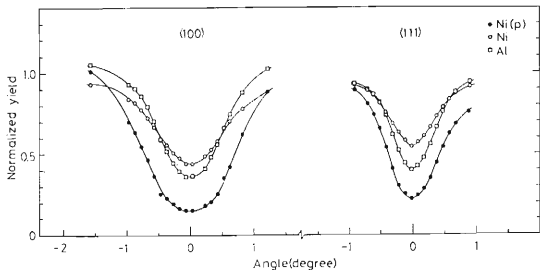

Fig. 2. Channeling angular profiles of Ni $K_{\alpha,\beta}$ X-rays (○), Al K_α (□) and backscattered protons (●) across the <100> and <111> axes for the $Ni_{0.75}Al_{0.15}Ti_{0.10}$ crystal.

References

1) T. Tanaka, E. Yagi, N. Masahashi, Y. Mizuhara, K. Tatsumi, and T. Takahari: *Nucl. Instrum. Methods Phys. Res. B,* in press.

RIKEN Accel. Prog. Rep. 23 (1989)

III-2-24. Crystallographic Polarity of Ideomorphic Faces on a Cubic Boron Nitride Single Crystal

T. Kobayashi, O. Mishima,* M. Iwaki, H. Sakairi, and M. Aono

A Rutheford backscattering spectroscopy (RBS) method can determine the crystallographic polarity of ideomorphic {111} faces of c-BN composed of light elements.

The large front and back faces (indicated in Fig. 1) are {110} planes as revealed by X-ray diffraction.

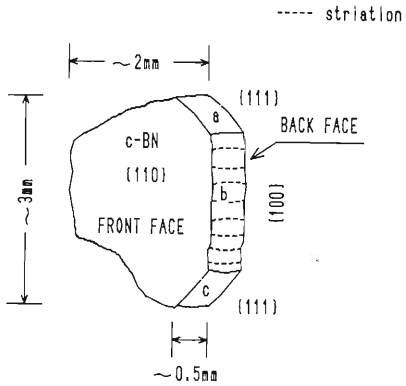

Fig. 1. Sketch of a single crystal of c-BN.

We carried out RBS-channeling experiments with a 1.5 MeV $^4He^+$ beam for the front and back {110} faces (not for the {111} faces themselves) illustrated in Fig. 1. The top view of the atomic arrangements of the front and back {110} faces are shown in Figs. 2a and 2b. Figures 2c and 2d are the side views of Figs. 2a and 2b, respectively, in which each string of atoms is shown with a thick bar. The structures shown in Figs. 2c and 2d have no vertical mirror plane perpendicular to the plane of these figures. Therefore, an asymmetric channeling dip will be observed. The direction of channeling angular scan was shown in Figs. 2c and 2d.

Figure 3 shows the channeling angular profiles of ^4He particles scattered with nitrogen atoms around the <110> channeling axes for the front and back {110} faces. The channeling dips observed for the front and back {110} faces are asymmetric and the asymmetry is reversed

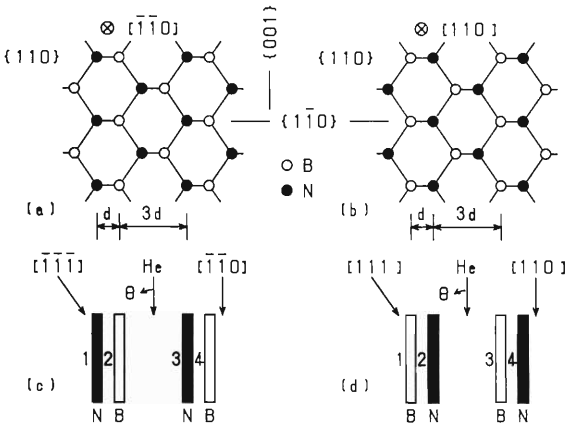

Fig. 2. Top views of the atomic arrangements of the front and back {110} faces of a c-BN crystal shown in Fig. 1 (a and b) and their side views (c and d).

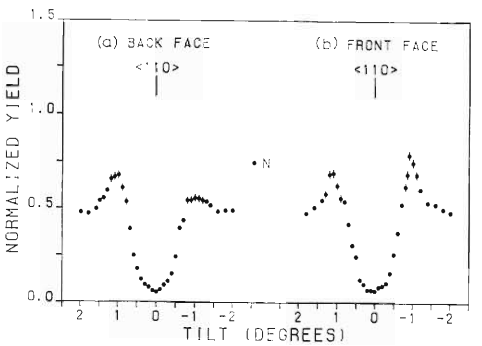

Fig. 3. Channeling angular profiles of ^4He particles scattered with nitrogen atoms in a c-BN single crystal around the <110> channeling axes for the front and back {110} faces.

between the front and back {110} faces. We conclude that the front {110} face corresponds to Figs. 2b and 2d and the back {110} face to Figs. 2a and 2c. The crystallographic polarity of the ideomorphic {111} faces a and c shown in Fig. 1 is, therefore, determined from the crystal structure of c-BN as follows: the {111} faces a and c in Fig. 1 are both terminated with a nitrogen plane.

* National Institute for Research in Inorganic Materials.

RIKEN Accel. Prog. Rep. 23 (1989)

III-2-25. RBS Investigation of $^{14}N^{+}$-Implanted Ti, Cr, Fe, Zr, and Nb Sheets

T. Fujihana, Y. Okabe, K. Takahashi, and M. Iwaki

The nitrogen concentration profile as a function of depth is one of the most important subjects in the research of N-implanted layers[1,2] and has been investigated by means of SIMS, AES, and so on. However, these analyses are accompanied by ion beam sputtering which presents the possibility that selective sputtering, cascade mixing, *etc.* would take place. It is important to compare the results of these analyses with the RBS measurements, which have no such effects of sputtering.

We describe the results of the RBS measurements on the compositions of N-implanted metal surface layers.

The implantation of $^{14}N^{+}$ into Ti, Cr, Fe, Zr, and Nb sheets was performed to a dose of 1×10^{18} ions/cm^2 at 100 keV and at 20 °C. The RBS measurement was carried out using 1.5 MeV $^{4}He^{+}$ ions. Backscattered particles were detected at an angle of 150 degrees.

Figure 1 shows the RBS spectra for unimplanted and N-implanted specimens. The backscattered yields from implanted N atoms were hardly observable, because the N-yields were much smaller than the yields from metals and the energy spectrum of N-yields was superposed on that of metal-yields. Thus, the yields of N atoms cannot be used for the calculation of atomic concentrations. By comparing the spectra for unimplanted and implanted specimens, however, the N-depth profile can be derived from a reduced backscattered yield from host metal-atoms. The height of the spectrum of the backscattered yield from metal-atoms in implanted layers can be determined by assuming the atomic ratio of N-metal compounds and by using the stopping cross section factor calculated from Bragg's rule and the surface energy approximation. The depth dependence of the N-atomic ratio for all specimens shows a trapezoidal distribution. Compounds having the N/Metal atomic ratio profile given by the flat topped plateaux are indicated in Fig. 1.

From these results we conclude that, in high dose N-implantation into metals, the N/Metal ratio cannot exceed a certain value and N atoms can migrate toward the surface during the implatation at as low as 20 °C. The depth profile of the implanted Natoms becomes a trapezoidal distribution, consequently.

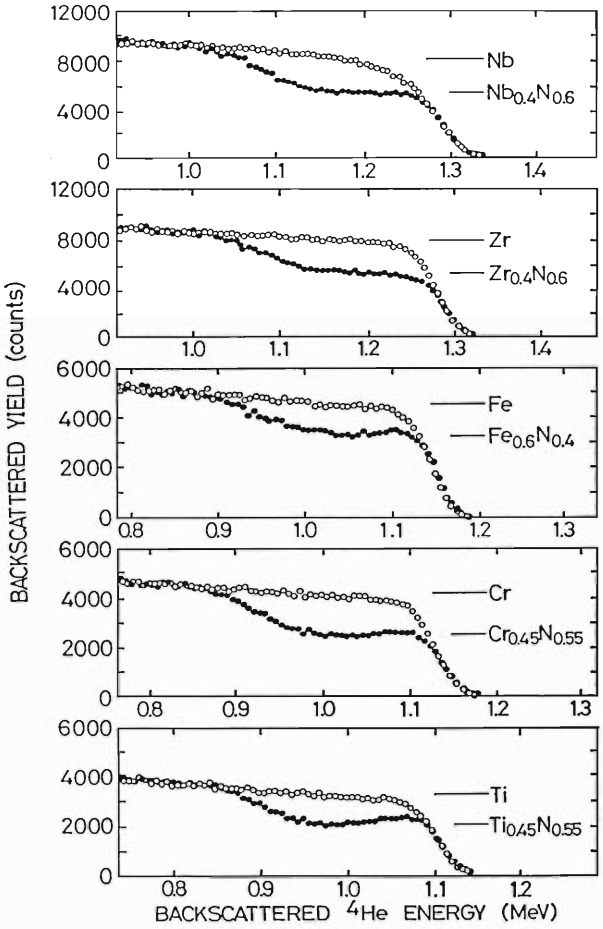

Fig. 1. RBS spectra for unimplanted and N-implanted Ti, Cr, Fe, Zr, and Nb to a dose of 1×10^{18} ions/cm^2.

References

1) T. Fujihana, Y. Okabe, and M. Iwaki: *Nucl. Instrum. Methods*, **B39**, 548 (1989).
2) T. Fujihana, Y. Okabe, and M. Iwaki: *Mater. Sci. Eng.*, **A115**, 291 (1989).

RIKEN Accel. Prog. Rep. 23 (1989)

III-2-26. RBS Investigation of N-implanted AlN_x Films on Glassy Carbon

K. Kobayashi, S. Namba, T. Fujihana, T. Kobayashi, and M. Iwaki

The possibility of modifying the compositional ratio of AlN_x ($0.2 \leqq x \leqq 1.4$) films by nitrogen ion implantation was studied.

AlN_x films with four compositional ratios were deposited on glassy carbon (GC) by activated reactive evaporation (ARE) in a nitrogen atmosphere at deposition rates of 30, 4, 0.8, and 0.7 nm/min. The thickness of as-deposited films measured by a Dektack was about 120 nm.

N-implantation into the AlN_x thin films was performed to a dose of 5×10^{17} N^+/cm^2 at 40 keV and at 1×10^{-6} Torr. This energy was chosen so as to make the average range of nitrogen tall within the thickness of the films.

Figure 1 shows the RBS spectra before and after N-implantation for four kinds of AlN_x films deposited on GC. The surface edges of Al, N, and O are indicated by short lines; the position of GC is also indicated.

We calculated each of N/Al in the films by a surface energy approximation, by assuming the shaded area of the yields of nitrogen to be the real yields of nitrogen to eliminate background from oxygen signals.

The ratios, N/Al, in the as-deposited films are 0.2, 0.8, 1.2, and 1.4 for (A), (B), (C) and (D), respectively. The ratios in the implanted films are approximately 0.7, 1.0, 1.0, and 1.1 for samples (a), (b), (c), and (d), respectively. Comparison between the ratios of N/Al in un-implanted and implanted films indicates that N-implantation into Al-rich films causes an increase in the ratio but it does not exceed the stoichiometric ratio of AlN; for N rich films, N-atoms move out of the surface and the ratio approaches the stoichiometric ratio of AlN consequently.

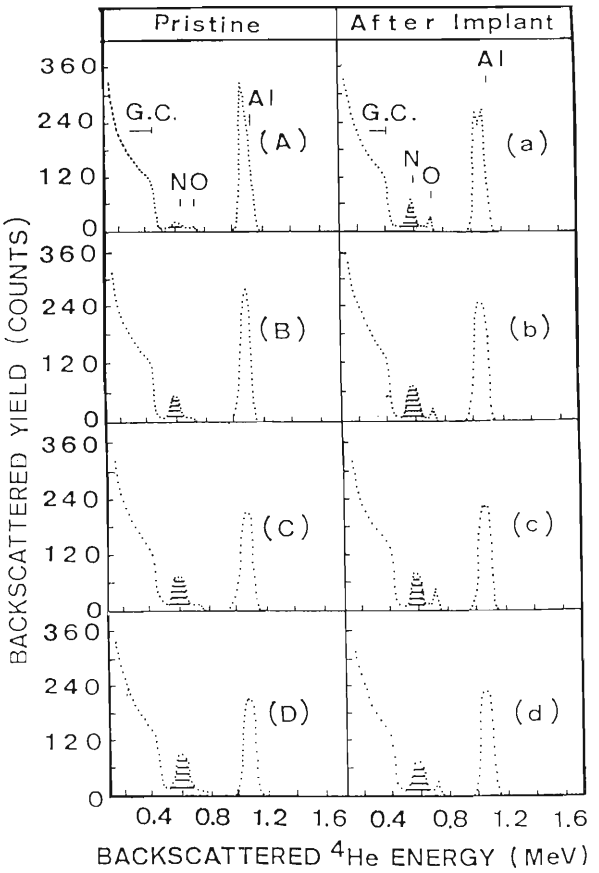

Fig. 1. RBS spectra for four kinds of AlN_x films on GC before and after N-implantation. The surface edges of Al, N, and O are shown by the short lines.

Thus, we concluded that N-implantation is useful for preparing stoichiometric AlN films from AlN_x ($x \neq 1$).

RIKEN Accel. Prog. Rep. 23 (1989)

III-2-27. Depth Profile of Tb Implanted in CaF_2

K. Aono, M. Iwaki, and S. Namba

Energy levels created by impurities (rare earth elements) in CaF_2 single crystals are used as a laser source. We previously studied luminescence during ion-implantation and the radiation damage or depth profiles of Eu implanted in CaF_2 by RBS-channeling using 1.5 MeV He^+.[1,2] In these studies, some results are found to be very different from those of implantation into other insulators; thus, ion implantation into CaF_2 has been studied with various ions.

In the present study, the depth profile of Tb implanted in CaF_2 was investigated by the same method as that previously[1,2] used. Terbium was implantated in CaF_2 to a dose of $\sim 4\times10^{14}$ ions/cm^2 at 100 keV in random directions at room temperature.

Figure 1 shows random and ⟨111⟩ aligned spectra observed for CaF_2 and Tb. The random spectra give the same shape as unimplanted specimens, indicating that no out-diffusion of Ca and F atoms has occurred through the surface. The Tb depth profiles in the random and ⟨111⟩ aligned spectra of implanted specimen are of a Gaussian-type. A difference is seen between the random and aligned spectra of the as-implanted specimen. On implantation, the scattering yield in the aligned spectrum shows a strong reduction compared with that in the random spectrum. Figure 2 shows the angular scans for the host Ca- and impurity Tb-yields around the ⟨111⟩ direction. Terbium has the same angular profile as Ca, suggesting that most of the Tb atoms occupy substitutional lattice sites. The depth corresponding to the Tb peak in the spectra is about 40 nm, which is a little larger than the projected range of Tb of about 31 nm predicted from the calculation by an E-DEP-1 code. The standard deviation calculated from the FWHM of the Tb spectra is about 8 nm, which is in good agreement with the predicted value of about 9 nm. The calculation by E-DEP-1 code is effective for specimens implanted to a high dose. We concluded therefore that the experimentally observed range of Tb atoms implanted in CaF_2 to a high dose may be in fairly good agreement with the predicted value.

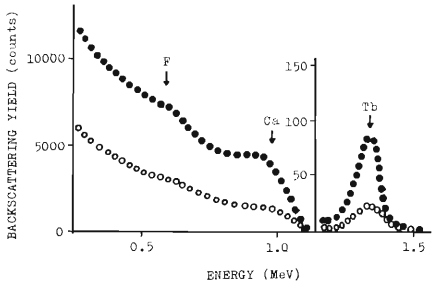

Fig. 1. Random (●) and ⟨111⟩ aligned (○) spectra for Tb-implanted CaF_2 with $\sim 4\times10^{14}$ ions/cm^2.

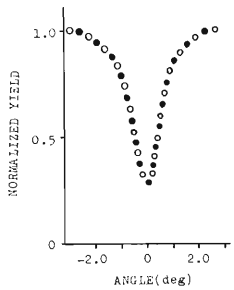

Fig. 2. Channeling angular profiles of Ca(●)- and Tb (○)- yields for the Tb-implanted ⟨111⟩ direction.

References

1) K. Aono, M. Iwaki, S. Namba: *Nucl. Instrum. Methods*, **B32**, 321 (1988).
2) K. Aono, M. Iwaki, and S. Namba: *ibid.*, in press.

RIKEN Accel. Prog. Rep. 23 (1989)

III-2-28. Correlation of Particle-Induced Displacement Damage in Si and GaAs. II

K. Kuriyama,* H. Takahashi,* N. Hayashi, H. Watanabe, I. Sakamoto, and I. Kohno

Recently, irradiation effects on semiconductors, particularly on GaAs, have been investigated by several authors. We studied the effect of high-energy proton irradiation on GaAs, as a part of investigations on the effects of radiation of different projectiles. And we have found the enhanced quenching of photoconductance.

Samples were undoped semi-insulating GaAs grown by liquid-encapsulated-Czochralski (LEC) method with an etch-pit-density (EPD) of 10^5/cm^2. The thickness was 400-460μm. Irradiation was performed by using the cyclotron at room temperature with 15-MeV protons, which have a mean range of about 760μm over the sample thickness. Photoconductance was measured at temperature ranges of 80 to 300 K in the same manner as in a gamma-ray irradiation study on GaAs.[1]

Figure 1 shows the temperature dependence of photoconductance at different doses. The quenching of photoconductance near 100 K is enhanced markedly with increasing proton dose. Irradiated sample E was annealed in a N_2-gas flow for 15 min at 200, 250, 300, and 350°C. The photoquenching was completely recovered by annealing around 350°C, but the photoconductance stayed at a lower value than that before irradiation. In the time-dependence of photoconductance on the irradiation dose, we observed a large time constant after more than 8×10^{12}p$^+$/cm^2 irradiation, while a single small time constant before irradiation. The large time constant after irradiation disappeared by annealing around 350°C for 15 min. We suggest that the large time constant is related to the defects created by proton irradiation. The mechanism of the enhanced quenching is not due to the increase of EL2 (the midgap electron trap center) concentration by proton irradiation, but to the decrease of EL2 compensated by proton-irradiation-induced defects. Since shallow donors created by irradiation provide electrons to the compensated

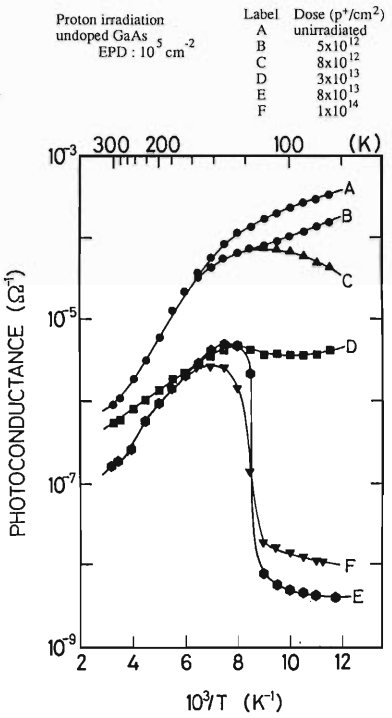

Fig. 1. Temperature dependence of photoconductance for samples irradiated to different doses.

EL2, EL2$^+$, these EL2$^+$ defects become quenchable neutral EL2^0 defects. Therefore, the transition from the normal EL2^0 to the metastable EL2* state is enhanced.

Experiments of proton irradiation of Si crystals are also being carried out to obtain damage factors[2] and to elucidate the correlation of the displacement damage produced by protons and neutrons.

References

1) K. Kuriyama, H. Kawahara, M. Satoh, and T. Kawakubo: *Appl. Phys. Lett.*, **53**, 1074 (1988).
2) N. Hayashi, N. Watanabe, I. Sakamoto, K. Kuriyama, H. Kawahara, and I. Kohno: *RIKEN Accel. Prog. Rep.*, **22**, 105 (1988).

* Hosei University, Koganei

RIKEN Accel. Prog. Rep. 23 (1989)

III-2-29. Diagnostics of ECR Plasma for Carbon Film Production

K. Yano, H. Oyama, K. Shimizu, M. Yanokura,
Y. Abe, H. Kokai, and Y. Sakamoto

A recent topic of materials produced by plasma CVD is carbon films, including diamond. ECR plasma with a high electron temperature was used for production of carbon films. An electron temperature of ECR plasma produced by means of Electron Cyclotron Resonance ranges from several to several tens of electron volts depending on discharge conditions, and is extremely higher than the temperatures of ions and gas molecules. For this reason, ECR plasma can effectively produce chemically active species via dissociation of material gas molecules. Furthermore, a feature of the ECR plasma is to operate under rather lower pressure ($\sim 10^{-4}$ Torr), which allows dissociated species to arrive onto a substrate without collision.

To clarify the relation between the characteristics of the carbon films and the discharge conditions of plasmas, species in the plasma were investigated by using a time-of-flight method ; it is difficult to use a QMA near the plasma owing to the existence of strong magnetic fields in the ECR plasma device.

The present ECR plasma device has been described in Ref.1. For mass analysis of charged particles coming out of the plasma along a magnetic field, a chamber was connected to the end of the discharge tube through an aperture of 1.5 mm in diameter. Deposited carbon films on a Si substrate were mainly investigated with Raman spectroscopy and ERD(Elastic Recoil Detection) by using an Ar^{4+} beam of about 50 MeV. The former was applied to the morphological studies of produced carbon films, the latter to the measurement of a hydrogen content in films and their thickness at the same time.

Carbon deposition experiments were carried out using mixed gas ECR plasma of methane and hydrogen.The feed gas pressure was usually fixed at 2.5×10^{-4} Torr throughout the experiments. The ratio of CH_4 in the mixture was varied from 0.17 to 0.55. The electron densities ranged from 1 to 3×10^{10} cm^{-3} and the electron temperatures ranged from 3 to 4 eV. Figure 1 shows the histogram of the results of mass analysis relating to hydrogen when ratio of CH_4 was changed. These results show that H_3^+ molecules were predominantly produced compared with H^+ and H_2^+ under every discharge condition. The mass analyses relating to hydrocarbon are in progress. Carbon films deposited when the ratios of CH_4 are 17, 33 and 44 % were revealed to be mixtures of amorphous and graphite from Raman spectra. The hydrogen content in films deposited was found by ERD to be 20-30% and films were several hundreds of nanometers in thickness.

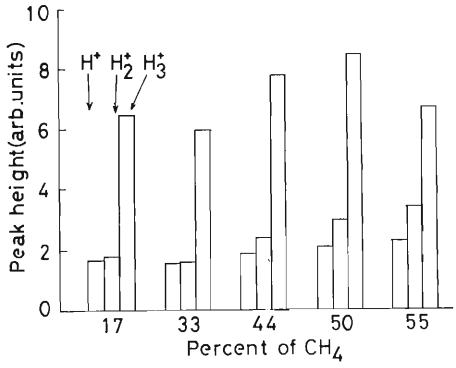

Fig. 1. Histogram of mass analysis results relating to hydrogen. The total feed gas pressure was 2.5×10^{-4} Torr.

References

1) K.Yano, H. Oyama, K. Shimizu, M. Yanokura, Y. Abe, H. Kokai, and Y. Sakamoto: ISPC-9, 3, 1444 (1989).

RIKEN Accel. Prog. Rep. 23 (1989)

III-2-30. Application of PIXE Analysis to Materials Sciences (II)

Y. Sasa, K. Maeda, and M. Uda

1) Comparison of PIXE and EPMA

Correct determination of the concentrations of coexisting trace elements is indispensable for the development of advanced materials. This can be executed by X-ray spectroscopy with a Si(Li) semiconductor detector. An electron-probe microanalysis method (EPMA) is widely used to map the distributions of elements in the surface region. However, its sensitivity is not so high, at most 0.1%, owing to its high background originated from the electron bremsstrahlung, and therefore this system is rather suitable for major and minor, but not trace elemental analysis. By contrast, a particle-induced X-ray emission method (PIXE) is expected to have multiple merits over EPMA such as a very low background, high sensitivity of detection, almost the same sensitivity for a wide range of concentration and elements, and moreover, the method can be used in any atmosphere. Up to now, however, data showing the superiority of PIXE over EPMA on the sensitivities or on the detection limits are scarce. Thus, we tried to show evidence for the advantage of PIXE over EPMA for trace analysis. Figure 1-a shows a PIXE spectrum of NBS Al alloy (SRM 1241a) obtained with 1.6 MeV protons. The same target was irradiated with 15 keV electrons to give an EPMA spectrum shown in Fig. 1-b). In spite of a long acquisition time of 30,000 seconds for the EPMA spectrum, only Mn and Fe Kα X-ray peaks are discernible due to its high background. On one hand, the PIXE spectrum measured for 1,700 seconds shows many intense X-ray peaks with a very low background. Signal to noise ratios (S/N) at the Mn Kα peak were estimated as 1/3 and 150/1 for the electron and the proton excitation, respectively. These results show that PIXE is superior to EPMA for trace element analysis.

2) Applications of PIXE

i) on the basis of the numerical analysis of PIXE spectra obtained with Al materials, we demonstrated that the intensity of continuous X-ray background can be used as a normalizing parameter to estimate the total amount of incident ions for quatitative trace analysis. The comparison of a spectrum for Al irradiated with 1.6 MeV H^+ and that with 2.4 MeV He^{2+} revealed that the latter gives a better sensitivity for trace elements of $Z \geq 32$.

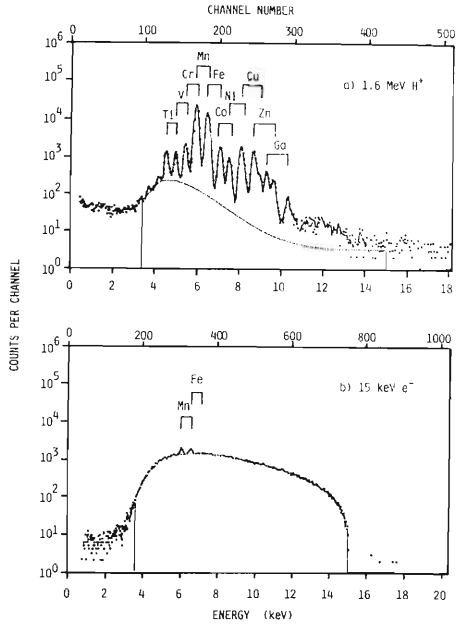

Fig. 1. X-ray spectrum of NBS Al alloy (SRM 1241a) irradiated with (a) protons and (b) electrons.

ii) Optimum conditions required for X-ray absorbers (kind of elements, thickness, and geometrical alignment) was inspected to analyze trace elements of atomic numbers adjacent to those of matrix elements in the analysis of impurities in Ga-As matrix electronics devices.

iii) We surveyed fundamental conditions for non-vacuum PIXE measurements on art, archaeological, and biological targets with a newly installed equipment. In these specimens, the overheating of samples and/or evaporation of components due to ion beam impacts in vacuum are serious problems. The analyses of letters written on paper sheets or on wooden chips with Chinese ink, colors on a figured paper, and saliva taken from young men with and without physical and mental stimulations are now being developed.

RIKEN Accel. Prog. Rep. 23 (1989)

III-2-31. PIXE Analysis of Human Spermatozoa Isolated from Seminal Plasma by a "Swim" Technique

K.Maeda, Y.Sasa, H.Kusuyama, K.Yoshida,* and M.Uda

A great effort has been made to determine the chemical compositions of semen and seminal plasma for the elucidation of the mechanism of fertilization. Horever, little work has been performed on the chemical compositions of spermatozoa themselves. The analytical data of spermatozoa reported in the literature were obtained from spermatozoon samples separated from seminal plasma by centrifugation,[1] or by centrifugation and washing.[2-4] In this report we describe the PIXE analysis of human spermatozoa isolated from semen by letting them swim into a kind of physiological saline, Tyrode's solution.[5] The 'swim' technique is generally adopted for selection of motile spermatozoa from semen of a low sperm quality, and is sometimes used for artificial fertilization.

Five semen samples were taken from patients afflicted with infertility. Half of each semen sample was used for the determination of spermatozoon density and motility of spermatozoa in semen and for the PIXE analysis of seminal plasma. The another half of each sample was put into a tapered plastic tube. Tyrode's solution containing NaCl as a major component was poured gently over the semen layer to keep the two layers separated. After allowing the spermatozoa to swim into the Tyrode's solution for 1 h, the upper layer was sucked out with a plastic pipet and transferred into another tapered tube. A spermatozoon-rich portion then was obtained by centrifugation, deposited on a 0.5 μm-thick Microfilm ($(H_9C_5O_3)_n$), and dried in a vacuum desiccator, and subjected to PIXE analysis. A beam of 1.6 MeV H^+ ions obtained from the Tandetron was used for excitation.

Since the target samples are composed of Tyrode's solution and spermatozoa, the chemical compositions of the spermatozoa were estimated after subtraction of peak intensities in the PIXE spectrum of pure Tyrode's solution from those of the samples. Here, the chlorine K X-ray peak intensity was used for evaluating the amount of Tyrode's solution contained in samples, because only Na and Cl are the major components of the solution.

The relative concentrations of P, K, Ca, Ti, Fe, Zn, and Br in the motile spermatozoa thus determined were compared with those in the seminal plasma. The compositions of spermatozoa were quite different from one sample to another, while the differences in the compositions of seminal plasma were not so large. The concentration ratios, Ca/K and Fe/K, in spermatozoa were considerably higher than in seminal plasma (a factor of 1.3-7 for Ca/K and of 2-14 for Fe/K). The concentration ratios of P/K, Zn/K, and Br/K in spermatozoa were not different from those in seminal plasma, *i.e.*, at most factor of 3. This is the first attempt to determine the chemical compositions of motile spermatozoa free from contaminations of seminal plasma and loss of component elements during washing.

References

1) P.J. Quinn, I.G. White, and B.R. Wirrick: *J. Reprod. Fertil.*, **10**, 379 (1965).
2) P.A. Pleban and D. Mei: *Clin. Chim. Acta*, **133**, 43 (1983).
3) G.S. Hall and R.M. Shelden: *Biol. Trace Elem. Res.*, **12**, 323 (1987).
4) K. Maeda, Y. Sasa, H. Kusuyama, K. Yoshida, and M. Uda: *RIKEN Accel. Prog. Rep.*, **22**, 119 (1988).
5) K. Maeda, Y. Sasa, H. Kusuyama, K. Yoshida, and M. Uda: *Nucl. Instrum. Methods*, in press.

* Saitama Medical Center, Saitama Medical School.

RIKEN Accel. Prog. Rep. 23 (1989)

III-3. Radiochemistry and Nuclear Chemistry

1. Emission Mössbauer Spectra of ^{57}Mn Formed in Chromium Compounds

K. Kubo, K. Mishima, T. Tominaga, M. Nakada, Y. Watanabe, K. Endo, H. Nakahara,* Y. Kobayashi, H. Sano,* M. Iwamoto, T. Okada, and F. Ambe

We previously reported an irradiation/measurement system for the Mössbauer study using a short-lived nuclide ^{57}Mn (1.45 min) as a suorce.[1,2] In this period we have measured emission Mössbauer spectra of ^{57}Mn formed by ^{54}Cr(α, p)^{57}Mn in a few chromium compounds.

An instrumental setup was described before.[2] In order to minimize the temperature drift in a piezoeletric bimorphtransducer, a temperature controller was installed, which kept the transducer slightly above ambient temperature. Irradiation-measurement was repeated with the following cycle: 90-s irradiation, 13-s migration to the measuring position, and 90-s Mössbauer measurement. A programmable controller repeated the cycle, operating a beam shutter and a signal gate. ^{54}Cr-enriched compounds used as targets were prepared from ^{54}Cr metal and $^{54}Cr_2O_3$. ^{54}Cr-enriched CrO_3 was synthesized by alkali-fusion of Cr_2O_3, oxidation with H_2O_2, removal of unnecessary ions, and evaporation of water. Target materials were fixed on a graphite sample holder and irradiated with 22-MeV α particles from the Cyclotron.

Target temperature was observed to rise during irradiation by several tens of Kelvins and to be slightly higher than room temperature at the time of measurement. The half-life of a 14.4 keV γ-ray was found to be an expected value, though repeated irradiation built up long-lived nuclide (s), leading to a poor Mössbauer S/N ratio. The typical counting rate was 0.5-2.0 counts/ch/min for 200 nA/cm^2 α flux. Figure la shows the Mössbauer spectrum of ^{57}Mn formed in metallic chromium. Because of its small thickness we could not obtain a good S/N spectrum, but an analysis assuming a single component gave an isomer shift of 0.32±0.13mm/s. In Cr_2O_3 two compontets were identified: an Fe(II) doublet with a large quadrupole splitting and an Fe(III) doublet (Fig. 1b). Although an earlier work[3] concluded that the Fe(III) component was a broad singlet, a doublet is clearly observed in our better resolved spectrum. There is no indication of the presence of Fe(V) or Fe(VI) species in CrO_3 (Fig. 1c): the spectrum can be explained with an Fe(III) doublet alone. Measurements are now in progress to improve the Mössbauer S/N ratio and obtain spectra with better statistics.

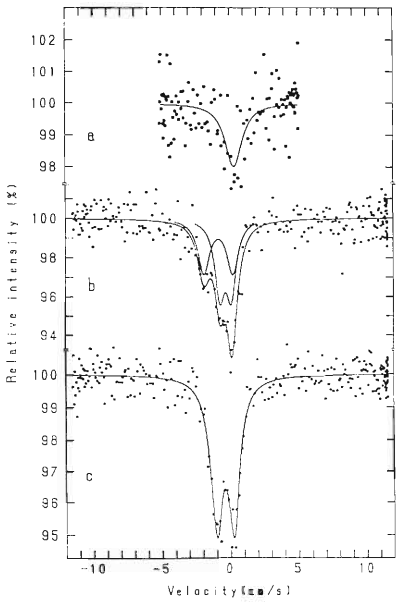

Fig. 1. Emission Mössbauer spectra of ^{57}Mn formed in chromium compounds against a SS absorber. a) Cr metal, b) Cr_2O_3, c) CrO_3.

References

1) Y. Watanabe, M. Nakada, K. Endo, Y. Kobayashi, H. Nakahara, H. Sano, K. Kubo, K. Mishima, Y. Sakai, T. Tominaga, T. Okada, K. Asai, N. Sakai, I. Kohno, M. Iwamoto, and F. Ambe: *RIKEN Accel. Prog. Rep.*, **22**, 121 (1988).
2) Y. Ikegami, K. Nishi, Y. Watanabe, K. Endo, K. Kubo, M. Iwamoto, and F. Ambe: *ibid.*, **22**, 152 (1988).
3) R.S. Preston and B.J. Zabransky: *Phys. Lett.*, **55A**, 179 (1975).

* Tokyo Metropolitan University.

RIKEN Accel. Prog. Rep. 23 (1989)

III-3-2. ^{99}Ru Mössbauer Spectroscopic Studies of Heusler Alloys (II)

Y. Kobayashi, M. Katada, H. Sano*, T. Okada,
K. Asai, M. Iwamoto, and F. Ambe

In this period, ^{99}Ru and ^{57}Fe Mössbauer spectroscopic and magnetization measurements were continued in order to clarify the complicated magnetic properties of ternary intermetallic compounds $Ru_xFe_{3-x}Si$ ($x=0.5$, 1, 1.5, 2) with a disordered Heusler structure.[1-3] A ^{99}Ru Mössbauer source nuclide, ^{99}Rh ($T_{1/2}=15.0$ d), was produced by irradiating a target of 97% enriched ^{99}Ru metal powder with 12 MeV protons accelerated by the cyclotron.[4]

Compounds with $x=0.5$ and 1 revealed very interesting and remarkable magnetism. ^{99}Ru Mössbauer spectra obtained with these compounds at 5 K (Fig. 1) can be analyzed with two components of magnetically split 18 lines. The results of X-ray studies support this observation. On the basis of a first-near-neighbour (1nn) model, assuming that most of the hyperfine field at the ^{99}Ru nuclei is caused by the 1nn Fe atoms and is related to the product of their number and magnetic moments, we found, from the ratio of the intensities of the two components, that Ru atoms occupy both [A,C] and [B] sites, but preferentially the [B] site.

On the other hand, two hyperfine magnetic fields (220 and 300 kOe) were observed in ^{57}Fe Mössbauer measurements. These magnetic fields were considered to be those for ^{57}Fe in the [A, C] and [B] sites in the Heusler structure, respectively, referring to the result on Fe_3Si. For the magnetic field distribution of Fe atoms, we found that the peak intensity at 300 kOe associated with Fe [B] increased and the intensity at 220 kOe associated with Fe [A,C] decreased with increasing Ru concentration (x) from 0 to 1. If the hyperfine magnetic field at ^{57}Fe on both sites in these compounds remains almost unchanged by introducing Ru atoms into Fe_3Si, the peak intensity at 300 kOe should not exceed that at 220 kOe irrespective of the site distribution of Ru atoms.

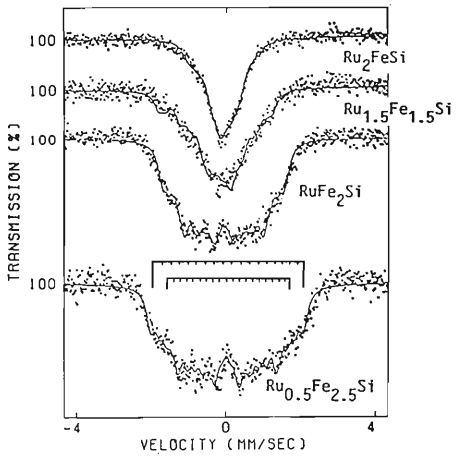

Fig. 1. ^{99}Ru Mössbauer spectra at 5 K of $Ru_xFe_{3-x}Si$ ($x=0.5$, 1, 1.5, 2), against the ^{99}Rh-Ru metal source at the same temperature.

Consequently, it is concluded that the hyperfine magnetic field of a part of Fe [A,C] goes up to 300 kOe in the compounds with $x=0.5$ and 1. This increase at Fe [A,C] is expected to be caused by the introduced Ru atoms of the 1nn shell, assuming no magnetic moment on Ru atoms. This possible increase in the moment of Fe [A,C] is consistent with a larger mean magnetic moment per Fe atom in $RuFe_2Si$ than in Fe_3Si and the site assignment of Ru atoms.

References

1) V. S. Patil, R. G. Pillay, A. K. Grover, P. N. Tandon, and H. G. Devare: *Solid State Commun.*, **48**, 945 (1983).
2) Y. Kobayashi, M. Katada, H. Sano, T. Okada, K. Asai, and F. Ambe: *J. Radioanal. Nucl. Chem. Lett.*, **136**, 387 (1989).
3) Y. Kobayashi, M. Katada, H. Sano, T. Okada, K. Asai, M. Iwamoto, and F. Ambe: *Hyperfine Interact.*, in press.
4) Y. Kobayashi, M. Katada, H. Sano, T. Okada, K. Asai, M. Iwamoto, and F. Ambe: *RIKEN Accel. Prog. Rep.*, **22**, 122 (1988).

* Tokyo Metropolitan University.

RIKEN Accel. Prog. Rep. 23 (1989)

III-3-3. Emission Mössbauer Studies on the Chemical States of ^{119}Sb and ^{119m}Te in S, Se, and Te

S. Ambe and F. Ambe

The chemical states of diluted Sb and Te impurity atoms in S, Se, and Te were studied by ^{119}Sn-emission Mössbauer spectroscopy employing no-carrier-added ^{119}Sb(half-life 38.0 h) and ^{119m}Te(half-life 4.68 d).

^{119m}Te was produced by bombarding a metallic tin plate with α-particles accelerated in the cyclotron. No-carrier-added ^{119m}Te was coprecipitated with S or Se by a reducing reaction. The precipitates were fused in an Ar atmosphere after purification by sublimation. No-carrier-added ^{119}Sb was precipitated together with Te by adding Cr^{2+} to a $^{119}Sb^{5+}$-Te^{4+} solution. The emission Mössbauer spectra of the samples were measured at 78 K by using a $BaSnO_3$ absorber.

The Mössbauer spectra of S(^{119m}Te) and Se(^{119m}Te) consist of a broad line with a shoulder, and are decomposed into a singlet and a doublet (Fig. 1). Comparing the parameters with those of tin sulfides or selenides, we ascribe the singlet to Sn(IV) and the doublet to Sn(II) surrounded by S or Se.

The Mössbauer spectra of coprecipitated, sublimed, and fused Te(^{119}Sb) samples consist of a slightly broadened asymmetric peak (Fig. 2). Fitting of the peak with two singlets gave a satisfactory χ^2-value, yielding isomer shifts at 2.90-2.94 mm/s (compoment I) and 3.26-3.44 mm/s (component II). Both isomer shifts are different from that of ^{119}Sb in Sb metal (2.68 mm/s[1]), indicating that ^{119}Sb atoms are not segregated as Sb metal in Te. Similarity of the isomer shift of the component I to that of ^{119m}Te metal[1] suggests that ^{119}Sb atoms are present as isolated single atoms. The isomer shift of the component II is in good agreement with that of ^{119}Sb in Sb_2Te_3 (3.39 mm/s[2]). The intensity of the component II is found to increase by fusion. Thus, we conclude that a greater part of ^{119}Sb atoms is dispersed in the coprecipitated or sublimed Te metals and on fusing most of the dispersed ^{119}Sb atoms come together to form $^{119}Sb_2Te_3$.

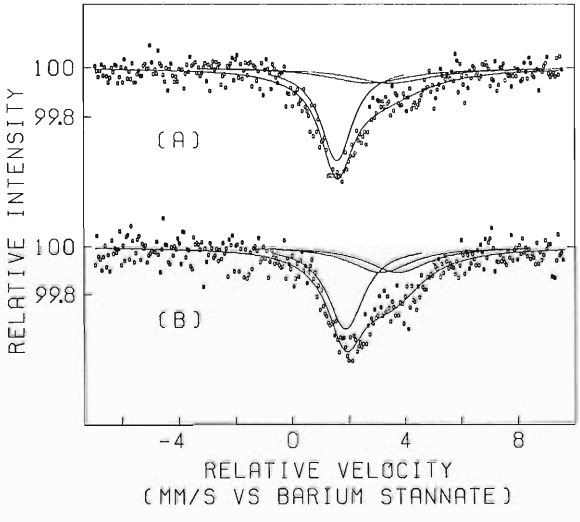

Fig. 1. Mössbauer spectra of (A) S(^{119m}Te) and (B) Se(^{119m}Te).

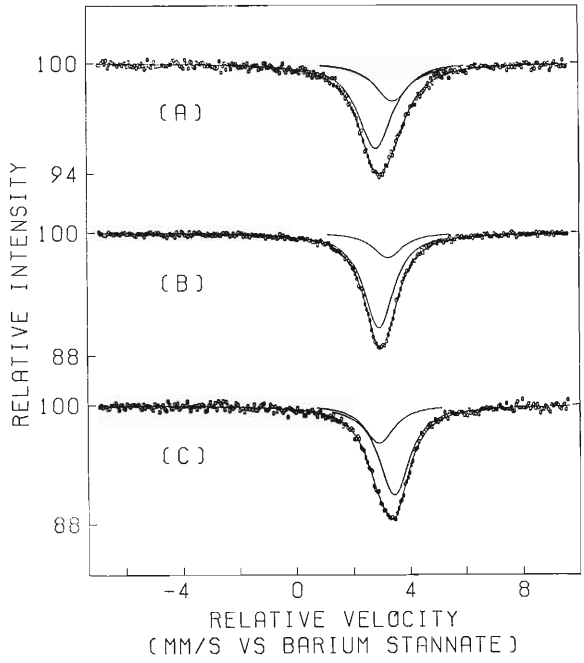

Fig. 2. Mössbauer spectra of (A) Te(^{119}Sb) coprecipitated, (B) sublimed, and (C) fused.

References

1) F. Ambe, S. Ambe, H. Shoji, and N. Saito: *J. Chem. Phys.*, **60**, 3773 (1974).
2) F. Ambe and S. Ambe: *ibid.*, **73**, 2029 (1980).

RIKEN Accel. Prog. Rep. 23 (1989)

III-3-4. Perturbed Angular Correlation of γ Rays of ^{99}Rh in α-Fe_2O_3

Y. Ohkubo and F. Ambe

Perturbed augular correlation (PAC) measurements are a powerful method to study hyperfine interactions. The ^{111}Cd 5/2+level ($t_{1/2}$=85 ns) produced by the decay of ^{111}In ($t_{1/2}$=2.8 days) has extensively been used for PAC measurements, mainly because of several technical reasons.[1] However, in applying the PAC technique to solid state physics and chemistry, it is desirable to measure PAC for a variety of chemical elements. In this period, we started to measure PAC for the ^{99}Ru 3/2+level ($t_{1/2}$=20.5 ns) in α-Fe_2O_3, using ^{99}Rh ($t_{1/2}$=15 days) as its parent. α-Fe_2O_3 is antiferromagnetic below and paramagnetic above 960 K (the Néel point). It is expected from its crystal structure that there is an axially symmetric field gradient at ^{99}Ru.

About 80 mg of isotopically enriched (96.63 at. %) ^{99}Ru powder was irradiated with 12-MeV protons available from the cyclotron. An irradiated Ru target was dissolved in KOH solution. Ru was oxidized to RuO_4 by Cl_2 and separated with a solvent extraction. The solution containing ^{99}Rh was treated with coprecipitaion and ion-exchange methods.[2] Fe^{3+} was added to the solution. ^{99}Rh was coprecipitated with ferric hydroxide by adding NH_4OH. The ferric hydroxide containing ^{99}Rh was dried in vacuum with P_2O_5 at 298 K and then fired in air at 1023 K for 2 hours.

A PAC spectrometer consisted of two BaF_2 (1.5 in $\phi \times 1$ in) detectors, standard NIM modules, and, an ADC and an MCA connected to a personal computer. Coincidence counts for detector combinations of 90 and 180 degrees were measured as a function of delay time between the emissions of 353 and 90 keV γ rays.

Measurements were made at 298 K, 873 K, 923 K, and 1023 K. The last temperature was chosen to be higher than the Néel point, above which only an axially symmetric electric field gradient is expected to cause perturbation. Measured time-differential PAC spectra are shown in Fig. 1. Perturbation due to magnetic interactions is seen clearly at 298 K and 873 K, not so at 923 K,

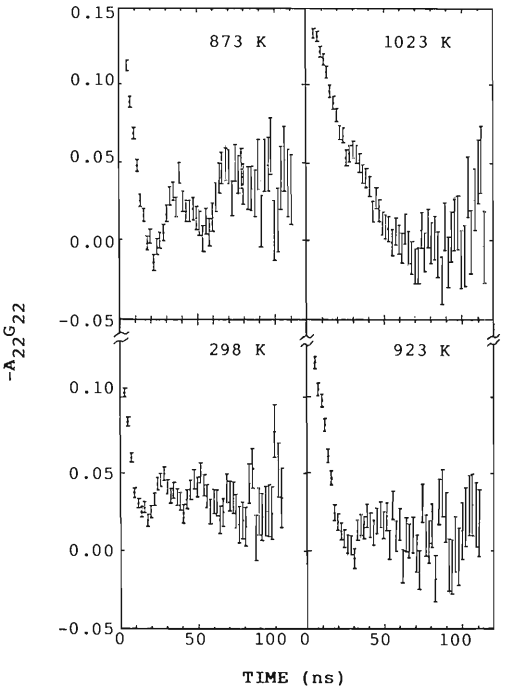

Fig. 1. Time-differential PAC spectra of ^{99}Ru (3/2+) in α-Fe_2O_3 measured at below and above its magnetic transition temperature.

and almost disappears at 1023 K. In the time range in Fig. 1, the second prominent peak due to electric quadrupole interactions is not seen because the quadrupole moments of the ^{99}Ru 3/2+ is not sufficiently large (the first prominent peak is at time= 0). These spectra are only preliminary. In order to make the data more accurate and extend the time scale to see the second prominant peak, we are setting up a PAC measurement system with 4 detectors. A Mössbauer emmision measurement of ^{99}Ru on α-Fe_2O_3 is also in progress.

References

1) K. Asai, F. Ambe, S. Ambe, T. Okada, and H. Sekizawa: *Phys. Rev. B*, in press.
2) D.F.C. Morris and M.A. Khan: *Radiochim. Acta*, **6**, 110 (1966).

RIKEN Accel. Prog. Rep. 23 (1989)

III-3-5. Angular-Momentum Effect in Heavy Ion-Induced Fusion Reactions

H. Baba, H. Kobayashi, H. Kusawake, Y. Ohkubo, T. Saito,
A. Shinohara, and N. Takahashi

Among various theoretical approaches concerning excitation functions for heavy ion-induced fusion reactions, the Bass model is known to describe their reaction mechanisms definitely.[1] Fused nuclei heavier than those in the medium-weight region decay *via* either of two competitive channels, fission or particle evaporation. In the region higher than a specific energy, the cross section for the latter channel was predicted to be proportional to the reciprocal of energy. This is established experimentally for nuclei lighter than lead. Much lighter fused systems, however, show no such energy dependence, when a cross section for particle evaporation is deduced by subtraction of an experimental fission cross section from a fusion cross section predicted by the Bass model. Thus, we aim to directly measure the cross sections for particle evaporation, and its dependence on energy, by a nuclear-chemical method. Reaction systems to be studied are combinations of various heavy ions and the targets of monoisotopic elements around lanthanoids. Furthermore we intend to consider a reaction mechanism in detail, especially an angular-momentum effect, in heavy ion-induced fusion reactions as described by the Bass model.

In the first experiment, we studied the reaction of a ^{141}Pr target with a 26-MeV/u ^{40}Ar beam. The target was a 6.3-mg/cm^2 thick Pr metal of 99.9% purity, sandwiched by two thin Al foils which served as catchers for reaction products with rather small momenta. Another Al foil of 13.5 mg/cm^2 in thickness was placed in the forward direction to catch the products escaping from the target with large momenta, products which would result from the fusion reaction. The projected linear momenta of the products are obtainable from the residing ratio between the target and the catcher. In case when beam energy was degraded, Al foils with appropriate thickness were placed upstream of the target. A stack of the target was mounted in an Al falling-ball and was irradiated at a falling-ball irradiation system installed in the E3 beam course.[2] At two energies, short- and long-term irradiations were carried out for 30 min, favorable for the detection of short-lived radioactive reaction products, and for 200 min for the detection of long-lived products, respectively. The projectile energies at the center of the target were calculated as 25 and 24 MeV/u. Beam intensities were monitored with a current integrator connected to a Faraday cup, and was typically 100-300 neA. After irradiation the falling balls were transferred to the hot laboratory in a few minutes, and the target and the most-downstream catcher were separately sealed for further gamma-ray spectrometry. Non-destructive gamma-ray spectrometry of the reaction products was carried out with three Ge spectrometers with resolutions of approximately 2 keV and relative efficiencies of 18%, 13%, and 10%. Counting efficiencies were obtained at several geometries by use of a calibrated standard source. We found radioactivities such as 2.1-h ^{138m}Pr. Detailed analysis of the gamma-ray spectra is in progress.

In the next experiment, we will study the reaction of a ^{165}Ho target with a 35-MeV/u ^{14}N projectile.

References

1) R. Bass: "Nuclear Reactions with Heavy Ions", Springer-Verlag, Berlin (1980).
2) M. Yanokura, Y. Ohkubo, S. Ambe, M. Iwamoto, and F. Ambe: *RIKEN Accel. Prog. Rep.*, **22**, 150 (1988).

RIKEN Accel. Prog. Rep. 23 (1989)

III-3-6. Preparation of a ^{48}V Source for the Measurements of Positron Lifetimes in Metals

S. Tanigawa, T. Kurihara, Y.-K. Cho, K. Watanabe,
T. Kubota, and Y. Itoh

The studies of lattice defects by positron annihilation have been successfully expanding. Two types of measurements are now in general use in this field. Positron lifetimes in materials are measured by using radioactive nuclides of a particular type that emits gamma radiation coincident in time with the emission of positron. The Doppler broadening of annihilation radiation due to the electron momentum distribution in materials is also measured by using positron emitting nuclides. When lattice defects are present, positrons trapped by them have a lifetime different from a normal value due primarily to the fact that trapped positrons sample a different population of electrons in the process of annihilation than do free positrons. The trapped positrons also sample a different distribution of the electron momenta and hence the Doppler broadening changes accordingly.

Regarding the choice of a proper positron-emitting nuclide and preparation of a source for lifetime measurement, some problems persist. It is highly preferable that the fraction of annihilation in a source itself or a material which supports the source is negligible. Furthermore, the physical and chemical state of the source should remain stable against various environmental changes which the specimen-source hybrid may experience during heat treatments, *e.g.*, quenching and annealing, or measurements of the lifetime as a fuction of temperature from cryogenic to high temperatures. One way to obtain a stable source of a negligible self-annihilation fraction is an internal-source method, where a proper amount, say 10^5 Bq of positron emitting nuclides are induced within a specimen itself by using a proper nuclear reaction. For lifetime measurements this method has great advantages of stability and absence of self-annihilation, but is only applicable to a few limited cases because it is rare to find a suitable nuclides to be induced in a specimen of interest by any nuclear reactions. Another difficulty is the effect of incident particles on a target specimen. The effects of radiation damage and gas bubbles become a serious problem. Particularly, in the case of α or ^{3}He irradiations, it is very hard to completely remove helium gas bubbles from a specimen without melting. We have developed a more convenient and practical type of thin foil source for the lifetime and lineshape measurements, using ^{48}V as a positron emitting nuclide. ^{48}V was induced in a 1 μm Ti foil with ^{48}Ti(p,n)^{48}V by the cyclotron.

A stack of ten sheets of commecially available Ti foil of 1 μm in thickness was irradiated with a proton beam of 16 MeV. The yield of ^{48}V per sheet was 6×10^3 Bq/μA$\cdot$h$\cdot$cm^2. After cooling off for a few days, the Ti foil containing ^{48}V was used in positron experiments. For a positron lifetime measurement, the birth signals of positrons are required, so that all the β^+-decay nuclides cannot be used as a positron source for the measurement. Fortunately, the disintegration scheme of ^{48}V enables one to perform the lifetime measurement. As the birth signal, one of two gamma-rays with energies of 1.31 and 0.98 MeV is available.

From preliminary lifetime measurements, the following superior points of the developed source were found: (1) the negligible fraction of annihilation in the source itself, (2) no mixing of long-lived components, (3) very high stabilities for the use at high temperature, in liquid metals and so on. The present development of a new source will expand the utility of positron techniques to various types of materials and environmental conditions.

RIKEN Accel. Prog. Rep. 23 (1989)

III-3-7. No-Carrier-added Radiobromination with ^{75}Br and ^{77}Br and Their Application to Neuro-Receptor Imaging in Nuclear Medicine

M. Suehiro* and M. Iwamoto

We have been studying various no-carrier-added-radiobromination methods for labeling of neuro-receptor-imaging agents.

Of these methods, a Gattermann reaction was successfully applied to the synthesis of a neuroleptic drug bromoperidol. A small amount of freshly-prepared copper powder plays a key role to allow a tracer-amount of no-carrier-added radiobromine to react very efficiently with diazonium salts of aminoperidol and to give a high radiochemical yield with high reproducibility. This is interesting because the Gattermann reaction with stable bromine usually gives a lower yield than a Sandmeyer reaction, whereas use of the Sandmeyer reaction for no-carrier-added radiobromination was found to be unsuccessful.[1] This difference is worth of further investigation.

Electrophilic no-carrier-added radiobromination by Chloramine T has also proved to be a good method for such a practical purpose: the reaction proceeds fast and irreversibly. However, chlorination occurs simultaneously, resulting in the formation of chlorinated compounds which have similar chemical structure and similar biological activity to no-carrier-added-radiobrominated compounds. We carefully studied the two reactions, *i.e.* bromination and simultaneously-occurring chlorination by Chloramine T, found the factors which regulate the rates of these reactions, and could determine the optimal conditions where bromination proceeds fast while chlorination occurs slowly.

Using this electrophilic radiobromination method, we succeeded in labeling a buthyrophenone neuroleptic drug, spiperone with ^{75}Br and ^{77}Br.[2]

These no-carrier-added-radiobrominated compounds were applied to the neuro-receptor imaging in nuclear medicine. Animal studies were performed to obtain the imformation on a structure-activity relationship. While bromospiperone gave high striatum-to-cerebellum retios, bromoperidol, which is also a buthyrophenone drug, failed not only to give high striatum-to-cerebellum ratios but also to show a wash-out effect by a large amount of unlabelled spiperone. However, unlike radioiodinated amphetamine analogues, the radiobrominated bromoperidol showed a dose-dependent saturation in terms of the brain-uptake.

References

1) M. Suehiro, F. Yokoi, T. Nozaki, and M. Iwamoto: *J. Label. Comp. Radiopharmaceut.*, **24**, 1143 (1987).
2) M. Suehiro, F. Yokoi, I. Arai, T. Nozaki, and M. Iwamoto: *Int. J. Appl. Radiat. Isotopes*, Submitted for publication.

* Tokyo Metropolitan Geriatric Hospital

RIKEN Accel. Prog. Rep. 23 (1989)

III-3-8. Production of Tracers, Their Application, and Search for New RI Probes Using a RIKEN Ring Cyclotron Beam

S. Ambe, Y. Ohkubo, M. Iwamoto, Y. Kobayashi,
M. Yanokura, and F. Ambe

Radioactive tracer technique is widely used in various fields of science, technology, and medicine. However, there are not a few elements for which radioactive nuclides suitable as a tracer can not be produced with conventional accelerators and reactors. A wide variety of radioactive nuclides can be produced by irradiation with a high-energy heavy-ion beam available from RIKEN Ring Cyclotron.

We aim to establish radiochemical methods for the production of tracers and multitracers and to employ them in solving various environmental and medical problems of the day.

As the first experiment along this line, Al, Cu, and Ag foils mounted in a ball were irradiated with a 26 MeV/u $^{40}Ar^{13+}$ beam in a falling-ball irradiation system installed in the E3 beam course.[1] After irradiation, balls were transported down to the hot laboratory. Non-destructive γ-ray spectra of reaction products were taken with Ge detectors, and then Cu and Ag targets were dissolved in nitric acid. The target elements were removed rapidly by precipitation as CuSCN and AgCl, respectively, to give solutions containing a number of carrier-free radioactive nuclides ready to be used as tracers.

The adsorption isotherms for the tracers was studied as follows. The solutions adjusted to given pH's were added with α-Fe_2O_3. After shaking the suspensions, α-Fe_2O_3 was removed by centrifugation. An aliquot of the supernatant was subjected to γ-ray measurement. Thus, the adsorption isotherms of a number of elements were determined simultaneously under the same experimental conditions. Results are now being analyzed.

References

1) M. Yanokura, Y. Ohkubo, S. Ambe, M. Iwamoto, and F. Ambe: *RIKEN Accel. Prog. Rep.*, **22**, 150 (1988).

RIKEN Accel. Prog. Rep. 23 (1989)

III-3-9. Segregation Coefficient of Carbon, Boron, and Oxygen in GaAs Crystal

Y. Itoh, Y. Kadota, H. Fukushima, and K. Tachi

It is important to control and suppress residual impurities such as carbon, boron, and oxygen in a LEC (liquid encapsulated Czochralski)-GaAs crystal.[1] In the LEC method, where molten GaAs is covered with a boric oxide encapsulant in a pyrolytic boron nitride crucible, and heated by a graphite heater. In this case, carbon, boron, and oxygen get into or out of the GaAs melt, and are not segregated into the GaAs crystal according to the normal freezing prosess. Therefore it is difficult to estimate the equilibrium segregation coefficients based on the distributions of these impurity concentrations.

Since the equilibrium segregation coefficients are indispensable to control the concentrations of these impurities in LEC GaAs crystal, we carried out the present study. Samples were prepared as follows. The GaAs ingot was cooled down rapidly at the solidified fraction of 0.5 and cut from the tail portion of the GaAs single crystal ingot and the remainder. The equilibrium segregation coefficient (k_0) can be obtained from the impurity concentrations of the tail portion (C_s) and the remainder (C_L), *i.e.* $k_0 = C_s/C_L$.

The concentrations of carbon and boron were measured by infrared spectrophotometry and secondary ion mass spectroscopy, respectively. Calibration factors were obtained with standard samples in which carbon and boron concentrations were known from deuteron activation analysis.[2-4] Oxygen concentration was determined directly by charged particle activation analysis.[5,6] Table 1 shows the results of the impurity analysis and the equilibrium segregation coefficients.

Recently, Clemans and Conway reported 2.1 ± 0.6 for k_0 of carbon using GaAs crystal grown by a vertical gradient freeze (VGF) growth method.[7] The good agreement of the value for carbon suggests that our method for the determination of k_0-values for boron and oxygen in LEC-GaAs crystal is reliable.

Table 1. Equilibrium segregation coefficients of carbon, boron and oxygen in LEC-GaAs.

Impurity	Method	Concentration (atoms/cm^3)		Segregation coefficient
Carbon	FTIR	Crystal	1.0×10^{14}	2
		Remainder	0.4×10^{15}	
			0.5×10^{15}	
Boron	SIMS	Crystal	2.8×10^{16}	1~4
			2.9×10^{16}	
		Remainder	6.1×10^{15}	
			2.2×10^{16}	
Oxygen	CPAA	Crystal	7.2×10^{15}	0.06~0.13
			1.1×10^{16}	
		Remainder	8.6×10^{16}	
			9.1×10^{16}	
			1.3×10^{17}	

References

1) L.B. Ta, H.M. Hobgood, A. Rehatgi, and R.N. Thomas: *J. Appl. Phys.*, **53**, 5771 (1982).
2) T. Nozaki, Y. Itoh, Y. Ohkubo, T. Kimura, and H. Fukushima: *Jpn. J. Appl. Phys.*, **24**, L801 (1985).
3) Y. Itoh, Y. Kadota, T. Nozaki, H. Fukushima, and K. Takeda: *ibid.*, **28**, 210 (1989).
4) Y. Kadoto, K. Sakai, T. Nozaki, Y. Itoh, and Y. Ohkubo: Semi-Insulating III-V Materials, Ohmusha, Tokyo, p. 201 (1986).
5) T. Nozaki: *J. Radional. Chem.*, **72**,527 (1982).
6) H. Fukushima, T. Kimura, H. Hamaguchi, T. Nozaki, Y. Itoh, and Y. Ohkubo: *J. Radioanal. Nucl. Chem. Artric.*, **112**, 415 (1987).
7) J.E. Clemans and J.H. Conway: Semi-Insulating III-V Materials, Ohmusha, Tokyo, p. 28 (1988).

RIKEN Accel. Prog. Rep. 23 (1989)

III-3-10. Improved Chemical Procedure for the Determination of Oxygen in Gallium Arsenide

H. Kirita, H. Fukushima, Y. Itoh, and K. Tachi

Charged-particle activation analysis is one of the most sensitive methods for trace carbon, nitrogen, and oxygen. We have assayed trace amounts of oxygen in a high purity gallium arsenide semiconductor.[1] When the oxygen concentration in gallium arsenide exceeds 10^{17} atoms/cm^3, we can ignore the radiochemical impurity. For the samples of lower oxygen concentrations of about 10^{15}atoms/cm^3, however, we cannot ignore the radiochemical impurity. We thus improved our chemical procedure to give satisfactory results.

To this end, the nuclear reaction, $^{16}O(^3He,p)^{18}F$, was used. The chemical procedure for ^{18}F separation is shown in Fig. 1, where double parentheses represent improved procedures. A suction pump is used for filtration.

Since ^{70}As, ^{72}As, and ^{76}Br are considered to be radiochemical impurities, the following points in our old method were improved. In order to prevent the adsorption of ^{70}As and ^{72}As on precipitated KBF_4, arsenite as a hold-back carrier was added. For fear that the microparticles of AgBr precipitate would leak to a filtrate, a filter paper, TOYO No. 5C, was replaced with a membrane filter of 0.45μm pore size.

As a result, the decay of the activity in precipitated KBF_4 agreed with the half life of ^{18}F, 109.8 min. Moreover no difference between the background activity and the activity 24 hours after the start of measurement was observed. Therefore we conclude that enough radiochemical purity of KBF_4 precipitate was obtained.

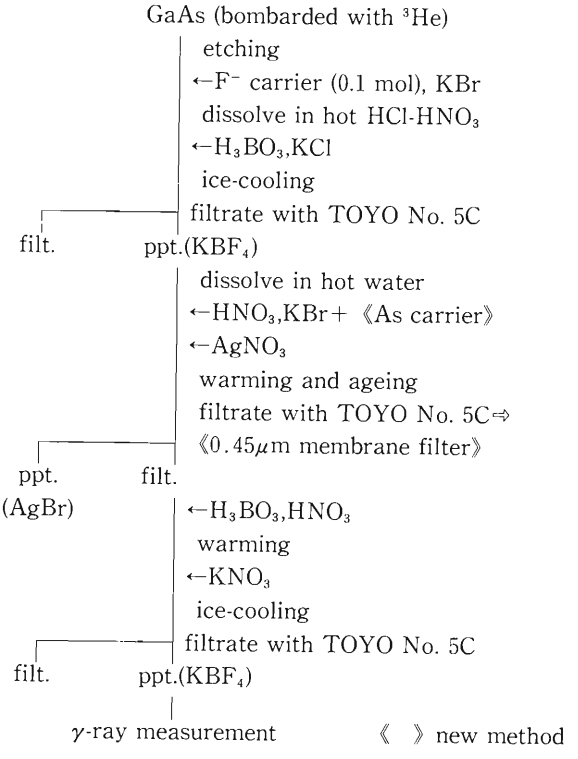

Fig. 1. Chemical Separation of ^{18}F.

References

1) H. Fukushima, T. Kimura, H. Hamaguchi, T. Nozaki, Y. Itoh, and Y. Ohkubo: *J. Radioanal. Nucl. Chem., Artic.*, **112**, 415 (1987).

RIKEN Accel. Prog. Rep. 23 (1989)

III-3-11. Elastic Recoil Detection Analysis of the Hydrogen Contents in Diamond-like Carbon Films

M. Minami, M. Aratani, M. Yanokura, and S. Okada

Diamond-like carbon (DLC) films are deposited on the surface in C-containing gases by chemical vapor deposition (CVD). Their physical properties are similar to those of a diamond: high hardness, high thermal conductivity, high electrical resistivity, optical transparency, and low friction coefficient. Attention has been paid on relationships between the hydrogen contents in the DLC films and their properties.

Measurement of hydrogen contents was made on the DLC films (150-500 nm) prepared from methane and ethylene by using electron cyclotron resonance (ECR) plasma CVD[1] on silicon substrates. Elastic recoil detection analysis (ERDA) was performed for measuring hydrogen contents with argon ions accelerated at 50 MeV with RILAC.[2]

A scattering chamber (100 cm in diameter) on the RILAC A-1 beam line was used. At the center of the chamber, the specimens were set up at an angle of 30° to an incident beam. Tow surface-barrier semiconductor detectors (SSD) were arranged at an angle of 35° (SSD-1) and at 50° (SSD-2) to the incident beam. In front of the SSD-1, an aluminium foil (10 μm) was located to detect only carbon and hydrogen ions by stopping recoiled silicon and scattered argon ions in the foil. The spot size of the incident ion beam was 2 mm×2 mm on the specimen.

Figure 1 shows the yields of recoiled carbon and hydrogen as a function of recoil energy. Contents were calculated from these yields by using scattering cross sections.[3] Results for three kinds of samples shown in Table 1 show that the hydrogen content in the DLC films is lower than those in soft polymer-like carbon films. We have concluded that the hydrogen content in the DLC film prepared from ethylene is lower than that from methane.

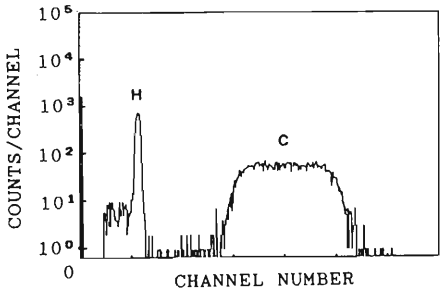

Fig. 1. ERDA spectra of recoiled carbon and hydrogen ions (SSD-1).

Table 1. Hydrogen contents in carbon films.

	Starting gas	Deposit rate (nm/min)	Hardness (kg/mm²)	H Contents (at%)
Polymer-like carbon films	CH_4	15.5	100	35~45
Diamond-like carbon films	CH_4	7.5	2,150	20~26
	C_2H_4	22	2,300	16~24

References

1) S. Okada, M. Hayakawa, S. Morishima, and S. Kunishima: 11th Int. Vacuum Congr. Köln, Sep. (1989).
2) H. Nagai, S. Hayashi, M. Aratani, T. Nozaki, M. Yanokura, I. Kohno, O. Kuboi, and Y. Yatsurugi: *Nucl. Instrum. Methods B*, **28**, 59 (1987).
3) J.F. Ziegler (Ed.): Handbook of Stopping Cross Sections for Energetic Ions in All Elements, Pergamon Press, New York (1980).

RIKEN Accel. Prog. Rep. 23 (1989)

III-3-12. Multielement Depth Profiling of Multilayered Systems

M. Aratani, M. Yanokura, M. Minami, and K. Saito*

Multilayered systems have recently been used widely for electronic devices, for example, ohmic contacts and Schotoky barriers. Material distributions in such systems are fairly complicated to be examined by conventional analytical techniques.

We applied a heavy-ion probe Rutherford scattering method to the study of the material distributions in multilayered systems Cu/Pd/Ni/Ti/Si (substrate). Detectors were located at both forward and backward angles for ions recoiled and scattered by ~10 nA 50-MeV Ar^{4+} incident ions from RILAC. Nine samples mounted on a ladder-type holder were installed at the center of a scattering chamber at angles of 20°-30° against the incident beam. The present report describes the change in the material distribution of this system after heat treatment at medium temperatures.

After heat treatment the initial spectrum of forward scattered ions (Fig. 1a) changed to that shown in Fig. 1b. In both spectra the scattered ions from the Cu surface appear at the same scattered energy, *i. e.*, at a channel number of 334 ch, because no energy loss takes place at the surface. Therfore, the high energy side of the second peak (around 340 ch) corresponds to the outermost Cu surface, and the low energy side of the peak corresponds to the Cu/Pd interface. The Pd layer under the Cu layer is observed as the first peak (around 395 ch), the high energy of which corresponds to the Pd/Cu interface. Therefore, the Cu/Pd interface phenomena such as atomic mixing and interfusion would be observed through the changes at these two positions in

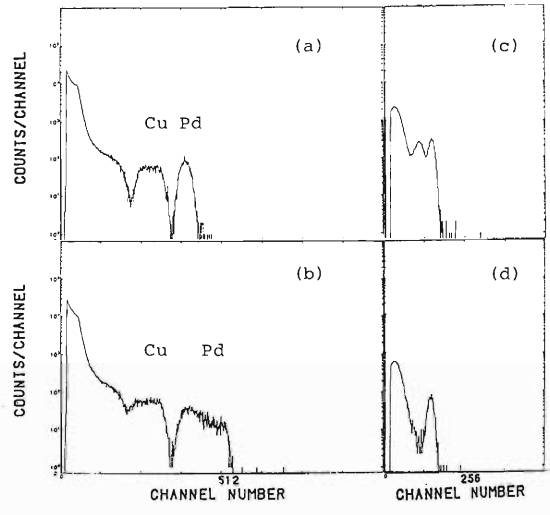

Fig. 1. Energy spectra for forward (75°) scattered ions before (a) and after (b) heat treatment, and for forward (50°) recoil hydrogen ions (15 μm Al absorber) before (c) and after (d) heat treatment form Cu/Pd/Ni/Ti/Si (20°).

the spectra. After heat treatment, the highest energy of the peak shifts to a higher channel. A standard sample of Pd foil reveals that the position corresponds to the Pd surface. Consequently we conclude that Pd atoms diffuse through the Cu layer and reach the Cu outermost surface, but no Pd atoms diffuse into the Pd layer.

Hydrogen atoms are also observed as an impurity. Hydrogen profiles before and after heat treatment are shown in Fig. 1c and Fig. 1d. Before treatment, hydrogen atoms distribute in the three layers, but after treatment, no hydrogen atoms are observed in the Pd layer.

* R&D Center, Toshiba Corporation.

RIKEN Accel. Prog. Rep. 23 (1989)

III-3-13. A New Technique for Preparation of an Enriched ^{100}Mo Disk of Very High Purity

I. Sugai,* M. Aratani, H. Kato,** M. Minami, and M. Yanokura

Neutrino physics requires enriched ^{100}Mo foils of very high purity to study double beta decay. The foils should not be contaminated with such radioactives as U, Th, and K.

We have developed a simple technique for preparation of a ^{100}Mo disk target with 50-80 mg/cm^2 in thickness and 30 mm in diameter. Chemically refined Mo powder was packed uniformly in a stainless-steel mold of 30 mm in diameter and carefully pressed in a vacuum. The Mo solid disk was then sintered in an electrical oven at 280-330°C for 13 hours in air.

The weight of the Mo disk increased by oxidation with heating temperature. We found that the quality of the Mo disk depends greatly on the degree of oxidation. After repeated sintering and pressing tests, we found that a Mo disk containing 3 % oxygen is mechanically strong. The key point in producing a pure and uniform ^{100}Mo disk target is also to use powder as fine as possible with rustling properties.

We measured the purity of Mo in the disks by an ERDA technique using a 50 MeV Ar^{4+} ion beam from the RILAC. Figure 1 shows the energy spectra of Ar ions scattered and light element ions recoiled from various disks. We can observe no elements other than oxygen and carbon on the curve shown in Fig. 1.

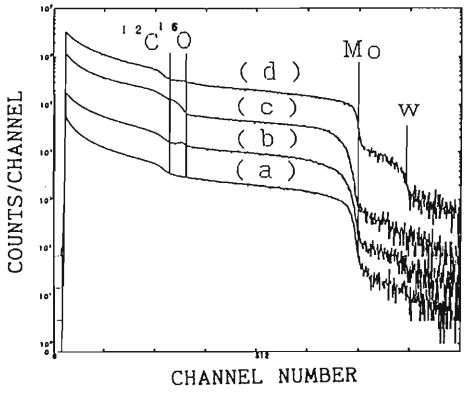

Fig. 1. Energy spectra of Ar ions scattered and light element ions recoiled from various disks. $E(Ar^{4+}) = 50$ MeV and $\theta_{Lab} = 52°$. Natural Mo disk targets prepared from metallic powder of 99.999 % purity not by sintering [curve (a)] and by sintering at 280°C [curve (b)], and from metallic powder of 99.95 % purity by sintering at 330°C [curve (c)]. An enriched ^{100}Mo foil obtained from Oak Ridge National Laboratory was also examined for comparison [curve (d)].

The Mo disks prepared by the present technique show extremely low contamination: 1.3 ppb U, 0.5 ppb Th, and 3.5 ppb K for the ^{100}Mo disk and < 0.5 ppb U, < 0.5 ppb Th, and < 0.5 ppb K for the natural Mo disk. Five disk targets of enriched ^{100}Mo and natural Mo prepared by the present method were successfully used for double-beta-decay neutrino experiments.

* Institute for Nuclear Study, University of Tokyo.
** Faculty of Education, Yamanashi University.

RIKEN Accel. Prog. Rep. 23 (1989)

III-3-14. Measurement of Light Element Contaminants in Superlong-Lived Carbon Stripper Foils

I. Sugai, M. Aratani, M. Minami, and M. Yanokura

Carbon stripper foils with long lifetimes are very important for cascade-type heavy ion accelerators. We have been developing long-lived carbon stripper foils by various methods aiming at high reproducibility and creditability.

Among many methods, controlled AC and DC arc-discharge (CADAD) method and an ion beam sputtering (IBS) method were found to be useful for the preparation of foils with very long lifetimes compared with an electron beam (E/B), commercialy available carbon foils (CM), and an old arc-discharge methods.[1,2] In particular, foils prepared by the IBS method showed as long a lifetime as 55 hours, which is about 110 times of that of a CM foil.

We call this special foil a supperlong-lived carbon stripper foil (SLLC). The lifetimes prepared by the IBS method, however, were widely distributed from maximum 55h to very short. The short lifetime results in very rapid rupture by irradiation.

We suppose that a main reason for the great difference in the lifetime of foils may be caused by the contamination of light elements such as hydrogen, oxygen, and nitrogen, and tried to search for such contaminants by ERDA (elastic recoil detection analysis) and RFS (Rutherford forward scattering) using a 50 MeV Ar^{4+} beam from the RILAC. In the present study carbon foils of 10-15 $\mu g/cm^2$ in thickness prepared by IBS and E/B were used, and CM foils are also used for comparison.

Figure 1 shows the typical spectra of these foils. We can clearly see the difference in the amounts of contaminations (oxygen and nitrogen) between foil (c) and foil (d) made by IBS using Kr^+ ion. No noticiable contaminations are seen between E/B (a) and CM (b) foils. Foil (d) was prepared from spectroscopically pure carbon rods and foil (c) from a standard pure carbon rod used as a supportor of a sputtering specimen. From the measurments the contaminations (oxygen and nitrogen) in foil (c) are estimated as approximately 3 $\mu g/cm^2$ for oxygen and 2 $\mu g/cm^2$ for nitrogen in thickness.

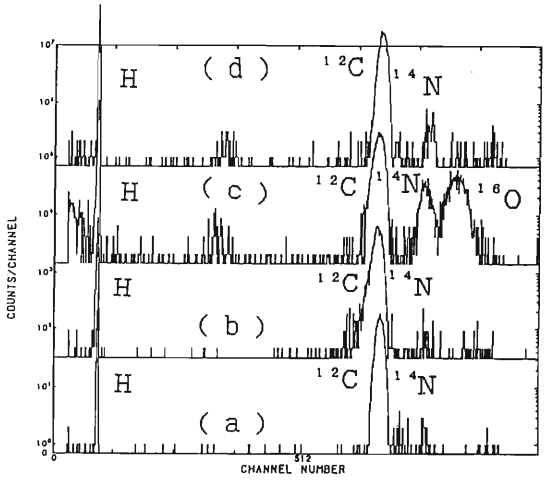

Fig. 1. Spectra of the particles scattered and recoiled from carbon foils ((a), E/B foil: (b), commercial foil: (c), IBS foil; and (d), IBS foil) at $E(Ar^{4+})=50$ MeV and $\theta_{Lab}=45°$.

These contaminations strongly affect the lifetime of carbon foils against the irradiation of high-intensity heavy ion beam. We also found traces of Fe and Ta, which come from the cavity of an ion-source and a thermal filament.

These results suggest that the foils prepared by IBS using Kr^+ present a clue for the preparation of superlong-lived carbon stripper foils.

References

1) I. Sugai *et al.*: *Nucl. Instrum. Methods*, **A236**, 576 (1985).
2) I. Sugai *et al.*: *ibid.*, **A251**, 596 (1986).

RIKEN Accel. Prog. Rep. 23 (1989)

III-3-15. Analysis of Deuterium in Palladium Electrodes by Heavy-Ion Rutherford Scattering

M. Yanokura, M. Minami, S. Yamagata, S. Nakabayashi,
M. Aratani, A. Kira, and I. Tanihata

Deuterium contents in palladium electrodes during or after electrolysis are crucial for so-called cold nuclear fusion in a test tube.[1,2] Electrodes used as a cathode for electrolysis of heavy water (D_2O) were analyzed by a heavy-ion Rutherford scattering method[3] in order to determine the deuterium content and the depth profile.

A hydrogen (H) signal prodominated in the electrodes etched with sulfuric acid and electrolyzed in a D_2O solution of $PdCl_3$, although the solution contained H_2O of less than 1 per cent. This finding indicates that hydrogen atoms can penetrate inside, but deuterium atoms cannot under this condition of surface teatment.

The successful method for surface treatment and pre-loading of deuterium is as follows. Electrodes were heated to 420°C in a vacuum of 10^{-6} torr for 2 h, equilibrated with 1 atm deuterium gas at 420°C for 1 h, and left for cooling for several hours. The electrodes were kept in heavy water after the treatment and also after electrolysis.

The electrodes thus treated showed a deuterium signal which was not accompanied by a hydrogen signal. Figure 1 shows the contents of deuterium as a function of the depth from the surface. The atomic ratio of deuterium to paradium is about unity in the electrode before electrolysis. After electrolysis for 120 h, the ratio increases to about 1.5, indicating that electrolysis promotes the accumulation of deuterium in palladium. The data for the unelectrolyzed electrode kept in a vacuum give a rough estimation for a loss of deuterium atoms from the surface layer due to diffusion.

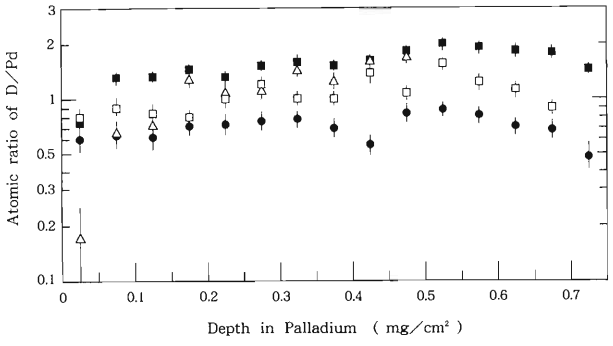

Fig. 1. Depth profile of deutirium in palladium plates.
□ pre-loaded with D_2 gas before electrolysis.
● kept in vacuum for 1 week.
■ kept in heavy water after electrolysis.
△ kept in the atomsphere after electrolysis.

References

1) M. Fleischmenn, S. Pons, and M. Hawkins: *J. Electroanal. Chem.*, **261**, 301 (1989).
2) S.E. Jones, E.P. Palmer, J.B. Czirr, D.L. Decker, G.L. Jensen, J.M. Thorne, S.F. Taylor, and J. Rafelisk: *Nature*, **338**, 737 (1989).
3) H. Nagai, S. Hayashi, M. Aratani, T. Nozaki, M. Yanokura, and I. Kohno: *Nucl. Instrum. Methods Phys. Res.*, **B28**, 59 (1987).

RIKEN Accel. Prog. Rep. 23 (1989)

III-4. Radiation Chemistry and Radiation Biology

1. High-Density Excitation by Heavy Ions: Track-Depth Resolved Emission Measurement Using a Micro Track Scope

K. Kimura, S. Yanagishita, and F. Sano

Stopping power data is only one knowledge by which one can estimate the extent of change in matter produced by ion iradiation. However, the stopping power give us neither knowledge on the density effect of intermediates nor the change of excitation processes with the change in ion energy, though this knowledge is decisively important in the low-energy region near the track termination where high-density excitation and new excitation processes may play an important role. We developed a micro track-scope which enables us to obtain the stopping power dependency of excited states, their interaction and dynamics, particularly near track termination.

Previously, we have measured track depth-resolved emission spectra, specific emissions (dL/dx) and efficiencies (dL/dE), and their decays along a 5 MeV/amu N-ion ion track in dense helium gas at 400 Torr and 5 K (density of helium was 0.006 g/cm^3 and the track length was 11 mm).[1,2] Helium gives relatively high emission yields under high-density excitation and hence is the most appropriate sample. One of results is that dL/dE increases still along the track with dercreasing stopping power after its maximum value. Is this result explicable by $dE/(r^2dx)$ or by increase in the probability of direct excitation and charge exchange? Is this correlated with new emission bands observed?[3] From what excitation density does the quenching begin? The depth resolution of about 0.1 mm of the previous methods was too crude to analyze the region near the maximum stopping power in detail.

Thus, we developed a new simple track-scope for the precise observation of UV- and UVU-emission intensities with much denser samples. The scope is composed of a square bundle of 10,000 quartz fibers of 2×2 mm^2 in diameter. The terminal of the array was set close (0.1 mm) laterally to the tracks of collimated ions of a cross section of 0.1×2 mm. The image was measured at another terminal by a position-sensitive photoncounter connected with an on-line computer. An experimental system was already reported in a previous report.[4]

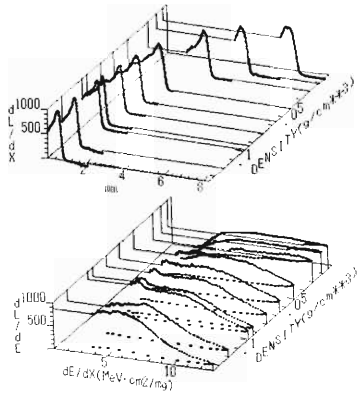

Fig. 1. Density dependences of dL/dX *vs.* track-depth and dL/dE *vs.* dE/dX 5 MeV N-ion tracks in helium. A junction of a lateral bar and the curve indicates an incident point of ions. All the curves are adjusted into the equal peak height.

Figure 1 illustrates dL/dE *vs.* dE/dx for visible emission as a function of the density of helium (helium is liquefied at 0.12 g/cm^3 at present temperature). It is a remarkable phenomenon that dL/dE has a plateau or increases near the track termination, considering that usual scintillators are quenched thoroughly in the corresponding range. In addition, dL/dE was dependent on the helium density and maximum near 0.06 g/cm^3. These results indicate that effective excitation processes other than what are contained in the calculation of the stopping power become important. These effective processes seem to be direct excitation and charge exchange processes.

References

1) K. Kimura: *J. Chem. Phys.*, **84**, 2002 (1986).
2) K. Kimura: *ibid.*, **84**, 2010 (1986).
3) K. Kimura, M. Kataoka, T. Azuma, Y. Ito, Y. Tabata, and Y. Aoki: *Phys. Lett. A*, **133**, 91 (1988).
4) K. Kimura, T. Yoshida, S. Imai, T. Nakamura, and N. Hamada: *RIKEN Accel. Prog. Rep.*, **21**, 137 (1987).

RIKEN Accel. Prog. Rep. 23 (1989)

III-4-2. Production of Makrofol Microfilters by ^{14}N Ion Irradiation

N. Nakanishi, Y. Kaneta, and S. Wakasa

Energetic charged particles give radiation damage to materials and, at the same time, leave latent tracks in them. The nuclear tracks registered in plastics have been used for identification of particles and their energies by chemical etching.

It is also known that pierced pores are observed in thin polymers bombarded with ions after chemical etching. We have applied the phenomenon to form microfilters, which are widely used in various fields such as chemical, food, medical and other industries.

Although fission fragments or accelerated heavy ions have been used for microfilter formation, we used 22 and 15 MeV ^{14}N beams from RILAC, because these beams are also available using a compact cyclotron. Polycarbonates, Makrofol of 10 and 20 μm in thickness were irradiated and chemically etched in a 6 N NaOH solution at 70°C. No satisfactory results have been obtained because of a relatively low Z/β of around 130. However, it was recognized that UV exposure after irradiation was very efficient in making pores in Makrofol films. One of good results is shown in Fig. 1.

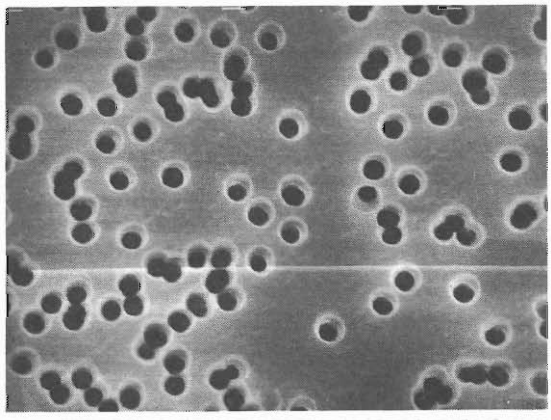

Fig. 1. Scanning electron micrograph of etched pores in a 10 μm MAKROFOL irradiated by 15 MeV $^{14}N^{3+}$ ions. Magnification ×5000.

RIKEN Accel. Prog. 23 (1989)

III-5. Instrumentation

1. A Proposal for Collinear Laser Spectroscopy of Refractory Elements

T. Murayama, M. Azuma, T. Inamura, T. Ishizuka, H. Katsuragawa,
M. Koizumi, S. Matsuki, Y. Matsumoto, K. Morita, I. Nakamura,
K. Shimomura, I. Sugai, and M. Takami

Collinear fast-beam laser spectroscopy has been very successful in studying nuclear radii and nuclear moments for the long isotopic chain of various elements in combination with isotope separators.[1] However, refractory elements such as Hf, W, and Os, which are of interest to study because of their high spin isomers and possible shape transitions, are currently inaccessible by using isotope separators with thermal ion sources.

Recently an ion-guided isotope separator (IGISOL) has been constructed at the Ring Cyclotron facility.[2] This machine easily provides the isotope-separated radioactive beams of refractory elements. We have designed an apparatus for the collinear laser spectroscopy, which will be installed at the straight section of one of the IGISOL beam lines. The schematic arrangement of experimental setup for the collinear laser spectroscopy is shown in Fig. 1. The apparatus is composed of a charge exchange cell, an LIF (Laser Induced Fluorescence) detection region, and an RIS (Resonance Ionization Spectroscopy) detection region. A laser beam will be delivered from the laser facility[3] to the experimental vault through a 160 meter-long optical fiber. The setup is designed to utilize a coincidence technique with atomic beams.[4]

First we shall study the energy spread of isotope-separated beams from the IGISOL by changing its skimmer potential. For this purpose a spark-type ion source is installed in the target chamber of the IGISOL. We measure the energy spread by observing the Doppler broadening of the flurescence spectrum of the transition ($3d'^2G_{9/2} \rightarrow 4p^2F_{7/2}$, $\lambda = 611.6$ nm) of meta-stable Ar^{+1} ion beams. The other candidate of test ion beams is lithium. In this case the strong transition ($1s2s^3S_1$ $F=5/2 \rightarrow 1s2p^3P_2$ $F=7/2$, $\lambda = 548.5$ nm) of meta-stable $^7Li^{+1}$ ion can be used.

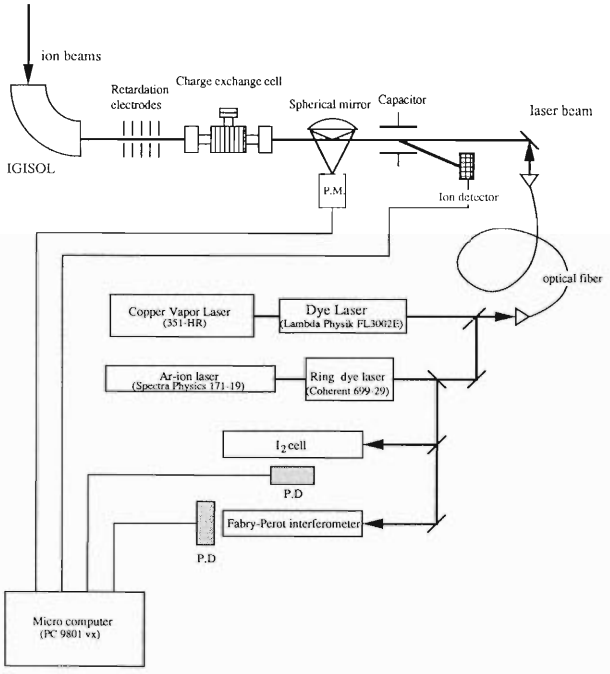

Fig. 1. Schematic diagram of the experimental setup of collinear laser spectroscopy at the Ring Cyclotron facility.

References

1) E.W. Otten: "Treatise on Heavy-Ion Science", Plenum Press, New York, Vol. 8, p. 517 (1989).
2) K. Morita, T. Inamura, K. Valli, T. Noumura, J. Tanaka, H. Miyatake, K. Sueki, Y. Hatsukawa, M. Fujioka, T. Shinozuka, K. Taguchi, H. Kudo, Y. Nagai, T. Tomiyama, H. Hama, M. Yoshii, and K. Furuno: *RIKEN Accel. Prog. Rep.*, **21**, 155 (1987).
3) T. Murayama, M. Takami, Y. Matsumoto, and T. Inamura: *ibid.*, **21**, 174 (1987).
4) D.A. Eastham, P.M. Walker, J.R.H. Smith, J.A.R. Griffith, D.E. Evans, S.A. Wells, M.J. Fawcett, and I. S. Grant: *Opt. Commun.*, **60**, 293 (1986).

RIKEN Accel. Prog. Rep. 23 (1989)

III-5-2. Low Energy Radioisotope Beam Channel "SLOW" for Surface Studies

T. Matsuzaki, K. Ishida, and K. Nagamine

A new type of low energy radioisotope beam channel "SLOW" has been developing in the E7 experimental area of RIKEN Ring Cyclotron (RRC). We will be able to use the SLOW beam channel for the studies of emission mechanisms of various low energy radioactive atoms from characterized surfaces and for the extraction of useful radioactive ions for surface-physics studies.

A heavy ion-induced nuclear reaction can produce many kinds of radioisotopes in a target at the same time. Part of the radioisotopes moderate to be rest in the target and could reach to the target surface by thermal diffusion. At the surface, the radioactive atoms could evaporate into a vacuum and could be ionized through various ionization mechanisms deeply correlated to the surface conditions.

The details of the basic design, its construction, and experimental program are described in Ref 1. Almost all the construction work of SLOW has been finished. At present, we are making a fine tuning of SLOW.

In order to decrease a residual magnetic field to less than 0.1 gauss, a magnetic shield around a SLOW beam line was constructed. A low magnetic field along the SLOW beam line is necessary for beam optical tuning using a thermal electron. The thermal electron will be produced by a hot tungsten filament and be accerelated to 10 keV. The beam line components will be tuned by the 10 keV electron beam. As described in Ref. 1, SLOW is composed of electrostatic lenses, and the beam optical conditions depend upon not a mass but only an electric charge for transporting ions. Therefore, we can do a beam tuning for negative-charged ions by this tuning and can get an optimum condition also for positive ions after changing the polarities of all electrodes of the components. In addtion, the experimental room "E7" is located beside the RRC accerelator room and beneath the AVF cyclotron injector room. The maximum magnetic field was found to be about 2 gauss for one direction at a SLOW beam channel, when the RRC was operated.

A high vacuum of 4×10^{-9} Torr was attained after long evacuation with a turbo-molecular pump and cryo-pump, without an outgassing procedure by baking. A baking heater was already wounded around the SLOW beam line. We have made a temperature control system for the baking procedure to keep the temperature of vacuum components by on/off control. A final vacuum test is scheduled after the baking procedure.

Slow is equiped with several instruments for surface characterization and treatment: a LEAD/AUGER spectrometer, a 5 keV Ar ion gun and an electric quadrupole mass spectrometer. They are installed above the target position of SLOW. These instruments were operated to prove their specifications.

At the end of SLOW, a multi-channel plate (MCP) will be installed to detect ions transpoted through the SLOW beam line. We have made a vacuum chamber to check an MCP by using a thermal electron beam. A test experiment of MCP is now in progress.

For the remote control of high voltage for electrodes of the beam line components, we have improved five main high voltage power supplies and newly bought six main power supplies. The remote control will be realized by supplying DC voltage (0-10V) to a main power supply from the control room.

We are now designing a pre-chamber, where we can treat and chracterize the surface of samples, independent of the main vacuum of the SLOW beamline.

References

1) T. Matsuzaki, K. Ishida, and K. Nagamine: *RIKEN Accel. Prog. Rep.*, **22**, 155 (1988).

RIKEN Accel. Prog. Rep. 23 (1989)

III-5-3. Thickness Uniformity Measurements of Large Area SSDs for Cosmic Ray Heavy Ion Telescope

T. Imai, T. Kohno, K. Munakata, A. Yoneda, and C. Kato

We have developed a cosmic ray heavy ion telescope having a very large geometric factor. The objectives of our observation are elemental and isotopic aboundances of galactic cosmic rays and solar energetic particles up to Fe/Ni nuclides. For our first experiment using RIKEN Ring Cyclotron, a N-beam of 42 MeV/u was used for the detector array shown in Fig. 1. The first two PSDs (Position Sensitive Detector) are two dimensional charge division type SSDs. Four PIN type energy detectors follow them.

In use of a $\Delta E \times E$ method for particle identification, the thickness uniformity of a ΔE detector is essential for the resolution of the telescope. We used a penetrating N-beam to measure the thickness uniformity, of the detector. Because the range of N-ions with an energy of 42 MeV/u is 2.6 mm in silicon, all N-ions entering the telescope shown in Fig. 1 stop in the last detector, PIN4.

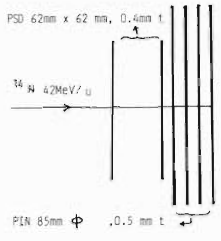

Fig. 1. Detector array for the experiment.

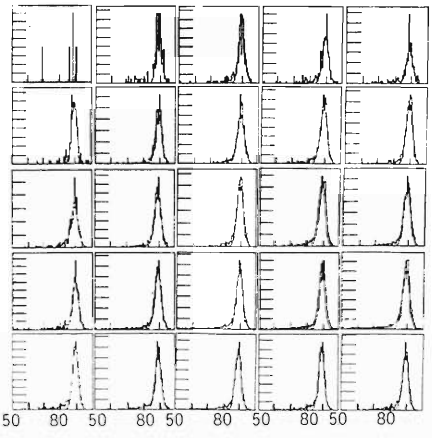

Fig. 2. Pulse height distributions of PIN1 in each mesh for 1/4 of the whole area.

Since energy straggling after PIN3 is large, we survey the pulse height distribution of PIN1 here. Using the information of PSD, we divided the position in the PSD into 10×10 meshes with each mesh size of 6.2 mm × 6.2 mm.

Shown in Fig. 2 are the pulse height distributions of penetrating N-ions in each mesh for 1/4 (5×5 meshes) of the whole area. The peak energies in each mesh are shown in Table 1. They are shown in % value of deviation from the mean value of the whole area. The pulse height distributions shown in Fig. 2 correspond to 1/4 of the upper-left of Table 1. The meshes where no sufficient events was obtained due to a beam profile are indicated as 100 %.

If these values represent the typical detector thickness in each mesh, almost all the meshes are within 0.5 % in thickness (standard deviation is 0.23 %). Our requirement for the thickness uniformity to indentify Fe isotopes is less than 0.5 % in FWHM. The width of each distribution, however, is about 30 % wider than the value expected from theoretical energy straggling. We consider that these distributions are not due to fine non-uniformity in each mesh, but due to some other reason.

Table 1. Peak energies of whole meshes represented by percent value deviation from the mean of the whole area.

% to AV. Energy = 89.09 MeV									
-100.00	0.20	0.27	0.19	-0.42	0.02	-100.00	-100.00	-100.00	-100.00
0.28	0.30	0.11	-0.01	0.07	0.08	0.14	0.19	-100.00	-100.00
0.39	0.22	0.18	0.04	0.05	0.05	0.08	0.27	-100.00	-100.00
0.54	0.32	0.22	0.21	0.14	0.16	0.09	0.02	0.45	-100.00
0.33	0.31	0.22	0.19	0.18	0.10	-0.01	-0.09	0.00	-100.00
0.27	0.04	0.19	0.08	0.15	-0.09	-0.07	-0.16	-0.15	-100.00
-0.07	-0.01	-0.08	-0.03	-0.07	-0.30	-0.38	-0.45	-0.53	-100.00
-0.09	-0.16	-0.19	-0.24	0.00	-0.37	-0.33	-0.73	-0.63	-100.00
-0.44	-0.32	-0.37	-0.33	-0.28	-0.39	-0.42	-0.23	-100.00	-100.00
-100.00	-0.22	-0.74	0.07	-0.32	-100.00	-100.00	-100.00	-100.00	-100.00

RIKEN Accel. Prog. Rep. 23 (1989)

III-5-4. Development of a Multiwire Drift Chamber for the Measurements of Proton Spectra

Y. Yashiro, H. Shimizu, M. Yosoi, and H. Ohnuma

We have made a new detector to measure energy spectra of protons. This detector features general-purpose utility, a large solid angle, and easiness of repair.

An exploded view of the detector is shown in Fig. 1. It consists of four anode frames (B, D, F, and H) and five cathode frames (A, C, E, G, and I), all made from aluminum. Each anode frame is 55×55 cm^2 in area and 2cm in thickness, and each cathode frame is 3mm in thickness, 62×62 cm^2 in area for A and I and 57×57 cm^2 for C, E, and G. All frames have an active area of 47×47 cm^2. The two external frames (A and I) are covered, on the outer surface, with 25 μm thick aluminized Mylar windows, and the inner surfaces of these frames and the both surfaces of other three cathode frames (C, E, and G) are covered with 12.5 μm thick Kapton films on which copper and chromium were deposited. Twenty-four anode wires and 24 field-shaping wires were connected to each anode frame alternately with a 1 cm spacing with a feed through (plastic connector). The anode wires are 20 μm gold-plated tungsten and the field-shaping wires are 80 μm gold-plated molybdenum. The anode wire plane spaced 1 cm from two cathode planes.

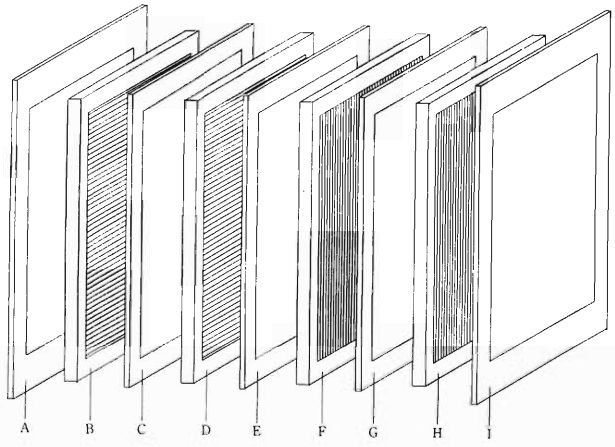

Fig. 1. Multiwire drift chamber.

A mixture of 50% argon and 50% ethane was used. To keep the cathode planes flat (for the uniformity of the electric field between the cathode and the anode plane), the gas is allowed to flow around all cells separated by the cathode planes. (For a similar multiwire chamber system, see T.D. Ford, G.A. Needham, F.P. Brady, J.L. Romero, and C.M. Castaneda: *Nucl. Instrum. Methods*, **228**, 81 (1984)).

RIKEN Accel. Prog. Rep. 23 (1989)

III-5-5. Timing Property of a Fast Timing Detector Using an Electron Multiplier

K. Yuasa-Nakagawa, T. Nakagawa, S.M. Lee, and I. Tanihata

We have made a simple timing detector which is very useful for a time-of-flight telescope. The detail of the mechanical construction of the detector system has been reported last year.[1] The timing character of this detector was measured by using ^{16}O(5.3 MeV/amu), ^{35}Cl (3.4 MeV/amu), and ^{81}Br (1.5 MeV/amu) beams from the 12UD tandem accelerator in the University of Tsukuba. Ions elastically scattered by a gold target (~60 μg/cm^2) were detected by the TOF telescope at 10 degrees. The electron multiplier was located at a distance of 103.5 cm behind an Au-target. The flight path between this detector and the stop one is 10 cm. The stop detector is a standard silicon surface barrier detector (SBD 100 mm^2, 150 μm thick).

Figure 1 shows time resolution performance for ^{16}O beams as a function of the acceleration voltage between the foil and the grid (V_{acc}). The time resolution rises with increasing V_{acc} and then saturates. The total transit time spread mainly consists of two components: (1) the spread of transit time between the foil and the first dynode and (2) the transit time spread in the electron multiplier. For overall time resolution we should also take into account the component of the SBD. Furthermore we can say that the component (1) is proportional to $1/V_{acc}$.[2] The solid line in Fig. 1 shows $\sqrt{(k_1/V_{acc})^2+(460)^2}$, ($k_1$ ~50). Gatti and Svelto[3] have shown that the variance of fluctuations in the arraival time of a total current pulse at the anode of the electron multiplier is proportional to $1/\sqrt{N}$. In Fig. 2, the best time resolutions for three particles are plotted as a function of $\sqrt{N}$. The solid line shows the relation, $t_t=\sqrt{(k_2/\sqrt{N})^2+t_{SBD}^2}$, where $k_2=3,300$ and $t_{SBD}=120$ps which we determined from other experimental results. We used the values determined in recent measurements[4] for the number of secondary electrons N. The time resolution rises with increasing N. From these results, we should use this type of detector with a foil, that emits a large number of secondary electrons, and that by applying high V_{acc} good total time resolution can be obtained.

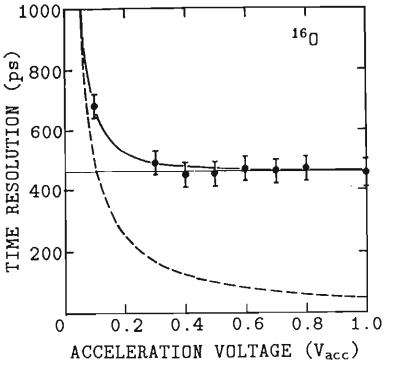

Fig. 1. Performance of time resolution for an 84.8 MeV ^{16}O beam as a function of the acceleration voltage V_{acc}.

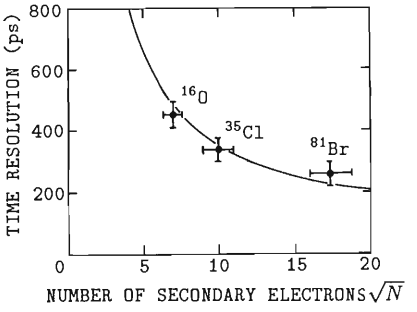

Fig. 2. Total time resolution as a function of the number of secondary electrons ($\sqrt{N}$).

References

1) T. Nakagawa, K. Yuasa-Nakagawa, and I. Tanihata: *RIKEN Accel. Prog. Rep.*, **22**, 159 (1988).
2) L.K. Anderson *et al.*: in "Advances in Microwaves" (Ed. L. Young), Vol. 5, No. 1 (1970).
3) E. Gatti *et al.*: Symp. Nuclear Instruments (Ed. J.B. Birks), p. 35 (1965); F. de la Barre: *Nucl. Instrum. Methods* **102**, 77 (1972).
4) H.G. Clerc, H.J. Gehrhardt, L. Richter, and K.H. Schmit: *ibid.*, **111**, 325 (1973).

RIKEN Accel. Prog. Rep. 23 (1989)

III-5-6. Improvement of the Sensitivity of a Proportional Counter by 1,4-Dioxane

H. Katsuragawa, T. Minowa, and T. Inamura

A proportional counter is capable of detecting a single electron-ion pair produced with high-energy particles and X rays, and by photoionization. Recently, using a proportional counter, we carried out resonance ionization spectroscopy of several metal elements.[1] In this study we found that, in spite of its high sensitivity, a proportional counter filled with a gas such as P-10 (90% Ar+10%CH_4) is insufficient for observation of atomic spectra where the number of Al and Fe atoms in the ionization area is less than 10.

We studied the sensitivity of a proportional counter filled with gas mixtures (total pressure 1,000 mmHg): Ar+methanol (40 mmHg), Ar+ethanol (20 mmHg), Ar+acetone (60 mmHg), and Ar+1,4 dioxane (40 mmHg). The proportional counter was made of stainless steel; the inner diameter was 10 cm and the diameter of an anode wire was 100 μm. At bias voltages lower than 1 kV, a source for electron-ion pair production was α particles from ^{210}Po (5.3 MeV), and at bias voltages higher than 1 kV X rays from ^{55}Fe (5.9 keV). Output signals from the proportional counter were amplified and stored in a multichannel analyzer (MCA). The multiplication gain was measured in the peak channel of MCA. Figures 1 and 2 show the gain curves for bias voltages lower than 1 kV and higher than 1 kV, respectively.

The multiplication gains increase slowly in the low bias region and increase exponentially in the high bias region. Because electron avalanche starts in an exponential region, electrons are only collected without multiplication in the low-bias region, where, except for 1,4-dioxane, the gain curves almost coincide with each other. The difference in the gain curve appears to be due to the loss of electrons depending on the properties of organic molecule. At higher biases the slopes of the multiplication gains are almost equal. The ratios of the multiplication gains were determined to be $g_d/g_a = 10^2$ and $g_e/g_a = 10$, where g_d, g_e, and g_a denote the multiplication gains for Ar+1,4 dioxane, Ar+ethanol, and pure Ar gas, respectively.

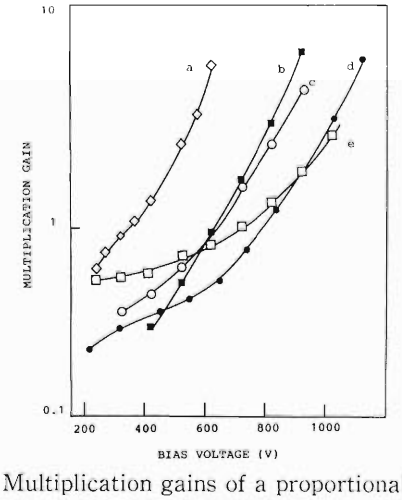

Fig. 1. Multiplication gains of a proportional counter. a, Ar+1,4-dioxane; b, Ar+methanol; c, Ar+ethanol; d, Ar+acetone; e, pure Ar.

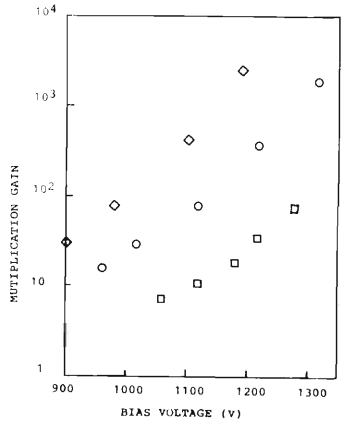

Fig. 2. Multiplication gains of a proportional counter. ◇, Ar+1,4-dioxane; ○, Ar+methanol; □, pure Ar.

The improvement of the multiplication gain can be explained qualitatively in terms of penning ionization, that is, collisional ionization between Ar^m and an organic molecule, where Ar^m denotes argon in the metastable state (11.5 eV). Part of argon atoms colliding with electrons in electron avalanche are excited to a metastable state.

The efficiency of penning ionization is greatly increased when the ionization energy (IE) of a molecule or an atom is slightly lower than the energy of its metastable state, and decreased rapidly as the difference between the two energy increased. For a Xe-filled proportional counter dimethylamine was reported to exhibit a pronounced penning effect.[2] The energy of the first metastable state of Xe is 8.3 eV, which is very

close to the IE of dimethylamine. We also found that 1,4-dioxane considerably improved the multiplication gain of the Ar-filled proportional counter. The exact IE of 1,4-dioxane is not known but the experimental result obtained here suggests that the IE is close to the energy of the metastable state of argon.

Since IE of ethanol is 10.5 eV and that of acetone is 9.7 eV, the penning ionization due to Ar^m will take place more efficiently for ethanol than for acetone. In fact Fig. 1 shows that the multiplication gain for ethanol is larger than that for acetone; this result can be explained qualitatively in terms of penning ionization.

References

1) H. Katsuragawa, T. Minowa, and T. Inamura: *Nucl. Instrum. Methods B*, **43**, 259 (1989).
2) B.D. Ramsey and P.C. Agrawal: *Nucl. Instrum. Methods A*, **278**, 576 (1989).

RIKEN Accel. Prog. Rep. 23 (1989)

III-5-7. Dosimetry by Means of a Liquid and a Gas Ionization Chamber

S. Konno, T. Takahashi, K. Nakano, and F. Yatagai

Precise determination of doses at a given point is very important in radiation biological studies and is carried out usefully, especially for high dose rate, by observing ionization currents generated in ionization chambers. We investigated two types of ionization chambers filled with liquid and with gas.

Type I chamber is filled with 2,2,4-trimethylpentane (isooctane) and has a sensitive volume of 0.63 ml. The distance between a collector electrode (anode) made of stainless-steel disk of 1.0 cm in diameter and a front window (cathode) made of aluminum of 0.2 mm in thickness is 2 mm. The chamber was irradiated with ^{60}Co γ-rays at room temperature.

Ionization currents are plotted against applied electric fields in Fig. 1. For reference, the ionization currents of 1 atm air in the same chamber are shown (A and C) in Fig. 2.

Type II chamber is equipped with two parallel-plate electrodes (anode and cathode) made of aluminized Mylar of 4 μm in thickness. The shielding electrode made of the same material is arranged outside the anode. The chamber having a sensitive area of 12.57 cm^2 is filled with 1 atm air as an ionizing medium.

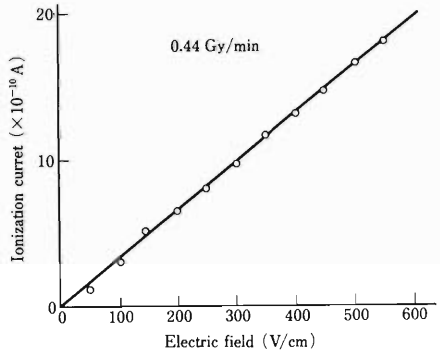

Fig. 1. Plot of ionization currents against applied electric fields for type I chamber filled with 2,2,4-trimethylpentane (isooctane) irradiated with ^{60}Co γ-rays.

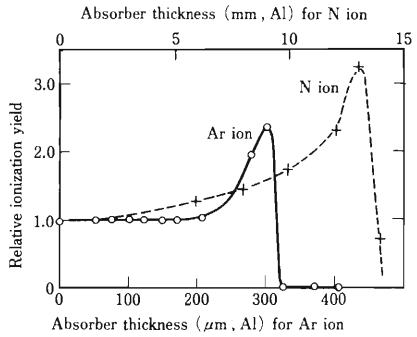

Fig. 2. Plots of ionization currents against applied electric fields for type I and II chambers filled with 1 atm air irradiated with ^{60}Co γ-rays. A and C, for type I chamber at dose rates of 0.35 Gy/min and 1.75 Gy/min, respectively; B and D, for type II chamber at dose rates of 1.23 Gy/min and 2.82 Gy/min, respectively.

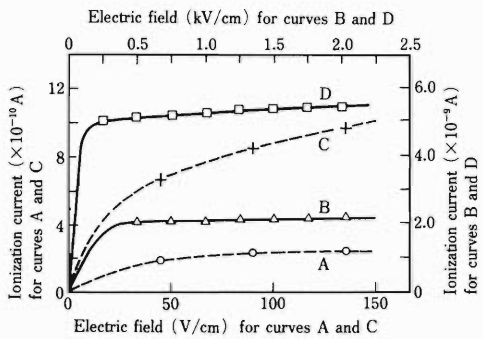

Fig. 3. Bragg curves obtained with type II chamber filled with 1 atm air for 26 MeV/u Ar ions and 135 MeV/u N ions.

Saturation currents for type II chamber irradiated with ^{60}Co γ-rays are shown (B and D) in Fig. 2. Bragg curves shown in Fig. 3 were preliminarily obtained for 26 MeV/u Ar ions and 135 MeV/u N ions from RIKEN Ring Cyclotron. Relative ionization yields were measured by using two type-II chambers filled with 1 atm air, which were set at the upstream and downstream positions of the beams with aluminum absorbers placed between them.

RIKEN Accel. Prog. Rep. 23 (1989)

III-5-8. Multiple Sampling Ionization Chamber

K. Kimura, H.S. Xu, Y. Tanaka,* I. Tanihata, and M. Yanokura

Since a multiple sampling ionization chamber (MUSIC) has been shown by a group at Lawrence Berkeley Laboratory[1] to be very powerful for particle identification of relativistic heavy ions up to an atomic number of $Z=57$, we constructed a MUSIC for RIPS heavy-ion experiments.

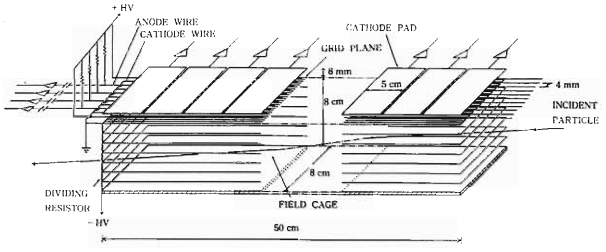

Fig. 1. Schematic view of MUSIC.

A schematic view of this chamber is shown in Fig. 1. It consists of a field cage (8 cm×8 cm×50 cm) and a multi-wire chamber (0.8 cm×8 cm×50 cm). These two parts are separated by a grid plane made of 1 mm spaced Cu-Be wires (100 μmϕ). The anode plane of the multi-wire chamber is made of 4 mm spaced Cu-Be wires (100 μmϕ), which run in parallel to incident particles. The cathode plane is divided into 10 pads (5 cm×8 cm) arranged along the anode wires. Total energy loss signals are obtained from the anode wires and multiple sampling of dE/dx-values can be done by the cathode pads.

This counter is capable of not only measuring the energy loss of heavy ions passing through a field cage but also ray tracing using timing signals from the cathode pads. For the ray tracing it might be better to operate the chamber as a proportional counter because better timing signals can be obtained. Such conversion is rather easily done by replacing the anode wires with thinner ones. As for energy resolutions, however, an ionization chamber mode should be better than a proportional chamber mode.

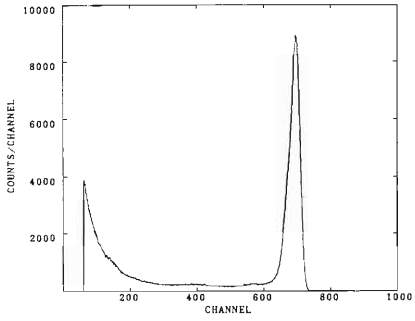

Fig. 2. Energy spectrum of deuterons observed by MUSIC. Deuterons, $E_d=10$ MeV, were scattered at $\theta=30$ from a Havar-foil and traversed about 30 cm of air before entering MUSIC.

We have tested the MUSIC using low-energy deuteron beams, $E_d=10$ MeV, from a Tandem accelerator at Kyushu University. The counter was filled with P-10 gas (Ar+CH_4 10%) of 1 atmospheric pressure. In order to see energy resolutions, deuteron energy was selected so that deuteron ranges do not exceed the counter length. Figure 2 shows an energy spectrum of deuterons scattered from a Havar-foil placed at the exit window of a scattering chamber. The energy resolution of this spectrum, 5%, is largely determined by the spreading of target masses in the Havar-foil and energy loss stragglings of deuterons in the air between MUSIC and Havar-foil, about 30cm. The intrinsic resolution of the counter is expected to be better than this value.

References

1) W.B. Christie *et al.*: *Nucl. Instrum. Methods*, **A255**, 466 (1987).

*Department of physics, Kyushu University, Fukuoka 812.

RIKEN Accel. Prog. Rep. 23 (1989)

III-5-9. Calculation of the Injection Scheme for Muon (g-2) Experiments at BNL

K. Ishida and K. Nagamine

Since the discovery of muon in 1947, the muon g-2 value has played an important role in establishing modern quantum electrodynamics, and in establishing that the muon behaves like a heavy electron. A series of experiments carried out at CERN was dedicated to increasingly precise determination of g-2 for muon.[1] Now a new experiment is in preparation at the Brookhaven National Laboratory (BNL) to establish the muon g-2 value to 0.35ppm.[2] A muon storage ring will be built with a shape of 14m in diameter, with a homogeneous magnetic field produced by superconducting coils in a C-shaped iron yoke and with a quadrupole electric field. The new experiment will provide a test of the electroweak theory and could also suggest new particles such as new generations of leptons up to 4 TeV.

Among many challenging issues, there exists a difficulty in storing muons into the ring. Two injection schemes have been considered; they are pion injection and muon injection. Schematic diagrams are shown in Fig. 1(a) and 1(b). We proposed pion injection with a kicker as shown in Fig. 1(c) as another injection scheme, which aims to trap pions in a ring using a kicker. In standard pion injection, pions are lost in less than one turn in the ring and have little chance to decay. By trapping pions we can expect all pions to decay in the ring yielding muons.

The efficiency of the muon storage was calculated by a Monte Carlo method using a calculated phase space of pions and muons at an injector as input. Table 1 shows that the efficiency of the pion injection with a kick is the best of the three. But, we have to estimate experimental errors due to beam backgrounds before final choice is made on the injection scheme.

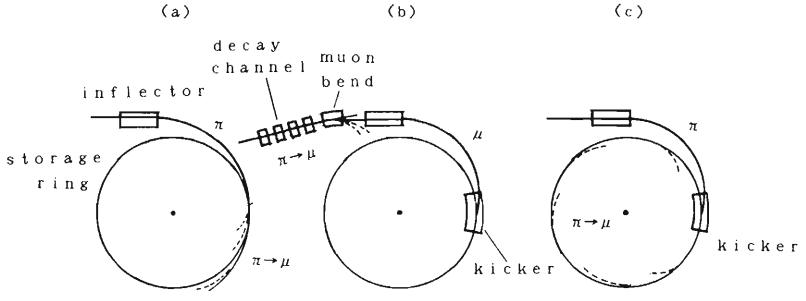

Fig. 1. Three injection schemes. (a), standard pion injection; (b), muon injection; (c), pion injection with a kick.

Table 1. Result of a Monte Carlo calculation of the efficiency of the muon storage.

	Pion injection	Muon injection	Pion injection with a kick
Number inflected/ proton interaction	92.7 ppm	0.15 ppm	92.7 ppm
Capture efficiency	100 ppm	0.33	1050 ppm
Number stored	9.3×10^{-9}	49.5×10^{-9}	97.3×10^{-9}
Proton bunches	2	1	1
Muon polarization	1	1	0.79
Relative gain in statistical accuracy	1	2.7	3.3

References

1) J. Bailey *et al.*: *Nucl. Phys.*, **B150**, 1 (1979).
2) V.W. Hughes *et al.*: AGS Proposal for g-2 experiment E821.

RIKEN Accel. Prog. Rep. 23 (1989)

III-5-10. Target Chamber for the Muon Catalyzed Fusion

T. Matsuzaki, K. Ishida, K. Nagamine,
E. Torikai, and S. Sakamoto*

The liquid hydrogen (D_2/T_2) target system was constructed for the direct measurement of the muon to alpha sticking probability in the muon catalyzed fusion process, by observing 8.2 keV muonic X-rays from (μHe) atom.[1]

The crosssectional view of the target chamber is shown in Fig. 1. A hydrogen gas container (~1,000 cc) is held in a vacuum space, enclosed by a secondary target chamber. The gas container, made of SUS316 stainless-steel supplied by Mill Sheet, is equiped with a tube and valve section for charging a target gas to be isolated from a gas filling system. A possible crack around the weldered parts is inspected by taking an X-ray photograph. The outside of the gas container is gold-plated to minimize hydrogen permeation. The container was degassed by baking, evacuating, and D2 gas purging, and risidual gas components were determined with an electric quardrupole mass spectorometer.

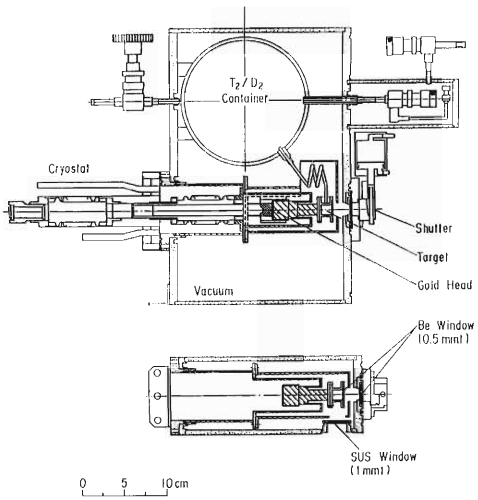

Fig. 1. Schematic view of the target chamber for the muon catalyzed fusion experiment; the vertical view (above) and the horizontal cut-view along the muon beam plane (below).

Hydrogen is introduced into a liquid target cell through a 4 mmϕ stainless-steel tube. The target cell made of a cupro-nickel alloy has a beryllium window (12 mmϕ and 0.5mm thick) for low energy observation using a Si(Li) detector. The beryllium window is hard-soldered on the window frame in a hot vacuum furnace. The inner surface of the target is coated with a 0.2 mm Ag sheet to absorb a photon background of Cu electronic X-rays from the wall.

The target cell is thermally attached to a copper heat-conducting rod and the other end of the rod is thermally contacted to a specially designed helium flow cryostat. The temperature of the cryostat head is monitored with a Rh-Fe thermometer and is automatically controled with an aid of a heater installed in the head. The target cell is surrouned by a copper thermal shield to prevent radiation loss. The shiled is cooled with a returning helium gas. The cryostat is evacuated separately and sealed. By using this cryostat, the target cell is cooled down to hydrogen liquification temperature and a 1cc liquid target can be formed.

Before final target gas loading, the fatigue and brittleness of beryllium windows and weldering parts of the target cell were carefully examined as making temperature cycles. A pressure proofing upto 2 atm and vacuum tightness were also checked for the target cell by using a helium leak detector as changing temperatures. A drop test was performed from a height of 9.1 m to the ground in order to assure the strengh of the target, where the target was packed into a transportation vessel. After the drop test, vacuum tightness and pressure proofing were reexamined.

Hydrogen gas (70%D_2 and 30%T_2) was loaded into the target at Japan Atomic Energy Research Institute.[2]

References

1) K. Nagamine, T. Matsuzaki, K. Ishida *et al.*: *Muon Catalyzed Fusion*, **1**, 137 (1987) and to be published.
2) M. Tanase *et al.*: to be published.

* Meson Science Laboratory, University of Tokyo.

RIKEN Accel. Prog. Rep. 23 (1989)

IV. NUCLEAR DATA

1. Status Report of the Nuclear Data Group

A. Hashizume, Y. Tendow, Y. Ohkubo, K. Kitao, and K. Sueki

The Nuclear Data Group has continued, as its last year's activities,[1] the following four items.

(1) The compilation of charged-particle induced reaction cross section data in cooperation with Nuclear Data Section in International Atomic Energy Agency (IAEA), a Data Center at Kurchatov Institute in Moscow, and others.[2] For the compilation of new EXFOR (Exchange Format for Experimental Data) files, we are concerned with the reactions of which products are used for mediobiological applications. The cross sections of the reactions producing the following isotopes were compiled in the EXFOR file: ^{11}C, ^{13}N, ^{15}O, ^{18}F, ^{28}Mg, ^{52}Fe, ^{67}Ga, ^{68}Ge, ^{68}Ga, ^{74}As, ^{77}Br, ^{82}Br, ^{77}Kr, ^{81}Rb, ^{82m}Rb, ^{111}In, ^{123}Xe, ^{123}Cs, ^{127}Xe, ^{123}I, ^{124}I, and ^{125}I nuclei.[1] In producing these isotopes, impurities are produced by competing reactions. We also compiled the reaction cross sections for various combinations of incident particles and target nuclei to produce these impurities.

An effort was made to complete the collection of the data[3-5] on the production of ^{18}F, ^{28}Mg, ^{67}Ga, ^{81}Rb, ^{123}I, and ^{123}Xe nuclides. We almost completed a set of data files of the cross sections of the reactions producing above nuclides. A computer code for least squares fitting has been developed and successfully applied for the ^{124}Te(p, 2n), ^{127}I(p, 5n), ^{122}Te(d, n), ^{127}I(d, 6n), ^{127}I(d, p5n), and ^{121}Sb(α, 2n)^{123}I reactions.

The compilation of the integrated and differential reaction cross-section data originated in Japan in the EXFOR files is continued.

(2) We are evaluating the details of collected cross-section data on the ^{12}C(p, pn)^{11}C, ^{27}Al(p, 3pn)^{24}Na, ^{63}Cu(p, 2n)^{62}Zn, and ^{65}Cu(p, n)^{65}Zn reactions to propose standard cross sections for monitor reactions.

(3) For the mass chain evaluation of nuclear structure data, the evaluation of the nuclear structure data on the $A=177$ mass chain is in progress.

(4) The references of annual reports and quarterly reports published in Japan during 1988 were compiled in the form of Nuclear Structure References Coding. This work is connected to the compilation of recent reference files at Brookhaven National Laboratory (BNL). We have responsibility of the compilation of references published in Japan and all references published 1987 and 1988 were sent to the BNL Data Center. All compiled references are published periodically as 'recent references' in Nuclear Data Sheets.

References

1) A. Hashizume, Y. Tendow, Y. Ohkubo, K. Kitao, and K. Sueki: *RIKEN Accel. Prog. Rep.*, **22**, 187 (1988).
2) A. Hashizume: Invited talk and proceedings of 'The International Conference on Nuclear Data for Science and Technology', Mito, May (1988).
3) K. Kitao, A. Hashizume, Y. Tendow, and Y. Ohkubo: This Report, p. 103.
4) A. Hashizume, Y. Ohkubo, Y. Tendow, and K. Kitao: This Report, p. 101.
5) Y. Tendow, A. Hashizume, and Y. Ohkubo K. Kitao: This Report, p. 105.

RIKEN Accel. Prog. Rep. 23 (1989)

IV-2. Cross-Section Data for ^{18}F Production

A. Hashizume, Y. Ohkubo, Y. Tendow, and K. Kitao

Fluorine-18 has gained large needs in the field of radiopharmaceuticals for *in vivo* function studieds with positron emssion tomography. For evaluation of cross sections of charged particle induced reactions, we have investigated the status of the experimental excitation functions and cross sections for the production reaction of ^{18}F. Collected data were tabulated in Table 1.

For $^{19}F(p, pn)+^{19}F(p, 2n)$ reactions, Gusakow measured an excitation function in the energy range 19-154 MeV. The maximum cross section is 230±30 mb at 34 MeV. Lambrecht reported 11.8±1.0 mCi/μAh with incident 31.7 MeV protons on a 11.5 m-mole F_2 target.

For $^{16}O(^3He, p)+^{16}O(^3He, n)$ reactions, the peak of the excitation curve is located at 7 MeV; the cross section is 390 mb. Threre is a discrepancy of about a factor of two between Nozaki's and Fitschen's results in the energy range 30-40 MeV. For $^{16}O(^3He, p)$ and $^{16}O(^3He, n)$ reactions, the following reactions causing impurities must be taken into account: (1) $^{16}O(^3He, 2\alpha)^{11}C$ with $T_{1/2}=20.3$ min, (2) $^{16}O(^3He, {}^6Li)^{13}N$ with $T_{1/2}=9.96$ min, and (3) $^{16}O(^3He, 3\alpha)^7Be$ with $T_{1/2}=53.6$ days.

Fluorine-18 is generally produced by $^{20}Ne(d, \alpha)^{18}F$ or $^{16}O(^3He, p)^{18}F$ reaction. Moreover, six kinds of reaction cross sections for a target ^{20}Ne have been studied as shown in Table 1. The productions via the short-lived precursor 1.67 s ^{18}Ne have also been studied.

Table 1. List of measured cross sections and yields of ^{18}F production.

Reaction	First author	Reference	Beam energy	Collected data
$^{19}F(p,pn)^{18}F$	B.L.Cohen	Phys.Rev.,99,723(1955)	21.5 MeV	cross sec.{(p,pn)+(p,2n)}
	H.P.Yule	Phys.Rev.,118,1591(1960)	82-426	excit.func.
	M.M.Gusakow	J.de Phys.Rad.,22,636(1961)	19-154	excit.func.{(p,pn)+(p,2n)}
	L.Valentin	Nucl.Phys.,62,82(1965),Phys.Lett.7,163(1963)	155,5700	cross sec.
	J.B.Cumming	Ann.Rev.Nuclear Science,13,261(1963)	82-2800	excit.func.(review)
	R.M.Lambrecht	Int.J.Appl.Radiat.Isotopes,29,175(1978)	31.7	yield
$^{19}F(p,2n)^{18}Ne$	R.M.Lambrecht	Int.J.Appl.Radiat.Isotopes,29,175(1978)	31.7	yield
$^{27}Al(p,d2\alpha)^{18}F$	N.M.Hintz	Phys.Rev.,88,19(1952)	21-118	excit.func.
	I.R.Williams	Phys. Rev.,162,1055(1967)	40-60	excit.func.
$^{20}Ne(d,\alpha)^{18}F$	R.M.Lambrecht	Int.J.Appl.Radiat.Isotopes,29,175(1978)	11	yield
$^{20}Ne(d,x)^{18}Ne$	H.Backhausen	Radioch.Acta,29,1(1981)	24-76	excit.func.
$^{16}O(^3He,p)^{18}F$				
$+^{16}O(^3He,n)^{18}Ne$	S.S.Markowitz	Analyt.Chem.34,329(1962)	5-30	excit.func.
	O.D.Brill	J.Nucl.Phys.(USSR),1,37(1965)	11-29	excit.func.
	T.Nozaki	Int.J.Appl.Radiat.Isotopes,25,393(1974)	2.4-42	excit.func.
	J.Fitschen	Int.J.Appl.Radiat.Isotopes,28,781(1977)	14-29	excit.func.
$^{20}Ne(^3He,x)^{18}F$	R.M.Lambrecht	Int.J.Appl.Radiat.Isotopes,29,175(1978)	10-55.7	yield
$^{20}Ne(^3He,\alpha n)^{18}Ne$	H.Backhausen	Radioch.Acta,29,1(1981)	18-31	excit.func
$^{20}Ne(^3He,\alpha p)^{18}F$	H.Backhausen	Radioch.Acta,29,1(1981)	17-32	excit.func
$^{20}Ne(\alpha,\alpha pn)^{18}F$	M.Furukawa	J.Phys.Soc.Japan,16,129(1961)	21-39	excit.func.
	R.M.Lambrecht	Int.J.Appl.Radiat.Isotopes,29,175(1978)	33-45	yield
$^{20}Ne(\alpha,\alpha 2n)^{18}Ne$	R.M.Lambrecht	Int.J.Appl.Radiat.Isotopes,29,175(1978)	33-45	yield

RIKEN Accel. Prog. Rep. 23 (1989)

IV-3. On Nuclear Reaction Data for the ^{28}Mg Production

A. Hashizume, T. Tendow, K. Kitao, and Y. Ohkubo

As a part of the compilation of nuclear reaction data concerning radioisotope production for medical applications, the excitation functions and production yields reported for ^{28}Mg were compiled and reviewed

A radionuclide ^{28}Mg ($T_{1/2}$=20.9 h) is one of the most useful radiotracers in life science and other applied fields. Other magnesium radioisotopes have shorter half-lives. Although ^{28}Mg is practically supplied *via* the ^{26}Mg(α, 2p) or ^{27}Al(α, 3p) reaction, eleven other reactions have been studied as shown in Table 1.

Table 1. ^{28}Mg Production reactions.

Reaction	First author	Reference	Beam energy (MeV)
^{30}Si(p,3p)	D.L. Morrison	(1)	130-425
^{31}P(p,4p)	D.L. Morrison	(1)	130-425
^{nat}S(p,5p)	D.L. Morrison	(1)	130-425
^{nat}Fe(p,x)	C.J. Orth	(2)	590
^{nat}Cu(p,x)	C.J. Orth	(2)	590
^{nat}U(p,spall.)	J. Alstad	(3)	170
^{27}Al(t,2p)	T. Nozaki	(4)	6-24
^{nat}Mg(t,p)	T. Nozaki	(4)	3-19
^{27}Al(α,3p)	J. Hudis	(5)	41
	D.R. Nethaway	(6)	33,11
	U. Martens	(7)	30-102
	T. Nozaki	(4)	33-45
	H.J. Probst	(8)	30-156
^{26}Mg(α,2p)	R.H. Lindsay	(9)	13-156
	T. Nozaki	(4)	22-40
	H.J. Probst	(8)	19-36.7
^{nat}Cu(^{12}C,x)	T. Lund	(10)	86 MeV/u

Reactions induced by alpha particles: As shown in Table 1, ^{26}Mg(α, 2p) and ^{27}Al(α, 3p) reactions were studied. Threshold energies of these reactions are 15.4 MeV and 24.8 MeV, respectively; the excitation curve have the maximum value of 3.0 mb at 40 MeV for the ^{26}Mg(α, 2p) reaction and the maximum value of 0.16 mb at 56 MeV for the ^{27}Al(α, 3p) reaction, respectively. Because of lower threshold energy and larger value of cross section, the ^{26}Mg(α, 2p) reaction is fitted for the production with a small cyclotron. Although the cross section of ^{26}Mg(α, p)^{29}Al is still larger in the 40 MeV region than that of the (α, 2p) reaction, the half-life of ^{29}Al is only 6.6 min; therefor there is no problem produced with this impurity after one hour. Major impurities produced when magnecium or aluminum is bombarded with alpha particles are ^{24}Na, ^{22}Na and ^{7}Be. When aluminum is bombarded at 140 MeV, the activity yield of ^{24}Na icreases two order of magnitude; therefore chemical separation is dispensable. Probst[8] reported that the yield of ^{26}Mg(α, 2p) and ^{27}Al(α, 3p) are 155 μCi/μAh and 20 μCi/μAh for an incident alpha-particle energy of 140 MeV.

Tritium induced reactions: The excitation functions of ^{26}Mg(t, p) and ^{27}Al(t, 2p) reactions were studied by Nozaki.[4] It should be noted that the peak values of these cross sections are about 80 times larger than that of ^{26}Mg(α, 2p) reaction. An yield of about 0.15 mCi/μAhr was reported[4] at an incident trition energy of about 20 MeV.

Other reactions: The cross sections induced by high-energy protons were measured as shown in Table 1. These reactions were studied mostly to examine reaction mechanism, not from the practical viewpoint. The cross sections of the ^{30}Si(p, 3p), ^{31}P(p, 4p), and S(p, 5p) reactions are 2.0, 0.2, and 0.05 mb, respectively, in the energy region of incident protons from 130 to 425 MeV. The cross sections increase slightly with increasing energy. When the iron and cupper are bombarded with 590 MeV protons, the spallation reaction cross sections to produce ^{28}Mg are 0.056 and 0.0251 mb, respectively.

References

1) D.L. Morrison and A.A. Caretto, Jr.: *Phys. Rev.*, **127**, 1731 (1962).
2) C.J. Orth, H.A. O'Brien, Jr., M.E. Schillaci, and B.J. Dropesky, J.E. Cline, E.B. Nieschmidt, and R.L. Brodzinsky: *J. Inorg. Nucl. Chem.*, **33**, 13 (1976).
3) J. Alstad, I.R. Haldorsen, A.C. Pappas, and M. Skarestad: *J. Inorg. Nucl. Chem.*, **37**, 873 (1975).
4) T. Nozaki, M. Furukawa, S. Kume, and R. Seki: *Int. J. Appl. Radiat. Isotopes*, **26**, 17 (1975).
5) J. Hudis: *J. Inorg. Nucl. Chem.*, **4**, 237 (1957).
6) D.R. Nethaway and A.A. Caretto, Jr.: *Phys. Rev.*, **109**, 504 (1958).
7) U. Martens and G.W. Schweimer: *Z. Phys.*, **233**, 170 (1970).
8) H.J. Probst, S.M. Qaim, and R. Weinreich: *Int. J. Appl. Radiat. Isot.*, **27**, 431 (1976).
9) R.H. Lindsay and R.J. Carr: *Phys. Rev.*, **118**, 1293 (1960).
10) T. Lund and D. Molzahn, B. Bergersen, E. Hagebo, I. R. Haldorsen, and C. Richard-Serre: *Z. Phys.*, **A306**, 43 (1982).

RIKEN Accel. Prog. Rep. 23 (1989)

IV-4. The Nuclear Cross Sections for ^{81}Rb Production

K. Kitao, A. Hashizume, Y. Tendow, and Y. Ohkubo

For the evaluation of cross sections of charged particle induced reactions, we have investigated the status of the experimental excitation functions and cross sections for the production reactions of ^{81}Rb ($T_{1/2}$=4.58 h). The short-lived daughter ^{81m}Kr ($T_{1/2}$=13.3 s) of ^{81}Rb has become important in the field of nuclear medicine because of its suitable characteristics as follows: (1) ^{81m}Kr is an inert gas; (2) It is a single photon emitter; (3) The energy of the photon of 190 keV is not so high as to give rise to collimator difficulties in a scintillation camera; and (4) ^{81m}Kr has a short physical half-life and a short biological half-life.

Hitherto, the production of radionuclide ^{81}Rb has been studied for the development of a ^{81}Rb-^{81m}Kr generator system, and many different reactions were proposed for ^{81}Rb production:[1-14]

Table 1. List of measured cross sections of ^{81}Rb production.

Reaction	Energy range (MeV)	Comments(target, monitor reaction,etc.)	References
^{79}Br(α,2n)^{81}Rb	40-12	Natural KBr, 2.1mg/cm^2.	11)
^{81}Br(^{3}He,3n)^{81}Rb*	40-12	Natural KBr, 2.1mg/cm^2.	11)
^{85}Rb(p,p4n)^{81}Rb	70-43	99.78% ^{85}RbCl, mixture with 99.99% Al. Monitor:^{27}Al(p,3pn)^{24}Na,^{65}Cu(p,pn)^{64}Cu.	8)
Rb,Br(p,spall)^{81}Rb	800	Natural RbBr;cumulative yield was given. Monitor:^{27}Al(p,spall)^{22}Na,^{24}Na,^{7}Be.	15)
^{90}Zr(p,4p6n)^{81}Rb	86-56	99.8% ^{90}ZrO, mixture with CuO. Monitor: ^{63}Cu(p,n),^{65}Cu(p,pn),^{90}Zr(p,2pn).	16)
^{90}Zr(p,4pxn)^{81}Rb	1000	96.8% enriched, on-line mass sep.	17)
^{91}Zr(p,4pxn)^{81}Rb	1000	81.3% enriched, on-line mass sep.	17)
^{94}Zr(p,4pxn)^{81}Rb	1000	91.2% enriched, on-line mass sep.	17)

* Including the ^{79}Br(^{3}He,n)^{81}Rb reaction.

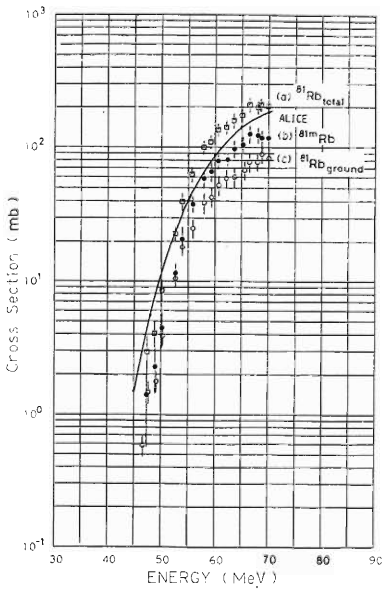

Fig. 1. Excitation functions for the (p, p4n) reaction on ^{85}Rb.[8] (a), The reaction leading to the ground state of ^{81}Rb: (b), leading to the isomeric state; (c), (a) plus (b). Calculations by an ALICE code are included.

^{80,82}Kr(p, xn), ^{82}Kr(p, 2n), ^{82}Kr(d, 3n), ^{85}Rb(p, p4n), ^{85}Rb(p, 5n), ^{81,79}Br(^{3}He, xn), and^{79,81}Br(α, xn). These reports are mostly on thick target yields, and only a few experimental data are available for our purpose. Table 1 shows a list of experiments which reported cross sections. Some experimental data were compared with the calculations using a code ALICE/Livermore82. These experimental cross sections are shown in Fig. 1 together with the calculation results. For critical evaluation, further experimental studies are needed.

References

1) T.J. Ruth *et al.*: *Int. J. Appl. Radiat. Isot.*, **31**, 51 (1980).
2) R.M. Lambrecht *et al.*: *ibid.*, **31**, 343 (1980).
3) E. Acerbi *et al.*: *ibid.*, **32**, 465 (1981).
4) J.J.L. Mulders *et al.*: *ibid.*, **34**, 717 (1983).
5) J.F. Lamb *et al.*: *J. Nucl. Med.*, **18**, 609 (1977).
6) A. Hanser *et al.*: *Int. J. Appl. Radiat. Isot.*, **32** , 775 (1981).
7) J.E. Gindler *et al.*: *ibid.*, **27**, 330 (1976).
8) T. Horiguchi *et al.*: *ibid.*, **31**, 141 (1980).

9) N.F. Peek *et al.*: *J. Nucl. Med.*, **15**, 522 (1974).
10) R.J. Schneider *et al.*: *Int. J. Appl. Radiat. Isot.*, **27**, 189 (1976).
11) Y. Homma *et al.*: *ibid.*, **30**, 345 (1979).
12) Y. Yano *et al.*: *J. Nucl. Med.*, **11**, 674 (1970).
13) L.G. Colombetti *et al.*: *ibid.*, **15**, 868 (1974).
14) J.C. Clark *et al.*: *Radiochem. Radioanal. Lett.*, **25**, 245 (1976).
15) P.M. Grant *et al.*: *Int. J. Appl. Radiat. Isot.*, **33**, 415 (1982).
16) M.V. Kantelo *et al.*: *Phys. Rev.*, **C14**, 64 (1976).
17) B.N. Belyaev *et al.*: *Izv. Acad. Nauk USSR, Ser. Fiz.*, **42**, 2392 (1978).

RIKEN Accel. Prog. Rep. 23 (1989)

IV-5. Excitation Function Data for ^{67}Ga Production

Y. Tendow, A. Hashizume, Y. Ohkubo, and K. Kitao

As a part of continuing efforts to compile nuclear reaction data relating to the radioisotope production for biomedical applications, the cross section or excitation function data for ^{67}Ga formation appearing in publications to date are reviewed.

Table 1. Excitation functions for ^{67}Ga.

Reaction	Energy(MeV)	σ max(mb at MeV)	Reference
^{67}Zn(p, n)	2.34 - 6.37	>420(at 6.37)	1)
	1.845 - 5.34	>130(at 5.34)	2)
^{68}Zn(p, 2n)	15 - 85	430(at 20)	3)
^{69}Ga(p, p2n)	20 - 56	372(at 35.9)	4)
^{71}Ga(p, p4n)	41 - 55	>84(at 55)	4)
^{66}Zn(d, n)	1.5 - 15.5	450(at 8.5)	5)
	4.5 - 11.3	225(at 8)	6)
^{65}Cu(^{3}He, n)	8.4 - 23.7	12.5(at 11.9)	7)
	8.1 - 70	7.9(at 12.4)	8)
^{65}Cu(α, 2n)	16.4 - 36.6	520(at 27)	9)
	15.2 - 40.1	630(at 28.1)	10)
	11.3 - 26.5	973(at 26.4)	7)
	18.4 - 60	897(at 26.7)	11)
^{64}Zn(α, p)	13.4 - 39.6	515(at 18.5)	12)
	9.1 - 36.9	452(at 19.6)	13)
^{nat}Zn(α, x)	14 - 36	280(at 19)	14)

A ^{67}Ga isotope (EC decay, $T_{1/2}$=3.261 d) has been used in medical diagnosis for the localization of malignant human tumors. Various targets and reactions have been used to produce ^{67}Ga. In Table 1,[1-14] the types of reaction, incident energy ranges, and maximum cross sections for the excitation functions measured so far are summarized. In consequence that natural zinc or copper targets are commonly used in a practical point of view, a reaction such as ^{66}Zn(d, n), ^{65}Cu(α, 2n), or ^{64}Zn(α, p) will be a choice. The only possible interfering gallium activity as an impurity is ^{66}Ga ($T_{1/2}$=9.4 h), which is easily cooled off owing to its short half-life. As for ^{66}Zn(d, n) excitation cross sections, there is a discrepancy of about a factor of two between existing two measurements.[5,6] For the ^{65}Cu(α, 2n) reaction, the largest values of cross sections are obtained with less discrepancies between measurements.[7,9-11] For the ^{68}Zn(p, 2n) reaction, there are two reports on its cross section at single energy points.[15,16] Single point cross sections for As(p, spall) and Rb+Br(p, spall) ^{67}Ga reactions are reported to be 28.4 and 41 mb, respectively, at a proton energy of 800 MeV.[17] Calculations of excitation functions based on a statistical theory have been extensively carried out in this mass region.

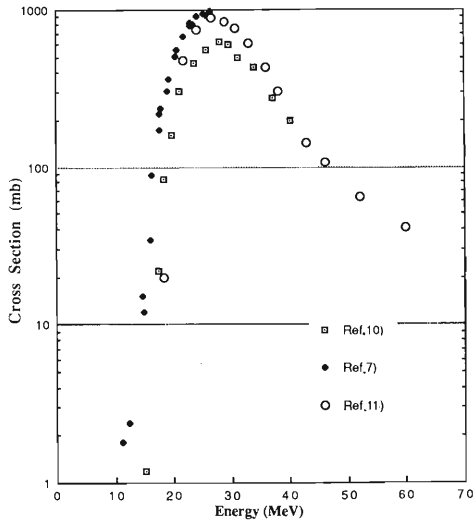

Fig. 1. Excitation functions for the ^{65}Cu(α, 2n)^{67}Ga reaction.

References

1) J.P. Blaser, F. Boehm, P. Marmier, and D.C. Peaslee: *Helv. Phys. Acta*, **24**, 3 (1951).
2) C.H. Johnson *et al.*: ORNL-2910, 25 (1960).
3) T. McGee, C.L. Rao, G.B. Saha, and L. Yaffe: *Nucl. Phys.*, **A150**, 11 (1970).
4) N.T. Porile, S. Tanaka, H. Amano, M. Furukawa, S. Iwata, and M. Yagi: *Nucl. Phys.*, **43**, 500 (1963).
5) D.C. Williams and J.W. Irvine, Jr.: *Phys. Rev.*, **130**, 265 (1963).
6) S.J. Nassiff and H. Munzel: *Radiochim. Acta*, **19**, 97 (1973).
7) E.A. Bryant, D.R.F. Cochran, and J.D. Knight: *Phys. Rev.*, **130**, 1512 (1963).
8) N.W. Golchert, J. Sedlet, and D.G. Gardner: *Nucl. Phys.*, **A152**, 419 (1970).
9) K.G. Porges: *Phys. Rev.*, **101**, 225 (1956).
10) N.T. Porile and D.L. Morrison: *ibid.*, **116**, 1193 (1959).
11) H.P. Graf and H. Munzel: *J. Inorg. Nucl. Chem.*, **36**, 3647 (1974).
12) N.T. Porile: *Phys. Rev.*, **115**, 939 (1959).
13) F.H. Ruddy and B.D. Pate: *Nucl. Phys.*, **A127**, 305 (1969).
14) Y. Nagame, M. Unno, H. Nakahara, and Y. Murakami: *Int. J. Appl. Radiat. Isot.*, **29**, 615 (1978).
15) B.L. Cohen and E. Newman: *Phys. Rev.*, **99**, 718 (1955).
16) L.B. Church and A.A. Caretto, Jr.: *ibid.*, **178**, 1732 (1969).
17) H.A. O'brien: IAEA Consultants' Meeting on Nuclear Data for Medical Radioisotope Production, April (1981).

RIKEN Accel. Prog. Rep. 23 (1989)

V. DEVELOPMENT OF ACCELERATOR FACILITIES

1. Ion Accelerator Development

1. Initial Operation of the Injector AVF Cyclotron

A. Goto, K. Hatanaka, M. Kase, Y. Yano, T. Kageyama,
S. Kohara, M. Nagase, H. Isshiki,* R. Abe,* S. Otsuka,*
H. Akagi,* T. Ishikawa,* and R. Ichikawa*

The injector AVF cyclotron was completed at the end of March 1989 on schedule. We then successfully extracted the first $^{14}N^{5+}$ beam with 7 MeV/u in April. In July we began to transport the nitrogen ion to RIKEN Ring Cyclotron (RRC) and succeeded in accelerating and extracting the ion with 135 MeV/u, at its maximum. Routine operation started in October; so far upon coupling with RRC two kinds of ions, 135MeV/u $^{14}N^{7+}$ (7 MeV/u $^{14}N^{5+}$) and 102 MeV/u $^{18}O^{8+}$ (5.5 MeV/u $^{18}O^{6+}$) have been used for experiments.

Characteristic features experienced in the last half-year operation are summarized as follows.

Isochronization: Signals from six pairs of non-destructive phase probes suggest that, after initial field setting, the fine adjustment of only a main coil current can give the phase excursion of less than $\pm 5°$. By further adjustment with one trim coil current, we can easily get a nearly ideal isochronous field.

Compression factor with a beam buncher: A single gap buncher producing a sawtooth-like wave by an optimal combination of f_0, $2f_0$, and $3f_0$ provides a compression factor of 5-6.

Transmission: The ratio between currents before injection and after extraction is 20 to 30% at a typical beam current of several $e\mu A$. It is noted that in this case part of a beam is cut with a slit at the upstream of the cyclotron.

Single turn extraction: The beam profile measured with a profile monitor placed downstream of the cyclotron indicates that single turn extraction can be achieved by careful tuning.

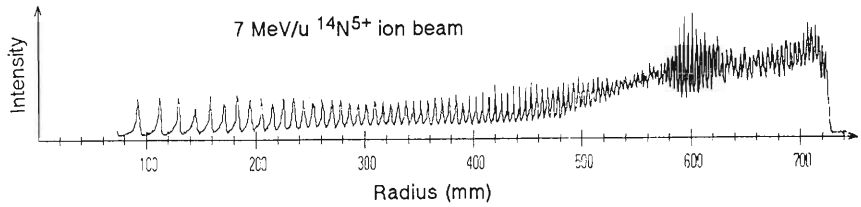

Fig. 1. Example of orbit pattern of 7 MeV/u $^{14}N^{5+}$ ions measured with a main radial probe. The number of revolutions is about 110.

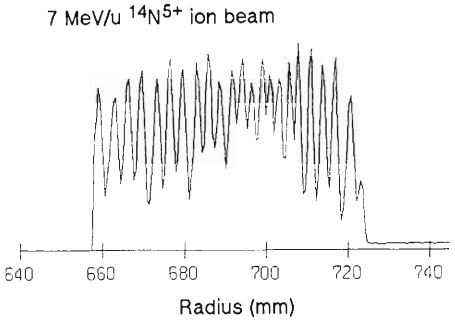

Fig. 2. Example of orbit pattern of 7 MeV/u $^{14}N^{5+}$ ions measured with a deflector probe placed in front of deflector. A small peak adjacent to the final orbit peak shows that in this case single turn extraction is not achieved. This small peak disappears by fine tuning of the dee voltage.

Stability: The cyclotron has been operated in a very stable condition. Retuning of the cyclotron, mainly readjustment of the main coil current, is necessary at most once in one-week operation, despite that the stability required for the coupled operation with RRC is severe.

Reliability: The tuning of the machine including the beam transport can be completed by a slight adjustment of the parameters that were determined in the previous run. The isochronous field distribution is reproduced well in every run.

Vacuum pressure: The pressure of 1×10^{-5} Pa is achieved with two cryopumps of 4,000 and 6,500 l/s.

*Sumijyu Accelerator Service, Ltd.

Although the cyclotron has worked successfully as mentioned above, there are still some open problems. They are:

The beam pattern measured with a radial probe is slightly different from the calculation.

Extraction efficiency is not so good (60 to 70 %) despite that the beams at extraction are separated quite enough for single turn extraction.

Transmission of a beam of high intensity (several tens of eμ Amperes) that is deliverd when a slit at the upstream of the cyclotron is fully open is less than 10 %. We expect that this is due mainly to insufficient tuning of the injection beam transport.

Figure 1 shows an example of beam orbit pattern measured with a main radial probe for the $^{14}N^{5+}$ beam. An example of beam orbit pattern measured with a deflector probe placed in front of deflector is shown in Fig. 2.

RIKEN Accel. Prog. Rep. 23 (1989)

V-1-2. Status of the RF System of RIKEN Ring Cyclotron

T. Fujisawa, S. Kohara, I. Yokoyama,
M. Nagase, Y. Taniguchi,* and Y. Kumata**

The RF amplifier system of RIKEN Ring Cyclotron consists of a series of three amplifiers; the pre-amplifier is of a wide-band solid-state type and the driver and final amplifiers are of tuned tetrode types.[1] The two amplifier systems have been operated without serious trouble since they were installed in 1986.[2] Recently, differences in operation parameters, such as RF output powers and DC tube currents, became noticeable between the two RF systems which were supposed to operate at the same state. Because accuracy of the meters of the system was suspected at first, they were recalibrated. The results are: the final output-power meter for the No. 1 system indicated 50% of actual output power and that for the No. 2 did 75%; the output-power meters of the wide-band amplifiers indicated reasonable powers; the dee voltage meter of the No. 2 system showed right values but the meter of the No. 1 showed 85% of actual dee voltage. After the calibrations, however, operating conditions were different from each other to generate the same dee voltage. Hence we measured the static characteristics of the final (RS2042SK) and driver (RS2012CJ) tubes. Figure 1 shows the results together with the characteristics delivered by the maker SIEMENS. From the figure, we conclude that the difference in the operating conditions were due to lowering of tube function in No. 1 system. Finally, we in-

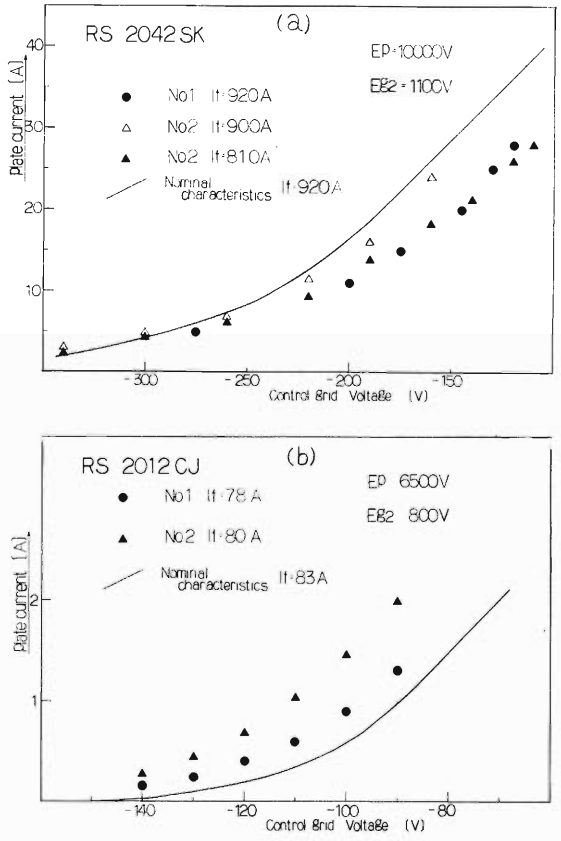

Fig. 1. Static characteristics of final (RS2042SK) and driver (RS2012CJ) tubes of the RF amplifiers for RIKEN Ring Cyclotron. The solid lines show the characteristics delivered by SIEMENS.

Table 1. Typical operating conditions of the amplifier systems of the RIKEN ring cyclotron at 28 MHz for an output power of 100 kW. The plate DC voltages are 10 kV for RS2042SKs and 6 kV for RS2012CJs.

	No. 1 amplifier system		No. 2 amplifier system	
Dee voltage	165 kV		169 kV	
Output power of WBA	260 W		150 W	
	RS2012CJ	RS2042SK	RS2012CJ	RS2042SK
Filament voltage	9.1 V	8.3 V	8.6 V	8.1 V
Filament current	81 A	890 A	78 A	820 A
G1 DC Voltage	123 V	340 V	123 V	340 V
G1 DC Current	220 mA	1,160 mA	219 mA	1,100 mA
G2 DC Voltage	900 V	1,200 V	810 V	1,110 V
G2 DC Current	57 mA	220 mA	33 mA	230 mA
Plate Current	2.4 A	19 A	1.9 A	16.1 A

* Denki Kogyo, Ltd.
** Sumitomo Heavy Industries, Ltd.

creased the filament currents and screen grid DC voltages of the tubes of the No. 1 system in order to generate the required dee voltage stably. Table 1 shows typical operating conditions after these adjustment. The stable operation has been restored and the dee voltages of the two resonators are consistent with each other within 3% at an input power of 100 kW.

References

1) K. Ogiwara, S. Kohara, Y. Kumata, Y. Taniguchi, and T. Fujisawa: *RIKEN Accel. Prog. Rep.*, **22**, 196 (1988).
2) T. Fujisawa, K. Ogiwara, S. Kohara, I. Yokoyama, Y. Oikawa, M. Nagase, I. Takeshita, Y. Chiba, and Y. Kumata: Proc. European Accel. Conf., Rome 1096 (1988).

RIKEN Accel. Prog. Rep. 23 (1989)

V-1-3. Status of the RF System for the Injector AVF Cyclotron

S. Kohara, A. Goto, M. Nagase, and Y. Kumata*

The RF system of the injector AVF cyclotron for RIKEN Ring Cyclotron (RRC) was installed at the AVF cyclotron vault and its characteristics were tested in March 1989. Because the details of the characteristics were already measured last year at Sumitomo Heavy Industries, Ltd. (SHI),[1,2] the test at RIKEN was simply made with respect to the following items:

1) characteristics of a resonator,

2) characteristics of an amplifier and the final power test, and

3) stabilities of an accelerating voltage and ripple factors of power supplies of a tube.

Resonant frequencies and Q-values were remeasured to check the characteristics of a reassembled resonator. The results reproduced well the values measured[1] at SHI.

A grounded-cathode tetrode (EIMAC 4CW 50,000E) amplifier is capacitively coupled to the resonator with a fixed vacuum coupling capacitor. The load impedance of the tube varies as the frequency is varied. The required accelerating voltage (33 kV) could not be obtained at the maximum frequency of 23 MHz when the fixed capacitor of 12 pF was used for the coupling capacitance in the power test at SHI.[2] Therefore the coupling capacitor was replaced from 12 to 16 pF to increase the load impedance of the tube. The load impedance at 23 MHz was increased from 450 to 700 Ω by the replacement. In the power test the required accelerating voltages (32-50 kV) have thus been obtained over the whole frequencies (12-23 MHz).

A photograph of the final amplifier is shown in Fig. 1. The input and the output circuits of the final amplifier are separated in upper and lower sides with an aluminum partition board so as not to interfere with each other.

The stabilities of the accelerating voltage and the ripple factors of the power supplies of the tube were within the specifications. The ripple factors of measured output voltages of the plate, the control grid, and the screen grid power supplies were 4×10^{-3}, 2×10^{-4}, and 3×10^{-4}, respectively. The stabilities of an amplitude and a phase of the maximum accelerating voltage (50 kV at 16 MHz) were measured to be within 2×10^{-4} and 0.2°, respectively. The results at a beam test shows that these stabilities were sufficient to accelerate a beam of good quality.

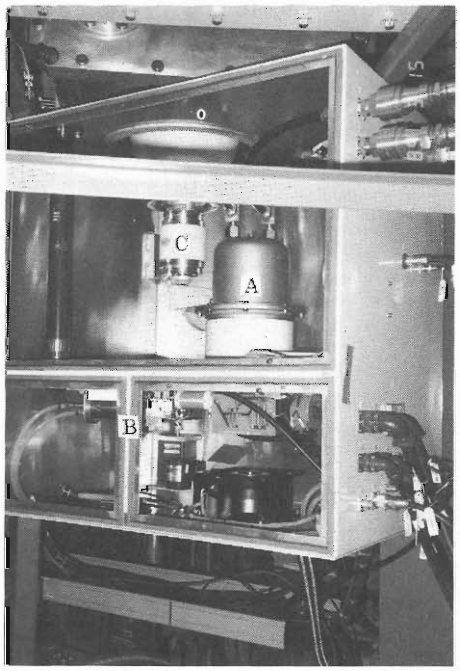

Fig. 1. Photograph of the final amplifier.
A: Tetrode (EIMAC 4CW50,000E),
B: Input circuit, C: Coupling capacitor.

The RF system has been working well without serious trouble since the first beam test.[3]

References

1) S. Kohara, A. Goto, and Y. Kumata: *RIKEN Accel. Prog. Rep.*, **22**, 209 (1988).
2) S. Kohara, M. Nagase, M. Saito, T. Kageyama, A. Goto, T. Fujisawa, and Y. Kumata: *ibid.*, **22**, 211 (1988).
3) A. Goto *et al.*: This Report, p.106.

* Sumitomo Heavy Industries, Ltd. (SHI).

RIKEN Accel. Prog. Rep. 23 (1989)

V-1-4. Beam Rebuncher between the Injector AVF Cyclotron and RIKEN Ring Cyclotron

A. Goto, M. Saito, S. Kohara, R. Abe,* A. Matsumoto,
T. Sasamoto, T. Watanabe, and Y. Yamada

A beam rebuncher system has been completed and set up in the course of the beam transport line from the injector AVF cyclotron to RIKEN Ring Cyclotron (RRC). Figure 1 shows a cut-away view of the rebuncher resonater. The design of the resonator was given in Ref. 1. Figure 2 gives the results of measurement of resonant frequencies, Q values, and shunt impedances. The measured shunt impedances indicate that the maximum required voltage of 40 kV at 65MHz (for 7MeV/u $^{14}N^{7+}$ ion; the first beam from the cyclotron) can be obtained with the power consumption of about 2 kW. For excitation of the resonator, a 3 kW wide-band amplifier of all-solid-state type is used that is delivered by THAMWAY Co., Ltd. The control system of the RF oscillator is similar to that of the rebuncher between the injector RILAC and RRC.[2]

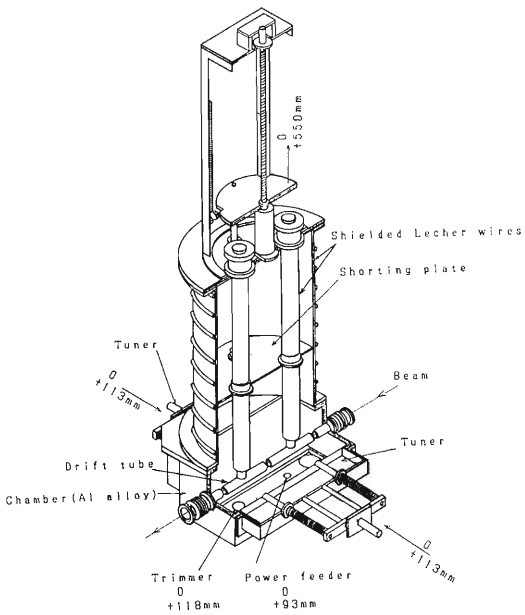

Fig. 1. Cut-away view of the rebuncher resonator.

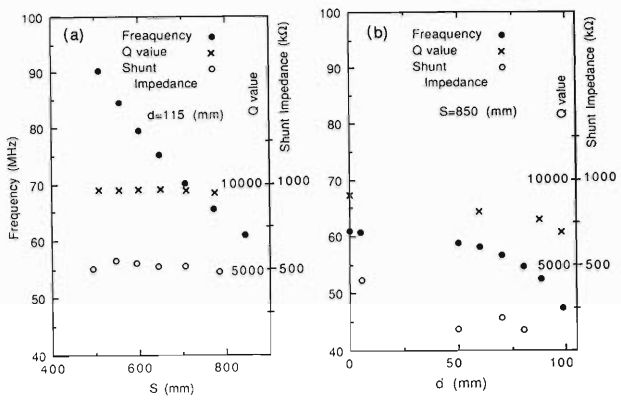

Fig. 2. (a) Measurements of resonant frequencies, Q values, and shunt impedances against the position of a movable shorting plate (s) for the maximum distance (d=115 mm) between a frequency tuner and drift tubes.
(b) The same as Fig. 2 (a) against the position of a frequency tuner (d) for the maximum s (s=850 mm).

The whole system has been working successfully for the last half a year since the first operation, though the wide-band amplifier once had a trouble due to transistors' breakdown.

References

1) A. Goto, M. Saito, S. Kohara, and R. Abe: *RIKEN Accel. Prog. Rep.*, **22**, 215 (1988).
2) A. Goto, T. Fujisawa, I. Takeshita, T. Urai, Y. Ikegami, and Y. Yamada: *RIKEN Accel. Prog. Rep.*, **20**, 176 (1986).

* Sumijyu Accelerator Service, Ltd.

RIKEN Accel. Prog. Rep. 23 (1989)

V-1-5. New Beam Current Monitor System at RILAC

M. Kase, T. Aihara,* and I. Yokoyama,

Electronics of RILAC beam current monitor system with beam slits and Faraday cups were replaced with a new-designed system which uses an intelligent interface circuit DIM (Device Interface Module)[1] as a sequensor. A block diagram is shown in Fig. 1.

The new system can be divided into three sections, *i.e.* DIM, a control desk monitor, and a group of circuits called as BDI (Beam Diagnostic Interface)[2] and BDU (Beam Diagnostic Unit). The BDI circuits are connected to DIM via a 50 bit digital bus line, and the BDU circuits are connected to the BDI circuits. The both kinds of circuits are built in plug in modules according with an Euro card standard, DIN41494. The contorol desk monitor has status lamps, five analog meters, and push buttons on its front panel.

The operation at the control desk monitor follows those of the former system,[3] except that beam currents from slits are displayed on a meter in a log scale to avoid a troublesome process of current-range selection. For example, if an operator push one button on the control desk monitor, then DIM is interrupted and starts following sequential actions. DIM sets the corresponding Faraday cup on a beam line, turns on a bias voltage to its supressor electrode, displays the beam current from it on an analog meter and removes all the Faraday cups laid upstream out of beam line. A micro-processor (Intel 8031) in DIM controls every function above according to a program written in a memory.

A main improvement in the new system is that it is connected to the RILAC control computer (Mitsubishi M60) via DIM-CIM-CAMAC in the same way as the RIKEN Ring Cyclotron control system.[1] The exactly same function as done on the control desk monitor can be executed from the control computer and also from a Ring Cyclotron control computer via a local area network. Furthermore the system has some automatic functions, programed in the control computer, such as automatic beam-current logging of all the slits and Faraday cups, automatic test of a Faraday cup actuator and electric isolation of signal line of slits and Faraday cups, and finally automatic beam tunning.

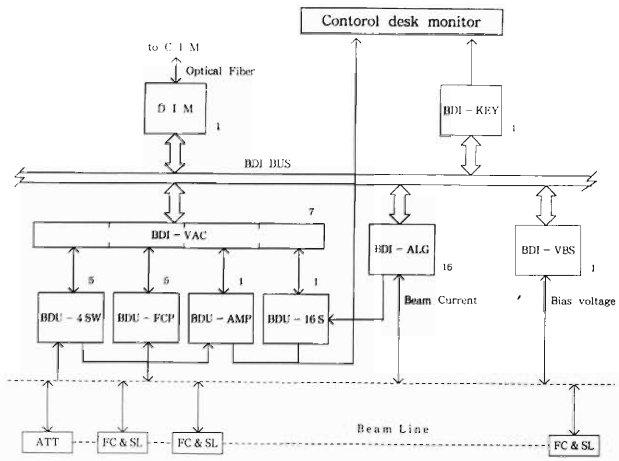

Fig. 1. Block diagram of the RILAC beam current monitor system. DIM has a processor (Intel 8031), memories (8 kb RAM and 8 kb ROM), 32 bit digital input/output, and 16 channel analog inputs. Forty-eight digital signals of DIM are used as a bus, BDI bus. BDI-VAC is a register I/O. BDI-ALG is a log amplifier with four inputs. BDI-VBS is a voltage supply (100-600 V). BDI-KEY is an interface between DIM and 64 key inputs. BDU-4SW is an analog switch (4 to 1) with high electric isolation. BDU-FCP is a controller of four pneumatic actuators of Faraday cups. BDU-AMP is a gain controllable linear amplifier for current signals from Faraday cups. BDU-16S is an analog signal selector for five analog meters of the control desk monitor. The figures shown nearby circuit denote the number of use in this system. BDU-FCP, BDU-4SW, BDI-ALG and BDI-VBS are connected to Faraday cup (FC), beam slits (SL), and beam attenuator (ATT).

References

1) T. Wada, J. Fujita, I. Yokoyama, T. Kambara, and H. Kamitsubo: *Sci. Papers I.P.C.R.*, **79**, 28 (1985).
2) M. Kase and I. Yokoyama: Proc. 6th Symp. Accel. Sci. Tech., p. 219 (1987).
3) M. Kase, I. Yokoyama, and M. Hemmi: *I.P.C.R. Cyclotron Prog. Rep.*, **14**, 115 (1980).

* Sumiju Accelerator Service

RIKEN Accel. Prog. Rep. 23 (1989)

V-1-6. Development of a 1083-nm Laser for a Polarized ^{3}He Ion Source Based on Optical Pumping

A. Minoh, T. Fujisawa, and Y. Taniguchi

A powerful 1083-nm laser is indispensable to make a polarized ^{3}He ion source based on optical pumping for RIKEN Ring Cyclotron.[1] The best candidate for a lasing material at 1083nm is the lanthanum neodymium hexa-aluminate (LNA).[2] As shown in previous experiments,[3] the 514-nm line of an Ar^+ laser is best for pumping LNA. We develop a laser system consisting of an LNA rod and an Ar^+ laser. High efficiency of fluorescence yield to a pumping power is very desirable to laser action.

The fluorescence spectrum of an LNA laser rod excited with an Ar^+ laser (514 nm) was measured in a wavelength region of 1020-nm to 1110-nm. The LNA laser rod made by Union Carbide Co. Ltd. was 5mm in diameter and 20mm in length. The crystal *c*-axis was set in the longitudinal direction. The Ar^+ laser beam was focused on the laser rod longitudinally. The fluorescence on the same direction was analyzed with a monochromator (JASCO CT-25) into which a 1083-nm light from ^{4}He gas discharge was introduced to calibrate the wavelengthes, and the Ar^+ laser beam was cut with a infrared transmission filter.

The obtained fluorescence spectrum shown in Fig. 1 exhibits two fluorescence peaks and the yield of 1054-nm light is larger than that of 1082-nm. The laser oscillation at the 1054-nm wavelength should be suppressed in a cavity to obtain 1083-nm laser oscillation.

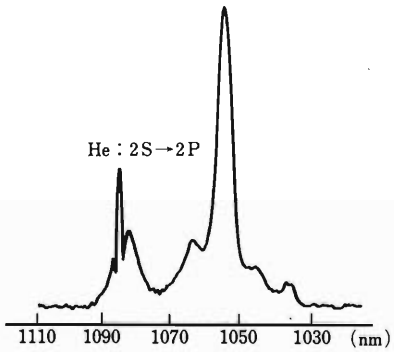

Fig. 1. Fluorescence spectra of Nd^{3+} in LNA and ^{4}He 2S-2P transition.

In order to design a laser cavity, the dependence of fluorescence intensities of 1082-nm on the Ar^+ laser power was measured on the Ar^+ laser beam line with a detector of a circular aperture subtending angle of 2 degree. Results are shown in Fig. 2, which indicates that the fluorescence intensities increase linearly with Ar^+ laser power and no induced emission effect appears at an input power up to 300 mW. The threshold pumping power for 1cm LNA laser crystal is reported to be 160mW.[2] These facts suggest that loss of the cavity should be as small as possible to obtain the laser action.

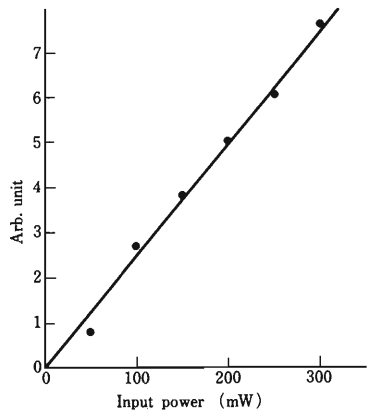

Fig. 2. Fluorescence intensities of the 1082nm as a funcion of the Ar^+ laser power.

References

1) T. Fujisawa, A. Minoh, Y. Taniguchi, S. Ishii, K. Hatanaka, and Y. Oshiro: *RIKEN Accel. Prog. Rep.*, **22**, 222 (1988).
2) L.D. Schearer, M. Leduc, D. Vivien, A. Lejus, and J. Thery: *IEEE Quant. Electron.*, **QE-22**, 713 (1986).
3) T. Fujisawa, A. Minoh, Y. Taniguchi, S. Ishii, and K. Hatanaka: *RIKEN Accel. Prog. Rep.*, **22**, 225 (1988).

RIKEN Accel. Prog. Rep. **23** (1989)

V-1-7. Magnetic Field Measuring System for the RIPS Magnets

H. Takebe, T. Kubo, K. Yoshida, and T. Nakamura

A new magnetic field measuring system using X-Y driving components was developed for the RIPS's* dipole, quadrupole, and sextupole magnets.[1] This X-Y moving system (Fig. 1) is sold as a robot component arm (Shibaura PH-106), which consists of two-directional pulse motors, drivers, and a control processor with an RS232C communication port.

A Hall element (Seiments SBV601s1) is connected to a DVM (FLUKE Co., 8502A) and a constant current supply as shown in Fig. 2.[2] The output data of an NMR gaussmeter (METRO Lab. 2050) and the DVM are fed into a personal computer (NEC PC9801vx) through a GPIB interface. The power supply for the magnet is also controlled by this computer using an interface which is the same as the DIM[3] system.

Figure 3 shows an example of the map data of the quadrupole magnet. Mechanical X-position errors along the Y-position were measured and the data were compensated by the computer. Figure 4 shows contour lines and a profile of the

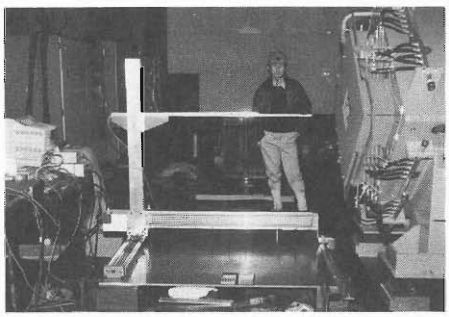

Fig. 1. X-Y driving components and a RIPS quadrupole magnet.

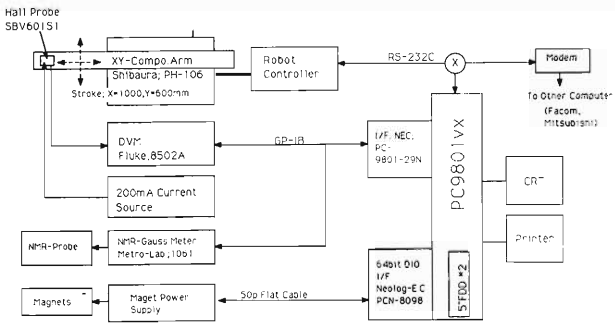

Fig. 2. A magnetic field measuring system for RIPS magnets.

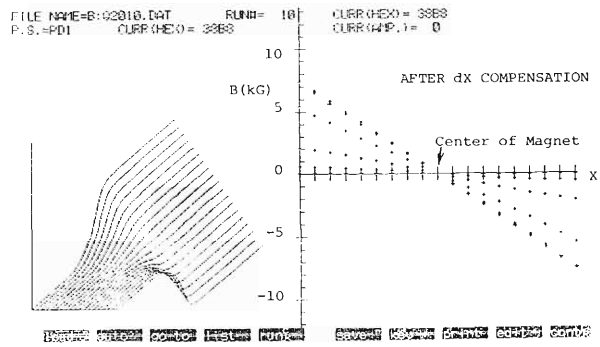

Fig. 3. Plot of raw data of the quadrupole magnet (Q2). The diameter of the Q2 is 172mm. X-position errors were compensated along Y-positions.

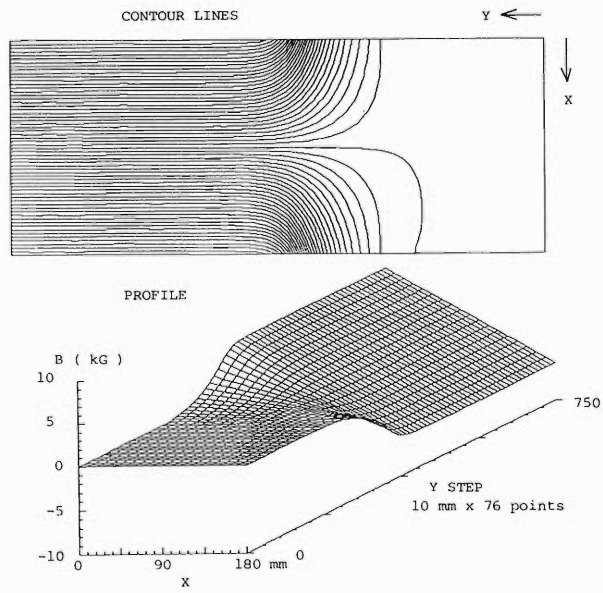

Fig. 4. Contour lines and a profile of map data of the quadrupole magnetic field.

obtained map data. The measuring program is written in a BASIC (MSDOS, N88BASIC), and the programs for plotting contour lines and profiles in a C-language.

* RIPS: RIKEN Projectile-fragment Separator.

References

1) T. Kubo *et al.*: *RIKEN Accel. Prog. Rep.*, **21**, 168 (1987).
2) H. Takebe *et al.*: *Sci. Papers I.P.C.R.*, **77**, 20 (1982).
3) H. Takebe, S. Motonaga, and T. Wada.: *RIKEN Accel. Prog. Rep.*, **19**, 174 (1985).

RIKEN Accel. Prog. Rep. 23 (1989)

V-2. Synchrotron Radiation Source Development

1. Status of the Synchrotron Radiation Project

H. Kamitsubo and M. Hara

The design study of the 6 GeV synchrotron radiation (SR) source was pursued in the past two years[1] and the lattice structure of 6 GeV was almost fixed. The R&D work on vacuum chambers, magnets, and RF cavities have been performed. In October 1988, RIKEN and Japan Atomic Energy Research Institute (JAERI) groups organized a joint team to promote the design and R&D work efficiently. The RIKEN group is in charge of the design study of a storage ring, and the JAERI group in charge of that of an injector linac and synchrotron. In May 1989, the advisory committee for this project had its first meeting.

In order to prepare the final proposal of the project, we again discussed the most desirable energy of the storage ring and led to a conclusion that the electron energy should be increased from 6 GeV to 8 GeV, because 6 GeV is not enough to get 20 keV X rays from a conventional undulator fundamental mode. We accordingly began the design studies of the 8 GeV storage ring and re-examined the design of injectors.

The injector consists of three linacs and a synchrotron. A 250 MeV linac is used to produce positrons, which are accelerated up to 1 GeV by the main linac. At the first stage of commissioning, we will inject electrons to the storage ring, so that we need to add another injector linac to the main linac. The synchrotron accelerates electrons (positrons) from 1 GeV to 8 GeV, and the lattice is of a FODO type. The major parameters of the injector linac and the synchrotron are listed in Tables 1 and 2.

The storage ring lattice is based on the Chasman-Green type and has 48 cells. A unit cell is composed of two bending magnets, ten quadrupoles, and seven sextupoles. The length of the straight section for an insertion device is 6.5 m and the circumference of the ring is 1436 m. The superperiodicity of the ring is 24, because the ring is operated in a mode that alternatively has high and low betatron functions at the straight sections.

After we fixed the lattice parameters, the advisory committee recommended us to modify the lattice structure so as to have several longer straight sections. It is not easy to introduce a few

Table 1. Major parameters of the injector linac.

Energy	1.0 GeV
Repetition rate	60 Hz
Frequency	2856 MHz
Multibunch mode (e^-)	
Peak current	100 mA
Pulse length	1 μs
Single bunch mode(e^-)	
Peak current	300 mA
Pulse length	1 ns
Multibunch mode (e^+)	
Peak current	10 mA
Pulse length	10 ns
Single bunch mode(e^+)	
Peak current	10 mA
Pulse length	1 ns

Table 2. Major parameter of the injector synchrotron.

Injection energy	1.0 GeV
Maximum energy	8.0 GeV
Currents	10 mA
Emittance horizontal	$1.92\ 10^{-7}$ m•rad
vertical	$1.92\ 10^{-8}$ m•rad
Energy spread	$1.1\ 10^{-3}$ (at 8 GeV)
Lattice	FODO 40 cells
Periodicity	2
Circumference	396.0 m
Repetition rate	1 Hz
Radiation loss per turn	11.55 MeV/turn
Nominal tunes(ν_x,ν_z)	11.73/8.78
Natural chromaticities	-15.3/-12.7
Momentum compaction	$9.53\ 10^{-3}$
Bending radius	31.385 m
Bending field	0.106 T / 0.85 T
Damping time(τ_x/τ_z/τ_θ)	937/938/469 ms (1.0 GeV)
1.83/1.83/0.92 ms (8 GeV)	
Frequency	508.58 MHz
Power source	Thyristor
Operation	On-axis injection
	8 pulse injection

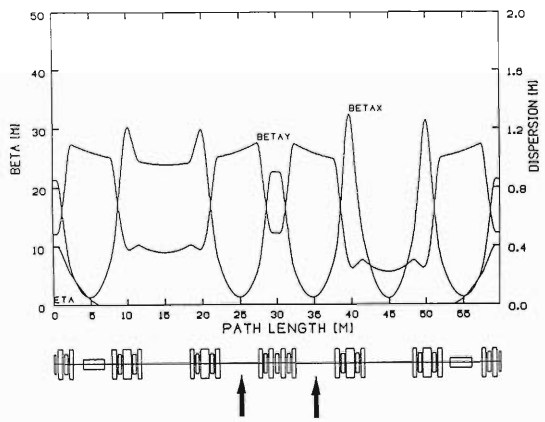

Fig. 1. Lattice functions over a straight cell. Bending magnets are extracted from the position indicated by arrows. Betatron functions are matched and tunes per cell are adjusted with a normal cell.

Table 3. Summary of Major parameters of the Storage Ring.

Energy	E(GeV)	8
Current(multi-bunch)	I(mA)	100
Current(single-bunch)	I(mA)	5
Circumference	C(m)	1435.95
Dipole magnetic field	B(T)	0.665
Bending radius	ρ(m)	40.098
Number of cells	Nc	48(44+4)
Length of straight section		
normal	L(m)	6.5
long	L(m)	36.42
Natural emittance	ε_n(π·m·rad)	7.18×10^{-9}
Critical photon energy	ε_c(keV)	28.32
Tune	ν_x	50.78
	ν_y	17.84
Synchrotron tune	ν_s	0.010198
Momentum compaction	α	1.49×10^{-4}
Natural chromaticity	ζ_x	-113.168
	ζ_z	-43.319
Energy loss in the arcs	U_0(MeV/rev)	9.04
Energy spread	σ_ε/E	0.00108
Damping time	τ_x(msec)	8.473
	τ_z(msec)	8.481
	τ_ε(msec)	4.242
Harmonic number	h	2436
R.F.voltage	V_{rf}(MV)	17
R.F.frequency	f_{rf}(MHz)	508.58

very long straight sections without deterioration of beam quality. We decided to make four 30-m straight sections. In the first phase of operation, four normal cells are changed to straight cells by extracting bending magnets. We can optically get almost the same betatron functions at the straight cell because the focusing force of the bending magnet is negligible. Magnet arrangement and betatron functions are shown in Fig. 1. At each straight cell, four long straight sections are on a line so that four different insertion devices can be installed on one beam line. In the next phase of operation, we can produce four entirely free 30 m straight sections by rearranging quadrupoles and sextupoles at the straight cells without changing the electron orbit. The final parameters of the storage ring are given in Table 3.

Prototypes of the bending, quadrupole, and sextupole magnets are under fabrication. The cold model of an RF cavity is also being fabricated. The R&D work on the vacuum chambers is in progress.

The site of the SR facility was decided at Harima Science Garden City in Hyogo prefecture. Ground breaking will start next February and the ground will be available for us in 1992. A tentative campus and accelerator arrangement are illustrated in Fig. 2.

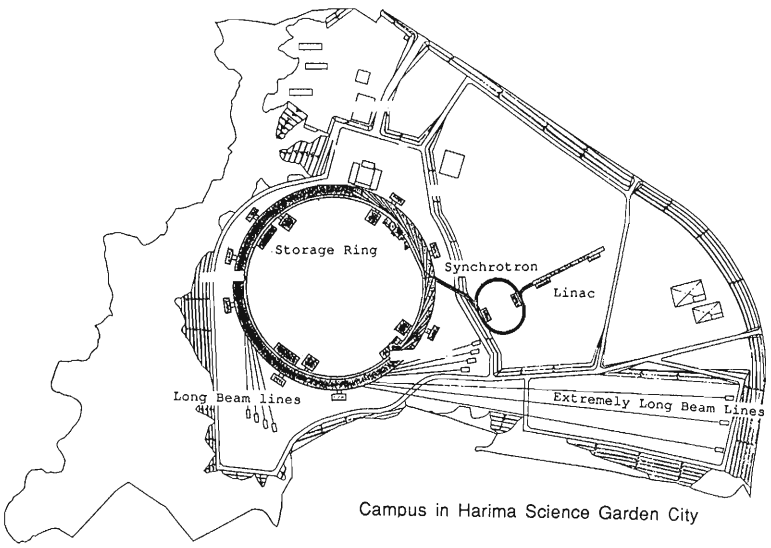

Fig. 2. Accelerator arrangement of the SPring-8 and the construction site.

RIKEN Accel. Prog. Rep. 23 (1989)

V-2-2. A Preliminary Study on the Storage Ring Commissioning

R. Nagaoka, K. Tsumaki, H. Tanaka, K. Yoshida, and M. Hara

For low-emittance synchrotron light sources, the problem associated with magnet alignment errors becomes above all serious. In particular, the misalignment of quadrupoles leads to the generation of large closed-orbit distortion (COD) which may exceed vacuum chamber dimensions even if the rms value is only few tenths of a milimeter. It is thus of great importance to set up a strategy to commission the low-emittance ring.

Two possible strategies were examined. One is to attempt commissioning in the low-emittance mode directly, by reducing the magnitude of COD by means of "first turn steering" to the extent that at least stationary revolution of the beam is guaranteed. Once this is done, one can proceed with the ordinary COD correction using normal pickup monitors and correctors, to make further refinements on the suppression of the residual COD.[1] The first turn steering is to detect the beam position in the very first turn at some positions in the ring and to steer the beam to the nominal positions with correctors located upstream. This process is iterated around the ring, the number of iteration depending on the sensitivity of the machine. To enable this operation, however, monitors must either be screens or highly sensitive pickups which are also capable of identifying the beam position in a single pass. We should note that this procedure does not strictly correspond to the correction of COD of the machine, since the beam would inevitably have an unknown betatron amplitude.

Another strategy is to commission the machine firstly in so-called detuned modes which are less sensitive to misalignment. One can expect the commissioning of detuned modes to be much facilitated. The idea is to perform the COD correction to the maximum extent, and then, by keeping the determined corrector strength, switch over to lower emittance modes. In designing the detuned optics modes, one should therefore take into account that the patterns of generated COD to be closely related to that of low emittance modes.

In both approaches, we turn off all sextupoles. The primary reason is to be free from dynamic aperture restrictions.[2] Moreover, there should be a considerable deterioration in the role of sextupoles itself under seriously distorted optics. Fortunately, the correction of COD should not be spoiled by adding the sextupoles in later steps. On the other hand, we may suffer from the weak

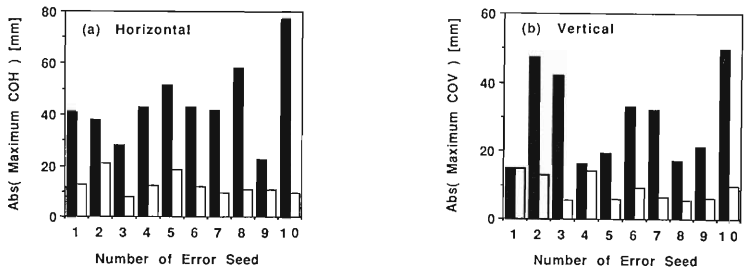

Fig. 1. Effect of first turn position steering. Maximum COD in a ring with quadrupole misalignment of 0.2 mm rms is calculated for 10 cases. Optics mode: Hybrid.[2] Dark bars, without steering; White bars, with steering at every high β section.[2]

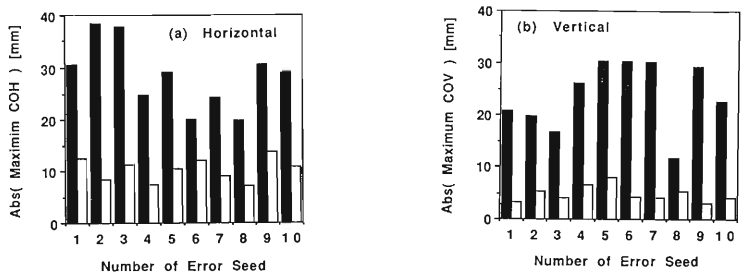

Fig. 2. Commissioning via detuned modes. Maximum COD in a ring with quadrupole misalignment of 0.2 mm rms is calculated for 10 different cases. Optics mode: Hybrid.[2] Dark bars, without correctors; White bars, with correctors whose strengths are determined by COD correction in the high β mode.[2]

beam intensity due to worsened chromatic behavior.

A simulation study was performed to examine the validity of two schemes described above. A computer code RACETRACK[3] was used by including a routine to simulate the procedure of first turn steering. In the direct commissioning scheme, we found that first turn steering is vital and greatly reduces the COD of the machine (Fig. 1). However, for machines with quadrupole misalignment of 0.2 mm rms, position steering at every two unit cells was not adequate to achieve the stationary revolution of the beam. In the indirect commissioning scheme using detuned modes, the performance of COD correction in detuned modes turned out to be effective in suppressing the COD of the low-emittance mode as much as to enable the commissioning (Fig. 2).

References

1) H. Tanaka, R. Nagaoka, K. Tsumaki, K. Yoshida, and M. Hara: *RIKEN Accel. Prog. Rep.*, **22**, 231 (1988).
2) R. Nagaoka, H. Tanaka, K. Yoshida, K. Tsumaki, and M. Hara: *ibid.*, **22**, 227 (1988).
3) A. Wrulich: DESY Rep., 84-026 (1984).

RIKEN Accel. Prog. Rep. 23 (1989)

V-2-3. Lattice Design for a Storage Ring with Long Straight Sections

R. Nagaoka, H. Tanaka, K. Tsumaki, K. Yoshida, and M. Hara

The lattice of the SPring-8 storage ring previously reported is composed of 48 identical Chasman Green (CG) cells with 6.5 m free straight sections.[1] During the last year, there appeared a strong opinion from the user's group to incorporate into the ring, some very long free straight sections of~30 m for which there are many attractive uses with the future synchrotron radiation technology. To meet this requirement, several proposals were made for the lattice structure. From the beam dynamics point of view, the most serious difficulty that must be overecome is the reduction of a dynamic aperture due to the breakdown of optics symmetry.

What finally came up as a compromise is to construct long straight sections by just taking away dipoles from some of CG cells. The idea behind this is that the distortion of optics due to the absence of dipoles should be so small that the optimized sextupole field would not be deteriorated.[1] Within this modification, there is thus a large advantage that most of the studies made heretofore for the previous design can be kept valid. Optics modes such as hybrid (Fig. 1) or high β can be equally well operated,[1] and as an ultimate option, we can operate the machine in a long straight section mode (Fig. 3) by further taking away all the magnets from cells without dipoles.

Table 1 lists the major paramters of the storage ring designed for this purpose. As before, the ring consists of 48 CG cells, from which dipoles are extracted from 4 cells preserving the 4-fold symmetry. It results in an increase in the dipole field by~9%, and in the emittance by~30%. Optics functions and dynamic apertures for the hybrid mode and the long straight section mode are shown in Figs. 1-4.

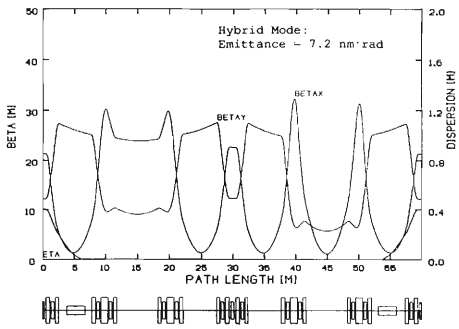

Fig. 1. Optics functions of the hybrid mode. A cell without dipoles is shown in the center. Optics matching is made at both ends of this cell to normal cells.

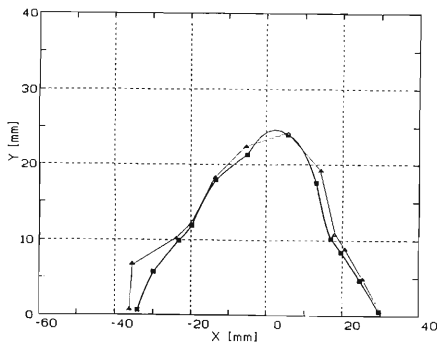

Fig. 2. Dynamic aperture of the hybrid mode calculated at a high β section (Squares). Compared with triangles is that of the ring composed of 48 normal cells.

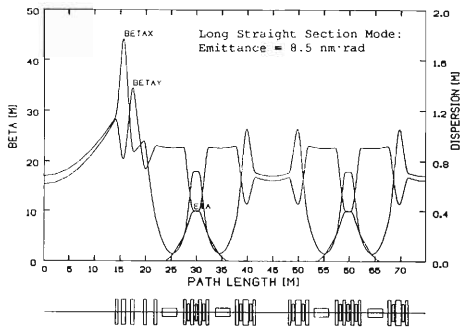

Fig. 3. Optics functions of the long straight section mode. High β mode is employed for normal cells. Optics matching is made at the center of adjacent achromatic arcs.

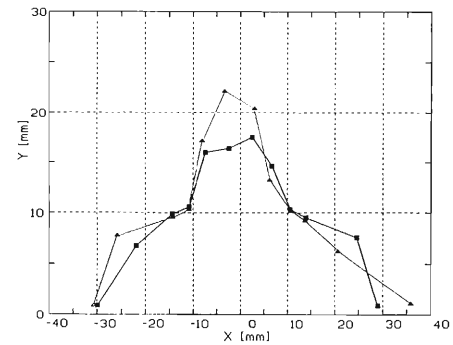

Fig. 4. Dynamic aperture of the long straight section mode. Squares: Calculated at the center of a long straight section. Triangles: Calculated at the center of normal straight section which is in the farthest position from long straight sections.

Table 1. Parameter list of the SPring-8 storage ring.

Energy		E (GeV)	8
Current (multi-bunch)		I (mA)	100
Current (single-bunch)		I (mA)	5
Circumference		C (m)	1435.95
Normal cell length		L_c (m)	29.916
Dipole magnet field		B (T)	0.665
Number of dipoles		N_b	88
Bending radius		ρ (m)	40.098
Energy loss in the arcs		U_0 (MeV/turn)	9.04
Critical photon energy		ε_c (keV)	28.32
Momentum compaction		α	1.49×10^{-4}
Harmonic number		h	2436
R.F. voltage		V_{rf} (MV)	17
R.F. frequency		f_{rf} (MHz)	508.58
Synchrotron tune		ν_s	0.010198
Damping time		τ_x (ms)	8.478
		τ_z (ms)	8.481
		τ_e (ms)	4.242
Energy spread		σ_e/E	0.00108
		Hybrid Mode	Long Straight Section Mode
Number of cells	N_c	48	36
Length of free straight section			
Normal	L (m)	6.5	6.5
Long	L (m)		28.096
Natural emittance	ε_n (πm•rad)	7.18×10^{-9}	8.49×10^{-9}
Betatron tune	ν_x	50.78	39.22
	ν_y	17.84	13.16
Natural chromaticity	ξ_x	−113.168	−71.591
	ξ_y	−43.319	−29.431

References

1) R. Nagaoka, H. Tanaka, K. Yoshida, K. Tsumaki, and M. Hara: *RIKEN Accel. Prog. Rep.*, **22**, 227 (1988).

RIKEN Accel. Prog. Rep. 23 (1989)

V-2-4. Recent Developments in the Computer Code "CATS"

R. Nagaoka, H. Tanaka, K. Tsumaki, K. Yoshida, and M. Hara

Some large improvements were made in the capability of the computer code "CATS", a code initaited to optimize the sextupole strength in enlargening the dynamic aperture of electron storage rings.[1]

In the lattice designing for a ring with long straight sections,[2] the previous analysis within a unit cell structure became totally unsatisfactory and optimizations in a larger structure became essential. Accordingly, the style of input file of CATS has been entirely modified. Following the fashion adopted in RACETRACK,[3] the input structure is divided into separate blocks which specify the desired type of execution. In particular, information on the ring is given in three blocks: A block defining the single elements which are characterized by their names, element types, lengths and strengths etc. A block defining magnet arrangement in a superperiod of the ring, characterized by element names. As in RACETRACK, this block also takes account of the repetition of the lattice structure. Finally, a block that defines the total ring structure in terms of number of superperiods and of reflective symmetry as to the initial point. This block also selects the option of using the initial values of optics functions. In case the initial values are not given, they are generated by the code from transfer matrices of the ring. The pre-defined initial coordinates are nevertheless useful in fitting the linear optics in a non-circular section of the lattice (see below).

Improvements are made also on fitting procedures. Beside the original routine to fit the sextupole strengths, two additional routines are included either to fit the linear optics or to fit the bumped orbit for injections. The fitting mode is specified in the input block. As before, by providing the necessary quantities, such as Twiss parameters or betatron tunes in the common blocks, an appropriate function to be least-square fitted is defined in the subroutine "MODLFN." Specification of the fitting parameters is made in the single element block. Also important to mention is the specification of the parameter range in the single element block, which is now taken into account in the fitting procedure. This is especially helpful in the sextupole optimization where one wishes to suppress the sextupole strength as weak as possible. As regards the sextupole optimization mode, a routine is added to correct the higher-order chromaticity[4] which makes a serious contribution in some of the optics modes. This correction can be used in combination with the correction of linear chromaticity or with that of geometric aberration.

There are still many other new features not referred here. With the new structure of the code, we wish further to extend the capability of CATS.

References

1) R. Nagaoka, H. Tanaka, K. Yoshida, K. Tsumaki, and M. Hara: *RIKEN Accel. Prog. Rep.*, **22**, 248 (1988).
2) R. Nagaoka, H. Tanaka, K. Tsumaki, K. Yoshida, and M. Hara: This Report, p. 119.
3) A. Wrulich: DESY Rep., 84-026 (1984).
4) H. Wiedemann: PEP-220 (1976).

RIKEN Accel. Prog. Rep. 23 (1989)

V-2-5. Linear Coupling Compensation for the Storage Ring of SPring-8

H. Tanaka, K. Yoshida,* R. Nagaoka, K. Tsumaki, and M. Hara

We investigated linear coupling in the storage ring of SPring-8 and its compensation.

We calculated a coupling coefficient κ_q[1,2] defined by Eq. 1 in two different ways, statistic calculation[3] and calculation with a tracking data,[4] and estimated the strength of the coupling.

$$\kappa_q e^{i\phi_q} = \frac{1}{2\pi}\int_{\theta}^{\theta+2\pi} d\theta k_s \sqrt{\beta_x\beta_y}\, e^{i[\Psi_x-\Psi_y-(Q_x-Q_y-q)\theta]} \quad (1)$$

where Ψ_i, β_i, and Q_i ($i=x$, horizontal plane; y, vertical plane) are the Floquet phase, the betaron function, and the betatron tune, ϕ_q is the phase of q harmonics corresponding to the strength of sine and cosine terms of κ_q, k_s is the strength of skew quadrupole components, and $\theta=2\pi s/L$ (s, azimuthal length; L, ring circumference) denotes the time variable. The parameter q represents the differential resonance condition and the resonance to be compensated often satisfies the condition that $\delta(\delta=Q_x-Q_y-q)$ is minimum. The parameter δ denotes the distance from the resonance. In our case, because the workpoint (Q_x and Q_y) of a normal hybrid mode is composed of 51.22 and 19.16, the resonance to be compensated is $Q_x-Q_y=32$ and δ is 0.06.

The data obtained in the two ways are:

$$\kappa_{32} \text{ by statistic calc.} = 0.05-0.055$$
$$\kappa_{32} \text{ by calc. with tracking} = 0.006-0.07$$

For above calculations, we used the follwing magnetic error conditions; a root mean square value (RMS value) of misalignment of a magnet is 0.2 mm, RMS values of a field and gradient error are 5×10^{-4}, and RMS value of a magnet tilt error is 0.5 mrad. The average value of κ_{32} obtained by the calculation with tracking data is about 0.03 and this is slightly lower than the value obtained by the statistic calculation which gives an expected value. This may be because all kinds of magnetic errors used in tracking simulation are cut off at the double root mean square value, and because a population is too small (10 rings). We presumed for the calculation of the coupling ratio of emittance that the expected value of κ_{32} exists in the range 0.03−0.055. With Eq. 2 which relates the coupling coefficient κ_q and the distance from the resonance δ to the coupling ratio of lateral emittance r, we found the expectet coupling ratio at the normal operation point to be about 20%−50%.

$$r=\kappa_q^2/(\kappa_q^2+\delta^2) \quad (2)$$

From the viewpoint of beam stability, it is difficult to make δ bigger than 0.10. This means that sharp reduction of the linear coupling is impossible without any coupling compensation (reduction of κ_q). As photon-beam users demand a wide tunability of the coupling ratio (about 1%−100%), we should compensate the coupling to

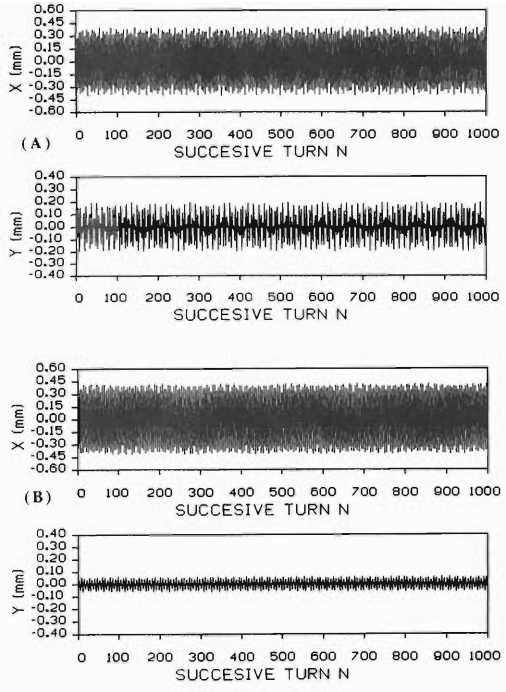

Fig. 1. Horizontal and vertical emittance beat. This is the result of linear coupling compensation for No. 1 in Table 1. X and Y represent horizontal and vertical oscillation amplitudes. (A) and (B) denote before and after the coupling compensation.

Table 1. Simulation result of the coupling compensation.
δ is 0.06 and lattice is the normal hybrid mode.

No.	Before compensation		After compensation	
	κ	Coupling ratio (%)	κ	Coupling ratio (%)
1	0.070	53	0.012	3.9
2	0.039	30	0.015	6.5
3	0.039	30	0.021	11
4	0.047	39	0.020	10

* Mitsubishi Electric Corp.

control the coupling ratio at the low value.

We tried to compensate the linear coupling with only two skew quadrupoles which satisfy the special phase relation that the resonance phase difference is exactly $\pi/2$. The resonance phase denotes an argument of the function in the right-hand side of Eq. 1. Theoretically, we can achieve the perfect compenstion with these two magnets. For 4 rings of relatively large $\varkappa_{32}$'s, the linear coupling compensation was simulated with RACETRACK[5] including special fitting routine for it. We show the results in Table 1 and an example of the beam oscillation before and after the linear coupling compensation in Fig. 1. We can find remarkable improvement in both coupling coefficient and coupling ratio in Table 1, but find that this method can not achieve a lower target, 1% coupling ratio. We should analyze the cause for this imperfect compensation and establish a new compensation scheme to satisfy our requirement.

References

1) F. Willeke *et al.*: AIP Conf. Proc. 184, **1**, 758 (1987).
2) G. Guignard *et al.*: CERN 76-06 (1976).
3) J.P. Koutchouk *et al.*: Proc. of Particle Accel. Conf., Washington, D.C., U.S.A., March (1987).
4) H. Tanaka *et al.*: Presented at the 7th Symp. on Accel. Sci. and Tech., Osaka, Japan (1989).
5) A. Wrulich *et al.*: DESY Rep., 84-026 (1984).

RIKEN Accel. Prog. Rep. 23 (1989)

V-2-6. Study of Injection for the Storage Ring of SPring-8

H. Tanaka, R. Nagaoka, K. Tsumaki, K. Yoshida, and M. Hara

In spite of many studies for improvement of dynamic stability, the dynamic aperture of the storage ring of SPring-8 is now only 15 mm for horizontal plane, as shown in Fig. 1, at worst in the presence of practical errors.[1] Owing to two sextupole magnets on the bump orbit, this dynamic aperture is further reduced to about 10mm at injection. In order to inject the beams into this sensitive ring with high efficiency, we investigated the dependence of injection efficiency on the following 5 kinds of errors and parameters which are suspected to be dominant, because the problem is too complicated to treat all errors and parameters simultaneously.

(a) Injected beam emittance;
(b) Injection trajectory errors;
(c) Twiss parameter matching errors;
(d) Septum leak field; and
(e) Bump magnet residual field.

The Parameter (a) determines the spread of an injected beam, (b) and (c) enlarge the amplitude of coherent betatron oscillation at injection, and (d) and (e) reduce the dynamic aperture by nonlinear perturbations. Our design goal is to determine the tolerance level of each error achieving the efficiency higher than 50%, which means that the worst efficiency in all case studies goes beyond 50%.

In decision of the tolerance of each error, we tried to make the contribution of each error as low as less than 10% of the efficiency decrease. If we could keep this criterion, we could easily achieve the goal. But the dependence of the injection efficiency is so different that we could not keep the above criterion on all errors and parameters. Within current limits of hardware design,

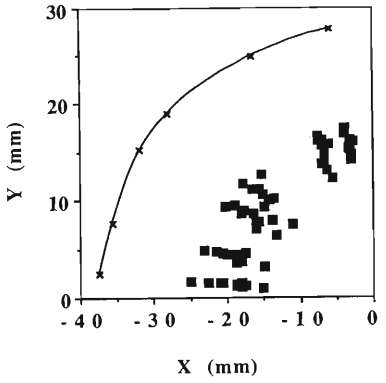

Fig. 1. 8 GeV hybrid lattice dynamic aperture. The tracking revolution number is 200 turn, the initial phase is 180 deg. (this is injection side), and the calculation point is at the beam injection point.
The Cross and dark square denote the dynamic perture without error and of 10 different rings with standard errors.[3]

Table 1. Tentative tolerance for the injection errors.

Item	Tolerance
Injection beam emittance	<200 nm rad
Injection trajectory errors	Angle 0.2 mrad
	Position 0.2 mm
Twiss parameter matching errors	$\beta > 25\%$
	$\alpha \pm 0.3$
Septum leak field	~30 G.m on bump orbit
	~1 G.m on reference orbit
Bump magnet residual field*	Damping coefficient
	$>10^5\ s^{-1}$
in the case of amplitude coefficient $<5\%$	
	Damping coefficient
	$>10^7\ s^{-1}$
in the case of amplitude coefficient $<50\%$	

*$B_{residual} = A \times F_0 \times \exp(-Bt) \times \sin(\omega t)$
F_0: Design magnetic field strength
A: Amplitude coefficient (−)
B: Damping coefficient (s^{-1})

we found that the injection trajectory error (angle error) and septum leak field mainly reduce the injection efficiency.[2] Therefore, these two tolerances become severe and make the specifications of hardware designs difficult. Consequently, we determined the tentative tolerances by adjusting the criterion so as to totally obtain the efficiency higher than 50%. The tolerances are shown in Table 1. Figure 2 shows the distribution of injection efficiencies for 80 machines under the error conditions that only twiss parameter matching is almost perfect and others have the same tolerance values. We can see from Fig. 2 that the worst efficiency is 60% and the average efficiency is about 90%. As we found by parameter search that the efficiency reduction due to the twiss parameter matching errors is slight, about several percent, we can expect to obtain sufficient efficiency ($>\sim$50%) at tentative tolerances.

We should investigate the following two things as soon as possible to estimate the tolerances correctly. One is injection trajectory matching to enlarge the effective dynamic aperture, which can make the tolerances of injection trajectory errors easier than what they are. The other is long life tracking to find the effect of the septum leak field correctly. Actually, there is possibility that the present results do not reflect on the slow damping effect of the septum leak field because

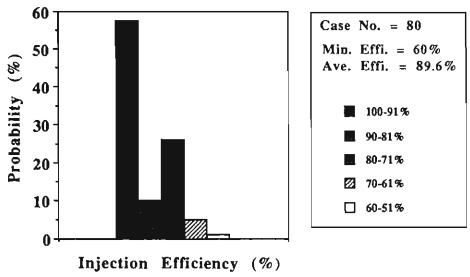

Fig. 2. Distribution of the practical injection efficiencies. Calculation is performed at the injection error that only twiss parameter matching is almost perfect and others have the same tolerance values. The tracking revolution number is 20 turn, the number of tracking particles are 200, and the ring errors is standard ones.[3]

of a small tracking revolution number, 20 turns. For this investigation, we should calculate the time structure of the septum leak field.

References

1) H. Tanaka, R. Nagaoka, K. Yoshida, K. Tsumaki, and M. Hara: *RIKEN Accel. Prog. Rep.*, **22**, 235 (1988).
2) H. Tanaka, R. Nagaoka, K. Tsumaki, and K. Yoshida: in preparation.
3) H. Tanaka, R. Nagaoka, K. Tsumaki, K. Yoshida, and M. Hara: *RIKEN Accel. Prog. Rep.*, **22**, 231 (1988).

RIKEN Accel. Prog. Rep. 23 (1989)

V-2-7. Design of a Quadruple Bend Achromat Lattice

K. Tsumaki, R. Nagaoka, H. Tanaka, and M. Hara

Generally, electron beams in a low-emittance storage ring are strongly focused to achieve low emittance. This fact generates many problems which are not principal difficulties for a high emittance storage ring: The dynamic aperture of such a low-emittance storage ring is too small and the sensitivity against field errors is very high. Thus, we need to design a storage ring which overcome these problems.

A Chasman-Green lattice with two bending magnets in a cell and a Triple Bend Achromat lattice with three bending magnets in a cell are well known as a low-emittance lattice for a synchrotron radiation source. In addition to these lattices, we designed a Quadruple Bend Achromat lattice (QBA) to obtain a better understanding of the dynamic characteristics of a low-emittance storage ring. This paper describes the lattice design of the Quadruple Bend Achromat lattice.

We imposed the following conditions in designing the lattice.

—Electron energy is 8 GeV and a bending magnet field strength is 0.6 T.
—Emittance is less than 10×10^{-9} m•rad.
—Circumference is less than 1500 m.
—The number of straight sections is more than 32.
—The length of the straight section is 6.5 m.
—A horizontal beta function is alternately high and low.

Under these conditions, our effort was focused on the designing of a lattice with a large dynamic aperture. To obtain a large dynamic aperture, the lattice should be detuned, but emittance also increases with detuning. On the other hand, the emittance decreases as the number of bending magnets increases. Accordingly, to obtain the large dynamic aperture with keeping the low emittance, we need to detune the lattice by increasing the number of bending magnets. On the basis of above idea, we designed a lattice which have four bending magnets in a cell (QBA lattice). Figure 1 shows the lattice functions and Table 1 shows the ring parameters.

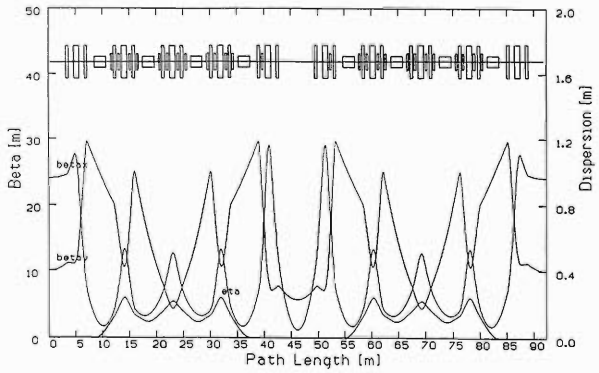

Fig. 1. Lattice functions of the QBA lattice.

Table 1. Major ring parameters.

Emittance	ε_0 (nm•rad)	5.0
Tune	ν_x (ν_{xc})	49.6 (3.10)
	ν_y (ν_{yc})	19.6 (1.23)
Chromaticity	ξ_x	−80
	ξ_y	−47
No. of cells	N	32
Circumference	C (m)	1477

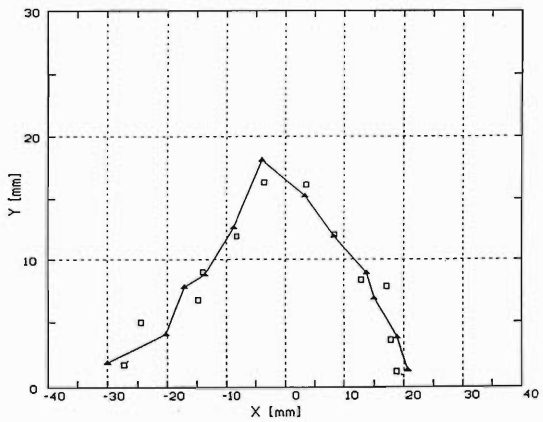

Fig. 2. Dynamic aperture of the QBA lattice. □, without harmonic sextupoles; ▲, with harmonic sextupoles.

The dynamic aperture obtained by particle tracking is shown by square marks in Fig. 2. These small dynamic apertures are mainly dominated by the first and third-order resonances induced by the strong sextupole fields of chromaticity correction sextupole magnets. To avoid these resonances, the amplitude dependent tune shift should be suppressed to be low.

To this end, sextupole fields were expanded to harmonics[1] and the contribution of each harmonics to amplitude dependent tune shift were studied. As a result, two harmonics were found

to have a large contribution to the amplitude dependent tune shift and limit the dynamic aperture. To suppress these harmful harmonics, additional sextupoles (harmonic sextupole) were placed in the non-dispersive section. We failed, however, to enlarge the dynamic aperture. If we suppress these harmonics to the extent where they are not the main source of a dynamic aperture limitation, the other harmonics grow and the dynamic aperture could not be enlarged. In this case, any definite single resonance does not limit the dynamic aperture, but a compound resonance limits the dynamic aperture. Consequently, the dynamic aperture cannot be enlarged by harmonic sextupoles. But dynamic aperture without harmonic sextupoles of the QBA lattice was larger than the Chasman-Green and the Triple Bend Achromat lattices.[2)]

References

1) R. Nagaoka, H. Tanaka, K. Yoshida, K. Tsumaki, and M. Hara: *RIKEN Accel. Prog. Rep.*, **22**, 248 (1988).
2) K. Tsumaki, R. Nagaoka, H. Tanaka, K. Yoshida, and M. Hara: Proc. 1989 Particle Accel. Conf. Chicago, March 20-23, 1989 (in press).

RIKEN Accel. Prog. Rep. 23 (1989)

V-2-8. Design of a Detuned Lattice

K. Tsumaki, R. Nagaoka, H. Tanaka, and M. Hara

Contrary to high-emittance storage rings, low emittance storage rings have small dynamic apertures and high sensitivity against errors. Accordingly, the commissioning of such rings is more difficult than high emittance storage rings. This difficulty leads to the idea that at first we should do commissioning with a detuned high emittance lattice instead of direct commissioning with a final-goal lattice. To this end, we designed a detuned lattice.

Design criteria: The lattice functions of a detuned lattice need to be similar to that of a final lattice,[1] because the generation pattern of a closed orbit must be similar to that of a final lattice. Thus it is desirable to detune the lattice without breaking the achromat condition of both straight sections in a cell. However, the lattice functions of a detuned lattice designed by keeping this condition has different behavior, and strong sextupole magnets for chromaticity correction are required. Therefore, we decided to break the condition of achromat of one straight section in a cell; we detune the lattice with two cells.

Table 1. Ring parameters of Detuned Chasman Green lattice.

	DCG1	DCG2	DCG3	DCG4	DCG5
Emittance(nm.rad)	16	23	37	53	82
Tune ν_x	33.20	31.20	28.20	25.20	22.80
ν_y	21.15	21.15	21.15	21.15	20.85
ν_{xc}	1.38	1.30	1.18	1.05	0.95
ν_{yc}	0.88	0.88	0.88	0.88	0.87

The betatron functions of straight sections are decided to have a medium value. On the basis of these criteria, we designed a detuned lattice of the emittance ranging from ~10 nm•rad to ~80 nm•rad.

Lattice functions and dynamic apertures: Lattice functions and dynamic apertures are shown in Fig. 1 and lattice parameters are shown in Table 1. These dynamic apertures are dominated by the first- and the third-order resonances driven by strong sextupole fields for chromaticity correction. The square mark is dynamic apertures only with sextupoles for chromaticity correction. The solid line is enlarged dynamic apertures by additional sextupoles (harmonic sextupoles) placed in a non-dispersive section. Figure 2 shows the operating point of each lattice on a tune diagram. Tunes of ν_{xc} and ν_{yc} are for one superperiod.

The dynamic apertures of lattices having emittaces from an 80 nm. rad level to a 50 nm•rad level (DCG5, DCG4) are limited by the resonances of $\nu_{xc}=1$ and $3\nu_{xc}=3$. However the driving term of these resonances can be easily canceled by only one harmonic sextupole. For a lattice having emittance of 30 nm•rad level (DCG3), the operating point is the middle of resonance lines $\nu_{xc}=1$ and $3\nu_{xc}=4$. As a result, the dynamic aperture is not small even though the emittance is smaller than the former two lattices. Tune of the lattice of 20 nm•rad level emittance (DCG2) approaches the resonance line of $3\nu_{xc}=4$ and the dynamic aperture is not large enough. Main driving terms are $\nu_{xc}=1$ and $3\nu_{xc}=4$. In this case it is difficult to cancel both driving terms by harmonic sextupoles. If the emittance reaches a 10 nm. rad level (DCG1), tune becomes larger than the resonance line of $3\nu_{xc}=4$. In this case, the dynamic aperture could be enlarged by two kinds of harmonic sextupoles. Dynamic apertures of these detuned lattices are large enough for injection of electron beams from the synchrotron.

Sensitivity against the errors: Figure 3 shows closed orbit distortions arising from random quadrupole displacements. X_{cod} and Y_{cod} are closed orbit distortions and dX and dY are expected values of alignment errors. Thus, we can find that expected values for closed orbit distortions are 3.5 mm and 4.1 mm for 0.1 mm

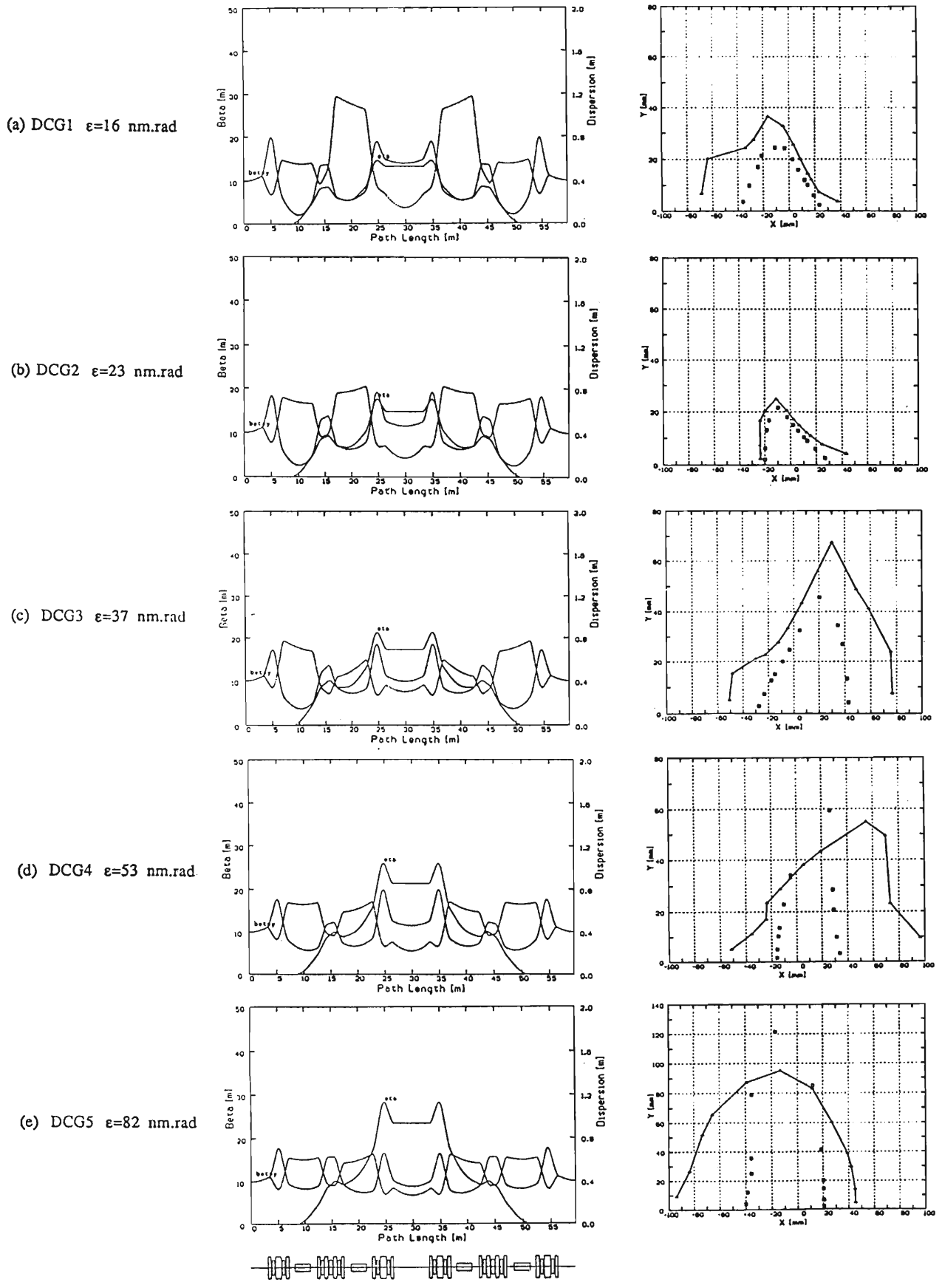

Fig. 1. Lattice functions and dynamic apertures.

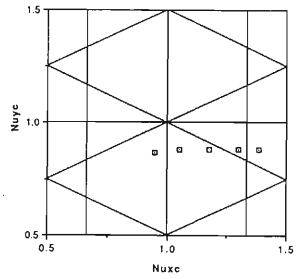

Fig. 2. Operating point on a tune diagram.

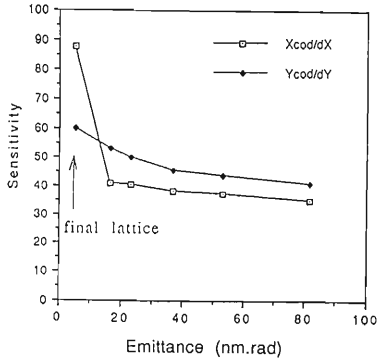

Fig. 3. Closed orbit distortions arising from random quadrupole displacements.

alignment errors of a quadrupole magnet for the ring of 80 nm•rad emittance. These values become 8.8 mm and 6.0 mm for the ring of 5 nm. rad emittance. Sensitivity of horizontal direction increases steadily when emittance decreases from 80 nm•rad to 16 nm. rad and changes from 41 to 88 for the final lattice. This shows that we may not need step-by-step commissioning from the ring of 80 nm•rad emittance to the final lattice, but only need to do it for the ring of 16 nm. rad emittance.

References

1) M.Hara *et al.*: XIV Int. Conf. on High Energy Accel., to be published in *Particle Accelerators*.

RIKEN Accel. Prog. Rep. 23 (1989)

V-2-9. Study of the Effect of Vibrations on Beam Stability

K. Tsumaki, R. Nagaoka, H. Tanaka, and M. Hara

If there are vibrations in magnets, the particles feel error fields, which deflect particle orbits. This effect becomes serious in low-emittance storage rings. Especially the closed orbit distortion (COD) due to quadrupole magnet vibration is remarkable. When the frequency of vibration is not so high, COD can be corrected by a feedback system, but when the frequency is high, feedback correction is not effective. As a result, growing beam size is observed as if emittance becomes large. If this "emittance growth" can not be neglected compared with intrinsic emittance, the meaning of low emittance is reduced. Thus, we studied the emittance growth due to the vibration of quadrupole magnets.

The cause of COD is due mainly to the displacement of the center of a quadrupole magnet by vibration. There are two types of vibration sources. One is the vibration of component equipments such as magnets and vacuum pumps and the other is the ground vibration. The former is further divided into two cases: all quadrupole magnets vibrate randomly and one specific quadrupole magnet vibrates. The ground vibration is treated as a plane wave and is assumed to propagate directly to a quadrupole magnet without attenuation.

The emittance growth is calculated using the expected values of COD originated from these vibrations. For single quadrupole vibration, the emittance growth due to vibration of a quadrupole magnet which has the strongest field was calculated since this gives the largest emittance growth. For plane-wave vibration, having not studied the power spectrum of vibration, we cannot calculate the emittance growth; thus, only magnification factor $M=\mathrm{COD}/\Delta d$ was calculated, where Δd is the amplitude of vibration.

Figure 1 shows the emittance growth $\Delta\varepsilon$ normalized by the intrinsic emittance ε_0 due to random quadrupole vibration. The coupling of horizontal and vertical betatron oscillation is assumed to be 10 %. As seen from Fig. 1, we need to suppress the random quadrupole vibration to be less than 0.15 μm for keeping the horizontal emittance growth within 10 %. For the vertical emittance growth of 10 %, the vibration of 0.05 μm amplitude is allowable. Figure 2 shows the emittance growth due to single quadrupole vibration. In this case, the vibration amplitude should be less than 1.2 μm for 10 % horizontal emittance growth and 0.7 μm for 10 % vertical emittance growth. Figure 3 shows the magnification factors due to ground vibration on the assumption that the propagation velocity of plane wave is 1,000 m/s. As seen from the figure, the magnification factor increases with increasing vibration frequency.

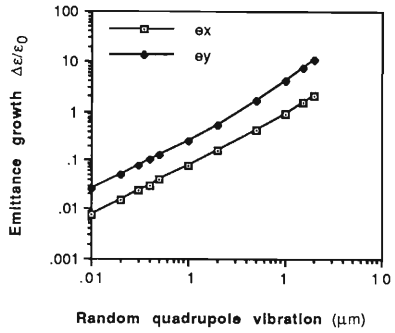

Fig. 1. Emittance growth due to random quadrupole vibration. —□—, horizontal emittance; —◆—, vertical emittance.

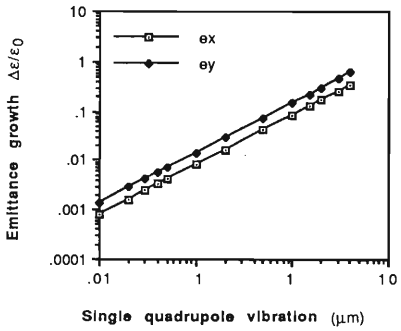

Fig. 2. Emittance growth due to single quadrupole vibration. —□—, horizontal emittance; —◆—, vertical emittance.

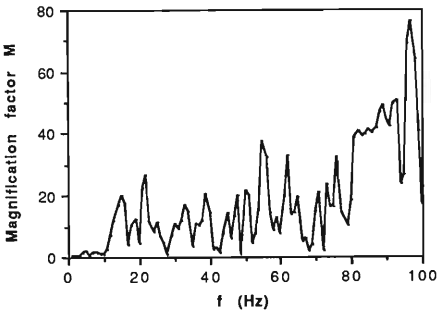

Fig. 3. Magnification factors due to ground vibration.

RIKEN Accel. Prog. Rep. 23 (1989)

V-2-10. Vacuum System for the SPring-8

S.H. Be, S. Yokouchi, Y. Morimoto, T. Nishidono,
Y.P. Lee,* and Y. Oikawa

The vacuum system consists of two differently shaped aluminum alloy (A6063-T5 whose strength is equivalent to that of T6) chamber extrusions, two types of absorbers, and various chamber components such as bellows, flanges and valves.

To achieve a beam lifetime of approximately 24 hours, the vacuum chamber with its pumping system should be designed so as to maintain the beam-on pressure of 1 nTorr or less. The main pumping system[1] is based on non-evaporable getter (NEG) strips, which are used in both the straight and bending chamber. In addition to the NEG strips, a distributed ion pump (DIP) is installed in a bending magnet chamber. A lumped NEG pump, a sputter ion pump, and a titanium sublimation pump are installed at a crotch and an absorber which are placed just downstream and upstream of a bending magnet, respectively.

Figure 1 shows a section of a unit cell with electron beam injection, showing the crotch (CR), absorber (AB), and magnets (QM, SM, KM). In a normal cell, there is no kicker magnet (KM). The details of the vacuum chamber,[2] crotch,[3] and others are described below.

In designing chamber components, a special effort must be made to minimize their impedance characteristics because, in a storage ring, the maximum achievable beam current depends greatly on their impedance. Therefore, the components must be designed so as to make the change in the cross secstion as little as possible. To minimize the impedance of the chamber components, the gaps between flanges must be

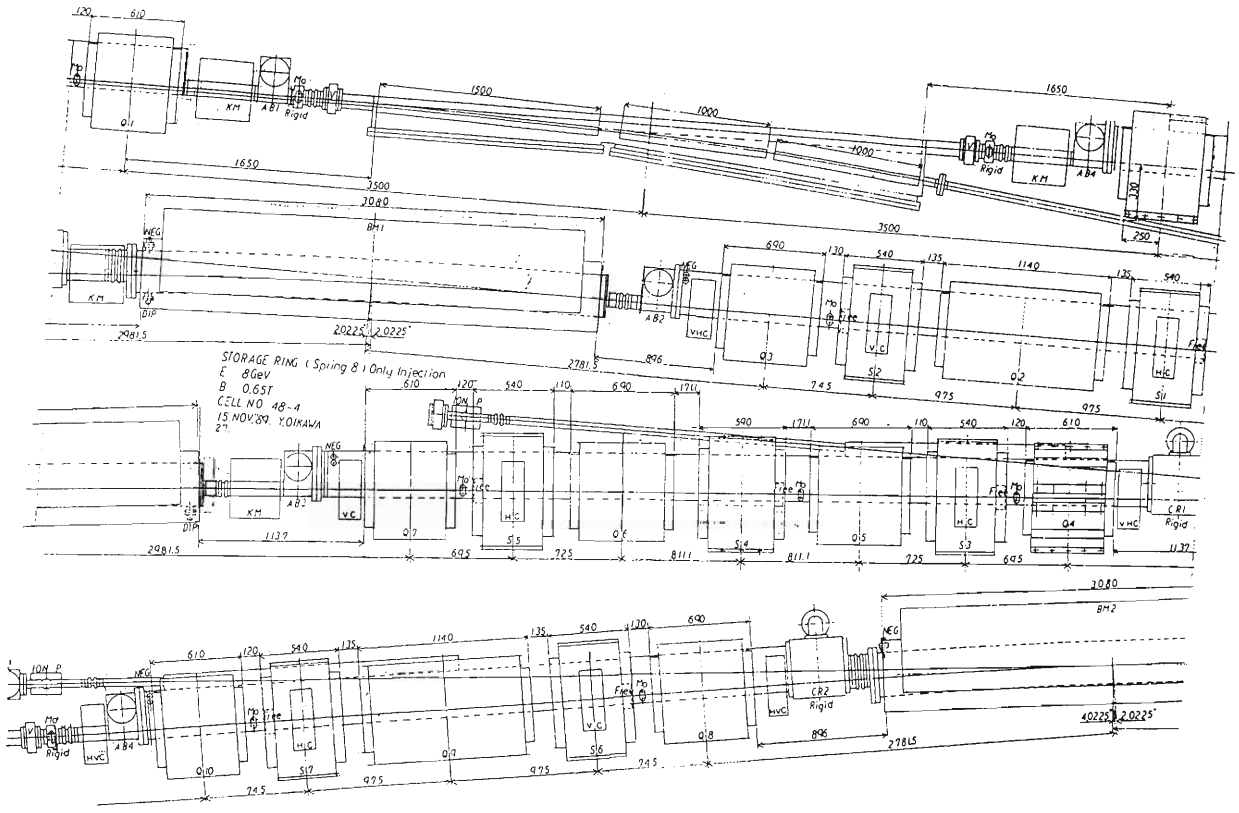

Fig. 1. A section of a unit cell with electron-beam injection, showing a crotch (CR), an absorber (AB) and magnets (QM, SM and KM).

* On leave from RIST, Pohang, Korea.

reduced, and the bellows must be shielded with an RF contact. A step change in the cross section of the vacuum chamber must be provided by means of a tapered transition, too. Our policies for the design of the vacuum system are: 1) The number of flanges and bellows should be as small as possible; 2) Monitors are mounted directly on the vacuum chamber without any special monitor chamber; 3) The connection between a kicker chamber and main vacuum chamber should be done by welding; 4) Crotches are fixed to have advantages in the mounting of the chamber; 5) The NEG assembly and DIP should be exchangeable for maintenance; 6) Welding around the ring should be kept down to the least.

The chamber for a straight section is installed with free mounts[4] and crotches as shown in Fig. 1. The crotch is completely rigid, not to allow chamber movement in any direction even during bakeout cycles. The free mount allows chamber's thermal expansion or contraction only in the electron beam direction, but not the vertical by means of a special mechanism. This mounting method should ensure the displacement of the vacuum chamber within the accuracy of less than 0.1 mm required for a beam position monitor (BPM).

Furthermore, the deformation of the chamber due to the pressure difference between atmosphere and vacuum is to be kept less than 0.1 mm. Therefore, the respective thicknesses of the beam chamber and a slot designed previously[5] are changed from 11 to 15 mm and from 6 to 10 mm, respectively. Thus we can keep the displacement to be less than 0.1 mm at the position of the BPM (see Fig. 2), which is to be installed between a sextupole magnet (SM) and a quadrupole magnet (QM). Figure 2 shows chamber geometries at the respective locations of SM (at upper part of the chamber) and QM (at lower part). The beam chamber and slot to be positioned in the SM and QM are cut by machining because of a special limitation.

The vacuum chamber for photon-beam extraction is shown in Fig. 3. An extraction chamber and an antechamber is connected with an electron beam welding.

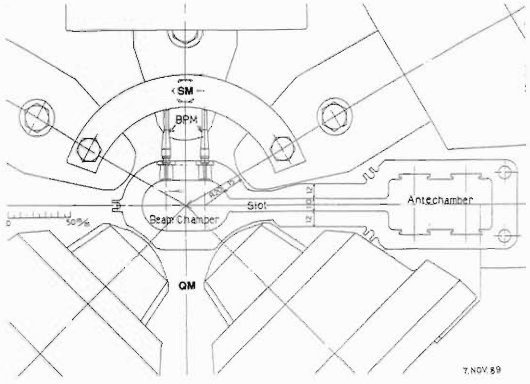

Fig. 2. Geometries of the vacuum chamber at the positions of quadrupole and sextupole magnets.

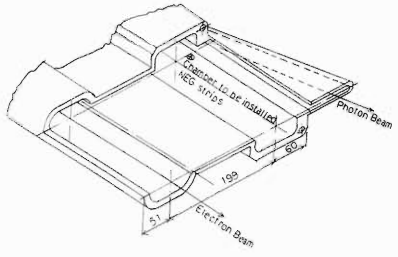

Fig. 3. Geometry of the chamber for extraction of a photon beam.

References

1) S. Yokouchi, H. Sakamoto, Y. Morimoto, and S.H. Be: *RIKEN Accel. Prog. Rep.*, **22**, 279 (1988).
2) H. Sakamoto, T. Bizen, S. Yokouchi, Y. Morimoto, T. Nishidono, Y.P. Lee, and S.H. Be: This Report, p. 145.
3) Y. Morimoto, Y. Yokouchi, T. Nishidono, Y.P. Lee, and S.H. Be: Proc. of 7th Meet. on Ultra High Vacuum Techn. for Accel. and Storage Ring KEK, (by G. Horikoshi and M. Kobayashi) March, p. 68 (1989).
4) T. Nishidono, S. Yokouchi, Y. Morimoto, Y.P. Lee, and S.H. Be: This Report, p. 143.
5) T. Nishidono, H. Kakui, S.H. Be, H. Sakamoto, S. Yokouchi, Y. Morimoto, and Y. Oikawa: *RIKEN Accel. Prog. Rep.*, **22**, 281 (1988).

RIKEN Accel. Prog. Rep. 23 (1989)

V-2-11. Outgassing Rates of 4 m-Long Model Chambers with and without NEG Strips

S. Yokouchi, H. Sakamoto, T. Nishidono, Y. Morimoto,
Y.P. Lee,* and S.H. Be

We test-manufactured two kinds of Al-alloy vacuum chambers for the R&D of the vacuum system[1] of SPring-8. One is modeled for a straight-section chamber (SSC) and the other for a bending magnet chamber (BMC), both made of extruded Al alloy[2] and 4m long.

We measured their outgassing rates (q) which are very important to achieve ultra-high vacuum for a required beam lifetime. Figure 1 shows a system for measuring q, which were obtained by a throughput method making use of

$$q = C\ (p_1 - p_2)/A \qquad (1)$$

where C is the conductance of an orifice (2.32 l/s for N_2), p_1 and p_2 the pressures in Torr at IG 1 and 2, respectively, and A the total surface area of a sample in cm^2.

Figure 2 shows q *vs.* the pumping time for SSC without NEG strips.[3] We obtained q of the orders of 10^{-10} Torr$\cdot l$/s$\cdot$cm^2 after $\sim$100 hour evacuation without baking. After a baking at 140°C for 40 hours, q was measured and found to be as low as 10^{-13} Torr$\cdot l$/s$\cdot$cm^2.

The q-value of BMC was also measured with NEG strips in it (Fig. 3). In this case, we have another source of q from the surface of NEG strips and their supports (SUS 304 and ceramics) as well as the chamber itself. The contribution from the NEG strips will, of course, vanish after activation. Since indifferent evaluation of q for each material was very difficult, we got an overall q by using Eq. (1) with overall A. q was $\sim 10^{-10}$ Torr$\cdot l$/s$\cdot$cm^2 after pumping for tens of hours without baking, almost the same as for SSC. On

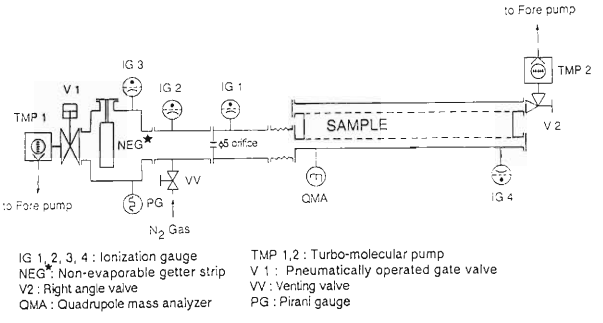

Fig. 1. Schematic diagram of a setup for measurement of outgassing rates. NEG strips were not installed in SSC, but in BMC. V2 is open for TMP 2 only when the chamber pressure is too high.

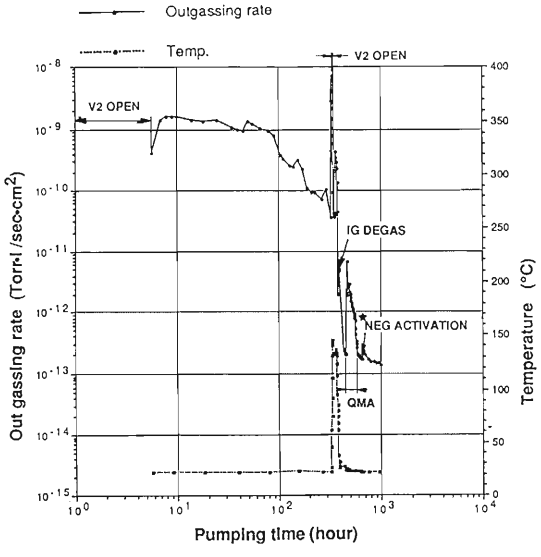

Fig. 2. q *vs.* the pumping time of SSC without NEG strips.
$A = 3{,}000$ cm^2.

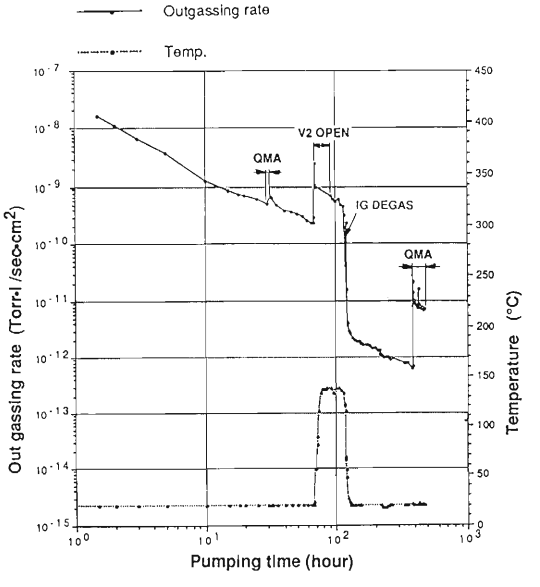

Fig. 3. q *vs.* the pumping time of BMC with NEG strips.
$A = 56{,}000$ cm^2 (30,700 cm^2 for the chamber itself, and 8,700 and 16,600 cm^2 for NEG strips and their supports, respectively).

* On leave from RIST, Pohang, Korea.

the other hand, q was higher an order of magnitude to be low 10^{-12}-high 10^{-13} Torr•l/s•cm^2 after baking under the same condition as SSC. This can be interpreted in terms that the bakeout was not enough for the NEG strips and their supports.

No problem is foreseen in a real storage ring where NEG is working as far as thermal outgassing from chambers is concerned, because we were able to get q smaller than 5×10^{-12} Torr•l/s•cm^2 (the required value for our vacuum system), only by a baking at 140°C for 40 hours.

References

1) S.H. Be, S. Yokouchi, Y. Morimoto, T. Nishidono, Y. P. Lee, and Y. Oikawa: This Report, p. 132.
2) H. Sakamoto, T. Bizen, S. Yokouchi, Y. Morimoto, T. Nishidono, Y. P. Lee, and S.H. Be: This Report, p. 145.
3) Y. P. Lee, S. Yokouchi, and S.H. Be: *J. Vac. Sci. Technol.* (to be published).

RIKEN Accel. Prog. Rep. 23 (1989)

V-2-12. Test of OFHC Flanges

S. Yokouchi, Y. Morimoto, T. Nishidono, Y.P. Lee,* and S.H. Be

Oxygen-free high-conductivity copper (OFHC) has been chosen as material for the crotch of the main storage ring of SPring-8. We are considering flanges of the same material because of its easy work and low cost, together with OFHC-Al alloy hybrid flanges. OFHC flanges were prepared, and their sealing characteristics have been investigated.

Figure 1 shows a completed flange. The material is OFHC of class 1, and Ag is added by 0.19% to enhance the hardness. The hardness was found to be H_v (5 kg)=112-124 at a reduction of 55%. A Helicoflex (HN200-H15048) was employed as a gasket, whose tube diameter, inner and outer diameters are 4.5, 101.8, and 110.8 mm, respectively. The surface is coated with pure Al in two layers. The required sealing force (F) was suggested to be 10,600 kgf for this flange pair. The material of the bolts used is SUS 304.

We studied the relationship between sealing force (F_f) and leakage. F_f can be obtained from the stress (σ_b) on the bolts identified by installed strain gauges. A He-leak test indicated no leak at room temperature (the minimum detectable leak rate (q_{min})=1×10^{-10} Torr·l/s) after fastening torque (T)=100 kgf·cm, where F_f=9,840 kgf (F_f/F=93%) and σ_b=15.2 kgf/cm^2. When T was raised further to 120 kgf·cm, F_f and σ_b were changed to 14,600 kgf (F_f/F=137.32%) and 22.5 kgf/cm^2 (above proof strength of the bolts), respectively, and still no leak shown at $q_{min}=2\times10^{-10}$ Torr·l/s even after baking at ~150°C. The relationship between F_f and leakage is not clear yet to be concluded even if we have some results including the aforementioned. We are continuing study on it.

The flanges under test were disassembled to measure the roughness of the surface, and were subjected to optical microscopy of the sealed surfaces. The surfaces of flanges were replicated for the measurement and observation. Figure 2 are photographs of the sealed surfaces of flange A and B, and those of the corresponding Helicoflex gaskets in Fig. 3 (a) and (b). Figure 3 includes another photographs to show the surface of an unused Helicoflex in (c). The measured results of surface roughness are also shown in Fig. 4 (a) and (b) for flanges A and B, respectively. It should be noticed that the surface of Helicoflex is changed to replicate that of the flange since the Helicoflex is softer pure-Al layers on the surface. Therefore, leakage paths[1] between flanges and gasket becomes tremendously small, in particular along the cross-sectional direction to provide an exellent sealing action against leakage.

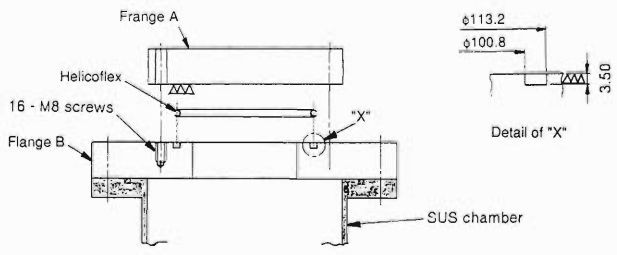

Fig. 1. Drawing of a completed flange.

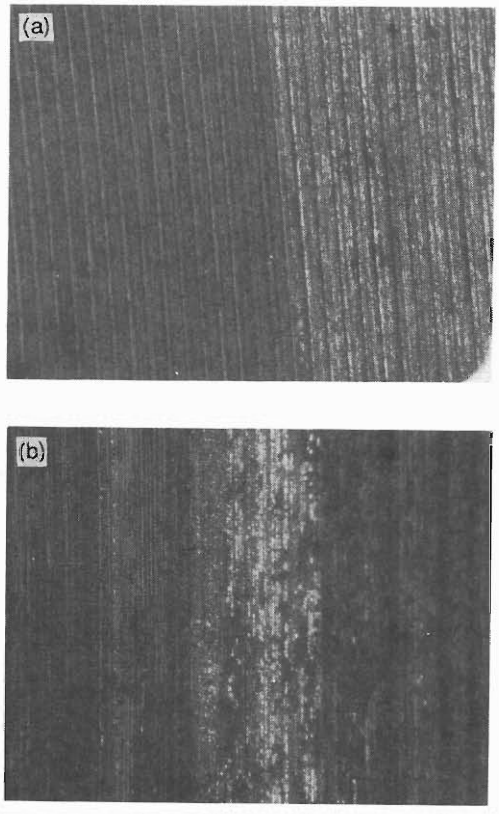

Fig. 2. Photographs (×62.5) of the sealed surfaces of flanges (a) A and (b) B.

* On leave from RIST, Pohang, Korea.

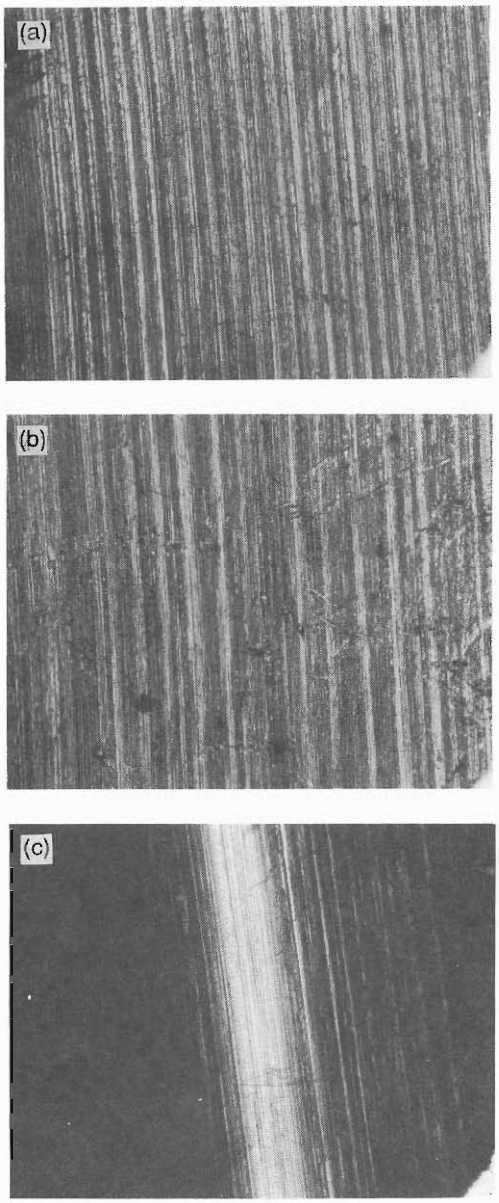

Fig. 3. Photographs (×62.5) of the sealed surfaces of Helicoflex gaskets (a) A and (b) B. (c) for the surface of an unused Helicoflex.

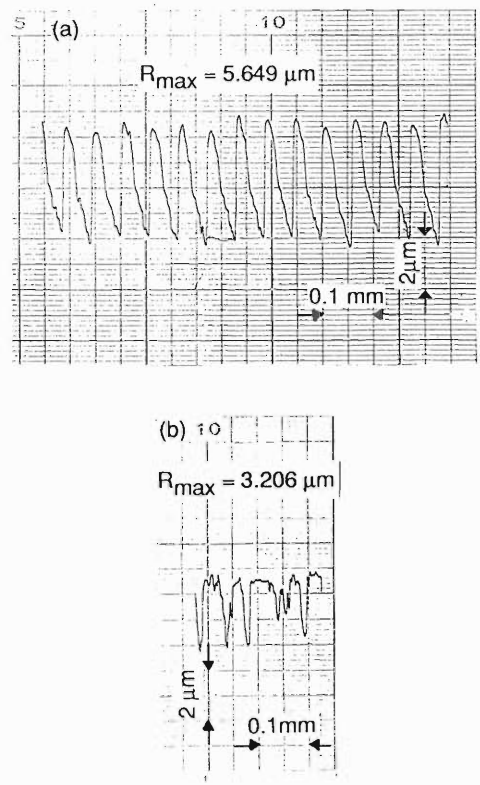

Fig. 4. Results of surface roughness measured for flanges (a) A and (b) B.

References

1) A. Roth: "Vacuum Technology", North-Holland, Amsterdam, p. 395 (1982).

RIKEN Accel. Prog. Rep. 23 (1989)

V-2-13. Manufacture of a Lumped NEG Pump

S. Yokouchi, Y. Yamano,* T. Nishidono, Y. Morimoto,
Y.P. Lee,** and S.H. Be

We test-manufactured a lumped NEG (non-evaporable getter)[1] pump for the crotch of SPring-8. The lumped NEG pump was designed to have large pumping speeds for CO and H_2 in the ultra-high vacuum range. Figure 1 shows a schematic drawing of the lumped NEG pump. The housing is made of Al alloy. A Helicoflex gasket is used between ϕ 460 flanges whose sealing surfaces are ion-plated with TiC.

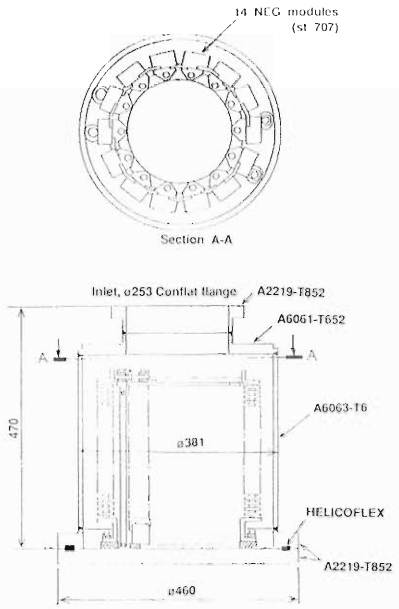

Fig. 1. Schematic drawing of the lumped NEG pump.

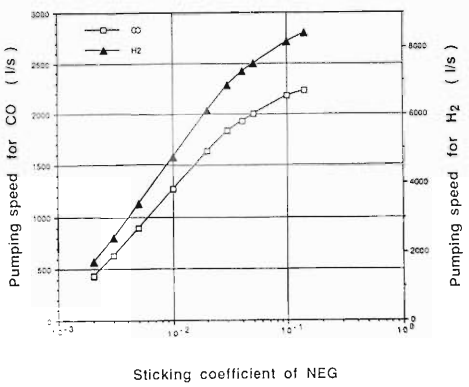

Fig. 2. Pumping speeds *vs.* the sticking coefficient for CO and H_2 at the inlet of the lumped NEG pump.

Fourteen NEG modules are mounted concentrically in the housing. We calculated pumping speeds for CO and H_2 at the pump inlet by a Monte-Carlo method. The results are shown in Fig. 2. Since the required pumping speed for CO is more than 1,500 l/s, the sticking coefficient on NEG should be larger than 1.5×10^{-2}. The pumping speed of NEG per unit area for CO (S) is related with the sticking coefficient (s_c) by $S=11.8s_c$ l/s·cm². Therefore, S turns out to be larger than 0.18 l/s·cm², which can be achieved practically according to experimental results[1] on NEG.

Copper tubes of 10 mm in diameter are attatched on the outer surface of the housing to eliminate the power generated during heating NEG. Since Cu cannot be welded or brazed to Al, the Cu tubes are bonded with an electrecally and thermally conductive binder (Silbest SIR 04) composed of epoxy resins, Ag powder, and volatile ingredients. We estimated a temperature rise in the housing to be lower than 40°C, assuming that generated power, water temperature, and a flow rate of water are 4.7 kW, 20°C, and 1.5 m/s, restectively.

The housing should be baked at 150°C to get the required ultra-high vacuum. Micro heaters, whose electric power is 1.3 kW, are also installed on the outer surface of the housing. The heater power is enough to rise the housing temperature up to 150°C with a few heat-insulation layers of polyimide film on which pure Al is vapor-deposited and embossed in a hemispherical shape.

We are planning to test and evaluate the performance of the lumped NEG pump for the R & D of SPring-8.

References

1) Y. P. Lee, S. Yokouchi, and S.H. Be: *J. Vac. Sci. Technol.* (to be punlished).

* Osaka Vacuum, Ltd.
** On leave from RIST, Pohang, Korea.

RIKEN Accel. Prog. Rep. 23 (1989)

V-2-14. Surface Analysis of Al-Mg-Si Vacuum Chamber

Y.P. Lee,* T. Nishidono, S. Yokouchi, Y. Morimoto, and S.H. Be

The extruded A6063-T5, whose strength is equivalent to that of T6, has been found to be appropriate as ultra-high vacuum material, especially for accelerators. The outgassing rate and desorption induced by high-energy photons and their photoelectrons are known to have correlation with the surface conditions. We have analyzed the surface of an extruded Al-Mg-Si model chamber for SPring-8 by Auger Electron Spectroscopy (AES) and Scanning Electron Microscopy (SEM) in mind for the gas loads. Furthermore, since some unexpected specks of extra corrosion were seen on one of our cleaned test chambers, we also figure out their nature and origin.

EXPERIMENTALS: AES and SEM were carried out with a JEOL JAMP 30 Auger Microprobe. For AES, E_p=5 keV and i_e=500 nA. When ion bombardment was required for depth-profile, an ion sputter gun was used at V_{ion}=3 keV and i_{ion}=30 nA with a homogeneous raster of 300μm×300μm

RESULTS AND DISCUSSION: Three distinct samples were prepared from the model chamber. Sample A and B represent the ordinary surface before and after cleaning process, respectively. 1,1,1,-trichloroethane was employed as the cleaning solvent. Sample C was picked up to include the extraordinary corrosion specks which didn't exist on the orginal extruded surface.

The intensity (I) of Al KLL peak is only 0.333 times that of Mg KLL peak on Sample A. This measured ratio is much smaller than the limit for bulk (89.941), suggesting a Mg oxide-rich layer for the top 30 Å as in Ref. 1. On Sample B, all I's were decreased compared with Sample A, suggesting a less dense oxide and contamination at the top. This may be attributed to the cleaning procedure. On the other hand, the top 30 Å is found more Mg oxide-rich than A to be $I_{Al\ KLL}$ / $I_{Mg\ KLL}$=0.206. Three characteristic points were investigated for Sample C. Point C-1 was picked up from the speck on the left in Fig. 1. Point C-2 is on the top smaller speck of the right side one, which looks another phase of corrosion-growth. The other probing point is on a heavily-oxidized particle of small size in the border itself for the left speck. All the points revealed no Mg KLL, and furthermore no oxidized Mg LVV on C-3, contrary to the aforementioned two samples. Even on C-1 and C-2, I ratios of oxidized Al LVV to oxidized Mg LVV are very large to be 7.983 and 20.045, respectively. These facts are interpreted by the predominancy of Al oxide through the top 30 Å of the surfaces. On the other hand, the $I_{0\ KVV}$'s are smaller than even Sample B, indicating a less dense oxide.

The AES depth-profiles of Sample B are shown in Fig. 2. Four characteristic zones are identified in Figs. 2 and 3. First of all, a superficial contamination zone (Zone 1) up to the oxygen maximum, and the Mg oxide-rich layer (Zone 2). This is followed by Zone 3, an Al oxide-rich layer at the beginning and then a mixed state of oxide and metal, and finally substrate (Zone 4). The durations of sputtering for the first 3 zones are defined by τ_1, τ_2 and τ_3, respectively. Zone 1 is not seen for sample B, which is probably an effect of cleaning. τ_3=23.667 min $\gg \tau_2$, and the total sputter-time at $1/e\, I_0^{max} \equiv t_{oxide}$ = 4.0 min. This corresponds to thickness ($\equiv Z_{oxide}$) of ~80 Å. All the values turn out to be only 51-65% with espect to Sample A. This can be understood by the aforementioned fact that we had a more Mg oxide-rich layer at the top before depth-profile than A. Figure 3 is for Point C-1 showing quite different behavior. τ_1 was found again to be 1.5 min, but no Zone 2 seen in agreement with the analysis on its natural surface. τ_3=168.5 and t_{oxide}=34.571 min (z_{oxide}~691 Å), which are 7.1 and 8.6 times the corresponding values of Sample B, respectively. This relatively

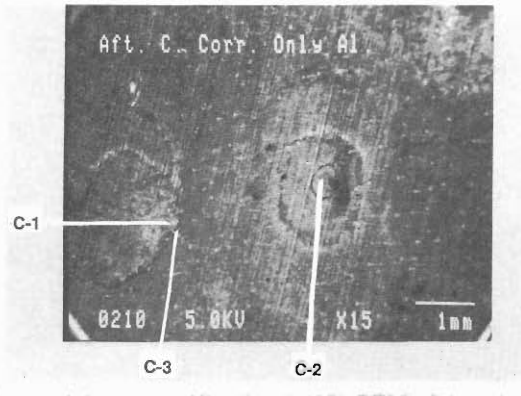

Fig. 1. A low-magnification (×15) SEM picture to see an overview of Sample C.

* On leave from RIST, Pohang, Korea.

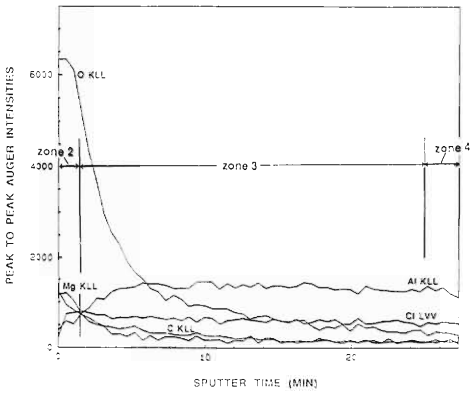

Fig. 2. AES depth-profile of Sample B.

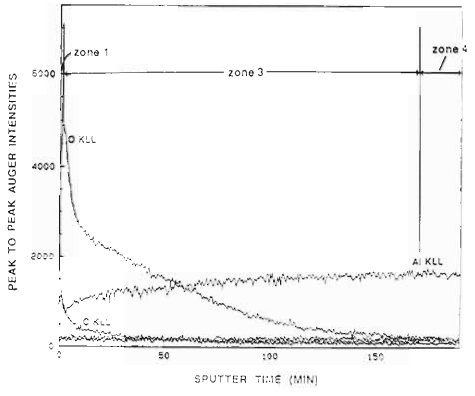

Fig. 3. AES depth-profile of Point C-1 on Sample C. Two nearly constant curves at a very low intensity are for Cl LVV and Mg KLL Auger peaks.

porous and thick oxide will provide a source itself of synchrotron-induced desorption as well as a channel for outgassing from the bulk of chamber wall.

When the alloy material goes through extrusion, Mg can be segregated or evaporated remarkably through an initial thin Al-oxide layer[2] owing to high temperature (480-520°C) during the process.[1,2] Therefore, Mg oxide is grown preferentially. Nevertheless, the amount of Mg is limited near the surface immediately before and during oxidation because its bulk composition is only 0.62 at.%. Consequently, the Mg-rich layer at the top should be thin,[2] and separated by a Mg-depletion layer from the ordinary bulk. Additional Al oxide-rich layer is grown beneath the initial Al oxide-rich layer. Nevertheless, the total thickness is smaller with the top Mg oxide-rich layer than that without it owing to the nature of Mg oxide-rich layer as a modifier.[3]

If the formed oxide layer at the top is broken away after extrusion, Al itself is exposed directly to chemical attack (especially during cleaning) and atmosphere. The grown Al oxide is less dense as already pointed out in terms of smaller $I_{0\ KVV}$'s for every point on Sample C than even B, and accordingly thicker than oxidation at extrusion. The cleaning procedure is thought to be the strongest interaction with the surface after extrusion. A small amount of strong acid like HCl can be dissociated from the cleaning solvent ($CH_3CCl_3 \rightarrow CH_2=CCl_2+HCl$), especially under the conditions of bright light, heat, water mixed, and catalytic metal mixed.[4] It can, then, etch out the superficial oxide at some places, particularly where the oxide layer has been shaken during high temperature and other preceding processes.

References

1) Y. Kato, K. Tsukamoto, E. Lsoyama, and T. Uchiyama: *J. Vac. Soc. Jpn.*, **28**, 785 (1985).
2) B. Goldstein and J. Dresner: *Surf. Sci.*, **71**, 15 (1978).
3) F.P. Fehlner: "Low-Temperature Oxidation", Wiley-Interscience, New York, pp. 29, 116 (1980).
4) S. Tsuji ed.: "Fine Cleaning Technology Manual", New Technology Development Center, Japan, p. 27.

RIKEN Accel. Prog. Rep. 23 (1989)

V-2-15. Performance Characteristics of a St 707 Non-evaporable Getter Strip

Y.P. Lee,* S. Yokouchi, Y. Morimoto, H. Sakamoto,**
T. Nishidono, and S.H. Be

A non-evaporable getter (NEG) can be manufactured even in a long linearly distributed shape for the conductance-limited vacuum chambers of particle accelerators including storage rings to provide a high pumping speed and large capacity in a simple, cheap, and flexible way. St 707 NEG strips are under consideration to be used as the main pump in both straight and bending chambers of this ring. We present the experimental characteristics at room temperature of the St 707 NEG strip in mind for our ring. The work includes a series of measurements of the pumping speeds (S) with respect to gases such as H_2, CO, N_2, and CO_2. The covered gas quantity sorbed (Q) is from as small as $\sim 2\times10^{-8}$ to $\sim 2\times10^{-3}$ Torr$\cdot l/cm^2$. We also demonstrate the dependence of the pumping speeds of H_2 and CO on the parameters such as initial gas loading (Q_0), gas injection-rate (q), and reactivation temperature (T_{act}) and time (t_{act}).

Experimentals: The experimental setup is essentially the same as in previous Progress Report.[1] The base pressure was in the range of high 10^{-11} Torr after a baking at $\sim$150°C for 37 h. The NEG was activated at 450°C by means of resistance-heating in a controlled way according to Sieverts' law[2] for H_2. For the other gases, Q_0 is regarded as zero after a reactivation at $\sim$450°C for 0.75 h. As soon as the reactivation had been done, the gate-valves to pumps were shut down and conductance adjusted for 20 l/s SIP, followed by the introduction of high-purity ($\geq$99.9%) gas at a constant throughput. S was, then, measured periodically by the conductance method.

Results and discussion: Figure 1 shows the comparison of S for H_2 at different Q_0's and the same $q=1\times10^{-5}$ Torr$\cdot l$/s. In general, a larger S is seen at a smaller Q_0, especially in the region of low Q although all the curves down to $S=0.2$ l/s$\cdot$cm^2 at $Q=10^{-3}$ Torr$\cdot l/cm^2$. The sorption of H_2 is carried out by bulk-diffusion mechanism as well as surface kinetics, and the results are coincident with a theoretical development on bulk gettering by Knize and Cecchi.[3] The Q's at bending (Q_b) in the first two and at the concave in the last curve are almost identical in the Figure. These Q's are considered as the transition point from surface-limited to bulk-limited mechanism. This process is, of course, competed with the adsorption process to the inner surfaces of the voids.[4] A simple transformation of Q in Fig. 1 to "Q" by "Q"$=Q_0+Q$ makes us to acquire a general curve from (S, "Q") = (0.34 l/s$\cdot$cm^2, 3×10^{-4} Torr$\cdot l/cm^2$) down to (0.2, 4×10^{-3}), which governs every Q_0 case (Fig. 2). S

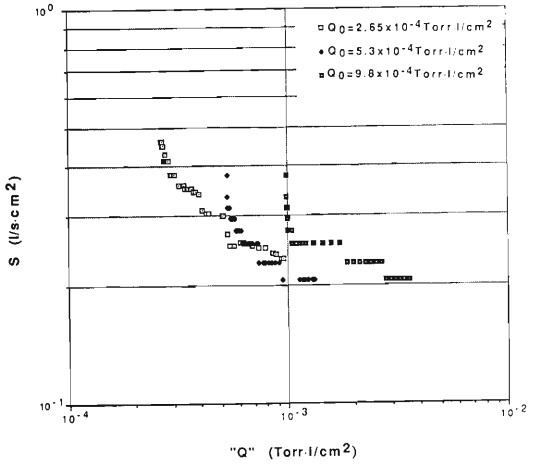

Fig. 1. Comparison of the pumping speeds for H_2 at different Q_0's and the same q.

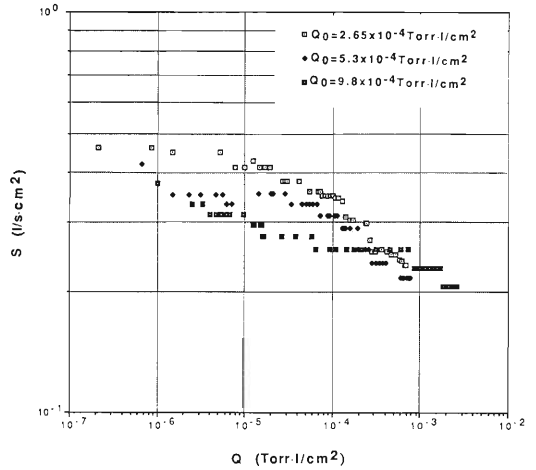

Fig. 2. "Q" version of Fig. 1.

* On leave from RIST, Pohang, Korea.
** Ishikawajima-Harima Heavy Industries Co., Ltd.

for H_2 was also compared at different q's and the same Q_0 to show little q-induced difference in S.

In Fig. 3, H_2, CO, CO_2, and N_2 are compared at the same q. Q_0 for H_2 is 2.65×10^{-4} Torr·l/cm^2, and the reactivation for CO, CO_2, and N_2 performed at 450°C for 0.5 h. S of H_2 was constant ($\Delta S=0.2l$/s·cm^2 from $Q\cong10^{-7}$ to 10^{-3} Torr·l/cm^2). On the other hand, that of CO decreases very rapidly to 3.3×10^{-3} S_0 at $Q=4\times10^{-4}$ with respect to 4×10^{-8} Torr·l/cm^2. S_0's of CO and CO_2 are fairly large, but that of H_2 is lower by an order of magnitude and smaller another order for N_2. The order of $H_2>N_2\sim CO\geq CO_2$ is seen with respect to Q_0. The physical meanings of Q_0's for N_2, CO and CO_2 are interpreted in a different sense. Since the bulk diffusion of these gases is not likely to happen at room temperature, this point indicates only the transition to the aforementioned adsorption mechanism[4] onto the inner surface. CO was also compared after different T_{act} and t_{act}'s, and at different q's. The efficiency of a NEG turned out to be ~40% after $T_{act}=280$°C. It was noticed that the full reactivation at 450°C can be completed only for 0.5 h, and the little dependence on q confirms only the surface relevant to the pumping for CO.[4]

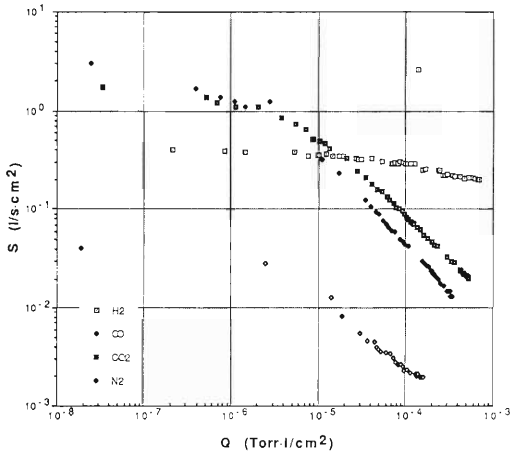

Fig. 3. Comparison of the pumping speeds for H_2, CO, CO_2, and N_2 at the same q.

References

1) S. Yokouchi, H. Sakamoto, Y. Morimoto, and S.H. Be: *RIKEN Accel. Prog. Rep.*, **22**, 283 (1988).
2) C. Boffito, B. Ferrario, and D. Martelli: *J. Vac. Sci. Technol.*, **A1**, 1279 (1983).
3) R.J. Knize and J.L. Cecchi: *J. Appl. Phys.*, **54**, 3183 (1983).
4) C. Benvenuti and F. Francia: *J. Vac. Sci. Technol.*, **A6**, 2528 (1988).

RIKEN Accel. Prog. Rep. 23 (1989)

V-2-16. Mounts of Vacuum Chambers

T. Nishidono, S. Yokouchi, Y. Morimoto,
Y.P. Lee,* and S.H. Be

Aluminum alloy extrusions (A6063-T5) are employed for the vacuum chambers of the SPring-8 storage ring, since the chambers are to be baked out at about 150°C to minimize their thermal outgassing rate, chamber mounts should be designed to be protected from thermal expansion during baking, and to keep the location of beam position monitors (BPM) unaltered after baking.

On the other hand, in the straight sections of the storage ring, the space are narrow between magnets; therefore bellows can not be used to compensate the thermal expansion of chambers, and BPM can not be mounted directly on the magnets. We are considering two types of mounts to overcome these difficulties. One is rigid and allows no chamber motion in any direction at the point of support "rigid mount". The other type of mount allows the chamber motion only in the longitudinal direction "free mount". The location of BPM can be fixed by this mount connected to a magnet at a given distance.

The schematic drawings of the mounts are shown in Fig. 1. We plan to use one rigid mount and two or three free mounts in a straight section of the storage ring.[1] We can adjust the BPM back to its original location with an accuracy as high as 0.1 mm after baking. The deformation of a chamber is induced by a temperature difference of a chamber during baking, resulting in a force

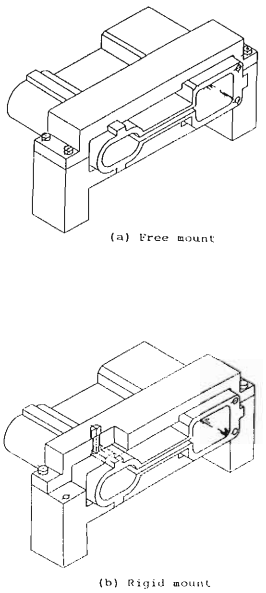

Fig. 1. Schematic drawings of the mounts.

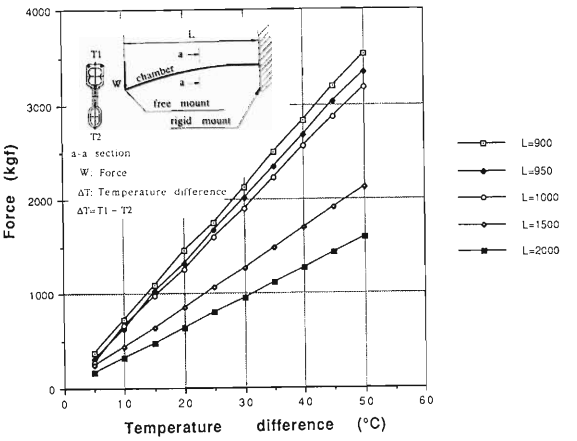

Fig. 2. Relationship between temperature difference and generated force.

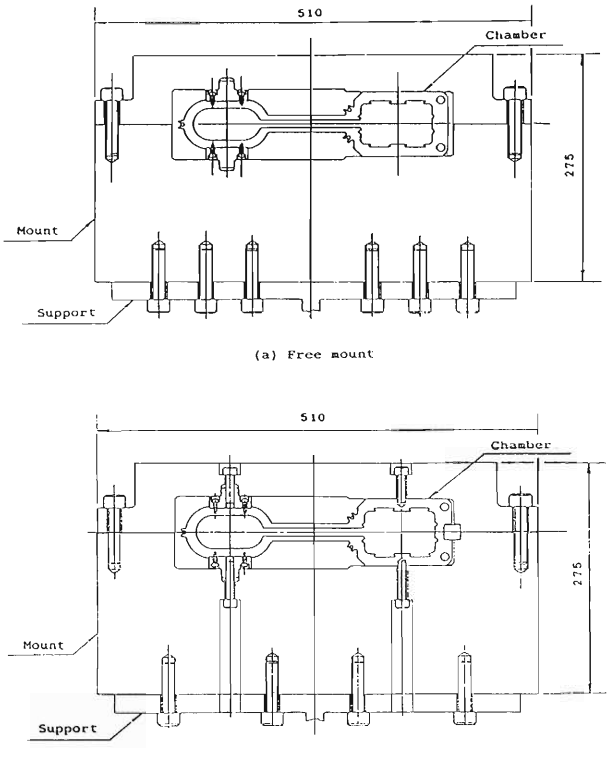

Fig. 3. Schematic drawings of the model mounts. The surface in contact with the chamber is coated with MoS_2 in free mount.

* On leave from RIST, Pohang, Korea.

against it at the mount. We calculated the force based on a model of simply supported beam. The relationship between temperature difference and corresponding force is shown in Fig. 2. We must design a mount which accommodates this force. The temperature difference was 10°C at baking.

We are on the way of the fabrication of mount models to check the restorability of BPM with desired accuracy. The schematic drawings of the model mounts are shown in Fig. 3.

References

1) S.H. Be, S. Yokouchi, Y. Morimoto, T. Nishidono, Y.P. Lee, and Y. Oikawa: This Report, p. 132.

RIKEN Accel. Prog. Rep. 23 (1989)

V-2-17. Fabrication of Vacuum Chamber, and Installation of the NEG Strips for SPring-8

H. Sakamoto,* T. Bizen,* S. Yokouchi, Y. Morimoto,
T. Nishidono, Y.P. Lee,** and S.H. Be

Prototype vacuum chambers for SPring-8 were completed, and their fabrication process was established at the same time. The structure and cross-sectional view of the aluminum-alloy vacuum chamber are shown in Figs. 1 and 2 for the straight and bending section, respectively. The both chambers have a length of 4 m.

Bakeout of the chambers is achieved with SUS 304 sheathed heaters (5 Ω/m Ni-Cr insulated with MgO) fixed on the surfaces, which can bring the temperature up to 150°C. The chambers are insulated thermally with three layers of laminated Kapton films (25 μm thick, aluminized, and embossed) to reduce heat losses. A thermal load at NEG activation is designed to be removed by means of water cooling at a flow rate of about 2 m/s in two channels of 10 mm in diameter.

The fabrication process of the chambers is shown in Fig. 3. The aluminum-alloy (A6063) chamber was extruded in a mixture gas of O_2 and Ar to build up a fine non-porous and dense

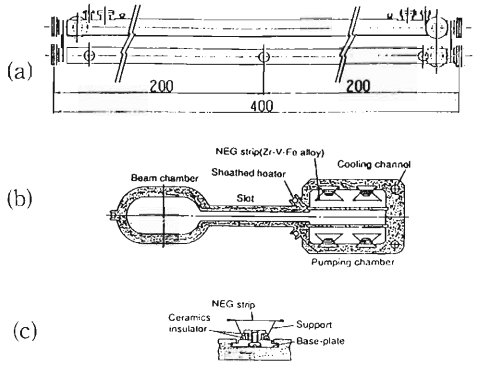

Fig. 1. Schematic drawings of the aluminum-alloy straight chamber. The structure (a) and cross-sectional view (b) of the chamber with NEG strips and the cross-sectional view of the NEG strip (c).

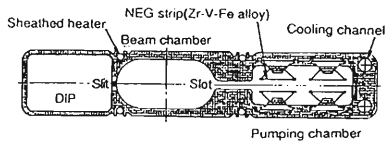

Fig. 2. Cross-sectional view of the bending chamber with NEG strips.

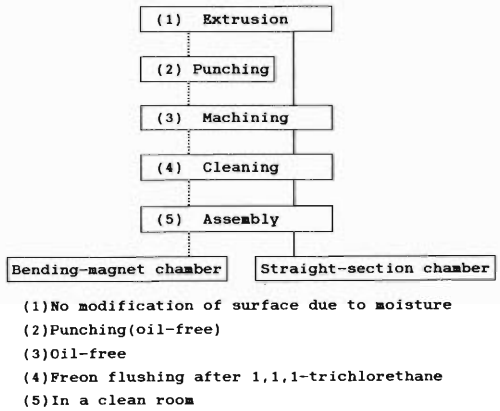

Fig. 3. Fabrication process of the aluminum-alloy vacuum chamber. Full lines indicate the fabrication process of the straight chamber, and dashed lines that of a bending chamber.

oxide-film on the surface. After T5 heat treatment, the strength of T5 became equivalent to that of T6. The chemical composition and mechanical properties of aluminum-alloy A6063 are shown in Table 1. The inner surface roughness R_{max} is 8 μm along the transverse direction. Deflection and torsion turned out to be within the tolerance based on the JIS H 4100 special class. The surface roughness and dimension tolerance are shown in Fig. 4. The flange material is aluminum-alloy A2219T852. The seal surface is coated with a film of TiC by an ion plating method in order to increase its hardness and corrosion resistance. The BMC has double line pumping slits (4 mm wide, 40 mm long, and 60 mm pitched) between the electron beam chamber and the DIP pump chamber. These slits were machined by oil-less punching. Oil-less machin-

Table 1. Chemical composition and mechanical properties of A6063 alumimum-alloy for the vacuum chamber.

	Chemical compositions (%)								
	Si	Fe	Cu	Mn	Mg	Cr	Zn	Ti	Al
A6063-T5	0.45	0.2	0.0	0.0	0.56	0.0	0.0	0.02	R.

	Mechanical properties		
	Tensile strength (kgf)	Proof stress (kgf/mm²)	Elongation
A6063-T5	26.0	23.2	11.4

* Ishikawajima-Harima Heavy Industries Co., Ltd.
** On leave from RIST, Pohang, Korea.

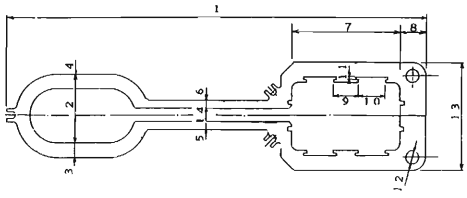

Unit : mm

No.	Designed value	Tolerances (JIS)	Measured value	No.	Designed value	Tolerances (JIS)	Measured value
1	317	±2.13	315.8	8	20	±0.46	18.86
2	40	±1.12	39.9	9	20	±0.46	19.80
3	11	±1.65	10.92	10	20	±0.46	20.46
4	11	±1.65	10.96	11	2.5	±0.36	2.77
5	6	±0.9	5.74	12	10	±0.51	10.11
6	6	±0.9	5.88	13	80	±0.86	79.35
7	80	±1.12	80.35	14	10	±2.13	9.14
Deflection		4.0	0.3	Torsion		9.5	4.0

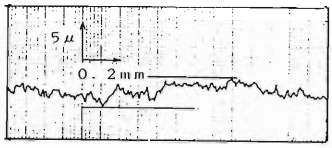

Fig. 4. Surface roughness and dimensional tolerance of the straight chamber. The chart shows the surface roughness along the transverse direction.

ing was widely employed to reduce contamination in the aspect of ultra-high vacuum.

Dust and machine oil were removed by 1,1,1-trichloroethane jet-cleaning (liquid pressure was 5 kgf/cm²) in a bath followed by freon flashing. The chambers were dried by blowing N_2 after cleaning. No particles over 100 μm in size were observed, and an analysis of the last solvent used indicated that oil contamination was less than 10 ppm. Unexpectedly, however several spots of heavy oxidation or corrosion were found on the surface of one chamber.

The flanges were welded (AC-TIG) to the chambers in Ar-shield gas. All assembly and welding were carried out in a clean room.

The structure of the NEG strip shown in Fig. 1 (c) was designed to be protected from synchrotron radiation, considering the limited space in a pump chamber. Thermal deformation is relaxed through the initial deflection of the NEG strip. On the other hand, the chamber geometry itself regulates a further deflection in case of activation at 450°C. The relationship between deflelction and temperature is shown in Fig. 5. We designed the initial deflection to be 5 mm for both chambers and the support distance to be 160 and 80 mm for the straight and the bending chamber, respectively.

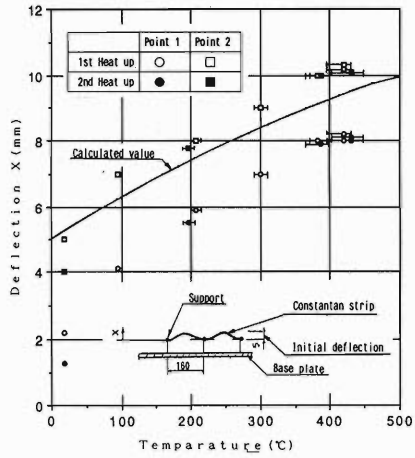

Fig. 5. Rerationship between temperature and deflection of the NEG strip.

RIKEN Accel. Prog. Rep. 23 (1989)

V-2-18. Deformation of Vacuum Chambers During Evacuation and Bakeout

T. Nishidono, S. Yokouchi, Y. Morimoto,
Y.P. Lee,* and S.H. Be

Aluminum-alloy chambers for the SPring-8 storage ring must be designed so as to stand the pressure difference between the atmospheric and vacuum. We estimated the stress and corresponding deformation of the vacuum chambers by means of a code based on a finite element method,[1] and also measured the deformation with dial-gauges as shown in Fig. 1. Calculations show that the maximum displacement takes place at the slot for either straight-section or bending-magnet chamber. No significant difference was found between calculated and measured values (Table 1) when we considered that the actual thickness of the chamber wall is 0.1-0.2 mm thinner than a designed value.

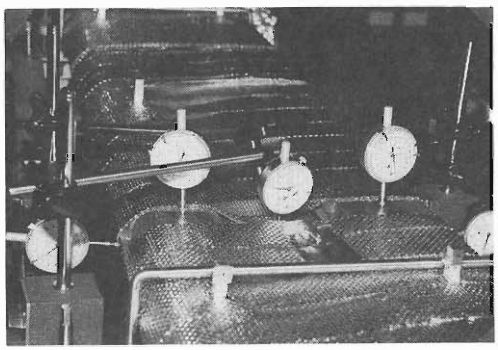

Fig. 1. Photograph of the measuring setup for the displacement of a straight-section chamber.

We also measured the displacement of a straight-section chamber (SSC) during bakeout. Measured values are shown in Table 2, together with values for evacuation from the atmospheric pressure. We presumed that the chamber was displaced only with respect to a fixed support. Since beam position monitors (BPM) are planned to be mounted on SSC, the displacement of SSC must be less than 0.1 mm for the sake of monitoring accuracy.

Table 1. Displacements at the slots of vacuum chambers.

	Straight-section chamber	Bending-magnet chamber
Calculated	0.45 mm	0.1 mm
Measured	0.6 mm	0.2 mm

Table 2. Measured displacement of a straight chamber during bakeout and during evacuation from the atmospheric pressure

Location[1)]	At evacuation (room temp.)		At bake out (~140 °C)
	Calculated value(mm)[2),3)]	Measured value(mm)[3)]	Measured value(mm)[3)]
A	−0.1	−0.2	+0.04
B	−	+0.1	+0.23
C	−0.45	−0.6	−0.53
D	−	+0.44	+0.64

Note: 1) Locations are shown below.
2) Values estimated by using a symmetrical half model.
3) All values with respect to the top of a support.

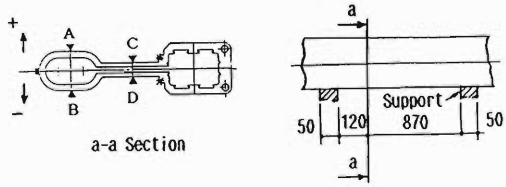

We are considering a thicker wall only for the region of BPM to permit the displacement to be less than 0.1 mm.[2] A bending-magnet chamber has been fabricated and subjected to investigation.

References

1) T. Nishidono, H. Kakui, S.H. Be, H. Sakamoto, S. Yokouchi, Y. Morimoto, and Y. Oikawa: *RIKEN Accel. Prog. Rep.*, **22**, 281 (1988).
2) S.H. Be, S. Yokouchi, Y. Morimoto, T. Nishidono, Y.P. Lee, and Y. Oikawa: This Report p. 132.

* On leave from RIST, Pohang, Korea.

RIKEN Accel. Prog. Rep. 23 (1989)

V-2-19. Leakage Test for Aluminum-Alloy Flanges

T. Nishidono, S. Yokouchi, Y. Morimoto, Y.P. Lee,* and S.H. Be

We are considering to use extruded aluminum-alloy chambers for the SPring-8 storage ring. Since the chambers should be baked out at about 150°C to minimize their thermal outgassing rate, aluminum-alloy flanges as well as stainless-steel flanges are required to be leakless even after many cycles of baking. Furthermore, the flanges are large in size because of the large cross section of the vacuum chamber.

We investigated how many flanges leak in an experimental setup and what is the origin of leakage, which was correlated closely to the measurements of the outgassing rate of extruded aluminum-alloy chambers, and the pumping speed of NEG strips. We also made a large-size aluminum-alloy flange (ICF406) and investigated.

We baked out the experimental setup 11 times for a year from June '88 to May '89. Sixteen flanges out of forty in the setup showed leakage. Most of these leaking flanges were heterogeneous pairs of aluminum-alloy and stainless-steel as shown in Table 1. All flanges in the setup were assembled with aluminum-alloy (A1050H18) gaskets. Not extra-tightening gaskets, but new softer gaskets (A1050H24) were found effective to protect the flanges from leakage. It is also worth pointing out that aluminum-alloy flanges and gaskets should be standardized for avoiding

Table 1. Leak statistics for the experimental setup.

Flange size	Material of flange									Total		
	Al+Al			Al+S.S.			S.S.+S.S.					
	Quan-tity	Leak	%	Quan-tity	Leak	%	Quan-tity	Leak	%	Quan-tity	Leak	%
034	--	--	--	2	1	2.5	3	0	0	5	1	2.5
070	7	3	7	10	4	10	1	0	0	18	7	7.5
114		--	--	2	2	5	--	--	--	2	2	5
152	1	1	2.5	1	1	2.5	1	0	0	3	2	5
203	5	0	0	6	4	10	1	0	0	12	4	10
Total	13	4	10	21	12	30	6	0	0	40	16	40

Note :
1) Leak rate is above 2~ 3×10^{-10} Torr · l/s .
2) The specifications are shown as follows:
Flange:
Material is aluminum alloy (A2219-T852).
Sureface treatment is CrN ion plating.
Bolts:
Material is aluminum alloy (A2024-T4).
Gasket:
Material is aluminum alloy (A1050H18).

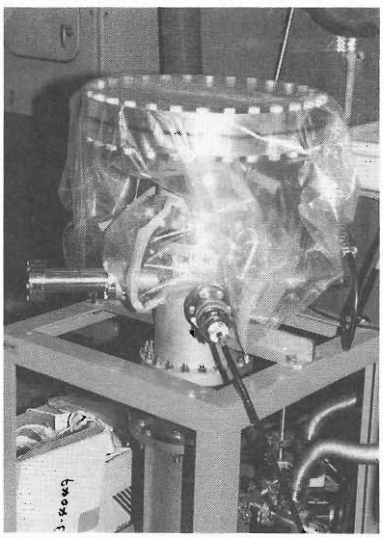

Fig. 1. Photograph of the experimental setup for a large-size flange.

Table 2. Specifications of an ICF406 flange.

Flange Material	Aluminum Alloy(Al-Si,AHS-T6)
Dimension	Outside Diameter : 406 mm Thickness : 32 mm
Sureface Treatment	TiN Ion Plating
Bolts Material	Aluminum Alloy(A2024-T4)
Size	M10
Quantity	30 pieces
Gasket Material	Aluminum Alloy(A1050H24)

* On leave from RIST, Pohang, Korea.

Table 3. Results of leakage tests after baking cycles.

Baking	Heat up Speed	Holding Temp.	Cool down Speed	Leak of ICF406 Flange	Notes
1st	12℃ /h	115 ℃ ×1h	Aired in room	No Leak (<8.9×10^{-11} Torr l/s)	
2nd	15℃ /h	145 ℃ ×2h	Aired in room	No Leak (<8.6×10^{-11} Torr l/s)	
3rd	19℃ /h	155 ℃ ×2h	Aired in room	No Leak (<1.4×10^{-10} Torr l/s)	
4th	18℃ /h	150 ℃ ×2h	Aired in room	No Leak (<1.8×10^{-10} Torr l/s)	Gasket changed
5th	29℃ /h	140 ℃ ×14h	Aired in room	No Leak (<2.4×10^{-10} Torr l/s	
6th	29℃ /h	140 ℃ ×19h	Aired in room	No Leak (<1.9×10^{-10} Torr l/s	

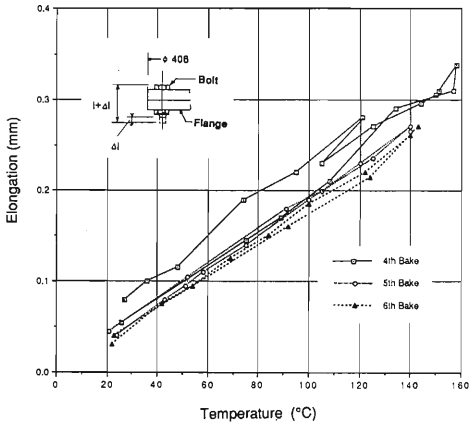

Fig. 2. Relationship between baking temperature and bolt elongation. Tightening force is calculated from the elongation.

problems arising from their scattered dimensions.

We constructed another experimental setup (Fig. 1) for large sized aluminum-alloy flange (ICF406), the specifications of which are listed in Table 2. The flange showed no leakage even after six baking cycles (see Table 3). The profile of gasket was round and the flange edge was about 0.05mm in depth. The flange was tightened with aluminum-alloy (A2024T4) bolts. We also found that tightening force was lowered with repeating baking; this may be caused by material or heat treatment of bolts (see Fig. 2).

We conclude that aluminum-alloy flanges have some problems, particulary in the case of baking. We continue the test to find whether they could be used safely for the SPring-8 storage ring.

RIKEN Accel. Prog. Rep. 23 (1989)

V-2-20. Hybrid Material Flange by Explosion Bonding

Y. Morimoto, H. Fukuyama,* K. Yamada,* S. Yokouchi,
T. Nishidono, Y.P. Lee,** and S.H. Be

A crotch is required to be connected to the vacuum system of the storage ring with flanges for easy maintenance and for unalteration of the other vacuum system. However, the material (copper) of the crotch is different from that (aluminum alloy) of the vacuum chamber, and ultra-high vacuum cannot be achieved by using flanges of these materials having different thermal properties. In addition, copper cannot be used as the material of the conflat flange because of its less tensile strength and hardness than those of aluminum alloy (A2219-T87). Hence, we have developed a hybrid material flanges to be mounted on the crotch.

Figure 1 shows the cross-sectional view of the hybrid material flange. One side is made of copper (OFHC CLASS 1) and the other side of aluminum alloy (A2219-T87). These two materials were bonded by an explosion-bonding method. A thin intermediate layer of pure aluminum (A1050-H24) serves to strengthen the bonding at the interface. We chose the explosion-bonding method because aluminum-copper welding is impossible and the bonding temperature is not allowed to be high. Since A2219-T87 is hardened by artificial aging at about 180°C, heating above 180°C reduces the hardness. The bonded piece was machined to the shape of a conflat flange, and the aluminum-alloy surface was coated with titanium nitride by ion plating. Finally, the copper side of the flange was welded to the main body of a crotch by using an electron-beam.

We investigated the adhesion at the exploded interface and the effect of heating during electron-beam welding. Figure 2 shows the cross section of the interface. The shearing strength at the interface was found to be 7.1~10.1 kg/cm², which exceeds 7 kg/cm² of pure aluminum A1050-H24. The changes in hardness, size, and leak rate at the interface were also measured after welding, and found to be −1~−2 Hb, less than 0.1 mm on copper and 0.15 mm on aluminum alloy, and less than 3×10^{-11} Torr · l/s, respectively. The

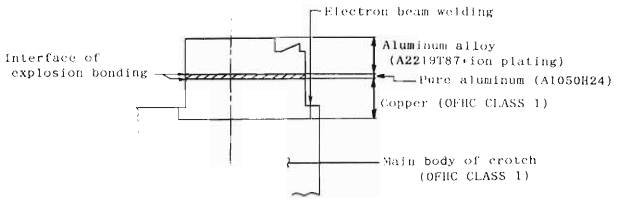

Fig. 1. Cross-sectional view of the hybrid material flange.

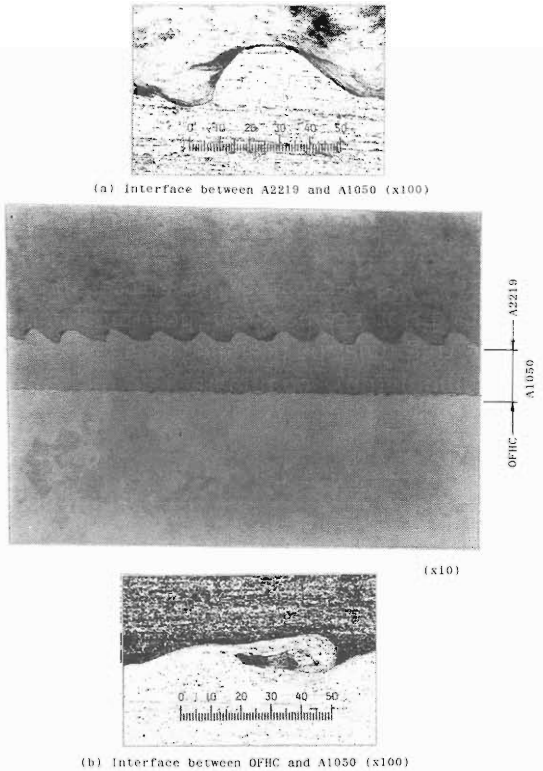

Fig. 2. Photograghs of the cross section at the exploded interface.

temperature of aluminum alloy during welding momentarily increased to 200°C. The depth of welding was only 2.4 mm, instead of anticipated 4 mm. We also noticed that the hybrid material flange was capable of withstanding heat cycles of baking (one cycle: 150°C for 24 h).

* Kobe Steel, Ltd.
** On leave from RIST, Pohang, Korea.

RIKEN Accel. Prog. Rep. 23 (1989)

V-2-21. Machining of OFHC with and without Oil

Y. Morimoto, H. Fukuyama,* K. Yamada,* S. Yokouchi,
T. Nishidono, Y.P. Lee,** and S.H. Be

The main body of a crotch should be machined from an oxygen-free copper (OFHC) block to the designed size and shape. The crotch is preferred to be machined with oil-free since crotches are used in ultra-high vacuum of a low 10^{-10} Torr or less. On the other hand, the oil-free machining ends up with a rougher surface than that with oil (see Table 1). It is required, therefore, to reduce the roughness to make its outgassing rate from the surface as low as possible.

Prior to the manufacture of a prototype crotch, we investigated the effect of oil on sample pieces prepared in the following ways to notice the effect: a) with the normal machine oil (Sample A), b) with the rust-free oil (Sample B), and c) without oil (Sample C). The difference between the normal and rust-free oil is in a boiling point: the former has a boiling point higher than the latter.

Figure 1 shows auger electron spectroscopy (AES) depth-profiles for Samples A, B, and C. The samples were cleaned carefully with trichloroethane and freon 113 immediately before analysis. The results indicate that the surface of Sample B was less contaminated with carbon (C) than that of Sample A and C. The contaminated depth in Sample A is five times thicker than that in Sample B.

Table 1 shows the roughness of the sample pieces which are machined by the same cutting methods as used in machining of the crotch. The roughness is correlated strongly with the cutting method. No quantitative tendency is seen, but, as a whole, when the rust-free oil is used, the roughness is somewhat lowered compared with that when oil is not used.

Table 1. Roughness of machined surfaces.

Cutting method	Direction of measurement	With rust-free oil R_{max} (μm)	Without oil R_{max} (μm)
Contouring by milling	Longitudinal	4.9	8.4
(racetrack shape)	Circumferential	5.6	6.3
Slotting	Longitudinal	10.6	2.4
Boring (small dia.)	Longitudinal	13.9	11.9
Boring (large dia.)	Longitudinal	14.8	5.7
Contouring (edge)	X direction	2.2	7.2
	Y direction	2.6	11.4
Milling (slit)	X (outside)	5.0	4.1
	Y (outside)	5.5	4.7
	X (inside)	6.1	12.7
	Y (inside)	9.5	26.3
Side cutting	Circumferential	3.9	5.8

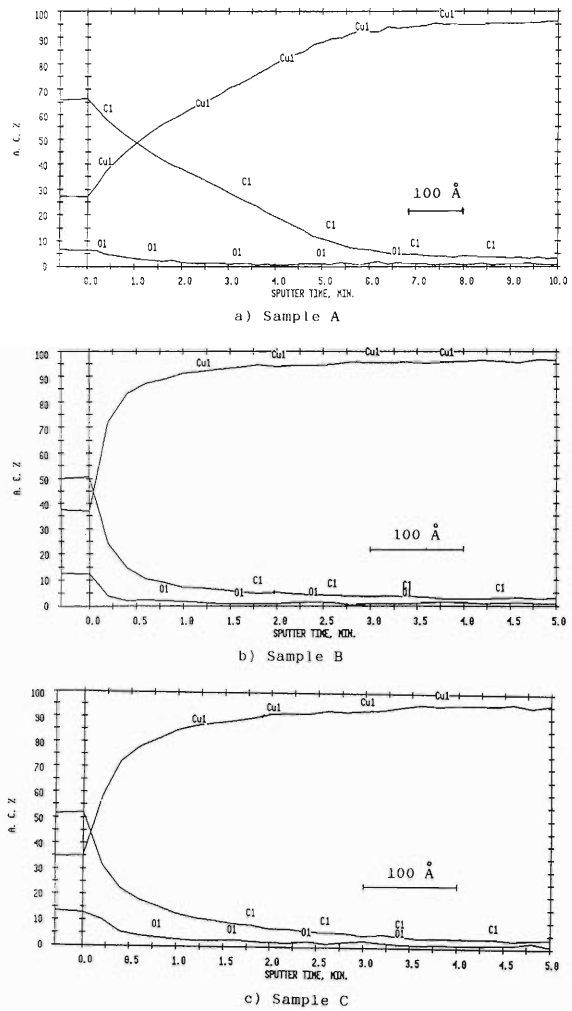

Fig. 1. AES depth-profiles for Sample A (normal machine oil), Sample B (rust-free oil), and Sample C (without oil).

A prototype of the crotch was machined with the rust-free oil in accordance with the above results. Since OFHC is easy to be oxidized, the machining with oil should be cautiously chosen to prevent contamination and oxidation during machining.

* Kobe Steel, Ltd.
** On leave from RIST, Pohang, Korea.

RIKEN Accel. Prog. Rep. 23 (1989)

V-2-22. Vacuum Performance Characteristic of the Crotch

Y. Morimoto, S. Yokouchi, T. Nishidono, Y.P. Lee,* and S.H. Be

The crotch is a component which absorbs synchrotron radiation (SR) from a bending magnet (BM) other than that supplied to the experimental facility. The geometry of the crotch and thermal analysis against an SR beam was presented in a previous report.[1] Since then, a prototype model of the crotch was fabricated, and we performed experiments to confirm the vacuum characteristics of the prototype model. Since 96 crotches are to be installed in the 8 GeV storage ring, it is important to learn their vacuum characteristics because ultra-high vacuum of a low 10^{-10} Torr or less is required for the storage ring to allow a beam lifetime greater than 20 h.

The crotches are made of OFHC (Oxygen-free high conductivity copper) CLASS 1, which has a very high purity of 99.996wt.% Cu or greater and a low outgassing rate. The low outgassing rate is given in manufacturing processes by vacuum treatment, which reduces the amount of gas containing in the metal. OFHC CLASS 1 also has a low outgassing rate due to SR-induced desorption, approximately fifty times less than that of aluminum alloy.

The schematic diagram of a test device is shown in Fig. 1. The test stand made of stainless steel (SUS 304) is connected to a crotch with a flexible tube. A 360 l/s turbo molecular pump (TMP), a orifice of 5 mm in diameter, and two BA nude gauges (BAG3, BAG4) are installed in the test stand. The outgassing rate for the crotch was measured by a throughput method using the orifice. The TMP is used for initial pump-down and baking. A 400 l/s sputter ion pump (SIP), a titanium-sublimation pump (TSP), and two extractor-type BA nude gauges (BAG1, BAG2) are also mounted on the crotch. During the measurements of the pressure in the crotch, the test stand is isolated from the crotch by closing a metal valve (MV3).

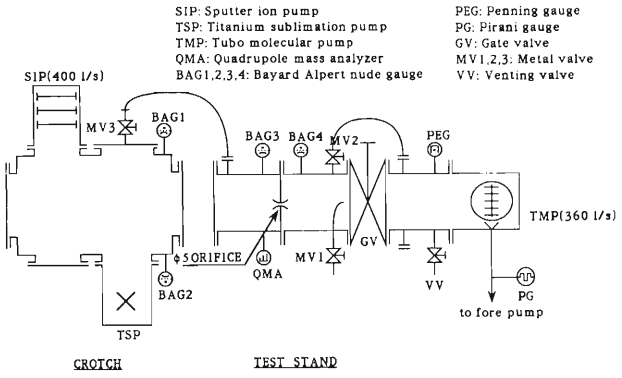

Fig. 1. Schematic diagram of the test device.

The measured pressures in the crotch are shown in Fig. 2 as a function of the pumping time. After two cycles of baking (150°C×24 h), the pressure decreased to 2.8×10^{-11} Torr. Under

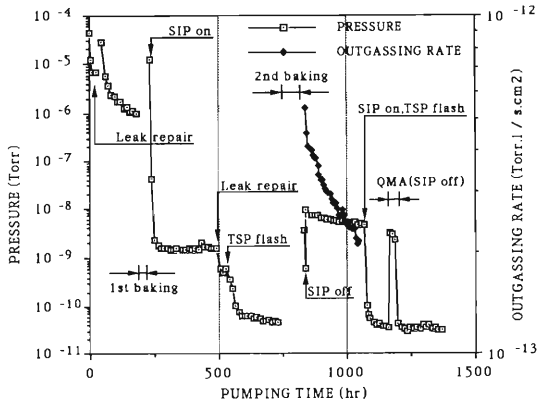

Fig. 2. Variations in pressure for the crotch with pumping time.

the same baking conditions, the outgassing rate of the crotch including SIP and TSP which are made of stainless steel was found to reduce to 2.1×10^{-13} Torr·l/s·cm^2. These values are fairly low compared with our anticipated pressures and outgassing rate of a low 10^{-11} Torr and 5×10^{-12} Torr·l/s·cm^2, respectively. Residual gas spectra obtained after the bake out were typical of a ultra-high vacuum system, *i.e.*, approximately 70% H_2, 20% CO. The remaining 10% was due to CH_4, CO_2, and H_2O.

References

1) Y. Morimoto, S. Yokouchi, H. Sakamoto, S.H. Be, and T. Shirakura: *RIKEN Accel. Prog. Rep.*, **22**, 292 (1988).

* On leave from RIST, Pohang, Korea.

RIKEN Accel. Prog. Rep. 23 (1989)

V-2-23. Calibration of Nude Ionization Gauges with a Spinning Rotor Gauge

H. Daibo, Y.P. Lee,* S. Yokouchi, T. Nishidono,
Y. Morimoto, and S.H. Be

Bayard-Alpert nude ionization gauges (BAG) are usually employed for the pressure measurements in various kinds of ultra-high vacuum systems including storage rings. Nevertheless, the measurement accuracy and reliability are far from perfect, and varied as manufacturers and even individual gauges. A spinning rotor gauge (SRG) is known as very reliable and accurate to have a fluctuation of only ±1% in the pressure range of 10^{-3}-10 Pa even for a long term.[1,2] We checked the performance of our SRG, (SRG-2, MKS Instruments, Inc.), and calibrated BAG's and extractor gauges (EG) with the SRG in the range of 10^{-6}-10^{-2} Pa. Figure 1 shows a schematic diagram of the calibration setup.

First of all, we have to understand the detailed behavior of offset (OFS) in order to use this SRG as a standard for other gauges, especially in a practical and extended pressure range of $\leq 10^{-4}$ Pa, because the lower limit of a measuring range is governed by the pressure resolution (Δp) of OFS and its stability. OFS is the residual pressure indication due to magnetic friction, and its fluctuation determines Δp. We investigated the effects on OFS of chamber pressure and kind of dominant residual gas as well as measurement parameters like sampling interval (SI) and measurement number (N). We also checked the effects of various input corrections, for example, chamber temperature (T) and temperature-corrected viscosity (η^T). Furthermore, the correlation between OFS and the time after SRG on

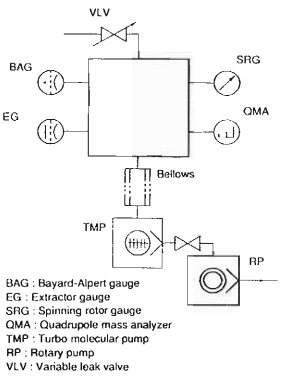

Fig. 1. Schematic diagram of the calibration setup.

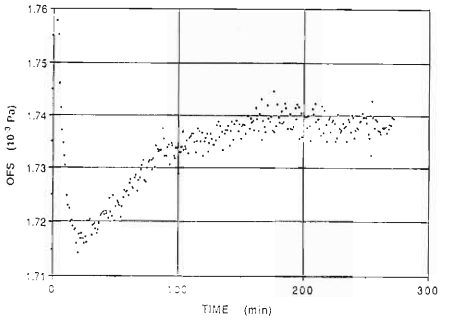

Fig. 2. Measurement of OFS behavior with respect to the time following the start of SRG operation. $SI=30$ sec and $N=1$, and the chamber pressure was $\sim 2\times 10^{-8}$ Pa.

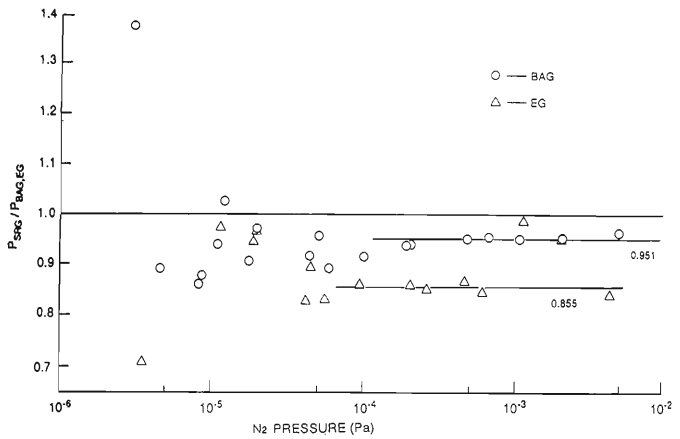

Fig. 3. Pressure comparisons between SRG and a BAG, and an EG. Horizontal lines are drawn at P_{SRG}/P_{BAG} ~0.951, and P_{SRG}/P_{EG} ~0.855 to indicate the correction factors for BAG and EG.

* On leave from RIST, Pohang, Korea.

was understood to turn out that SRG is not stable for the first few hours (Fig. 2). Finally, the optimum OFS for N_2 was determined to be 1.7414×10^{-3} Pa on the average and Δp in the order of 10^{-6} Pa, $\sim$ 3 hours after SRG on at a base pressure of $\sim2\times10^{-8}$ Pa without any manipulation of the residual gases. The OFS was measured at $SI=30$ sec and $N=10$ after input-corrections for T and η^T.

Once this quantity of OFS had been input, the pressures between SRG and a BAG, and an EG (Fig. 3) were compared in the pressure range of 10^{-6}-10^{-2} Pa. The chamber pressure was controlled by means of N_2 through a variable leak valve (VLV in Fig. 1). We found that the pressure ratios are nearly stable and close to unity above high 10^{-5} Pa. The correction factors for BAG and EG were acquired to be $\sim$0.951 and 0.855, respectively, for the region giving stable ratios.

References

1) G. Reich: *J. Vac. Sci. Technol.*, **20**, 1148 (1982).
2) M. Hirata, H. Isogai, K. Kokubun, and M. Ono: *J. Vac. Soc. Jpn.*, **28**, 898 (1985).

RIKEN Accel. Prog. Rep. 23 (1989)

V-2-24. Design of RF Cavities for the SPring-8 Storage Ring

T. Kusaka, T. Yoshiyuki, T. Moro,* and M. Hara

The SPring-8 storage ring has been determined to use 508.6 MHz cavities, which are located in four 6.5-m straight sections with low betatron functions. We examined two types of RF systems and compared the RF characteristics of a single-cell cavity and a 3-cell cavity.[1,2] Because the transverse impedance of a TM_{111}-like mode was so high, threshold currents due to transverse coupled bunch instabilities in both RF cavities were lower than the desired beam current of 100 mA.

Therefore, we decided the following design policies of the cavities for the SPring-8 storage ring and chose an RF system using thirty-two single-cell cavities.

(1) Intrinsic higher-order mode impedances of the cavities are reduced as low as possible.

(2) Shunt impedance in the accelerating mode is more than 6.8 MΩ/cell in order to suppress excessive thermal load in the cavity.

(3) Cavity structure is made simple for easy fabrication, cooling, and maintenance.

The designed RF cavity, shown in Fig. 1, is a spherically shaped cavity similar to superconducting cavities now widely used. Several ports are prepared for an input coupler, a frequency tuner, a monitor, and damping couplers which suppress higher-order modes. Computed impedances for the axially-symmetric structure are shown in Fig. 2 and compared with those of a re-entrant model cavity.[2] The impedances are calculated for cavities made of Oxygen-Free High Conductivity copper. Shunt impedance in the accelerating mode is 7.4 MΩ, which is about 20% lower than that of the re-entrant cavity. However, the maximum transverse impedance decreases by approximately one-half; thus, coupled-bunch instabilities are suppressed and a threshold current is raised above the design current 100 mA.

We are going to fabricate a model cavity and confirm its RF characteristics and plan high power tests using a 1-MW klystron to determine the detailed specification of practical cavities.

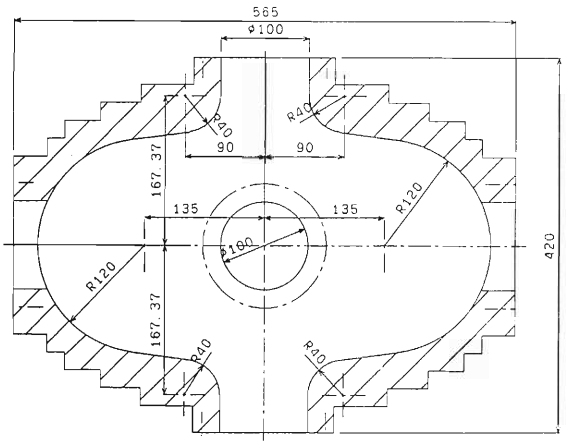

Fig. 1. Cross section of the designed spherically shaped cavity.

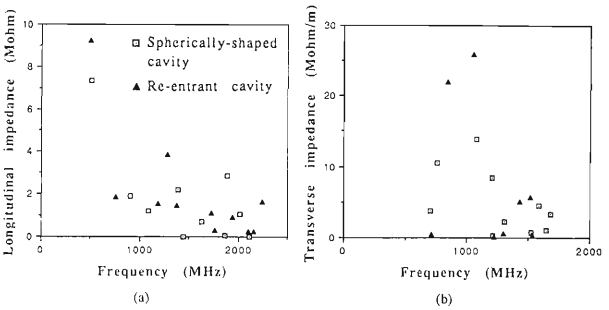

Fig. 2. Comparison of computed impedances between two types of cavities. (a), in longitudinal impedances; (b) in transverse impedances.

References

1) T. Yoshiyuki, T. Kusaka, and M. Hara: *RIKEN Accel. Prog. Rep.*, **22**, 265 (1988).
2) T. Kusaka, K. Inoue, T. Yoshiyuki, A. Miura, and M. Hara: *ibid.*, p. 268 (1988).

* College of Humanities and Sciences, Nihon University.

RIKEN Accel. Prog. Rep. 23 (1989)

V-2-25. Thermal Analysis of the Cavity for the SPring-8 Storage Ring

T. Kusaka, K. Inoue,* T. Yoshiyuki, and M. Hara

It is important to calculate the temperature distribution and thermal deformation in the cavity structure and to estimate the loss in shunt impedance resulting from the decrease in electrical conductivity. In the RF system of the SPring-8 storage ring, an RF power of 40 kW will be dissipated in the wall of the single-cell cavity.[1] The power is distributed as shown in Fig. 1.

A general-purpose computer code, ABAQUS,[2] based on a finite element method was used to calculate the thermal characteristics of the cavity. The cavity is cooled with eight parallel thin channels around the beam axis. The conditions of the calculation are listed in Table 1. The temperature distribution is shown in Fig. 2 (a).

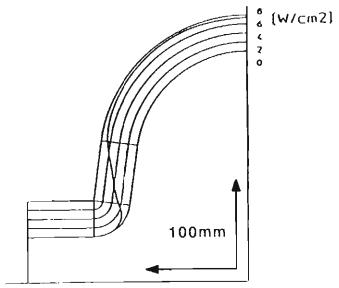

Fig. 1. Power distribution at a total power of 40 kW/cell.

Table 1. Conditions of calculation.

Cavity material	OFHC
Thermal conductivity	9.2×10^{-15} (kcal/mm·°C·s)
Cooling water	
Velocity	1.5 (m/s)
Temperature	24 (°C)
Surface heat transfer coefficient	1.9×10^{-6} (kcal/mm²·°C·s)
Linear expansion coefficient	1.7×10^{-5} (1/°C)
Young's modulus	12,000 (kg/mm²)
Poisson's ratio	0.33

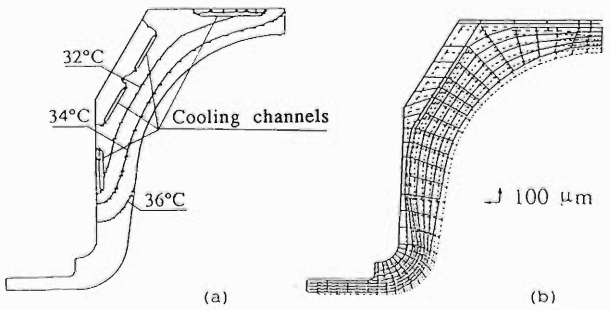

Fig. 2. (a) Temperature distribution of the cavity; (b) deformation of the cavity; the dashed lines show the original mesh and the solid lines show the displaced mesh.

The surface temperature of the cavity is uniformly about 36°C. Therefore, the shunt impedance is about 3.4% lower than the theoretical value at room temperature. Figure 2 (b) shows deformation due to thermal stress. The calculated resonant frequency change is about 80 kHz, which can easily be compensated with a frequency tuner. The cavity for high power tests will be designed on the basis of the computed results.

References

1) T. Kusaka, T. Yoshiyuki, T. Moro, and M. Hara: This Report, p. 155.
2) Hibbitt, Karlsson & Sorensen, Inc., "ABAQUS User's Manual" (1988).

* Kobe Steel, Ltd.

RIKEN Accel. Prog. Rep. 23 (1989)

V-2-26. Impedance Calculation of RF Cavities with a Three-Dimensional MAX3D Code

T. Kusaka, T. Moro,*and M. Hara

In designing RF accelerating cavities in low-emittance storage rings, it is important to calculate the longitudinal and transverse coupling impedances of RF cavities in resonant modes, because the growth rate of coupled-bunch instability is dependent on the value of impedance in higher-order modes.[1] Thus, we extended the functions of three-dimensional MAX3D code[2] to impedance calculation.

The RF characteristics of a cylindrical cavity were computed to check the accuracy of calculation. A test cavity, 46 cm in diameter and 30 cm in length, was divided into 18 elements along the radial direction and 15 elements along the longitudinal direction. The results are listed in Table 1. Computed impedances are good agreement with analytical ones below a frequency of 1 GHz.

Table 1. Comparison of calculated results with analytical ones for a cylindrical cavity.

Mode	Frequency (MHz)			Q-value			Impedance (MΩ or MΩ/m)		
	calculated	analytical	error (%)	calculated	analytical	error (%)	calculated	analytical	error (%)
TM010	498.74	498.88	-2.8×10^{-2}	44,299	44,039	5.9×10^{-1}	8.694	8.630	7.5×10^{-1}
TE111	627.58	628.94	-2.2×10^{-1}	49,172	49,778	−1.2	2.2×10^{-3}	0	
TM011	706.86	706.07	1.1×10^{-1}	36,794	36,537	7.1×10^{-1}	3.715	3.697	4.8×10^{-1}
TM110	794.54	794.89	-5.5×10^{-2}	55,409	55,590	-3.3×10^{-1}	6.597	6.666	−1.0
TE211	806.86	806.92	-7.8×10^{-3}	50,518	50,610	-1.8×10^{-1}	2.9×10^{-5}	0	
TM111	940.34	938.88	-1.6×10^{-1}	42,850	42,132	1.7	19.03	19.55	−2.6

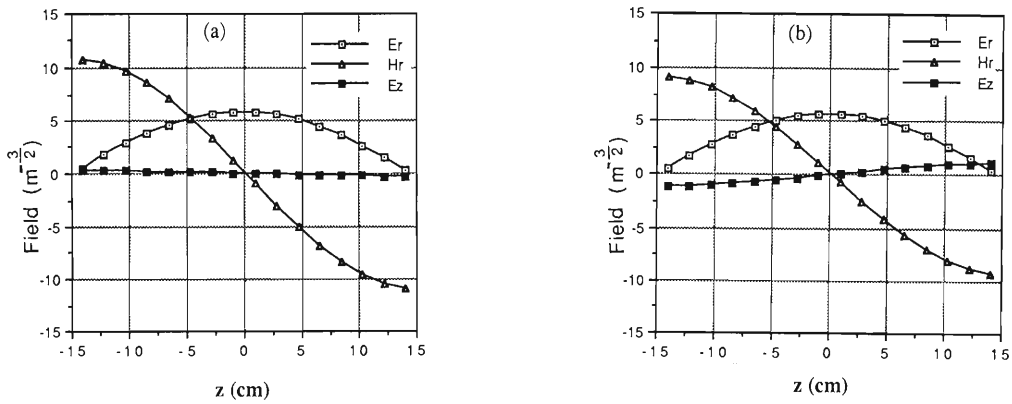

Fig. 1. Electromagnetic field distributions along the beam axis; (a), with no tuner; (b), with tuner insertion of 5.1 cm.

We investigated the effect of a plunger-type ferquency tuner.[3] The tuner with a sectional area of 60 cm^2 changes the field distributions of resonant modes, when the electric field exists in the tuner position. The comparison of the electromagnetic fields in a TM_{111}-like mode is shown in Fig. 1. A longitudinal electric field is produced at the beam axis by tuner insertion. This means that a beam is coupled to the TM_{111}-like mode even if the beam passes through the center of the cavity. We will study the effect of a tuner on impedances and beam stability in a practical cavity structure.

* College of Humanities and Sciences, Nihon University.

References

1) H. Kobayakawa, Y. Yamazaki, Y. Kamiya, and M. Kihara: *Jpn. J. Appl. Phys.*, **25**, 864 (1986).
2) M. Hara, T. Wada, K. Mitomori, and F. Kikuchi: Proc. 11th Int. Conf. on Cyclotrons and their Applications, p. 337 (1987).
3) T. Kusaka, A. Miura, T. Wada, and M. Hara: *RIKEN Accel. Prog. Rep.*, **22**, 268 (1988).

RIKEN Accel. Prog. Rep. 23 (1989)

V-2-27. Loss Parameter Measurements of a Model Cavity for the SPring-8 Storage Ring

T. Yoshiyuki, T. Kusaka, M. Hara, and S.H. Be

Beam coupling impedance is an important parameter to evaluate beam instabilities.[1] Since RF cavities have a large contribution to the impedance, we first measured the loss parameter of a model cavity with nose cones[2] to estimate the impedance. A coaxial wire method[3] is widely used for bench measurements of the impedance. A measurement setup is shown in Fig. 1. By introducing a thin wire into vacuum chamber components, the surface current distribution on the inner surface can be obtained, which corresponds approximately to the current distribution produced by a bunched electron beam. A nearly Gaussian pulse generated with a pulse generator travels through a thin wire at the axis of a beam either in a reference chamber or in a component under test of the same mechanical length. Both reference signal $i_0(t)$ and object signal $i_m(t)$ are recorded sequentially, and stored in a sampling oscilloscope. The data stored in the oscilloscope are sent to a controller and then a longitudinal loss parameter $k_{\parallel}(\sigma_1)$, which represents the energy loss[4] and is related to the beam coupling impedance,[5] is calculated by

$$k_{\parallel}(\sigma_1)=2Z_0\int i_0(t)(i_0(t)-i_m(t))dt\Big/\left[\int i_0(t)dt\right]^2 \quad (1)$$

where Z_0 is the characteristic impedance of the reference chamber ($=276\ \Omega$) and σ_1 the length of a Gaussian pulse.

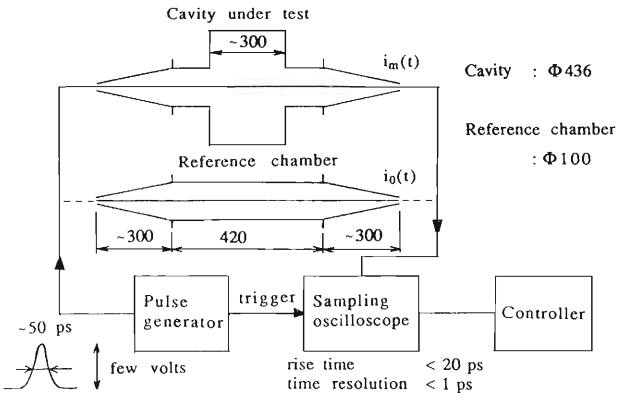

Fig. 1. Setup for the measurement of the loss parameter.

Figure 2 shows the recorded output pulses from the reference chamber and the cavity. The measured loss parameters, together with the calculational results by TBCI,[6] are plotted in Fig. 3 as a function of the bunch length. The loss parameters were obtained for four pulse widths; about 50, 100, 150, and 200 ps. The measured data are overestimated somewhat, but the measurements and calculations show the same distribution properties. Overestimation is considered to be due to that the generated pulse had no perfect Gaussian distribution and the coaxial line in a tapered chamber didn't match well with a 50 Ω cable and connectors.

Next we have to improve the measurement precision by increasing the number of measured data and keeping the connections between flanges, connectors, and a wire and a connector. After that we measure the loss parameters of a vacuum chamber with an antechamber, Conflat flanges, and an RF contact, aiming to minimze the energy loss of the SPring-8 storage ring.

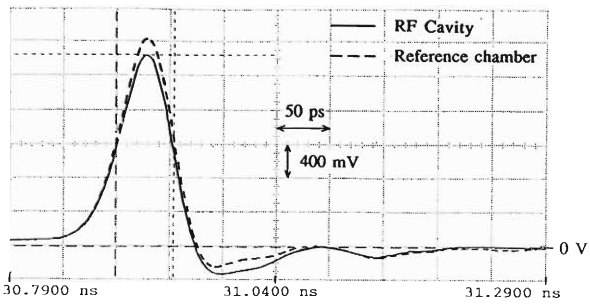

Fig. 2. Recorded output pulses $I_0(t)$ for the reference chamber and $I_m(t)$ for the RF cavity.

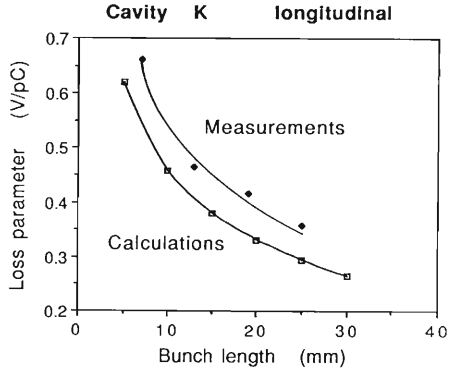

Fig. 3. Loss parameters of the RF cavity for measurements and numerical simulations.

References

1) T. Yoshiyuki, T. Kusaka, J. Ohnishi, and S.H. Be: *RIKEN Accel. Prog. Rep.*, **22**, 276 (1988).
2) T. Kusaka, K. Inoue, T. Yoshiyuki, A. Miura, and M. Hara: *ibid.*, **22**, 268 (1988).
3) M. Sands and J. Rees: SLAC-report PEP-95 (1974).
4) T. Yoshiyuki, T. Kusaka, M. Hara, and S.H. Be: This Report, p. 160.
5) B. Zotter: CERN LEP-TH/87-34 (1987).
6) T. Weiland: *Nucl. Instrum. Methods*, **212**, 13 (1983).

RIKEN Accel. Prog. Rep. 23 (1989)

V-2-28. Impedance Calculations of the SPring-8 Vacuum Chamber

T. Yoshiyuki, T. Kusaka, M. Hara, and S.H. Be

An important ingredient to evaluate beam instabilities is impedance, which is usually employed to describe the interaction of a beam with environment.[1] An electromagnetic field, which is generated by a electron bunched beam circulating through a given section of the vacuum chamber, can be computed numerically by means of a two dimensional code TBCI.[2] It computes wake potentials as a function of delay with respect to the head of a bunch, together with a loss parameter K which represents an energy loss ΔU by a charge Q in a lo gitudinal case as follows: $\Delta U = KQ^2$, when a Gaussian-distributed rigid bunch is traveling in structures. The loss parameters of different vacuum chamber components are computed as a function of the bunch length and summed for the whole storage ring. Broad-band impedances can be calculated from loss parameters by using a broad-band resonator model.[3]

The simulation was carried out for longitudinal (monopole fields) and transverse impedance (dipole fields) independently, and applied to RF cavities, bellows, flanges, and transitions to insertion device (ID) chambers.

As far as RF cavities are concerned, the calculation was carried out for single-cell cavities with nose cones, which were designed before, and for those without nose cones, which are under design as a low impedance cavity in higher-order modes (HOM) for the storage ring.[4] The loss parameters for both cases are plotted in Fig. 1 as a function of the bunch length. The loss parameters of the cavity without nose cones are larger than those of the cavity with nose cones in the

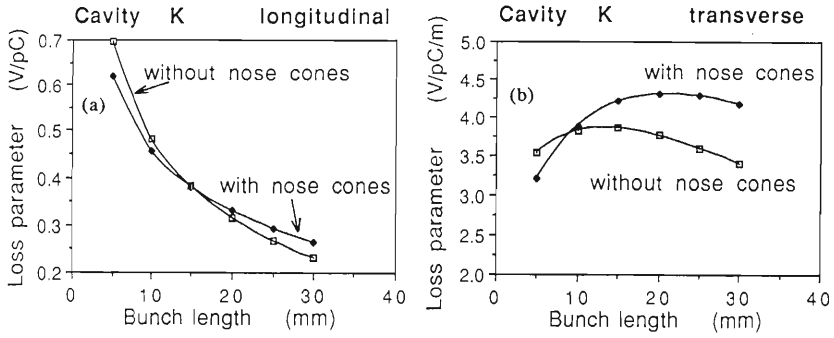

Fig. 1. Loss parameters for cavities with and without nose cones: (a), longitudinal case; (b), transverse case.

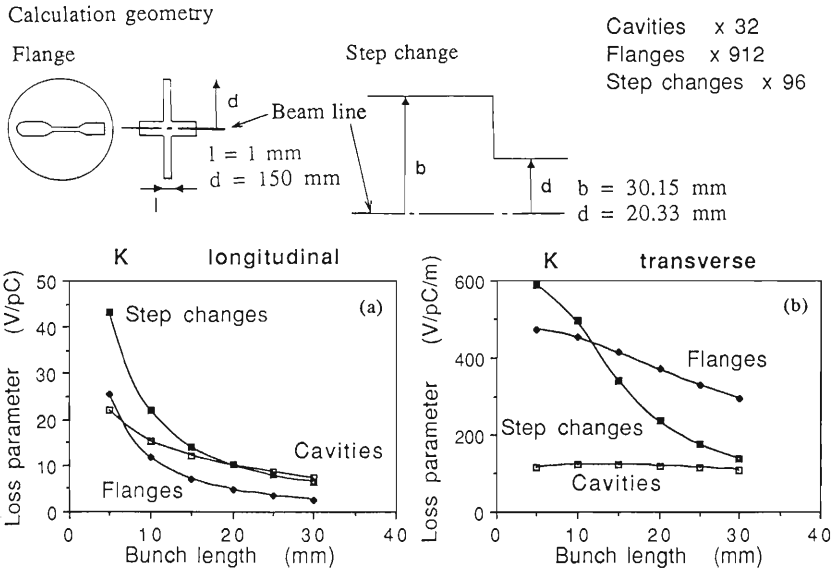

Fig. 2. Total loss parameters of the whole storage ring for typical components: (a), longitudinal case; (b), transverse case.

region of the short bunch length. This is because while the HOM impedances which exert a harmful effect on a beam, below cut-off frequency of the beam chamber connected to the cavity, are suppressed in the cavity without nose cones,[4] other HOM impedances which have little effect on the beam become large, especially above cut-off frequency.

Figure 2 shows the total loss parameters of the whole ring, when only the elements which have large contributions to the impedance are taken into account.Bellows themselves have large loss parameters, but the loss parameters are steeply reduced by screening with RF contacts. It turns out that, in a longitudinal case, step changes give a large effect on the impedance, and the step changes and flanges do in a transverse case. As far as the step changes are concerned, however, as the transitions to ID chambers consist of tapered parts, the loss parameters are, in fact, reduced further.

In conclusion, the contribution to impedance is mainly attributed to flanges and RF cavities. In particular, the impedance of flanges needs to be decreased more. In the next step, we calculate the loss parameters of asymmetric geometries using a three dimensional (3D) code MAFIA,[5] because TBCI is only used for geometries with a rotational symmetry. There is yet room for improvement, since the 3D simulation has many limitations such as the number of meshes, the minimum bunch length, and computational time.

References

1) T. Yoshiyuki, T. Kusaka, J. Ohnishi, and S.H. Be: *RIKEN Accel. Prog. Rep.*, **22**, 276 (1988).
2) T. Weiland: *Nucl. Instrum. Methods*, **212**, 13 (1983).
3) B. Zotter: CERN LEP-TH/87-34 (1987).
4) T. Kusaka, T. Yoshiyuki, T. Moro, and M. Hara: This Report, p. 155.
5) R. Klatt *et al.*: Proc. of the 1986 Linear Accel. Conf., SLAC (1986).

RIKEN Accel. Prog. Rep. 23 (1989)

V-2-29. Design of Magnets for the 8 GeV Storage Ring

S. Motonaga and J. Ohnishi

Basic design of dipole, quadrupole, and sextupole magnets for the 8 GeV storage ring has been finished, and their prototypes are being fabricated at factories. The unit cell of the storage ring is of so-called Chasmann-Green type and composed of 2 bending, 10 quadrupole, and 7 sextupole magnets. The ring has 48 cells and the circumference is 1436m. There are 4 symmetrically-located long straight sections of 34 m and 44 short straight sections of 6.5 m in the ring. The long straight section is realized by removing two bending magnets from the unit cell. Then total numbers of dipole, quadrupole, and sextupole magnets are 88, 480, and 336, respectively. For closed-orbit distortion (COD) correction, dipole and sextupole magnets have correction coils which can produce additional vertical and horizontal correction fields. In addition to these, 192 steering magnets are installed.

Table 1. Required field quality of the dipole, quadrupole, and sextupole magnets.

Magnet	Dipole	Quadrupole	Sextupole
Maximum field strength	0.665 T	18 T/m	360 T/m^2
Gap distance or bore radius	65 mm	45 mm	55 mm
Effective field length	2.863 m	0.5, 0.6, 1.1 m	0.6, 0.45 m
Field uniformity	$\Delta Bl/Bl$	$\Delta Gl/Gl$	$\Delta Gl/Gl$
	$<5 \times 10^{-4}$	$<5 \times 10^{-4}$	$<1 \times 10^{-3}$
	x=±40 mm	x=±35 mm	x=±35 mm
	y=±17 mm	y=±15 mm	y=±15 mm

The field quality required for these magnets is given in Table 1, and parameters designed for them are listed in Table 2. Magnetic field have been calculated by using a 2-D program code LINDA and TRIM.

Table 2. Designed parameters for lattice magnets.

		Dipole	Quadrupole			Sextupole	
Number of magnets		88	192	192	96	288	48
Maximum strength		0.665 T		18 T/m		300 T/m^2	360 T/m^2
Effective length	(m)	2.86	0.5	0.6	1.1	0.45	0.6
Gap or Bore radius	(mm)	65		45		55	
Magnetomotive force	(AT)	3.5×10^4		1.5×10^4		7.0×10^3	8.3×10^3
Turns per pole		14		16		22	
Conductor size	(mm)	14x23-ϕ10		11.5x16-ϕ5		8x8-ϕ3.5,	ϕ4.0
Current	(A)	1250		940		320	380
Current density	(A/mm^2)	5.1		5.8		5.9	7.0
Voltage	(V)	20.3	10.8	13.0	23.8	18.3	27.2
Power	(KW)	25.3	10.2	12.2	22.4	5.9	10.3
Cooling water circuits		2	4	4	8	6	6
Water flow	(l/min)	18.1	7.3	8.7	16.0	4.2	7.4
Pressure drop	(bar)	5.0	2.0	3.2	2.6	2.3	4.1
Temperature rise	(°C)	20		20		20	

All magnets are made by laminating 0.5mm thick silicon steel plates to guarantee the field of all magnets as identical as possible.

Dipole magnets: The dipole magnet has a C-shaped rectangular configuration as shown in Fig. 1 and its designed parameters are listed in Table 2. The pole is flat over a horizontal range of 200 mm and has radial shims of 2 mm in thickness at both ends. The calculation of the magnetic field predicts that $\Delta Bl/Bl$ will be less than 1×10^{-4} over a horizontal range of 100 mm.

Quadrupole magnets: The cross-sectional view of the quadrupole magnet is shown in Fig. 2. All magnets have the same pole contour. The structure was designed to remove parts of the yoke on both radial side at a median plane, because an enlarged vacuum chamber having a photon beam channel is to be installed. There are three different lengths provided; 1.1 m, 0.6 m, and 0.5 m. Designed parameters are given in Table 2. Calculated field gradients are shown in Fig. 3. The region of a uniform field gradient within 1.0×10^{-3} is expected to be in a radius of 35mm.

Sextupole magnets: Two types of magnets having different yoke structures have been designed: one is completely six-hold symmetric and the other is asymmetric. All magnets have

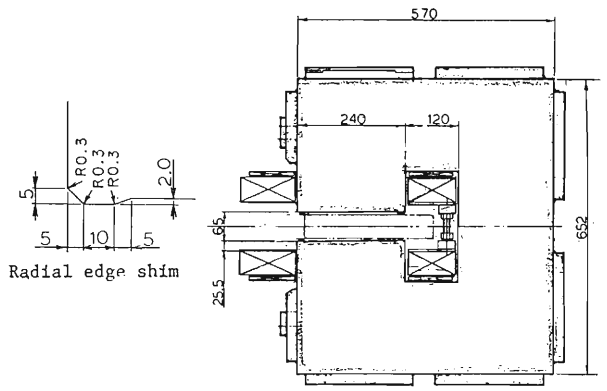

Fig. 1. Cross-sectional view of a prototype dipole magnet.

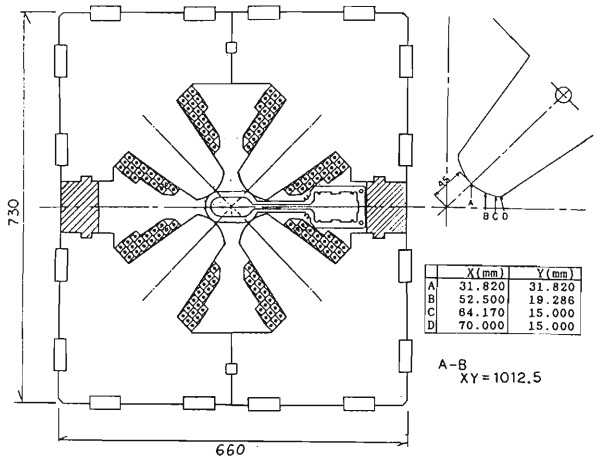

Fig. 2. Cross-sectional view of a prototype quadrupole magnets. The top and bottom halves are jointed through a non magnetic material to keep a space for inserting of a vacuum chamber. Field calculations were carried out on two types of yoke structures with and without a magnetic circuit in the yoke at median plane. The field gradient was found to be the same in both types.

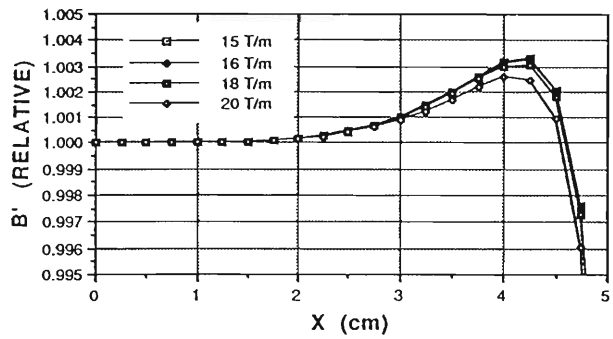

Fig. 3. Radial distribution of the field gradient (B') of the quadrupole magnet. The B' is designed to be intensified along the radial direction for compensation of the reduction in the longitudinal integrated gradient field over the magnet due to the fringing field.

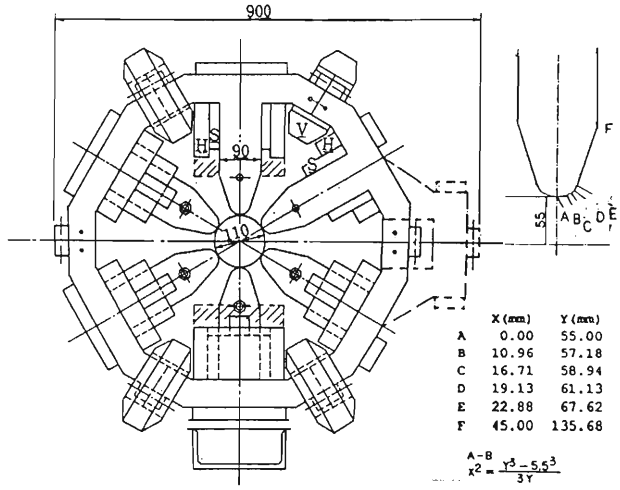

Fig. 4. Cross-sectional view of a sextupole magnet. Two different types have been designed: one is completely symmetric (a solid line) and the other is asymmetric in the yoke structure (a dotted line). Auxiliary coils for COD correction were wound on the sextupole magnets; 'H' and 'V' indicate coils for providing a vertical and horizontal dipole fields, respectively.

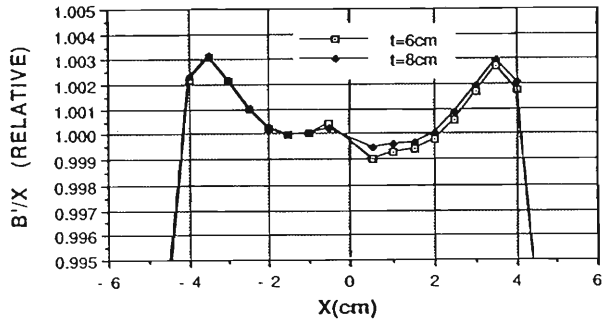

Fig. 5. Calculated field distributions of the sextupole magnet having an asymmetric yoke structure. Disagreement in the radial field distribution occuring from the center toward two sides (+, −) results from the quadrupole component. The maximum value of the component is equivalent to the gradient errors of the quadrupole magnet and will exert no serious influence on a beam.

the same pole contour shaped with $r^3\cos^3 q$ with a radial shim as shown in Fig. 4. The designed parameters are given in Table 2. The region of a uniform field gradient within 1.5×10^{-3} is expected to be in a radius of 35mm from a calculation. Figure 5 shows the field distributions caluculated for a sextupole magnet having an asymmetric yoke structure.

Correction magnets: The maximum field strength of 0.02 T. m is required, which gives 0.8 mrad kick to a beam.

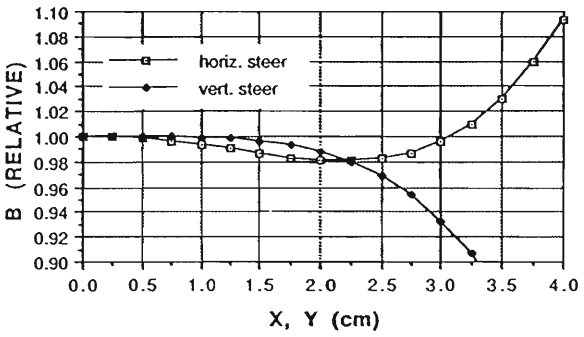

Fig. 6. Calculated field distributions of horizontal and vertical dipoles produced in the sextupole magnet. $B_{x(y)}$ on a $x=0$ plane is plotted for the horizontal field and $B_{y(x)}$ on a $y=0$ plane for vertical. The uniform region of field less than 2% is expected over a radius of 20 mm.

Vertical correction field for horizontal steering are provided with individual small magnets. Six of 7 families of the sextupole magnets provide a vertical or a horizontal dipole correction field. Ninety-six individual correction magnets prrovide both horizontal and vertical correction fields. Other small magnets also provide a horizontal dipole field. The detailed design of individual correction dipole magnets is now in progress. Figure 6 shows calculated distributions of a horizontal and a vertical dipole field produced by the streering elements added to the sextupole magnets.

The prototypes of the lattice main magnets are under construction. Real magnets will be designed by taking account of the results of the field measurements in prototypes.

RIKEN Accel. Prog. Rep. 23 (1989)

V-2-30. Design of Power Supplies for SPring-8 Storage Ring Magnets

H. Takebe, S. Motonaga, and H. Kamitsubo

On the basis of the machine parameters decided for the SPring-8 storage ring, the fundamental design of a power supply (PS) system and the connection (Fig. 1) of magnets were investigated this year. Table 1 shows a required strength for seven operating modes (two cell mode, hybrid mode, and Detuned Chasman-Green (DCG) modes) of the SPring-8 decided by the Lattice group. The Currents for the magnets were calculated from these values, using magnetic effective field lengths and excitation factors.[1] The maximum currents, voltages, stabilities, ripple currents, and power consumptions for the magnets are listed in Tables 2-5. Since a magnetic field ripple induced by a current ripple is reduced by a aluminum vacuum chamber, the allowance of the ripple current is about three times larger than the current stability. The number of the PS's located in PS-rooms A,B,C and D are indicated in these Tables.

The maximum current of a bending magnet (BM) for 8 GeV (0.66 Tesla) is 1320A. All the BM's are connected in series, and excited by one

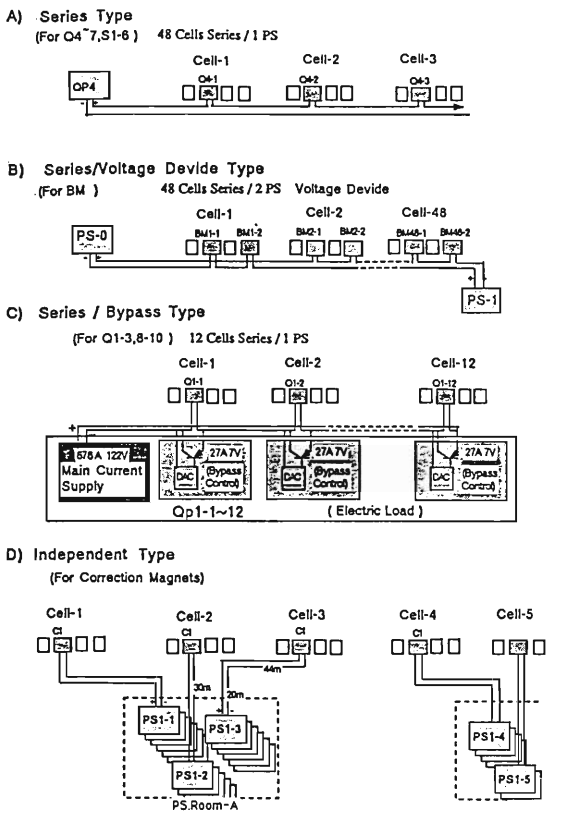

Fig. 1. Four connection types of the magnets and power supplies.

Table 1. Required strength of Q and Sx magnets for seven operation modes.

Magnet	P.S.	Hybrid	middle β	high β	DCG 8	DCG 6	DCG 4	DCG 3	Max	Min	Min/Max
					(Detuned Chasman Green)				(Absolute Value)		
QD1	QP1	-0.2422	-0.4354	-0.2348	-0.3365	-0.2829	-0.2992	-0.3005	0.4354	0.2348	54%
QF2	QP2	0.3759	0.4121	0.3711	0.4077	0.3720	0.3409	0.3140	0.4121	0.3140	76%
QD3	QP3	-0.3905	-0.2531	-0.3906	-0.4094	-0.4081	-0.3552	-0.3319	0.4094	0.2531	62%
Q4	QP4	-0.5077	-0.6000	-0.5077	-0.3870	-0.4105	-0.3765	-0.3581	0.6000	0.3581	60%
Q5	QP5	0.5555	0.5799	0.5555	0.4213	0.3334	0.3165	0.2969	0.5799	0.2969	51%
Q6	QP6	0.5555	0.5799	0.5555	0.3850	0.3608	0.3213	0.2970	0.5799	0.2970	51%
Q7	QP7	-0.5077	-0.6000	-0.5077	0.4074	-0.2877	-0.3095	-0.3074	0.6000	0.2877	48%
QD8	QP8	-0.5297	-0.2531	-0.3906	-0.4536	-0.4412	-0.4489	-0.4237	0.5297	0.2531	48%
QF9	QP9	0.5749	0.4121	0.3711	0.3506	0.3632	0.3591	0.3489	0.5749	0.3489	61%
QF10	QP10	-0.4309	-0.4354	-0.2348	-0.2875	-0.3467	-0.3234	-0.3091	0.4354	0.2348	54%
S1	SP1	3.5463	0.0000	2.0800	0.0000	0.0000	0.0000	0.0000	3.5463	0.0000	0%
S2	SP2	-4.0383	0.0000	-2.0616	0.0000	0.0000	0.0000	0.0000	4.0383	0.0000	0%
S3-5	SP3	-4.3757	-3.3593	-3.5308	-1.4909	-2.0060	-1.1570	-1.2709	4.3757	1.1570	26%
S4	SP4	7.7652	2.9091	3.1285	1.9722	2.4202	1.4021	1.5019	7.7652	1.4021	18%
S5	SP5	-4.3757	-3.3593	-3.5308	-1.4909	-2.0060	-1.1570	-1.2709	4.3757	1.1570	26%
S6	SP6	-3.0021	0.0000	-2.0616	-1.4909	-2.0060	-1.1570	-1.2709	3.0021	0.0000	0%
S7	SP7	4.8322	0.0000	2.0800	1.9722	2.4202	1.4021	1.5019	4.8322	0.0000	0%

Emittance(n.m)	5.3		5.7	23.1	36.8	53.3	81.7
Tune							
(Vertical)	19.16	18.251	16.16	21.149	21.149	21.149	20.851
(Horizontal)	51.22	42.25	42.22	31.2	28.2	25.2	22.8

PS (Fig. 1-B). The total resistance of 97 magnets is 1.57 ohm and cable is 0.095 ohm; thus, the total voltage of the PS is 2233V. Table 2 lists these parameters for the BM PS. In order to reduce the terminal voltage of the magnet and cable against the earth, the PS is divided into two devices and the voltage is divided into four (~550V). The current stability and the ripple are 1×10^{-5} and 3×10^{-5}, respectively. Temperature controlled cooling water (25 ± 0.5°C) is supplied for the PS's shunt resistance. The reference voltage for the current control is given by a hi-precision 16 bit DAC (Digital to Analog Converter). This DAC and amplifier are enclosed in a temperature controlled housing.

Required maximum currents and voltages for quadrupole (Q)-magnets are listed in Table 3. To reduce the number of the PS's and power consumption, the same Q-magnets of the cells are connected in series (Fig. 1-A). Q4, Q5, Q6 and Q7 magnets are connected in series with 48 cells. Other same named Q-magnets, (Q1, Q2, Q3, Q8, Q9, and Q10) are connected in series, but are adjusted by bypass control circuits[2] to correct the insertion device distortions (Fig. 1-C). The current corrections for the insertion devices are needed for 0.2% (Q2, Q3, Q8 and Q9), 4% (Q1) and 2% (Q10) to the maximum current.[3] Table 4 shows required currents, voltages, resistances, and others for the sextupole (Sx)-magnets. Magnets for the Sx-1 to 6 are connected in series in all cells. Two SD magnets are operated at the same current (the same PS).

Table 2 to 5. Required parameters for B, Q, Sx, Co-magnets.

Table 2 Dipole Magnet

Magnet Name	PS Name	Max.Curr. (A)	V (PS)	Stability	Ripple	Power (kW)	No.PS	Total Power (kW)	Connect Type	No.of PS in Room A	B	C	D
B	BP	1340	2233	1.0E-05	3.0E-05	2993	1	2993	B	1			

Table 3 Quadrupole Magnet (Bypass Type)

Magnet Name	PS Name	Max.Curr. *(A)	V (PS) V	Stability	Ripple	Power (kW)	No.PS	Total Power (kW)	Connect Type	No.of PS in Room A	B	C	D
QD1	QP1	676.3	121.5	1.0E-04	3.0E-04	82.2	4	329	C	1	1	1	1
QF2	QP2	640.8	216.6	1.0E-04	3.0E-04	138.8	4	555	C	1	1	1	1
QD3	QP3	636.0	131.1	1.0E-04	3.0E-04	83.4	4	333	C	1	1	1	1
QD4	QP4	932.8	638.7	1.0E-04	3.0E-04	595.7	1	596	A	1			
QF5	QP5	901.9	712.7	1.0E-04	3.0E-04	642.8	1	643	A	1			
QF5	QP6	901.9	712.7	1.0E-04	3.0E-04	642.8	1	643	A	1			
QD4	QP7	932.8	638.7	1.0E-04	3.0E-04	595.7	1	596	A	1			
QD6	QP8	823.8	162.8	1.0E-04	3.0E-04	134.1	4	536	C	1	1	1	1
QF7	QP9	893.8	294.6	1.0E-04	3.0E-04	263.3	4	1053	C	1	1	1	1
QD8	QP10	676.3	121.5	1.0E-04	3.0E-04	82.2	4	329	C	1	1	1	1
							28	5613					

Table 4 Sextupole Magnet

Magnet Name	PS Name	Max.Curr. *(A)	V (PS) V	Stability	Ripple	Power (kW)	No.PS	Total Power (kW)	Connect Type	No.of PS in Room A	B	C	D
S1	SP1	577.0	359.6	1.0E-04	3.0E-04	207	1	207	A	1			
S2	SP2	656.8	409.3	1.0E-04	3.0E-04	269	1	269	A	1			
S3-5	SP3	710.5	811.4	1.0E-04	3.0E-04	576	1	576	A	1			
S4	SP4	948.4	670.3	1.0E-04	3.0E-04	636	1	636	A	1			
S6	SP5	489.0	304.8	1.0E-04	3.0E-04	149	1	149	A	1			
S7	SP6	787.2	490.6	1.0E-04	3.0E-04	386	1	386	A	1			
							6	2224					

Table 5 Correct/Steering Magnet

Magnet Name	PS Name	Max.Curr. (A)	V (PS) V	Stability	Ripple	Power (kW)	No.PS	Total Power (kW)	Connect Type	No.of PS in Room A	B	C	D
S1	CP1	20.0	16.3	1.0E-03	3.0E-03	0.33	48	15.6	D	12	12	12	12
S2	CP2	20.0	19.1	1.0E-03	3.0E-03	0.38	48	18.3	D	12	12	12	12
S3	CP3	20.0	16.3	1.0E-03	3.0E-03	0.33	48	15.6	D	12	12	12	12
S5	CP4	20.0	16.3	1.0E-03	3.0E-03	0.33	48	15.6	D	12	12	12	12
S6	CP5	20.0	19.1	1.0E-03	3.0E-03	0.38	48	18.3	D	12	12	12	12
S7	CP6	20.0	16.3	1.0E-03	3.0E-03	0.33	48	15.6	D	12	12	12	12
C1H	CP7	40.0	14.4	1.0E-03	3.0E-03	0.57	48	27.6	D	12	12	12	12
C1V	CP8	40.0	14.4	1.0E-03	3.0E-03	0.57	48	27.6	D	12	12	12	12
C2	CP9	40.0	14.4	1.0E-03	3.0E-03	0.57	48	27.6	D	12	12	12	12
C3	CP10	40.0	14.4	1.0E-03	3.0E-03	0.57	48	27.6	D	12	12	12	12
C4H	CP11	40.0	14.4	1.0E-03	3.0E-03	0.57	48	27.6	D	12	12	12	12
C4V	CP12	40.0	14.4	1.0E-03	3.0E-03	0.57	48	27.6	D	12	12	12	12
B-C1	CP13	15.0	16.6	1.0E-03	3.0E-03	0.25	48	11.9	D	12	12	12	12
B-C2	CP14	15.0	16.6	1.0E-03	3.0E-03	0.25	48	11.9	D	12	12	12	12
							672	288.4					

*Max.Curr is a a 110% of the calculated value.
4 PS room Type

All PS.No
707

Total Power
11118 kW

L(PS-Mag)=225m

Q1-3.8-10.St.Co	Cable Length 0.45km
Q4-7.Sx.BM	Cable Length 4.2km

All the coils for correction (Co) magnets have independent PS's (Fig. 1-D), including Sx installed correction coils. Six horizontal correction coils in one Sx magnet are connected in series; thus, the total number of Co-PS's are 672.

A reference voltage to a transistor regulator is supplied from a 16 bit DAC, which is controlled by 15 or 12 bit registers through isolation davices. This register is strobed in a local processor (L-CPU) which communicate to the host processor.[4] A 24 bit status (power on/off, fuse, transistor break down, temperatures, oven, polarity, ext-interlocks, door, water flows, *etc.*) is read by this L-CPU. An actual current (shunt voltage) is monitored by an ADC (Analog to Digital Converter) and checked by the L-CPU every few tens of seconds. If the difference between the ADC and DAC values exceed some allowance or an error occurs in the status, an error flag is send to the host computer.

The total power consumption of the magnets of the storage ring is about 11.1 MW.

References

1) J. Ohnishi *et al.*: Accelerator Science Symposium, Osaka, Japan, Dec. 12-14 (1989).
2) H. Takebe, S. Motonaga, and T. Wada: *RIKEN Accel. Prog. Rep.*, **19**, 174 (1985).
3) Effect of Insertion Devices on Beam Dynamics of the 8 GeV Light Source Storage Ring. R. Nagaoka *et al.*: Particle Accelerator Conference in Chicago, U.S.A., Mar. (1989).
4) M. Nagase, H. Takebe, T. Wada, and K. Shimizu: 11th Int. Conf. on Cyclotron and Their Applications, Tokyo, Oct., p. 410 (1986).

RIKEN Accel. Prog. Rep. 23 (1989)

V-2-31. Development of Field Measurement Systems for SPring-8

J. Ohnishi, H. Takebe, and S. Motonaga

The storage ring of SPring-8 contains a great number of magnets (88 dipoles, 480 quadrupoles, 336 sextupoles, and about 192 correctors), which have to be satisfied with very stringent field quality.[1] Before installation, we have to measure the magnetic field of all the magnet in order to ensure that they are satisfied with requirement and to acquire individual characteristics of each magnet. On the other hand, the magnetic field measurement is significant in development of the magnets. At present, full-scale prototypes of a dipole, quadrupole, and sextupole are under construction. Their field measurement will be performed for the verification and improvement of designs.

We construct several kinds of facilities for the measurement:

(1) Hall probes and search coils are used for the measurement of 3-dimensional field distribution (mapping). The 3-dimensional scanning is performed with a moving table (4 m×0.3 m×0.3 m).

(2) A long flip coil, as shown in Fig. 1, measure the integrated dipole field $\int B(x)\,dl$ in a dipole magnet. The coil is wounded by two turns around a rod made from glass-fiber-reinforced epoxy, which is supported with an aluminium bar and can be adjusted horizontally. When we make the coil flipped (rotated in a half turn for about a second) in a dipole magnet, a current is induced. We can measure a quantity proportional to $\int B(x)\,dl$ by integrating the induced current during flipping. An absolute value of the field integral can be acquired from a measurement with a Hall probe.

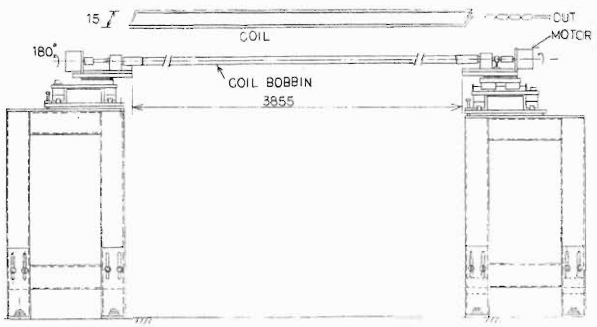

Fig. 1. Side view of the long flip coil, and the coil configuration.

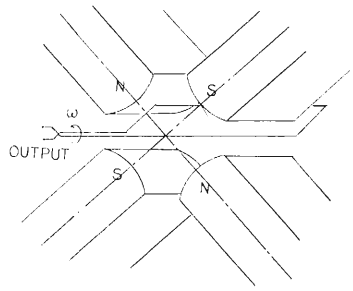

Fig. 2. Schematic of the harmonic coil located in a quadrupole magnet.

(3) We use a rotating coil for the measurement of higher-order multipole fields in a quadrupole and sextupole magnet. When it is rotated continuously in the magnet, as shown in Fig. 2, a current is induced with periodicities and has multiple components of a revolution frequency (about 16.7 Hz), which correspond to multipole components of magnetic fields. Therefore, we can measure each strength of multipole fields from an FFT analysis of output from the rotating coil.

We have completed the construction of a search, long flip, and rotating coil. At present, we are adjusting and testing them.

References

1) S. Motonaga and J. Ohnishi: This Report, p. 162.

RIKEN Accel. Prog. Rep. 23 (1989)

V-2-32. Injection Devices for the SPring-8

H. Miyade, H. Tanaka, J. Ohnishi, and S. Motonaga

A beam from the synchrotron is injected into the storage ring at one of the 6.5 m long straight sections, where the horizontal betatron function has large value. Figure 1 shows the beam injection section. The injection devices are composed of three septum magnets and four bump magnets.

The first and the second septum magnets have the same specification. These magnets are operated with a direct current. The third is a passive type[1] and is operated with a pulsed current. When a pulse width is 40 μs, a stray field is expected to be $\sim$40 G•m on a bump orbit.

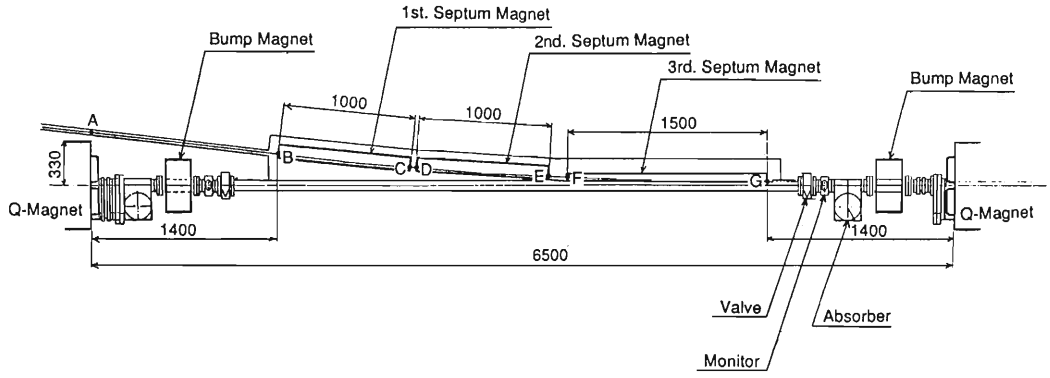

Fig. 1. Schematic diagram of the injection section.

Table 1. Parameters of the septum and bump magnets.

	Septum		Bump	
	1st, 2nd	3rd	BP1	BP2
Length (m)	1	1.5	0.2	0.4
Bending angle (mrad)	34.91	45.38	0.5831	2.26
Peak field (T)	0.931	0.807	0.0777	0.151
Number of turns	4	1	1	1
Inductance (μH)	70.4	2.64	0.45	0.91
Current waveform*	DC	HS	HS	HS
Peak current (A)	1,480	6,420	3,830	7,450
Pulse width (μs)	—	40	4	4
Repetition rate (Hz)	—	60	60	60

*DC: Direct current, HS: Half sine wave.

There are two types of bump magnets: one type of magnets are installed in the both ends of the injection section and the others are beside bending magnets. The magnets are operated by the pulsed current with a pulse width of 4 μs. The core is made of ferrite and a vacuum chamber is made of ceramic.

The parameters of the septum and bump magnets are listed in Table 1.

References

1) N. Marks and M.W. Poole: *IEEE Trans. Mag.*, **MAG-17**, 1579 (1981).

RIKEN Accel. Prog. Rep. 23 (1989)

V-2-33. Commissioning of a Multipole Wiggler, MPW#13

S. Sasaki, M. Hara, S. Yamamoto,* T. Shioya,* M. Kato,* and H. Kitamura*

The construction of a multipole wiggler, MPW #13, has been completed at the Photon Factory (PF).[1,2] Machine studies are necessary for obtaining the parameters for stable opertion of the PF storage ring, before providing synchrotron radiation from the MPW#13 for experimental use. The most significant influences of the device on the ring are tune shift and closed orbit distortion (C. O.D.). We report these items successively.

Tune shift measurement: An insertion device (I.D.) may shift the tune number of betatron oscillation to such an extent that the tune moves to the stop-band of a destructive resonance line. Therefore, the tune shift must be measured so that correction parameters are obtained not to shift the tune value prior to the operation of the I.D. for providing synchrotron radiation.

The tune shift comes from the focusing force of an I.D., arising from the edge focusing effect of each magnetic pole. The tune shift is caused even by an insertion device which has on error field.

An insertion device having vertical magnetic field such as MPW#13 causes a vertical tune shift, $\Delta\nu_y$. For such a device the tune shift can be expressed as,

$$\Delta\nu_y \approx \beta_y L_{ID}/8\pi\rho_w^2 \qquad (1)$$

where β_y is the beta function at the device position, L_{ID} is the length of the insertion device, and ρ_w is the radius of curvature of the electron orbit corresponding to the peak magnetic field.[3,4]

We measured the tune as a function of the magnetic field of MPW#13: we observed the fattening of a beam image on the monitor screen of synchrotron radiation in the visible region while we were varying the frequency of a perturbator, so that we could detect the resonance frequency of betatron oscillation. Actually, by this method we could obtain the fractional part of the tune when a measured resonance frequency was divided by a revolution frequency.

Figure 1 shows the fractional tune as a function of the peak magnetic field of MPW#13 with a value calculated from Eq. 1. Agreement between the calculated values and the measured values is fairly well; the small discrepancies can be attributed to the measurement errors of the

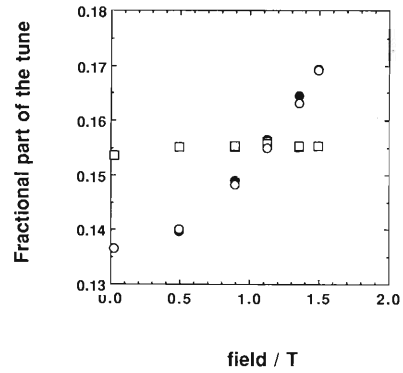

Fig. 1. Fractional part of the tune against the peak magnetic field of MPW#13. Closed circles, measured values of a vertical tune, ν_y; open circles, calculated values of a vertical tune, ν_y^{calc}; open squares, measured value of a horizontal tune subtracted by 0.25, $\nu_x - 0.25$.

resonance frequency, the deviation of magnetic field distribution from that assumed in deriving Eq. 1, and the uncertainties of the values for β_y and the effective length of the insertion device taken in the calculation; the β_y value used in the calculation is the designed value in linear optics.

C.O.D. Correction: C.O.D. arises from the finite value of the field integral of an I.D. along the device axis. Usually an I.D. is designed so as not to have a net integral field along the axis. Therefore C.O.D. can not occur unless field error, which is the deviation from the designed field distribution, exits.

Among the influences of C.O.D. to a storage ring, the shift and/or tilt of photon beam axes of synchrotron radiation is more serious than the beam dynamics aspect of the electron beam in the storage ring. If an insertion device generates any C.O.D., a cure should be made so as not to move the axes of photon beam lines around the storage ring during the change of the gap of the device.

In our case C.O.D. is corrected by controlling the currents of electromagnets attached to both ends of MPW#13.

C.O.D. correction parameters have been obtained in the following way. (1) We selected two sets of position monitors whose discrepancies were largest between two different gap settings. (2) We measured the beam position values of the position monitors selected at a given gap as reference. (3) The gap was set to one

* Photon Factory, National Laboratory for High Energy Physics (KEK-PF), Oho 1-1, Tsukuba, Ibaraki 305, Japan

of the measurement points. (4) Three sets of current values were selected, and for each set of the current values position monitor values were measured. (5) At this stage we obtained information to solve the linear equation for zero deviations of the position monitor values from the reference values. (6) The currents obtained in step (5) were applied to correction magnets, and position deviations were measured to confirm whether the deviation of the position monitor values were satisfactory small. (7) If the position monitor deviation were not small enough, newest three sets of current values were used for step (5), and the procedure was repeated. These procedures were applied to both x- and y-directions.

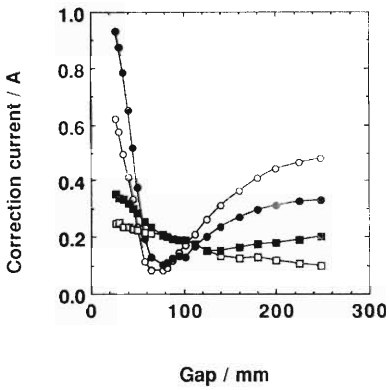

Fig. 2. C.O.D. correction current applied to the correction electromagnets of MPW#13 against the gap. Open circles, correction currents of the electromagnet attached upstream of MPW#13 for the horizontal direction; closed circles, downstream horizontal correction currents; open squares, upstream vertical correction currents; closed squares, downstream vertical correction currents.

Figure 2 shows the correction currents for the C.O.D. correction as a function of the gap.

This device has been funded in part by the Science and Technology Agency with Special Coordination Funds for the Promotion of Science and Technology.

References

1) S. Sasaki, M. Hara, S. Yamamoto, T. Shioya, and H. Kitamura: *RIKEN Accel. Prog. Rep.*, **21**, 252 (1987).
2) S. Sasaki, S. Yamamoto, T. Shioya, and H. Kitamura: *Rev. Sci. Instrum.*, **60**, 1859 (1989).
3) K. Halbach: "Field of Undulators and Wigglers", Workshop on Magnetic Errors, Brookhaven (1986).
4) L. Smith: "Effect of Wigglers and Undulators on Beam Dynamics", EGS Technical Note-24 (1986).

RIKEN Accel. Prog. Rep. 23 (1989)

VI. RADIATION MONITORING

1. Routine Monitoring of the Cyclotron, RILAC, and TANDETRON

I. Sakamoto, S. Fujita, M. Yanokura, T. Kobayashi, K. Ogiwara,
T. Katou, Y. Matuzawa, M. Miyagawa, S. Kagaya, S. Shinohara,
M. Iwamoto, and I. Kohno

The present report describes the results of routine radiation monitoring carried out for the cyclotron, RILAC, and TANDETRON from January to December 1989.

The Aspects of leakage radiation from the cyclotron are described in a succeeding report.[1)]

(1) Contamination in the cyclotron building

The surface contamination has been kept below 10^{-1} Bq/cm^2 on the floors of the cyclotron building. The contamination was wiped off twice a year. Immediately after this decontamination, the activities on the floor of most of the above places were reduced below 10^{-2} Bq/cm^2.

When radioactive substances were handled in the hot laboratory and chemical laboratories, the air in a draft chamber was activated. The air in the draft chamber was exhausted, and the radioactivity in the exit was found to be 10^{-8} Bq/cm^3.

(2) Drainage

Radioactivities in drain water from the cyclotron and the linac buildings were found to be of the order of 10^{-4}-10^{-3} Bq/cm^3. The total activity in aqueous effluents was 38 kBq.

(3) Radiation monitoring for RILAC and TANDETRON

The leakage radiation during operation of RILAC was measured outside the linac building every three months. No leakage of γ rays and neutrons from the linac buiding was detected. No contamination due to residual activities was found on the floor of control area and conditioning air in the linac building.

X-ray monitoring was carried out for TANDETRON, when a niobium target was bombarded with 2.0 MeV $^{11}B^+$ ions of 0.2 nA, and the maximum irradiation dose rates measured around TANDETRON was 0.012 mSv/h No leakage X-rays were detected around the target chamber and outside the TANDETRON room.

(4) Personnel monitoring

The number of RIKEN accelerator workers increased to 1.4 times of that in the preceding period.

The external exposure dose for personnel were measured by using γ ray and neutron film badges. The dose received by accelerator workers from January to December 1989 are shown in Table 1. The external doses were detected for two nuclear chemists; 0.4 and 0.1 mSv, respectively. The collective dose owing to thermal and fast neutron exposures was below the detection limit.

Table 1. Annual external exposure doses received by RIKEN accelerator workers from January to December 1989.

Workers	Number of persons				Collective dose (mSv)
	Dose undetectable	0.1-1 (mSv)	>1 (mSv)	Total	
Accelerator physicists and Operators *	47	0	0	47	0
Nuclear physicists	113	0	0	113	0
Researchers in other fields	148	2	0	150	0.5
TANDETRON workers	12	0	0	12	0
Health physicists	7	0	0	7	0
Total	327	2	0	329	0.5

* Operators : For Ring cyclotron, Cyclotron, and RILAC.

Average annual dose per person, 0.0015 mSv; Maximum individual annual dose was 0.4 mSv.

References

1) I. Sakamoto, S. Fujita, and I. Kohno: This Report, p.172.

RIKEN Accel. Prog. Rep. 23 (1989)

VI-2. Leakage-Radiation Measurements in the Cyclotron Building

I. Sakamoto, S. Fujita, and I. Kohno

Leakage radiation was measured at various points in the cyclotron building in September 1989, when a target placed on the beam line No. 2 was bombarded with 18-MeV helium-3 ions at a beam intensity of 2 μA.

γ-Ray dose rates were measured with an ionization chamber survey meter, and dose-equivalent rates for fast and slow neutrons were measuered with a "rem counter"*. The results are shown in Fig. 1.

The leakage doses measured during January and December 1989 with γ-ray and neutron film badges placed at two positions (points A and B in Fig. 1) on the underground passage are shown in Table 1.

Of the dose values measured every month at point A, the maximum total dose of 7 mSv was observed in September, when the values for γ-rays and thermal and fast neutrons were 5.6, 0.2, and 1.2 mSv, respectively.

High fast-neutron doses observed at point A in September, November, and December were 1.2, 0.8, and 2.0 mSv, respectively. At point A, the high fast-neutron doses were due mainly to activation analysis and radioisotope production carried out on the beam line No. 2 during these periods.

Table 1. Leakage-radiation doses (1 cm dose-equivalent in mSv) on the underground passage of the cyclotron building during January and December 1989.

Month	Point A*				Point B*			
	γ rays (mSv)	Thermal neutrons (mSv)	Fast neutrons (mSv)	Total (mSv)	γ rays (mSv)	Thermal neutrons (mSv)	Fast neutrons (mSv)	Total (mSv)
1.89'	0.4	0	0.1	0.5	0	0	0	0
2	1.9	0.1	0.2	2.2	0	0	0	0
3	2.3	0.2	0.5	3.0	0	0	0	0
4	2.7	0.1	0.3	3.1	0	0	0	0
5	2.1	0.1	0.4	2.6	0	0	0	0
6	2.8	0.1	0.7	3.6	0	0	0	0
7	0	0	0	0	0	0	0	0
8	0	0	0	0	0	0	0	0
9	5.6	0.2	1.2	7.0	0	0	0	0
10	2.2	0.1	0.7	3.0	0	0	0	0
11	5.4	0.2	0.8	6.4	0.4	0	1.5	1.9
12	4.4	0.2	2.0	6.6	0	0	0	0
Total	29.8	1.3	6.9	38	0.4	0	1.5	1.9

* See Fig. 1

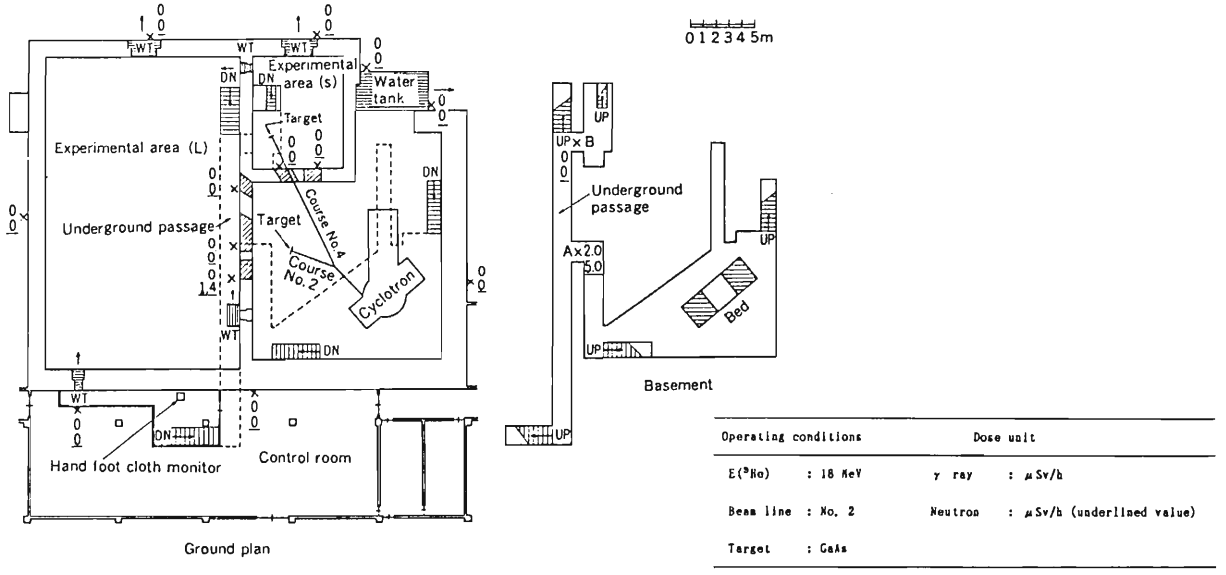

Fig. 1. Leakage-radiations (neutrons and γ rays) in the cyclotron building.

* A Neutron Rem Counter NSN1 manufactured by Fuji Electoric Co., Ltd. Japan.

RIKEN Accel. Prog. Rep. 23 (1989)

VI-3. Radiation Monitoring in the Ring Cyclotron Facility

S. Fujita, I. Sakamoto, T. Inamura, and H. Kamitsubo

The Radiation Safety Control System worked steadily from January to December, 1989, performing radiation monitoring continuously and automatically.

Additional beam lines became available for experimental vaults E4, E5, and E6. Figure 1 shows the indoor monitoring positions and the beam lines in the Ring Cyclotron facility. An injector AVF Cyclotron was also installed in April.

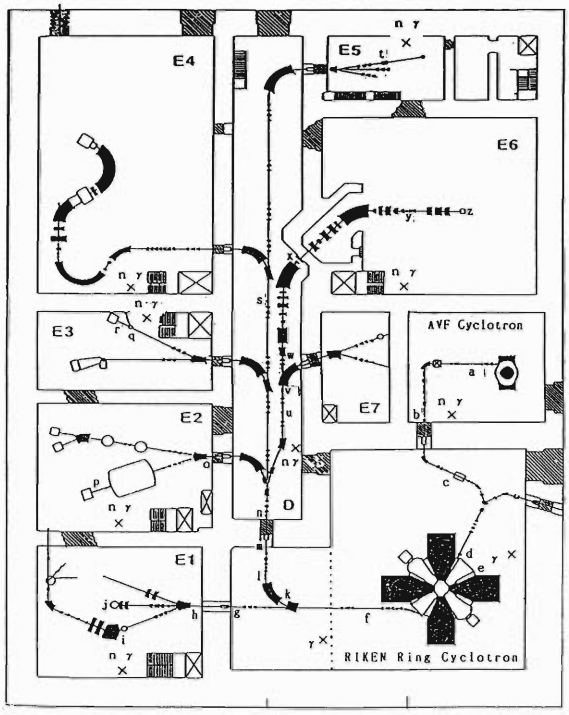

Fig. 1. Plan view of the Ring Cyclotron facility as of 1989. Monitoring positions are denoted by ×. Residual-activity detection points on the beam lines are denoted by alphabets.

When a routine overhaul was made in August, the dose rates due to residual activities of the Ring Cyclotron and the AVF Cyclotron were measured with a NaI-scintillation survey meter (NaI) and an ionization-chamber survey meter (IC). (Measurements were made about one month after the operation of the machine was stopped). The results are shown in Fig. 2 together with detection points. For the Ring Cyclotron residual activities were found as low as last year.[1)]

From October 16 to November 5, experiments were carried out with a ^{14}N beam of 135 MeV/u

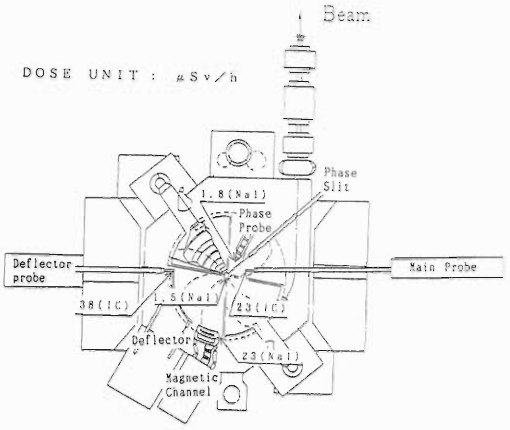

Fig. 2. Detection points around the injector AVF Cyclotron. Dose rates are indicated in units of μSv/h.

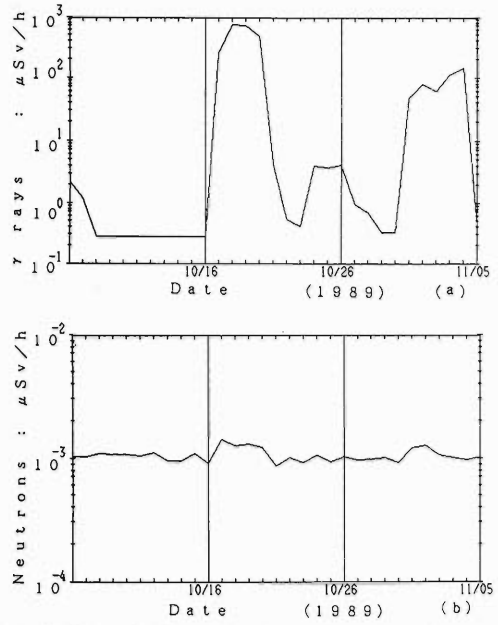

Fig. 3. Daily variations in the radiation level measured in the Ring Cyclotron facility. Detectors are (a) an ionization-chamber in the Ring Cyclotron vault, and (b) a BF_3 counter in the computer room. The beam current at the highest dose rate was about 30 nA.

in experimental vaults E1, E3, and E5, and with an ^{18}O of 100 MeV/u in E6. Figure 3 shows the daily variations in dose rates recorded during this period : (a) with an ionization chamber in the Ring Cyclotron vault; (b) slight leakage neutrons of about 5×10^{-4} μSv/h were recorded in the computer room above a bending magnet to guide beams from the Ring Cyclotron vault to the

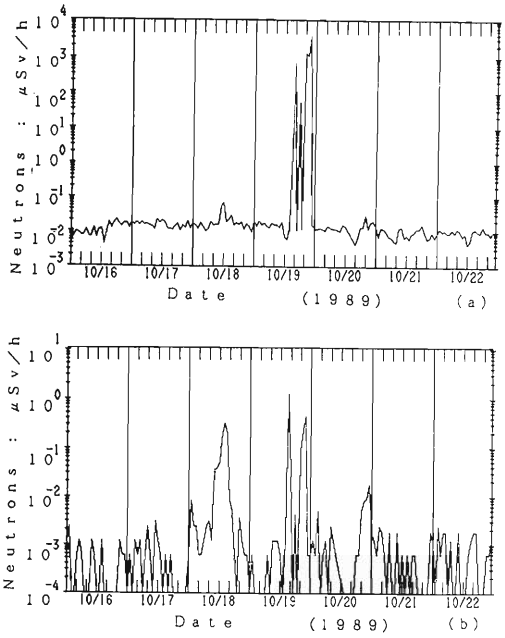

Fig. 4. Daily variations in the radiation level measured in the Ring Cyclotron facility. Detectors are (a) a BF_3 counter in the experimental vault E3, and (b) a BF_3 counter in the experimental vault E4. The beam current at the highest dose rate was about 30 nA.

beam disutribution corridor. No leakage gamma rays and no neutrons were detected with environmental monitors standing outside the building.

On October 19 an experiment was carried out with a ^{14}N beam of 135 MeV/u, the highest energy used this year, in the experimental vault E3. Figure 4 shows the daily variations in dose rates recorded in the neighboring vault E4 as well as in E3: (a) with a BF_3 counter in the experimental vault E3; (b) leakage neutrons were recorded in the experimental vault E4. Leakage neutrons due to beam tuning in the beam disutribution corridor were also recorded: on October 18 and at midnight of October 20. However, its level is well below the safety limit (1 mSv/week).

From October 23 to November 4, residual activities were detected along the beam lines with a NaI-scintillation survey meter and an ionization-chamber survey meter. Table 1 summarizes the measured dose rates.

Table 1. Summary of residual activities measured along the beam lines in units of μSv/h. Alphabets indicate detection points. (See Fig 1.)
Dp stands for detection points. NaI stands for a NaI-scintillation survey meter; and IC for an Ionization survey meter.

Dp	NaI	IC	Date	Dp	NaI	IC	Date
a	11	4.6	Nov. 04	n	38	23	Nov. 04
b	17	7.6	Nov. 04	o	1.8	1.8	Oct. 26
c	5.3	0.8	Nov. 04	p	17	3.8	Oct. 26
d	23	11	Oct. 23	q	3.8	2.4	Oct. 28
e	9.1	--	Oct. 23	r	7.6	3.0	Oct. 28
f	--	91	Nov. 04	s	6.8	4.1	Oct. 28
g	9.1	--	Oct. 23	t	9.1	--	Oct. 23
h	1.5	--	Oct. 26	u	--	38	Nov. 04
i	0.8	--	Oct. 26	v	--	61	Nov. 04
j	30	--	Oct. 23	w	--	76	Nov. 04
k	--	30	Nov. 04	x	14	13	Nov. 04
l	--	15	Nov. 04	y	12	9.1	Nov. 04
m	12	--	Oct. 23	z	4.6	5.3	Nov. 04

References

1) S. Fujita, I. Sakamoto, T. Inamura, and H. Kamitsubo: *RIKEN Accel. Prog. Rep.*, **22**, 307 (1988).

VII. LIST OF PUBLICATIONS

1. Accelerator development and accelerator physics

1) K. Hatanaka and H. Nonaka: "Status of the RIKEN ECRIS", Proc. Int. Conf. on the Physics of Multiply Charged Ions and Int. Workshop on E.C.R. Ion Sources, Grenoble, p. C1-827 (1989).

2) H. Kamitsubo, S. H. Be, M. Hara, R. Nagaoka, S. Sasaki, and T. Wada: "6-GeV Synchrotron Radiation Project", *Rev. Sci. Instrum.*, **60**, 1719 (1989).

3) S. Yamamoto, T. Shioya, S. Sasaki, and H. Kitamura: "Construction of Insertion Devices for Elliptically Polarized Synchrotron Radiation", *Rev. Sci. Instrum.*, **60**, 1834 (1989).

4) T. Shioya, S. Yamamoto, S. Sasaki, M. Katoh, Y. Kamiya, and H. Kitamura: "Construction and Operation of the Multipole Wiggler, MPW#16, at the Photon Factory", *Rev. Sci. Instrum.*, **60**, 1855 (1989).

5) S. Sasaki, S. Yamamoto, T. Shioya, and H. Kitamura: "Construction of a Multipole Wiggler, MPW#13, at the Photon Factory", *Rev. Sci. Instrum.*, **60**, 1859 (1989).

6) G. Isoyama, S. Yamamoto, T. Shioya, H. Ohkuma, S. Sasaki, T. Mitsuhashi, T. Yamakawa, and H. Kitamura: "Construction of a Multiundulator, Revolver No. 19, at the Photon Factory", *Rev. Sci. Instrum.*, **60**, 1863 (1989).

7) Y. Morimoto, S. Yokouchi, H. Sakamoto, Y. P. Lee, Y. Oikawa, and S. H. Be: "Design of Crotch and its Thermal Analysis for 8 GeV Stovage Ring", Proc. 7th Meeting on Ultra High Vacuum Techniques for Accelerators and Storage Ring, KEK, March, p. 68 (1989).

8) H. Sakamoto, S. Yokouchi, Y. Morimoto, Y. P. Lee, Y. Oikawa, and S. H. Be: "Vacuum System of 8 GeV Storage Ring", Proc. 7th Meeting on Ultra High Vacuum Techniques for Accelerators and Storage Ring, KEK, March, p. 74 (1989).

9) S. Yokouchi, H. Sakamoto, Y. Morimoto, and S. H. Be: "Vacuum Characteristics of NEG Strip", *J. Vac. Soc. Jpn.*, **32**, 385 (1989).

2. Nuclear physics and nuclear instrumentation

1) M. Oshima, E. Minehara, S. Kikuchi, T. Inamura, A. Hashizume, H. Kusakari, and M. Matsuzaki: "Rotational Perturbation to the Natural-Parity Rotational Band of ^{163}Dy", *Phys. Rev. C*, **39**, 645 (1989).

2) M. Yasue, H. Sato, H. Hasegawa, J. Takamatsu, T. Terasawa, T. Nakagawa, K. Hatori, and R. J. Peterson: "Deformed Nature of the 6^- States in ^{26}Al Observed by the (α, t) Reaction", *Phys. Rev. C*, **39**, 2159 (1989).

3) K. Saito, T. Maruyama, and K. Soutome: "Collective Modes in Hot and Dense Matter", *Phys. Rev. C*, **40**, 407 (1989).

4) H. Tamura, T. Yamazaki, M. Sano, Y. Yamamoto, M. Wakai, and H. Bando: "Compound Hypernucleus Interpretation of the ^{4}H Formation Probabilities in the Stopped K^-Absorption", *Phys. Rev. C*, **40**, 483 (1989).

5) M. Oshima, M. Matsuzaki, S. Ichikawa, H. Iimura, H. Kusakari, T. Inamura, A. Hashizume, and M. Sugawara: "Electromagnetic Transition Probabilities in the Natural-Parity Rotational Band of ^{173}Yb", *Phys. Rev. C*, **40**, 208 (1989).

6) M. Wakai, H. Bando, and M. Sano: "Mesonic Atom Production in High-Energy Nuclear Collisions", *Z. Phys. A*, **333**, 213 (1989).

7) W. Yokota, T. Nakagawa, M. Ogihara, T. Komatsubara, Y. Fukuchi, K. Suzuki, W. Galster, Y. Nagashima, K. Furuno, S. M. Lee, T. Mikumo, K. Ideno, Y. Tomota, H. Ikezoe, Y. Sugiyama, and S. Hanashima: "Energy Damping Feature in Light Heavy-Ion Reaction", *Z. Phys. A*, **333**, 379 (1989).

8) T. Yanagimachi, T. Doke, H. Hasebe, T. Imai, T. Kashiwagi, J. Kikuchi, T. Kohno, W. P. Liu, K. Munakata, T. Motobayashi, H. Murakami, K. Nagata, A. Nakamoto, and H. Yamaguchi: "New Two-Dimensional Position Sensitive Silicon Detector with Good Position Linearity and Resolution", *Nucl. Instrum. Methods A*, **275**, 307 (1989).

9) N. Koori, M. Hyakutake, M. Matoba, H. Ijiri, Y. Fujita, Y. Uozumi, S. Shirato, T. Motobayashi, T. Ohsawa, and K. Sagara: "High Resolution Measurement of Protons Emitted From Medium-Energy Neutron Induced Reaction by Means of a Magnetic Spectrograph", *Nucl. Instrum. Methods A*, **278**, 737 (1989).
10) K. Masuda, T. Doke, H. Ichinose, J. Kikuchi, E. Shibamura, and T. Takahashi: "Energy Resolution for Alpha Particles in Liquid Argon Doped with Allen", *Nucl. Instrum. Methods A*, **279**, 560 (1989).
11) T. Motobayashi, M. Louvel, S. M. Lee, and S. Joeng: "Particle Identification of Heavy Ions with Large Silicon Detectors", *Nucl. Instrum. Methods A*, **284**, 526 (1989).
12) S. Kubota, T. Motobayashi, M. Ogiwara, H. Murakami, Y. Ando, J. Ruan (Gen), S. Shirato, and T. Murakami: "Response of BaF_2, BaF_2-Plastic, and BGO Scintillators to Neutrons with Energies between 15 and 45 MeV", *Nucl. Instrum. Methods A*, **285**, 436 (1989).
13) H. Katsuragawa, T. Minowa, and T. Inamura: "High Density Atomic Beam Source by a Laser Ablation Method", *Nucl. Instrum. Methods B*, **43**, 259 (1989).
14) T. Nakagawa and K. Yuasa-Nakagawa: "Timing Properties of Time-of-Flight Detector", *Jpn. J. Appl. Phys.*, **28**, 498 (1989).
15) M. Yasue and Y. Fuchi: "Calibration of the Detection Angle in the Magneticl Spectrometer System", *Jpn. J. Appl. Phys.*, **28**, 943 (1989).
16) M. Yasue, M. Ikeda, M. Sakurai, K. Yoshida, and M. Tsukahara: "CAMAC Data Taking System for Experiments Using Continuous Ion Beams from a Cyclotron", *Jpn. J. Appl. Phys.*, **28**, 945 (1989).
17) K. Niita, T. S. Biro, W. Cassing, A. L. de Paoli, and U. Mosel: "Particle Production within a Selfconsistent Transport Approach to Heavy-Ion Colliaions", (Proc. Int. Workshop on Nuclear Dynamics at Medium and High Energies, Bad Honnef, W-Germany, Oct. 1988), *Nucl. Phys. A*, **495**, 91c (1989).
18) H. Bando, M. Sano, J. Zofka, and M. Wakai: "Production of Hypernuclei in Relativistic Ion Beams", *Nucl. Phys. A*, **501**, 900 (1989).
19) R. Samhammer, H. Hofmann, and S. Yamaji: "Self-Consistent Transport Tensors for Collective Motion in Several Dimensions", *Nucl. Phys. A*, **503**, 404 (1989).
20) K. Niita, W. Cassing, and U. Mosel: "Hard Photon Production within a Self-consistent Transport Approach to Heavy-Ion Collisions", *Nucl. Phys. A*, **504**, 391 (1989).
21) A. Manabe, I. Arai, M. Ninomiya, H. Nunokawa, M. Tanaka, K. Tomizawa, K. Yagi, T. Nagae, H. Sano, S. Sasaki, K. Tokushuku, J. Chiba, and T. Kobayashi: "Polarization and Cross Sections of Λ Hyperons Produced at Backward Angles in the Reaction $\pi+{}^{12}C\rightarrow\Lambda+X$ at 4 GeV/c", *Phys. Rev. Lett.*, **63**, 490 (1989).
22) A. L. De Paoli, K. Niita, W. Cassing, and U. Mosel: "Eta Production in Heavy Ion Collisions", *Phys. Lett. B*, **219**, 194 (1989).
23) M. Sano, M. Wakai, and H. Bando: "Possibility of H-Particle Production in High-Energy Nuclear Collisions", *Phys. Lett. B*, **224**, 359 (1989).
24) H. Okamura, A. Sakaguchi, S. Hatori, H. Sakai, N. Matsuoka, M. Fujiwara, T. Noro, T. Motobayashi, S. Satoh, T. Yamaya, O. Satoh, and S.-I. Hayakawa: "Excitation of Spin- and Isospin-Flip States with the $(d,d_{s=0})$ Reaction", *Phys. Lett. B*, **227**, 204 (1989).
25) K. Hagel, A. Peghaire, G. M. Jin, D. Cussol, H. Doubre, J. Peter, F. Saint-Laurent, G. Bizard, R. Brou, M. Louvel, J. P. Patry, R. Regimbart, J. C. Steckmeyer, B. Tamain, Y. Cassagnou, R. Legrain, C. Lebrun, E. Rosato, R. Macgrath, S. C. Joeng, S. M. Lee, Y. Nagashima, T. Nakagawa, M. Ogihara, J. Kasagi, and T. Motobayashi: "Incomplete Fusion in Nucleus-Nucleus Central Collisions. Study of ^{40}Ar on ^{27}Al from 25 to 85 MeV/u", *Phys. Lett. B*, **229**, 20 (1989).
26) H. Hofmann, R. Samhammer, and S. Yamaji: "Nuclear Collective Motion: Markovian or Not?", *Phys. Lett. B*, **229**, 309 (1989).
27) T. Motobayashi, C. Perrin, J. Carbonell, C. Wilkin, S. Kox, F. Merchez, Nguyen van Sen, D. Rebreyend, G. Guillaume, J.

Arvieux, J. Yonnet, B. Bonin, A. Boudard, M. Garcon, J. Guillot, and G. Gaillard: "Measurements of Tensor Analyzing Powers in the ^{1}H(d, 2p)n Reaction at 200 MeV", *Phys. Lett. B*, **233**, 69 (1989).

28) K. Nagamine: "Muon Catalyzed Fusion: Basic Understandings and Application", Proc. Int. Symp. on Advanced Nuclear Energy Research—Near-Future Chemistry in Nuclear Energy Field—, JEAR-Report, Tokyo, p. 265 (1989).

29) K. Nagamine: "Muon Catalyzed Fusion", *Chemistry*, **44**, 653 (1989) (in Japanese).

30) K. Asahi, M. Ishihara, T. Ichihara, M. Fukuda, T. Kubo, Y. Gono, A. C. Mueller, R. Anne, D. Bazin, D. Guillemaud-Mueller, R. Bimbot, W.-D. Schmidt-Ott, and J. Kasagi: "Spin Alignment in Projectile Fragmentation at Intermediate Energies", Proc. Int. Symp. on Heavy Ion Physics and Astrophysical Problems, Tokyo, July 21-23, 1988 (World Scientific, Singapore), eds. S. Kubono, M. Ishihara, T. Nomura, p. 173 (1989).

3. Atomic and solid-state physics

1) H. Fukuda, T. Ishihara, and S. Hara: "Application of Hyper-spheroidal Coordinates to HD^+", *Phys. Rev. A*, **39**, 35 (1989).

2) K. Hino and T. Watanabe: "Theory of the Relativistic Radiative Electron Capture Incorporating Effects of the Internal Conversion Process", *Phys. Rev. A*, **39**, 3373 (1989).

3) S. Hara and T. Ishihara: "X-ray Spectrum due to the Deexcitation of a Muonic Molecule $p\alpha\mu$", *Phys. Rev. A*, **39**, 5633 (1989).

4) N. Toshima, T. Ishihara, A. Ohsaki, and T. Watanabe: "Impact-parameter Treatment of Classical Trajectory Monte Carlo Calculations for Ion-Atom Collisions", *Phys. Rev. A*, **40**, 2192 (1989).

5) S. Hara and T. Ishihara: "Bound and Resonant States of Muonic Molecules Below the $n=2$ Level of Muonic Atoms", *Phys. Rev. A*, **40**, 4232 (1989).

6) I. Shimamura: "Series of Resonance States of Muonic Molecules", *Phys. Rev. A*, **40**, 4863 (1989).

7) R. Kadono, J. Imazato, T. Matsuzaki, K. Nishiyama, K. Nagamine, T. Yamazaki, D. Richter, and J. M. Welter: "Quantum Diffusion of Positive Muons in Copper", *Phys. Rev. B*, **U39**, 23 (1989).

8) E. Yagi, S. Nakamura, F. Kano, T. Kobayashi, K. Watanabe, Y. Fukai, and T. Matsumoto: "Hydrogen Trapping by Solute Atoms in Nb-3at%Mo Alloys as Observed by the Channeling Method", *Phys. Rev. B.*, **39**, 57 (1989).

9) K. Kobayashi, S. Namba, T. Fujihana, Y. Dai, and M. Iwaki: "Effect of Incident Angles of N Implantation on Recrystallization of AlN_x Films", *Nucl. Instrum. Methods B*, **37/38**, 704 (1989).

10) E. Yagi: "Lattice Location Study on Krypton Atoms in Aluminium by Means of the Channelling Method", *Nucl. Instrum. Methods Phys. Res. B*, **39**, 68 (1989).

11) T. Fujihana, Y. Okabe, and M. Iwaki: "Effects of Implantation Temperature on The Hardness of Iron Nitrides Formed with High Nitrogen Dose", *Nucl. Instrum. Methods B*, **39**, 548 (1989).

12) T. Watanabe and L. Végh: "Scattering Correlation in Multiple Ionization by Electron-, Proton-, Antiproton-, and Multicharged Ion Impact", *Nucl. Instrum. Methods Phys. Res. B*, **40/41**, 89 (1989).

13) T. Watanabe and K. Hino: "Theoretical Study of Radiative Electron Capture in Ion-Atom Collisions", *Nucl. Instrum. Methods Phys. Res. B*, **42**, 494 (1989).

14) H. Katsuragawa, T. Minowa, and T. Inamura: "High Density Atomic Beam Source by a Laser Ablation Method", *Nucl. Instrum. Methods B*, **43**, 259 (1989).

15) K. Ando, S. Kohmoto, Y. Awaya, T. Tanuma, and S. Tsurubuchi: "Analysis of Mg IX 2s3d-2s4f Transition of Beam-Foil Spectra", *Chin. J. Phys.*, **26**, 303 (1988).

16) T. Watanabe, K. Hino, Y. Awaya, T. Kambara, and Y. Kanai: "Studies of Heavy Ion-Atom Collisions at the RIKEN Cyclotron (RRC)", *Chin. J. Phys.*, **27**, 140 (1989).

17) H. Yamaguchi, I. Hashimoto, H. Mitsuya, K. Nakamura, E. Yagi, and M. Iwaki: "The Random Motion of Bubbles in Kr-Implanted Aluminum", *J. Nucl. Mater.*, **161**, 164 (1989).

18) Y. Sakamoto, K. Yano, H. Oyama, H.

Kokai, S. Itoh, and A. Miyahara: "Deterioration of Molybdenum Disulphide (MoS_2) by Hydrogen Plasma Irradiation", *J. Nucl. Mater.*, **162-164**, 932 (1989).

19) E. Yagi, I. Hashimoto, and H. Yamaguchi: "Evolution of Krypton Precipitates in Kr-Implanted Aluminium", *J. Nucl. Mater.*, **169**, 158 (1989).

20) K. Shimizu, K. Yano, H. Oyama, H. Kokai, and Y. Sakamoto: "The High Speed Measurement of Plasma Parameters", Proc. 9th Int. Symp. on Plasma Chemistry, **II**, 831 (1989).

21) K. Yano, H. Oyama, K. Shimizu, M. Yanokura, Y. Abe, H. Kokai, and Y. Sakamoto: "Diagnostics of ECR Plasma for Carbon Film Production", Proc. 9th Int. Symp. on Plasma Chemistry, **III**, 1444 (1989).

22) V. Zoran, A. Enulescu, I. Piticu, R. Nes, G. Wintermeyer, T. Kambara, M. Gabr, and R. Schuch: "Enhanced Inner-Shell Double Ionization of Heavy Elements in Closed, Asymmetric Collisions", Spectroscopy and Collisions of Few-Electron Ions, World Sci. Pub. Co., p. 410 (1989).

23) Y. Awaya, Y. Kanai, T. Kambara, T. Mizogawa, A. Hitachi, and B. Sulik: "The Multiple Inner-Shell Ionization of Target Atoms by 0.8-26 MeV/u Heavy Ion Impact", Spectroscopy and Collisions of Few-Electron Ions, World Sci. Pub. Co., p. 462 (1989).

24) T. Minowa, H. Katsuragawa, and T. Inamura: "Neutral Atomic Beam Generated by a Spark Discharge Method", *Rev. Sci. Instrum.*, **60**, 3280 (1989).

25) H. Maeda, Y. Mizugai, Y. Matsumoto, A. Suzuki, and M. Takami: "Highly Excited Even Rydberg Series of Lu I Studied by Two-step Laser Photoionisation Spectroscopy", *J. Phys. B: At. Mol. Opt. Phys.*, **22**, L511 (1989).

26) K. Hino and T. Watanabe: "Angular Distribution and Linear Polarization of X-Rays Induced by Radiative Electron Capture Processes", Atomic Physics 11, ed. S. Haroche (World Scientific, Singapore), **11**, 653 (1989).

27) T. Kambara, Y. Awaya, Y. Kanai, R. Schuch, K. Shima, and D. Trautmann: "Impact Parameter Dependent Probability of Au L_3-Shell Ionization by 40.7 MeV Ar Ions", *J. Phys. Soc. Jpn.*, **58**, 3929 (1989).

28) K. Ishii, H. Hamanaka, S. Morita, M. Ohura, Y. Yamamoto and Y. Awaya: "High Resolution PIXE with Crystal Spectrometer and Position Sensitive Proportional Counter", *Vacuum*, **39**, 97 (1989).

29) P. H. Mokler, S. Reusch, Th. Stohlker, R. Schuch, M. Schulz, G. Wintermeyer, A. Muller, Y. Awaya, and T. Kambara: "Resonant Transfer and Excitation in Swift, Heavy Few-Electron Projectiles", *Radiat. Eff. Def. Solids*, **110**, 39 (1989).

30) E. Yagi: "Lattice Location Study on Hydrogen in Metals by Means of Channelling Method Using a Nuclear Reaction $^1H(^{11}B, \alpha)\,\alpha\alpha$", Ion Beam Interactions with Solids, Report of the Special Project Research Supported by the Grant-in-Aid for Scientific Research from the Ministry of Science, Education and Culture of Japan 1985-1987, p. 327 (1989).

31) T. Fujihana, Y. Okabe, and M. Iwaki: "The Relationship Between Crystal Structure and Hardness of Nitrogen Implanted Iron Surface Layers", Mater. Res. Soc. Symp. Proc., **128**, 415 (1989).

32) H. Narumi, F. Shimizu, H. Hasegawa, and T. Watanabe: "Report on the 11th Int. Conf. on Atomic Physics", *Butsuri*, (in Japanese), **44**, 343 (1989).

33) H. Tawara and T. Tonuma: "Production of Highly Charged Secondary Ions by Energetic, Heavy Ion Impact: Features and Applications", *Butsuri*, (in Japanese), **44**, 740 (1989).

34) T. Watanabe, A. Ohsaki, K. Nakanishi, and K. Iguchi: "Classical-Trajectory Monte Carlo Calculation for Collision Processes of Coulomb-Interacting Three-Body Systems", *Indian J. Phys.*, **63B(1)**, 114 (1989).

35) H. B. Gilbody, A. Salin, R. Aumayr, A. Bárány, Dz. S. Belkic, F. J. de Heer, R. Hoekstra, R. K. Janev, Y. Nakai, R. D. Rivarola, H. Tawara, and T. Watanabe: "Review of the Data Base for Collisions of C^{q+} Ions with H, H_2 and He", *Phys. Scri.*, **T28**, 8 (1989).

36) I. Shimamura: "Intramolecular Nuclear Fusion in Hydrogen-isotope Molecules", *Prog. Theor. Phys.*, **82**, 304 (1989).

37) I. Shimamura: "Cross Sections for Colli-

sions of Electrons with Atoms and Molecules", *Sci. Papers I. P. C. R.*, **82**, 1 (1989).
38) E. Yagi, T. Kobayashi, K. Watanabe, Y. Fukai, and T. Matsumoto: "Trapping of Hydrogen by Solute Atoms in Nb-Mo Alloys as Observed by the Channelling Method", *Proc. Jpn. Acad.*, **65**, Ser. B, 38 (1989).
39) K. Ando: "Beam-Foil Spectroscopy", *Frontier in Physics*, **25**, Kyouritu Pub., p. 1 (1989) (in Japanese).
40) E. Yagi, S. Nakamura, F. Kano, T. Kobayashi, K. Watanabe, Y. Fukai, and T. Matsumoto: "Hydrogen Trapping by Solute Atoms in Nb-Mo Alloys as Observed by the Channelling Method", *Z. Phys. Chem. N. F.*, **B163**, 201 (1989) (Extended abstract).
41) D. Herlach, V. Claus, K. Fürderer, J. Major, A. Seeger, L. Schimmele, M. Schmolz, W. Staiger, W. Templ, and E. Yagi: "Positive Muons as Light Hydrogen Isotopes: Location and Motion of Positive Muons in α-Iron Studied over Five Temperature Decades", *Z. Phys. Chem. N. F.*, **B164**, 1041 (1989).

4. Radiochemistry, radiation chemistry and radiation biology

1) M. Yanokura, M. Aratani, S. Saito, K. Tanaka, and B. G. Yu: "Heavy Ion Scattering Analysis Applied to the Electronic Materials Part 2", Proc. of the Symp. on Ion Beam Technology, Hosei Univ., p. 123 (1988).
2) K. Tachi, M. Aratani, T. Kato, M. Yanokura, T. Sato, M. Otsuka, and M. Tsujiguchi: "Light Element Depth Profiling by RILAC Applied to the Study on the Composition of Anodic Oxide Films on Titanium", Proc. of the Symp. on Ion Beam Technology, Hosei Univ., p. 151 (1988).
3) Q. Qiu, E. Arai, M. Aratani, M. Yanokura, T. Nozaki, Y. Ohji, and R. Imura: "Application of Deuterium Analysis by Means of the D(^{3}He,p)^{4}He Reaction", Proc. of the Symp. on Ion Beam Technology, Hosei Univ., p. 167 (1988).
4) Y. Kobayashi, M. Katada, H. Sano, T. Okada, K. Asai, N. Sakai, S. Ambe, and F. Ambe: "Mössbauer Spectroscopic Studies of Ruthenium Trichlorides", *Hyperfine Interact.*, **41**, 487 (1988).
5) M. Aratani: "Heavy-Ion Beam Analysis Applied to Surface Characterization for Material Study", *Radioisotopes*, **37**, 43 (1988).
6) M. Aratani, M. Yanokura, B. G. Yu, Q. Qiu, and T. Nozaki: "Hydrogen and Alkali Depth Profiling of the Soda-Lime-Silica Glass Surface by 50 MeV Ar Probe Rutherford 2π Scattering", Proc. of Sino-Japanese Symp. on Desert, **1**, 85 (1988).
7) M. Suehiro, F. Yokoi, T. Nozaki, and M. Iwamoto: "No-carrier-added Radiobromination Via the Gattermann Reaction", *J. Labelled Compd. & Radiopharm.*, **24**, 1143 (1988).
8) T. Nozaki, Y. Itoh, and Q. Qiu: "Dissolution of Hydrogen and Nitrogen in Silicon", *J. Radioanal. Chem.*, **124**, 341 (1988).
9) I. Kaneko, K. Eguchi-Kasai, T. Kosaka, K. Nakano, A. Maruhashi, and T. Takahashi: "DNA-Lesion and Cell Deart by α-Particles and Nitrogen Ions", *Adv. Space Res.*, **9**, 73 (1989).
10) I. Sugai, *et al.*: "Hybrid-Type Long-Lived Carbon Stripper Foils", *Nucl. Instrum. Methods Phys. Res. A*, **282**, 164 (1989).
11) M. Yanokura, M. Minami, S. Yamagata, S. Nakabayashi, M. Aratani, A. Kira and I. Tanihata: "An Approach to the Cold Fusion Through Hydrogen Isotopes Analysis by the Heavy Ion Rutherford Scattering", *Chem. Lett., CMLTAG* (12), p. 2197 (1989).
12) S. Ambe: "Adsorption of No-Carrier-Added ^{119}Sb(V) Ions onto Metal Oxide and Hydroxide Surfaces from Aqueous Solutions", *Radiochim. Acta*, **46**, 145 (1989).
13) S. Ambe, T. Okada, and F. Ambe: "Mössbauer and Tracer Studies of Metal Oxide/Aqueous Solution Interface", Proc. Int. Symp. Advanced Nuclear Energy Research—Near-Future Chemistry in Nuclear Energy Field—, p. 407 (1989).
14) T. Takahashi, T. Kosaka, K. Kasai, K. Nakano, F. Yatagai, and I. Kaneko: "Recent Topics on the Effect of High LET Radiation on Microorganisms and Cultured Mammalian Cells", *Radiation*, **16**, 146 (1989) (in Japanese).
15) Y. Kobayashi, M. Katada, H. Sano, T. Okada, K. Asai, and F. Ambe: "^{99}Ru and ^{57}Fe Mössbauer Spectroscopy of a

Ruthenium Alloy, $RuFe_2Si$", *J. Radioanal. Nucl. Chem. Lett.*, **136**, 387 (1989).
16) Y. Itoh, Y. Kadota, T. Nozaki, H. Fukushima, and K. Takeda: "CPAA Study on Carbon, Boron and Oxygen in LEC-GaAs", *Jpn. J. Appl. Phys.*, **28**, 210 (1989).
17) Y. Itoh, Y. Sugita and T. Nozaki: "Effect of Carbon and Oxygen Precipitation on Gold Diffusion in Silicon", *Jpn. J. Appl. Phys.*, **28**, 290 (1989).
18) K. Kimura: "Effects of High Density Excitation by Heavy Ion Irradiation", *Ion. Radiat.*, **16**, 131 (1989).
19) K. Kimura, T. Matsuyama, and H. Kumagai: "High-density Excitation by Heavy Ions: Techniques of Fast Measurements of Emission Decay of BaF_2 Single Crystal", *Radiat. Phys. Chem.*, **34**, 575 (1989).
20) K. Nakagawa, A. Ejiri, M. Nishikawa, and K. Kimura: "Density Effect on Structures in Photoconductivity Excitation Spectra of Supercritical Xenon Doped with Anthracene Molecules", *Chem. Phys. Lett.*, **155**, 278 (1989).

(Papers Presented at Meetings)

1. Accelerator development and accelerator physics

1) S. H. Be, S. Yokouchi, Y. Morimoto, H. Sakamoto, Y. P. Lee, and Y. Oikawa: "Vacuum System for the 8 GeV Storage Ring", 1989 IEEE Particle Accelerator Conf., Chicago, U.S.A., Mar. (1989).
2) A. Goto, S. Kohara, M. Nagase, T. Kageyama, K. Hatanaka, M. Kase, Y. Yano, M. Saito, H. Takebe, K. Ikegami, N. Nakanishi, Y. Kumata, and T. Tachikawa: "Injector AVF Cyclotron at RIKEN", 12th Int. Conf. on Cyclotrons and Their Applications, Berlin, May (1989).
3) Y. Yano: "Status Report on RIKEN Ring Cyclotron", 12th Int. Conf. on Cyclotrons and Their Applications, Berlin, May (1989).
4) T. Watanabe, H. Iwasaki, M. Matsuoka, and H. Yokomizo: "A New X-Ray SR (SP Ring) Project at Harima (Japan)", Workshop on High Heat Load X-Ray Optics, Argonne, USA, Aug. (1989).
5) S. H. Be, S. Yokouchi, Y. Morimoto, H. Sakamoto, T. Nishidono, Y. P. Lee, and Y. Oikawa: "Conceptual Design of Vacuum System for 8 GeV Storage Ring", 30th Annu. Meeting Jpn. Vac. Soc., Tokyo, Oct. (1989).
6) Y. Morimoto, S. Yokouchi, H. Sakamoto, T. Nishidono, Y. P. Lee, and S. H. Be: "Manufacture of Crotch for 8 GeV Storage Ring", 30th Annu. Meeting Jpn. Vac. Soc., Tokyo, Oct. (1989).
7) T. Nishidono, S. Yokouchi, Y. Morimoto, Y. P. Lee, and S. H. Be: "Test of Aluminum Alloy Flange", 30th Annu. Meeting Jpn. Vac. Soc., Tokyo, Oct. (1989).
8) S. Yokouchi, H. Sakamoto, T. Nishidono, Y. Morimoto, Y. P. Lee, Y. Hirano, and S. H. Be: "Manufacture of Vacuum Chamber for 8 GeV Storage Ring", 30th Annu. Meeting Jpn. Vac. Soc., Tokyo, Oct. (1989).
9) Y. P. Lee, S. Yokouchi, T. Nishidono, H. Morimoto, N. Hinako, H. Sakamoto, and S. H. Be: "The Performance Characteristics of a St 707 Non-Evaporable Getter Strip for 8 GeV Storage Ring", 30th Annu. Meeting Jpn. Vac. Soc., Tokyo, Oct. (1989).
10) H. Miyade, H. Tanaka, J. Ohnishi, and S. Motonaga: "Study of Injection Magnets of 8 GeV Light Source Storage Ring", 1989 Fall Meeting Phys. Soc. Jpn., Miyazaki, Oct. (1989).
11) A. Goto, K. Hatanaka, M. Kase, Y. Yano, T. Kageyama, S. Kohara, M. Nagase, H. Takebe, K. Ikegami, M. Saito, N. Nakanishi, Y. Kumata, and T. Tachikawa: "Status of Injector AVF Cyclotron at RIKEN", 1989 Fall Meeting Phys. Soc. Jpn., Miyazaki, Oct. (1989).
12) H. Miyade, H. Tanaka, J. Ohnishi, and S. Motonaga: "Study of the Injection Devices for SPring-8", 7th Symp. on Accelerator Science and Technology, Osaka, Dec. (1989).
13) S. H. Be, S. Yokouchi, Y. Morimoto, T. Nishidono, Y. P. Lee, and Y. Oikawa: "SPring-8 Vacuum System", 7th Symp. on Accelerator Science and Technology, Osaka, Dec. (1989).
14) S. Yokouchi, Y. P. Lee, T. Nishidono, Y. Morimoto, and S. H. Be: "Construction and Surface Analysis of the Al-alloy Vacuum Chamber for SPring-8", 7th

Symp. on Accelerator Science and Technology, Osaka, Dec. (1989).

2. Nuclear physics and nuclear instrumentation

1) T. S. Biro, W. Cassing, U. Mosel, K. Niita, and G. Wolf: "Non-Equilibrium γ-Production in Heavy-Ion Collisions", Int. Workshop on Gross Properties of Nuclei and Nuclear Excitations XVII, Hirschegg, Austria, Jan. (1989).
2) K. Niita, T. S. Biro, W. Cassing, A. L. De Paoli, U. Mosel, and M. Schäfer: "Particle Production in Heavy-Ion Collisions from 20 MeV/u to 2 GeV/u", 26th Int. Winter Meet. on Nuclear Physics, Bormio, Itary, Jan. (1989).
3) T. Inamura: "Storage Ring and Laser Nuclear Spectroscopy", Symp. on Study of Nuclei Far from Stability, Tanashi, Jan. (1989).
4) K. Asahi: "Towards Spectroscopic Studies of Exotic Nuclei Using Intermediate Energy Heavy Ion Beams", RIKEN Symp. on Scientific Results at RIKEN Ring Cyclrotron, Wako, Mar. (1989).
5) K. Asahi: "Reaction Products in Heavy Ion Reactions at Intermediate Energies and Their Application to Condensed Matter Physics", RIKEN Symp. on Chemical Applications of Nuclear Methods, Wako, Mar. (1989).
6) T. Inamura: "Storage Ring and Laser Nuclear Spectroscopy", Warkshop on TARN II, Tanashi, Mar. (1989).
7) A. Hitachi, E. Otobe, H. Ichinose, T. Sano, T. Doke, K. Masuda, and T. Takahashi: "Photoionization Efficiency of Organic Molecules in Liquid Argon", 44th Annu. Meeting Phys. Soc. Jpn., Hiratsuka, Mar. (1989).
8) K. Ishida, T. Matsuzaki, K. Nagamine, H. Kitazawa, and E. Torikai: "Test Experiment of a Large Solid Angle Secondary Beam Cource Using Axially Symmetric Magnetic Field", 44th Annu. Meeting Phys. Soc. Jpn., Hiratsuka, Mar. (1989).
9) K. Nagamine, T. Matsuzaki, K. Ishida, Y. Watanabe, Y. Miyake, K. Nishiyama, M. Iwasaki, S. Sakamoto, H. Kurihara, E. Torikai, H. Umezawa, H. Kudo, M. Tanase, K. Kurosawa, M. Kato, M. Sugai, and M. Fujie: "X-ray Measurement of the α-sticking Probability in Muon Catalyzed Nuclear Fusion for D-T Mixture I, II", 44th Annu. Meeting Phys. Soc. Jpn., Hiratsuka, Mar. (1989).
10) K. Soutome, T. Maruyama, and K. Saito: "Relativistic Hartree-Fock Calculation of Finite-Temperature Nuclear Matter", 44th Annu. Meeting Phys. Soc. Jpn., Hiratsuka, Mar. (1989).
11) M. Fukuda, M. Adachi, M. Koguchi, N. Inabe, M. Ishihara, K. Asahi, T. Ichihara, T. Kubo, H. Kumagai, I. Tanihata, and T. Nakagawa: "Measurement of Interaction Gross Section at Intermediate Energies", 44th Annu. Meeting Phys. Soc. Jpn., Hiratsuka, Mar. (1989).
12) M. Koguchi, K. Asahi, M. Fukuda, M. Adachi, A. Tamura, H. Takanashi, T. Suzuki, T. Ichihara, and M. Ishihara: "Development of a Rotating Catcher System for Beta Decay Studies in the Region Far from Stability", 44th Annu. Meeting Phys. Soc. Jpn., Hiratsuka, Mar. (1989).
13) M. Koizumi, T. Inamura, M. Takami, K. Matsumoto, T. Murayama, and I. Sugai: "Nuclear Spectroscopy by a Resonance Ionization Method", 44th Annu. Meeting Phys. Soc. Jpn., Hiratsuka, Mar. (1989).
14) S. Yamaji and H. Hormann: "Self-Consistent Transport Theory for Collective Motion", 44th Annu. Meeting Phys. Soc. Jpn., Hiratsuka, Mar. (1989).
15) M. Sano: "Strangeness Production in High-Energy Nuclear Collisions", The NATO Advanced Studies Institute on 'Nuclear Equation of State', Peniscola, Spain, May (1989).
16) K. Asahi, M. Ishihara, H. Takanashi, M. Koguchi, M. Adachi, M. Fukuda, N. Inabe, D. Mikolas, D. Morrissey, D. Beaumel, T. Ichihara, T. Kubo, T. Shimoda, H. Miyatake, and N. Takahashi: "Production of Spin-Polarized Radioactive Beams Using Projectile Fragmentation at Intermediate Energies", 23th Yamada Conf. on Nuclear Weak Process and Nuclear Structure, Osaka, June (1989).
17) K. Asahi, M. Ishihara, H. Takanashi, M. Koguchi, M. Adachi, M. Fukuda, N. Inabe, D. Mikolas, D. Morrissey, D. Beaumel, T. Ichihara, T. Kubo, T. Shimoda, H. Miyatake, and N. Takahashi: "First Observation of Spin Polar-

ization in Projectile Fragments from Intermediate Energy Heavy Ion Collision", 1989 Int. Nuclear Physics Conf., Sao Paulo, Aug. (1989).
18) K. Nagamine: "Proposal for Slow μ^- Production via Muon Catalyzed Fusion", Int. Workshop on μCF, Oxford, Sep. (1989).
19) K. Nagamine: "X-ray Observation of α-Sticking Phenomena in Muon Catalyzed Fusion for Liquid and High T_2 Concentration D_2/T_2 Mixture", Int. Workshop on μCF, Oxford, Sep. (1989).
20) M. Fukuda, K. Asahi, T. Ichihara, N. Inabe, M. Ishihara, T. Kubo, H. Kumagai, T. Nakagawa, I. Tanihata, M. Adachi, M. Koguchi, H. Sagawa, and S. Shimoura: "Measurement of Reaction Cross Sections Using ^{11}Be Beam", 1st Int. Conf. on Radioactive Nuclear Beams, Berkeley, Oct. (1989).
21) K. Asahi, M. Ishihara, H. Takanashi, M. Koguchi, M. Adachi, M. Fukuda, N. Inabe, D. Mikolas, D. Morrissey, D. Beaumel, T. Ichihara, T. Kubo, T. Shimoda, H. Miyatake, and N. Takahashi: "Spin-Polarized Radioactive Beams from Intermediate Energy Heavy Ion Collision", 1st Int. Conf. on Radioactive Nuclear Beams, Berkeley, Oct. (1989).
22) H. Ichinose, T. Doke, J. Kikuchi, A. Hitachi, K. Masuda, E. Shibamura, and T. Takahashi: "Energy Resolution of Liquid-Xenon Photoionization Detector", 1989 Fall Meet. Phys. Soc. Jpn., Miyazaki, Oct. (1989).
23) K. Nagamine: "Muon Catalyzed Fusion", 1989 Fall Meet. Phys. Soc. Jpn., Miyazaki, Oct. (1989).
24) T. Nakagawa, K. Yuasa-Nakagawa, and W. Bohne: "Timing Properties of Surface Barrier Detector and Channel Plate Detector with Central Hole", 1989 Fall Meet. Phys. Soc. Jpn., Miyazaki, Oct. (1989).
25) K. Soutome, S. Yamaji, M. Wakai, and M. Sano: "Coulomb Dissociation of ^{11}Li", 1989 Fall Meet. Phys. Soc. Jpn., Miyazaki, Oct. (1989).
26) T. Takei, K. Ieki, N. Iwasa, and K. Yoshida: "Angular Momentum Transfer in Incomplete-Fusion Reaction", 1989 Fall Meet. Phys. Soc. Jpn., Miyazaki, Oct. (1989).
27) H. Okuno, K. Asahi, and M. Ishihara: "Momentum Distribution of Projectile Fragments at Intermediate Energies", 1989 Fall Meet. Phys. Soc. Jpn., Miyazaki, Oct. (1989).
28) K. Asahi, M. Ishihara, H. Takanashi, M. Koguchi, M. Adachi, M. Fukuda, N. Inabe, D. Mikolas, D. Morrissey, D. Beaumel, T. Ichihara, T. Kubo, T. Shimoda, H. Miyatake, and N. Takahashi: "Spin-Polarized Secondary Beams from Projectile Fragmentation at Intermediate Energies", 1989 Fall Meet. Phys. Soc. Jpn., Miyazaki, Oct. (1989).
29) K. Morita, T. Nomura, J. Tanaka, N. Ikeda, Y. Hatsukawa, Y. Nagai, A. Yoshida, K. Kunihiro, K. Omata, T. Toriyama, M. Fujioka, T. Shinozuka, H. Kudo, T. Inamura, M. Koizumi, and K. Yoshimura: "On-line Test of RIKEN ISOL II", 1989 Fall Meet. Phys. Soc. Jpn., Miyazaki, Oct. (1989).
30) K. Yoshida, J. Kasagi, H. Hama, M. Sakurai, M. Kodama, K. Furutaka, T. Kubo, M. Ishihara, K. Ieki, W. Galster, and A. Galonsky: "High Energy γ rays Observed in Ti, ^{92}Mo, ^{122}Sn+^{40}Ar Reactions at 26 MeV/nucleon", 1989 Fall Meet. Phys. Soc. Jpn., Miyazaki, Oct. (1989).
31) K. Yoshida, J. Kasagi, H. Hama, M. Kodama, K. Furutaka, M. Sakurai, T. Kubo, M. Ishihara, K. Ieki, W. Galster, and A. Galonsky: "Neutron Emissions from Ti, ^{92}Mo, ^{122}Sn+^{40}Ar Reactions at 26 MeV/nucleon", 1989 Fall Meet. Phys. Soc. Jpn., Miyazaki, Oct. (1989).
32) K. Yoshida, J. Kasagi, H. Hama, M. Sakurai, M. Kodama, K. Furutaka, T. Kubo, M. Ishihara, K. Ieki, and W. Galster, and A. Galonsky: "$2\pi BaF_2$ Detector", 1989 Annu. Meeting Phys. Soc. Jpn., Miyazaki, Oct. (1989).

3. Atomic and solid-state physics

1) H. Katsuragawa, T. Minowa, M. Otsuki, and T. Inamura: "Laser Resonance Ionization Spectroscopy—On Laser Ablation Method—", RIKEN Symp. on Laser Nuclear Spectroscopy, Wako, Dec. (1988).
2) T. Fujimoto and I. Shimamura: "State Densities and Ionization Equilibrium of Atoms in a Dense Plasma", Symposium on the Studies of Elementary Processes in X-Ray Lasers, Arima, Jan. (1989).
3) Y. Aikawa, K. Ando, S. Kohmoto, Y. Awaya, T. Tonuma, S. Tsurubuchi, S.

Hashimoto: "Analysis of Mg IX 2s3d-2s4f Transition of Beam-Foil Spectra", 1989 Spring Meeting Phys. Soc. Jpn., Hiratsuka, Mar. (1989).
4) K. Kobayashi, S. Namba, T. Fujihana, K. Yabe, and M. Iwaki: "Relation between Composition of AlN_x Film and Recrystallization of AlN by N-Implantation", 20th Symposium on Ion Implantation and Submicron Fablication, Tokyo, Mar. (1989).
5) T. Kambara: "Atomic Physics Research with an Ion Cooler Ring", Workshop on TARN2, Tanashi, Mar. (1989).
6) H. Sakaue, Y. Kanai, K. Ohta, T. Inaba, S. Ohtani, H. Suzuki, K. Wakiya, T. Takayanagi, T. Kambara, and Y. Awaya: "Electron Spectroscopic Studies by Using RIKEN ECRIS", Workshop on Highly Charged Ions: New Physics and Advanced Techniques, Berkeley, Mar. (1989).
7) Y. Awaya, T. Kambara, and Y. Kanai: "Facilities and Experimental Studies of Atomic Physics at RIKEN Ring Cyclotron", Workshop on Highly Charged Ions: New Physics and Advanced Techniques, Berkeley, Mar. (1989).
8) I. Shimamura: "Introduction: Symposium on Two-Electron Excited States", 44th Annu. Meet. Phys. Soc. Jpn., Hiratsuka, Mar. (1989).
9) M. Otsuki, T. Hosino, T. Minowa, H. Nakahama, H. Katsuragawa, and T. Inamura: "Resonance Ionization Sectroscopy of Neutral Atoms Generated by a Spark Discharge Method", 44th Annu. Meet. Phys. Soc. Jpn., Hiratsuka, Mar. (1989).
10) T. Suzuki, T. Minowa, H. Horibe and H. Katsuragawa: "Detection of Laser Cooling Effect by Resonance Ionization Spectroscopy", 44th Annu. Meet. Phys. Soc. Jpn., Hiratsuka, Mar. (1989).
11) E. Yagi: "Behavior of Kr Atoms in Aluminium", 44th Annu. Meet. Phys. Soc. Jpn., Hiratsuka, Mar. (1989).
12) Y. Kanai, T. Kambara, Y. Awaya, N. Stolterfoht, and B. Sulik: "N KLL Auger Electrons Emitted from N^{2+}-He Collisions", 44th Annu. Meet. Phys. Soc. Jpn., Hiratsuka, Mar. (1989).
13) K. Kawatsura, M. Sataka, H. Naramoto, Y. Nakai, T. Yamazaki, K. Komaki, K. Kuroki, Y. Kanai, T. Kambara, Y. Awaya, and N. Stolterfoht: "Zero-Degree Auger Electron Spectroscopy by High Energy Heavy-Ion Impact (I)", 44th Annu. Meet. Phys. Soc. Jpn., Hiratsuka, Mar. (1989).
14) Y. Hibino, T. Mukohyama, H. Adachi, Y. Sasa, M. Tachibana, K. Fuwa, and M. Uda: "Calculation of the Emission Probability of F $K\alpha$ Satellites", 44th Annu. Meet. Phys. Soc. Jpn., Hiratsuka, Mar. (1989).
15) P. H. Mokler, S. Reusch, Th. Stohlker, R. Schuch, M. Schulz, G. Wintermeyer, Z. Stachura, A. Warczak, A. Muller, Y. Awaya, and T. Kambara: "Resonant Transfer and Excitation in Swift, Heavy Few-Electron Projectiles", 1st Int. Symp. on Swift Heavy Ions in Matter, Caen (France), May (1989).
16) Y. Awaya: "Reports on Activities of the User's Sub-Group of "Atoms and Molecules", 1989 1st Meeting of the Soc. for Next Generation X-Ray Synchrotron Radiation, Kobe, May (1989).
17) K. Aono, M. Iwaki, and S. Namba: "Luminescence During Eu, Fe and Cr Implantation into CaF_2", 5th Int. Conf. on Radiation Effects in Insulators, (Abstracts, p. D4), Hamilton, Canada, Jun. (1989).
18) K. Aono, M. Iwaki, and S. Namba: "Radiation Damage in Eu Implanted CaF_2 Observed by the Channeling Method", 9th Int. Conf. on Ion Beam Analysis, (Abstracts, p. 13), Kingston, Canada, Jun. (1989).
19) K. Tanaka, N. Masahashi, K. Tatsumi, Y. Mizuhara, T. Takahari, and E. Yagi: "Lattice Location of B Atoms in $Ni_{0.75}Al_{0.15}Ti_{0.1}$ Intermetallic Compounds as Observed by the Channelling Method", 9th Ion Beam Analysis Conf., Kingston, Canada, Jun. (1989).
20) T. Fujihana, Y. Okabe, K. Takahashi, and M. Iwaki: "RBS, AES and XRD Investigations of Nitrogen Implanted Ti, Cr, Fe, Zr and Nb Sheets", 9th Ion Beam Analysis Conf., Kingston, Canada, Jun. (1989).
21) H. Sakaue, K. Ohta, N. Inaba, Y. Kanai, S. Ohtani, K. Wakiya, S. Suzuki, N. Takayanagi, A. Danjo, M. Yoshino, T. Kambara, and Y. Awaya: "Ejected Electron Spectra from Doubly-Excited Helium-Like Carbon Ion ($2ln l'$)", 16th Int. Conf. on the Physics of Electronic and Atomic Collisions, New York, Jul.

(1989).
22) H. Tawara, T. Tonuma, H. Kumagai, and T. Matsuo: "Production of Highly Charged Recoil Ions under Electron Stripping and Capture Processes of Ne^{q+} Projectiles in Collisions with Ne Atoms", 16th Int. Conf. on the Physics of Electronic and Atomic Collisions, New York, Jul. (1989).
23) K. Hino and T. Watanabe: "Cross Section for Radiative Electron Capture Calculated by a Relativistic Impulse Approximation; Total and Differential Cross Section and Linear Polarization", 16th Int. Conf. on the Physics of Electronic and Atomic Collisions, New York, Jul. (1989).
24) K. Hino and T. Watanabe: "Cross Section for Radiative Electron Capture Calculated by a Relativistic Impulse Approximation; Formulation", 16th Int. Conf. on the Physics of Electronic and Atomic Collisions, New York, Jul. (1989).
25) S. Reusch, P. H. Mokler, A. Warczek, Z. Stachura, T. Kambara, R. Schuch, M. Schultz, G. Wintermeyer, and A. Müller: "The Two-Photon Decay of the $^1S_0$ State in $_{32}Ge^{30+}$ Produced by Resonant Transfer and Excitation", 16th Int. Conf. on the Physics of Electronic and Atomic Collisions, New York, Jul. (1989).
26) S. Reusch, P. H. Mokler, A. Warczek, Z. Stachura, T. Kambara, R. Schuch, M. Schultz, G. Wintermeyer, and A. Müller: "Resonant Transfer and Excitation in Hydrogenic Ge-Projectiles", 16th Int. Conf. on the Physics of Electronic and Atomic Collisions, New York, Jul. (1989).
27) T. Kambara, Y. Kanai, Y. Awaya, H. Vogt, and H. Schmidt-Böcking: "Impact Parameter Dependence of K X-Ray Asymmetry in 10 and 30 MeV Ne-Ne Collisions", 16th Int. Conf. on the Physics of Electronic and Atomic Collisions, New York, Jul. (1989).
28) Y. Awaya, A. Hitachi, T. Kambara, Y. Kanai, K. Kuroki, and T. Mozigawa: "Radiative Electron Capture Cross Section for 26 MeV/u Ar^{18+} Ions on Carbon Target", 16th Int. Conf. on the Physics of Electronic and Atomic Collisions, New York, Jul. (1989).
29) Y. Kanai, T. Kambara, Y. Awaya, B. Sulik, and N. Stolterfoht: "High Resolution K-LL Auger Spectra of Nitrogen Projectiles", 16th Int. Conf. on the Physics of Electronic and Atomic Collisions, New York, Jul. (1989).
30) H. Fukuda and T. Ishihara: "Quantum Mechanical Calculation of Slow He^{++} + H Collisions", 16th Int. Conf. on the Physics of Electronic and Atomic Collisions, New York, Jul. (1989).
31) I. Shimamura: "Intramolecular Room-Temperature Nuclear Fusion in Hydrogen-Isotope Molecules", 14th Meet. of the Soc. for Atomic Collision Research, Jpn., Sagamihara, Aug. (1989).
32) I. Shimamura: "Series of Resonance Levels of Muonic Molecules", 14th Meet. of the Soc. for Atomic Collision Research, Jpn., Sagamihara, Aug. (1989).
33) K. Kanai, T. Kambara, Y. Awaya, H. Sakaue, K. Ohta, K. Wakiya, H. Suzuki, T. Takayanagi, N. Inaba, S. Ohtani, A. Danjo, and M. Yoshino: "Two-Electron Transfer Process in C^{6+}, B^{5+}-He System", 14th Meet. of the Soc. for Atomic Collision Research, Sagamihara, Aug. (1989).
34) Y. Awaya: "A Plan of 8-GeV Synchrotron Radiation Facilities by the Science and Technology Agency", 14th Meet. of the Soc. for Atomic Collision Research, Sagamihara, Aug. (1989).
35) A. Koyama: "Incident Angle-Dependence of Peak Energy of Al-LVV Auger Electrons for Ar^{12+} Impact", 13th Int. Conf. on Atomic Collisions in Solids, Aarhus Aug. (1989).
36) K. Kawatsura, M. Sataka, Y. Yamazaki, K. Komaki, Y. Kanai, H. Naramoto, K. Kuroki, T. Kambara, Y. Awaya, Y. Nakai, and N. Stolterfoht: "Angular Momentum Distribution of Autoionizing Rydberg States Produced by 64-MeV S Ions in Collision with He and C-Foils", 13th Int. Conf. on Atomic Collisions in Solids, Aarhus, Aug. (1989).
37) E. Yagi: "Materials Science Researches by Using Ion Beams in the Institute of Physical and Chemical Research (RIKEN Institute)", Symp. Application of Ion Beams to Materials Research, Tokyo, Aug. (1989).
38) Y. Awaya, T. Kambara, Y. Kanai, T.

Mizogawa, M. Terasawa, H. Schmidt-Böcking, H. Vogt, and R. Doner: "Impact Parameter Dependence of K X-Ray Asymmetry in 10 and 26 MeV Ne-Ne Collisions", 11th Int. Seminar of Ion-Atom Collisions, Manhattan (Kansas State), Aug. (1989).

39) Y. Sasa, K. Maeda, and M. Uda: "Application of PIXE Analysis to Materials Science", 5th Int. Conf. on Particle Induced X-Ray Emission and Its Analytical Applications, Amsterdam, Aug. (1989).

40) H. Takahashi, H. Kawahara, K. Kuriyama, N. Hayashi, I. Sakamoto, and I. Kohno: "Photoquenching Phenomena of Photoconductance in Proton Irradiated Semi-Insulating GaAs", Fall Meet. Jpn. Soc. Appl. Phys., Fukuoka, Sep. (1989).

41) I. Shimamura: "Series of Resonances in Muonic Molecules dtμ and ddμ", Int. Symp. on Muon-Catalyzed Fusion, Oxford, Sep. (1989).

42) Y. Awaya: "R & D Plans of the User's Sub-Group of Atoms and Molecules", Symp. on How to Use 8-GeV Synchrotron Radiation Facilities, Tokyo, Sep. (1989).

43) K. Shimizu, K. Yano, H. Oyama, H. Kokai, and Y. Sakamoto: "The High Speed Measurement of Plasma Parameters", 9th Int. Symp. on Plasma Chemistry, Pugnochiuso, Sep. (1989).

44) K. Yano, H. Oyama, K. Shimizu, M. Yanokura, Y. Abe, H. Kokai, and Y. Sakamoto: "Diagnostics of ECR Plasma for Carbon Film Production", 9th Int. Symp. on Plasma Chemistry, Pugnochiuso, Sep. (1989).

45) I. Shimamura and T. Fujimoto: "State Densities and Ionization Equilibrium of Atoms in Dense Plasmas", 7th Topical Conf. on Atomic Processes in Plasmas, American Physical Society, Gaithersburg, Oct. (1989).

46) E. Yagi: "Lattice Location Study on Hydrogen in Metals by Means of the Channelling Method", 1989 Fall Meet. Phys. Soc. Jpn., Kagoshima, Oct. (1989).

47) K. Ishii, Y. Sasa, K. Maeda, M. Uda, S. Morita, and M. Takami: "Study on the Production of Continum X Ray by Heavy Ion Impacts", 1989 Fall Meet. Phys. Soc. Jpn., Kagoshima, Oct. (1989).

48) K. Kawatsura, Y. Yamazaki, M. Sataka, Y. Kanai, K. Komaki, H. Naramoto, K. Kuroki, T. Kambara, Y. Awaya, Y. Nakai, and N. Stolterfoht: "Zero-Degree Auger Electron Spectroscopy by High Energy Heavy-Ion Impact (II)", 1989 Fall Meet. Phys. Soc. Jpn., Kagoshima, Oct. (1989).

49) H. Sakaue, K. Ohta, M. Hisajima, N. Inaba, Y. Kanai, S. Ohtani, K. Wakiya, T. Takayanagi, H. Suzuki, A. Danjo, M. Yoshino, T. Kambara, and Y. Awaya: "Emitted Electrons from 21nl′ Excited States Caused by Two-Electron Capture in $^{13}C^{6+}$, $^{11}B^{5+}$+He Collisions", 1989 Fall Meet. Phys. Soc. Jpn., Kagoshima, Oct. (1989).

50) M. Mogi, T. Mukohyama, H. Adachi, Y. Sasa, M. Tachibana, Y. Hibino, K. Fuwa, and M. Uda: "Production Mechanism of Chemical Effects on Satellite Spectra of F Kα", 1989 Fall Meet. Phys. Soc. Jpn., Kagoshima, Oct. (1989).

51) T. Minowa, M. Kubota, E. Endo, M. Otsuki, and H. Katsuragawa: "Resonance Ionization Spectroscopy Organic Molecules", Fall Meet. Phys. Soc. Jpn., Kagoshima, Oct. (1989).

52) T. Kambara, Y. Kanai, Y. Awaya, T. Mizogawa, M. Terasawa, H. Schmidt-Böcking, H. Vogt, and R. Doner: "Impact Parameter and Azimuthal Angle Dependent X K Ray Emission Probability in 10-30 MeV Ne-Ne Collisions", 1989 Fall Meet. Phys. Soc. Jpn., Kagoshima, Oct. (1989).

53) Y. Awaya, M. Kimura: "Reports on the Workshop on Atomic Physics and Related Studies by Using 8-GeV Synchrotron Radiation Facilities", 1989 Fall Meet. Phys. Soc. Jpn., Kagoshima, Oct. (1989)

54) T. Okada, N. Sakai, K. Asai, Y. Sasa and T. Yamadaya: "Orientation of $YBa_2Cu_3(Fe)O_{7-y}$", 1989 Fall Meet. Phys. Soc. Jpn., Kagoshima, Oct. (1989).

55) T. Okada, N. Sakai, K. Asai, and T. Yamadaya: "Mössbauer Study of $Bi_2Sr_4Fe_3O_{12}$", 1989 Fall Meet. Phys. Soc. Jpn., Kagoshima, Oct. (1989).

56) I. Shimamura: "Series of Resonances in Muonic Molecules", RIKEN Symp. on the Basis and Applications of the Muon-Catalyzed Fusion Phenomena, Wako, Nov. (1989).

57) I. Shimamura: "The Use of Supercomputers for Atomic Physics Researches at Daresbury Laboratory",

RIKEN Symp. on Large-Scale Computations in Science and Technology, Wako, Dec. (1989).

4. Radiochemistry, radiation chemistry and radiation biology

1) M. Aratani: "Hydrogen Depth Profiling of the Hydro-thermally Treated Surfaces", RIKEN Symp. on Fundamental Studies Using a Few MeV/nucleon Heavy-Ions and Applications to the High Technology Material Characterization, Wako, Mar. (1988).

2) M. Aratani, M. Yanokura, I. Sugai, S. Osada, and H. Kato: "Simultaneous Multinuclide Depth Profiling by Means of Argon Probe Rutherford Scattering", 32th Symp. on Radiochemistry, Tokai, Oct. (1988).

3) M. Aratani, M. Yanokura, B. G. Yu, Q. Qiu, and T. Nozaki: "50 MeV Ar Probe Rutherford 2π Scattering Applied to the Simultaneous Multinuclide Depth Profiling for Material Characterization", 10th Conference on the Application of Accelerators in Research and Industry, Denton, Texas, Oct. (1988).

4) M. Aratani, M. Yanokura, B. G. Yu, Q. Qiu, and T. Nozaki: "Hydrogen and Alkali Depth Profiling of the Soda-Lime-Silica Glass Surface by 50 MeV Ar Probe Rutherford 2π Scattering", Sino-Jpn. Symposium on Desert, Urumqi, China, Nov. (1988).

5) Q. Qiu, E. Arai, M. Aratani, M. Yanokura, T. Nozaki, Y. Ohji, and R. Imura: "Application of Deuterium Analysis by Means of the $D(^3He,p)^4He$ Reaction", Symp. on Ion Beam Technology, Hosei Univ., Koganei, Dec. (1988).

6) M. Yanokura, M. Aratani, S. Saito, K. Tanaka, and B. G. Yu: "Heavy Ion Scattering Analysis Applied to the Electronic Materials Part 2", The Symp. on the Ion Beam Technology, Hosei Univ., Koganei, Dec. (1988).

7) S. Ambe, T. Okada, and F. Ambe: "Mössbauer and Tracer Studies of Metal Oxide/Aqueous Solution Interface", Int. Symp. Advanced Nuclear Energy Research—Near-Future Chemistry in Nuclear Energy Field—, Oarai, Feb. (1989).

8) M. Aratani: "Sammary of Application of RILAC to Recent Material Studies", RIKEN Symp. Heavy Ion Linear Accelerator Applied to the Study of Hi-Technology Material Characterization, Wako, Feb. (1989).

9) K. Kimura: "High Density Excitation of Matter by Heavy Ion Irradiation", Yayoi Symp. Tokyo Univ., Tohkai, Feb. (1989).

10) M. Minami: "Host-Guest Profiling of Diamond-like Carbon Films", RIKEN Symp. Heavy Ion Linear Accelerator Applied to the Study of Hi-Technology Material Characterization, Wako, Feb. (1989).

11) Y. Kobayashi, M. Katada, H. Sano, K. Asai, T. Okada, M. Iwamoto, and F. Ambe: "Mössbauer Studies on Heusler Alloys", Int. Symp. on Advanced Nuclear Energy Research, Oarai, Feb. (1989).

12) K. Kimura, K. Uehara, T. Suzuki, K. Watanabe, and T. Matsuyama: "Emission Spectra of Heavy Ion Irradiated BaF_2", 44th Annu. Meet. Phys. Soc. Jpn., Hiratsuka, Mar. (1989).

13) K. Kimura: "Effects of High Density Excitation Induced by Heavy Ions", RIKEN Symp. Interaction of Heavy Ion with Matter, Wako, Mar. (1989).

14) H. Doumoto, K. Maeda, Y. Sasa, and M. Uda: "Elemental Analysis of Human Saliva by PIXE", 1989 Spring Meet. Jpn. Soc. Appl. Phys., Chiba, Apr. (1989).

15) H. Miura, Y. Sasa, K. Maeda, and M. Uda: "Application of PIXE Anlysis to Decoding of Old Manuscripts", 1989 Spring Meet. Jpn. Soc. Appl. Phys., Chiba, Apr. (1989).

16) S. Ambe, Y. Ohkubo, M. Iwamoto, and F. Ambe: "Preparation of No-Carrier-Added ^{111m}Cd for the Measurement of γ-γ Perturbed Angular Correlation", 58th National Meet. Chem. Soc. Jpn., Tanabe, Apr. (1989).

17) T. Takahashi, F. Yatagai, T. Katayama, Y. Suzuki, K. Watanabe, T. Kasuya, and T. Doke: "Inactivation of *B. Subtilis* Spores by Ar, Fe, and U ions", 7th Track Detector Symp., Tokyo, Apr. (1989).

18) M. Yanokura, K. Yoshida, I. Tanihata, M. Aratani, M. Minami, S. Nakabayashi, and A. Kira: "Ion Beam Analysis of Pd Electrodes After Electro-Chemical Reactions in D_2O", Workshop on Cold Fusion Phenomena at Santa Fe, Santa

Fe, May (1989).
19) K. Kimura: "Study on the Primary Processes of Ion Irradiation", Symposium on Chemical Reactions Viewed Through Pico-Nanosecond Time Windows, Chem. Soc. Jpn., Kanto Section, Wako, Jun. (1989).
20) H. Kusuyama, K. Okada, K. Yoshida, K. Maeda, Y. Sasa, and M. Uda: "Trace Elemental Analysis of Washed Human Spermatozoa", 2nd Meet. of the Int. Soc. for Trace Element Research in Humans, Tokyo, Aug. (1989).
21) K. Maeda, Y. Sasa, H. Kusuyama, Y. Yoshida, and M. Uda: "PIXE Analysis of Human Spermatozoa Isolated from Seminal Plasma", 5th Int. Conf. on Particle Induced X-Ray Emission and Its Analytical Applications, Amsterdam, Aug. (1989).
22) T. Takahashi, H. Kumagai, T. Kosaka, K. Kasai, K. Nakano, F. Yatagai, S. Konno, I. Kaneko, K. Hatanaka, and T. Kanai: "Dosimetry in the RIKEN Ring Cyclotron Biology Facility", 32th Annu. Meeting Jpn. Radiat. Res. Soc., Kitakyushu-shi, Aug. (1989).
23) K. Kimura: "High Density Excitation Induced by Heavy Ions", Symp. Res. Found. B of Minis. Edu., Tokyo, Aug. (1989).
24) M. Minami, M. Aratani, M. Yanokura, and S. Okada: "Characterization of Diamond-like Carbon Films by ERDA", 50th Fall Meet. Jpn. Appl. Phys., Fukuoka, Sep. (1989).
25) T. Takahashi, F. Yatagai, Y. Suzuki, K. Watanabe, and T. Tabata: "Analysis of Inactivation Cross Sections for Heavy Ions of *B. subtilis* Spores and *E. coli* K-12", 3rd Annu. Meet. Jpn. Soc. for Biological Sciences in Space, Tokyo, Sep. (1989).
26) H. Kirita, H. Fukushima, Y. Imazawa, T. Ooishi, Y. Kobayashi, M. Koshikawa, T. Miura, Y. Itoh, and K. Tachi: "Determination of Oxygen in Gallium Aresenide by Charged-Particle Activation Analysis", 33th Symp. on Radiochemistry, Hiroshima, Oct. (1989).
27) S. Ambe, and F. Ambe: "Mössbauer Studies on Chemical States of ^{119}Sb and ^{119m}Te in S, Se, and Te", 33th Symp. on Radiochemistry, Hiroshima, Oct. (1989).
28) M. Aratani, M. Yanokura, and M. Minami: "Heavy-Ion Scattering Spectroscopy Using RILAC Applied to Characterization of Multi-Layered Films Containing Heavy Elements", 33th Symp. on Radiochemistry, Hiroshima, Oct. (1989).
29) K. Niisawa, M. Aratani, M. Yanokura, and T. Nozaki: "Rutherford Scattering Analysis for Exchange of Environmental Water with D-substituted Soda-Lime Glass", 33th Symp. on Radiochemistry, Hiroshima, Oct. (1989).
30) M. Yanokura, I. Tanihata, M. Aratani, M. Minami, A. Kira, S. Nakabayashi, and S. Yamagata: "Quantitative Depth Profiling of Hydrogen Isotopes Analysis by the Heavy Ion Rutherford Scattering", 33th Symp. on Radiochemistry, Hiroshima, Oct. (1989).
31) M. Yanokura, I. Tanihata, M. Aratani, M. Minami, A. Kira, S. Nakabayashi, and S. Yamagata: "Quantitative Depth Profiling of Hydrogen Isotopes Analysis in Electrode by The Heavy Ion Rutherford Scattering", 33th Symp. on Radiochemistry, Hiroshima, Oct. (1989).
32) Y. Ohkubo, Y. Yanagida, and F. Ambe: "Measurements of γ-Ray Perturbed Angular Correlation for Ru-99 Using Rh-99", 33th Symp. on Radiochemistry, Hiroshima, Oct. (1989).
33) K. Kimura, F. Sano, and S. Yanagishita: "Depth Resolved Emission Profile of N Ion Impinged Condensed Helium", 32th Meet. Radiat. Chem. Jpn., Hiroshima, Oct. (1989).
34) K. Kimura, F. Sano, and S. Yanagishita: "Depth Resolved Emission Measurement of N Ion Tracks in Condensed Helium", Fall. Meet. Phys. Soc. Jpn., Miyazaki, Oct. (1989).
35) I. Sugai and T. Hattori *et al.*: "Development of Long-Lived Carbon Stripper Foils-II", Autumn Meet. of Phys. Soc. Jpn., Miyazaki, Oct. (1989).
36) T. Takahashi: "Track Structure Theory and Lethal Effect of Heavy Ions", 2nd Symposium of Advanced Radiation Research, Tokyo, Nov. (1989).

VIII. SUBJECTS UNDER CONTRACT

(Jan.-Dec. 1989)

1) "Radiochemical Analysis of ^{16}O, ^{14}N, and ^{12}C in Si Crystal and GaAs"	H. Kirita Japan Chemical Analysis Center
2) "Radiation Damage of Solar Cells"	T. Ohga Nippon Telephone Telegram Co., Ltd.
3) "Improvement of Thyristors by Proton Irradiation"	K. Tomii Semiconductor R&D Lab., Matsushita Electric Work Co., Ltd.
4) "Improvement of Thyristors by Proton Irradiation"	H. Akiyama LSI Lab., Mitsubishi Electric Co., Ltd.
5) "Improvement of Thyristors by Proton Irradiation"	M. Kitagawa and A. Ohsawa Toshiba Co., Ltd.
6) "Improvement of Thyristors by Proton Irradiation"	Y. Shimizu Hitachi Co., Ltd.
7) "Improvement of Thyristors by Proton Irradiation"	K. Muraoka and S. Sasaki Toyo Electric Co., Ltd.
8) "Radiation Damage of Cover Glass for a Solar Cells"	T. Hayashi and A. Ohnishi Institute of Space and Astronomical Science

IX. LIST OF SEMINARS

(Jan.-Dec. 1989)

Ion Accelerator

1) G. Münzenberg, GSI (West Germany), 22 February
"The New Experimental Facilities for Relativistic Heavy Ions and the Projectile Fragment Separator at GSI"

2) D. Mikolas, Michigan State Univ. (USA), 28 February
"Recent Developments at NSCL, Michigan State University"

3) T. Nomura, Institute for Nuclear Study (Tokyo), 2 March
"Production of Super-Heavy Nuclei by the Reaction (HI, α xn)"

4) H. Delagrange, GANIL (France), 15 March
"Photons from 1 MeV to 1 GeV and TAPS Project"

5) T. Shimano, Tokyo Institute of Technology (Tokyo), 15 May
"Signature Inversion due to γ-Vibrations"

6) A. C. Mueller, IPN Orsay (France), 8 June
"Experiments with Secondary Fragments Beam at LISE and Future Developments"

7) H. Enyo, Kyoto Univ. (Kyoto), 9 June
"High-Energy Nuclear Collisions at CERN-SPS"

8) I. S. Towner, Chalk River Nuclear Lab. (Canada), 16 June
"Quenching of Spin Matrix Elements in Finite Nuclei"

9) K. Niita, Giessen Univ. (West Germany), 22 June
"Hard Photon Production in Heavy-Ion Collisions"

10) O. Klepper, GSI (West Germany), 22 June
"Gamow-Teller β-Decays of Even-Even Nuclei near ^{100}Sn"

11) T. Watanabe, Osaka Univ. (Osaka), 7 July
"2ν $\beta\beta$-Decays of ^{100}Mo Studied by an Ultra-Low Background β-γ Spectrometer ELEGANTS-IV"

12) T. Numao, TRIUMF (Canada), 13 July
"Search for the Rare Decay $K\rightarrow\pi\nu\bar{\nu}$"

13) K. Ikeda, Niigata Univ. (Niigata), 18 July
"Studies of ^{11}Li with a ^{9}Li+2n Cluster Model"

14) Y. Tosaka, Niigata Univ. (Niigata), 18 July
"Structure of ^{11}Li in the Cluster Orbital Shell Model"

15) H. Sagawa, Univ. of Tokyo (Tokyo), 18 July
"Analysis of Loosely-Bound Neutrons with a Direct Reaction Model"

16) S. Nagamiya, Columbia Univ. (USA), 20 July
"Heavy-Ion Experiments at BNL and CERN—Now and Future"

17) J. S. Chan, The Univ. of Tsukuba (Ibaraki), 26 July
"Production of Intermediate-Mass Fragments in Medium Energy Heavy-Ion Reactions"

18) K. Katori, Osaka Univ. (Osaka), 7 September
"Production of Light Elements and Their Structures"

19) H. T. Duong, Aime Cotton Lab., Orsay (France), 19 September
"Experiments on the Bohr-Weisskopf Effect at ISOLDE, CERN"

20) C. Signorini, INFN and Salerno Univ. (Italy), 23 October
"The LNL Recoil Mass Spectrometer"

21) F. Chojnacki, Warsaw Univ. (Poland), 25 October
"Warsaw Ion Guide System and Study of Unstable Nuclei"

22) M. Di Toro, Catania Univ. (Italy), 26 October
"Reaction Mechanisms in Medium Energy Heavy-Ion Collisions"

23) H. J. Kluge, Mainz Univ. (West Germany), 2 November
"A Laser Ion Source and Its Application for Trace Analysis"

24) A. Ohnishi, Kyoto Univ. (Kyoto), 9 November
"Production of High-Energy Photons in Medium Energy Heavy-Ion Reactions"

25) N. Carjan, Centre détudes Nucleaires de Bordeaux-Gradignan (France), 14 November
"Macroscopic Models for Asymmetric Fission and De-Excitation of Compound Nuclei by Complex Fragment Emission"

26) Y. Hama, São Paulo Univ. (Brazil), 21 November
"Hadron Interferometry"

Synchrotron Radiation

1) J. A. Niederer, Brookhaven National Laboratory (USA), 29 March
"More Madness; Accelerator Physics, Control & Computer Science"

2) K. Yoshida, Inst. Nuclear Study (Tokyo), 28 June
"1.3 GeV Electron Synchrotron at INS"

3) H. Sasaki, Kawasaki Steel (Tokyo), 26 July
"Magnet Design for Synchrotron and Storage Ring"

4) R. Schmitz, DESY (West Germany), 11 August
"Accelerators and Control System at DESY"

5) H. Nishimura, LBL (USA), 11 August
"Simulation and Control in Accelerators"

6) A. Jackson, LBL (USA), 17 August
"Status on LBL ALS Project"

7) A. Jackson, LBL (USA), 18 August
"Beamdynamics Calculation of ALS"

8) K. Kim, LBL (USA), 18 August
"Brightness and Coherence through Wigner Function Formulation"

9) T. Okano, Inst. Industrial Science (Tokyo), 27 October
"Vacuum System in Synchrotron Radiation Source"

10) G. Saxson, Daresbury (England), 1 November
"Design of RF System in Electron Storage Ring"

11) A. Wrulich, Synchrotron Trieste (Italy), 7 November
"Design of Synchrotron Trieste"

12) T. Katsura, KEK (Tsukuba), 21 November
"Monotor System at Photon Factory"

13) T. Yamakawa, KEK (Tsukuba), 8 December
"Injection System Design in Storage Ring"

14) E. Forest, LBL (USA), 26 December
"Hamiltonian Free Theory in Beam Dynamics"

X. LIST OF PERSONNEL

Steering Committee

AMBE Fumitoshi 安部文敏
CHIBA Yoshiaki 千葉好明
HASHIZUME Akira 橋爪 朗
ISHIHARA Masayasu 石原正泰*
KATSUMATA Koichi 勝又紘一
KOHNO Isao 河野 功
NAGAMINE Kanetada 永嶺謙忠
TANIHATA Isao 谷畑勇夫
YANO Yasushige 矢野安重
AWAYA Yohko 粟屋容子
HANAOKA Fumio 花岡文雄
INAMURA Takashi 稲村 卓
KAMITSUBO Hiromichi 上坪宏道
KIRA Akira 吉良 爽
MATSUOKA Masaru 松岡 勝
TAKAMI Michio 高見道生
WATANABE Tsutomu 渡部 力

* Chairman

Cyclotron Operation and Maintenance Group

FUJITA Shin 藤田 新
KAGEYAMA Tadashi 影山 正
OGIWARA Kiyoshi 荻原 清
IKEGAMI Kumio 池上九三男
KOHARA Shigeo 小原重夫
TAKEBE Hideki 武部英樹

Linac Operation and Maintenance Group

CHIBA Yoshiaki 千葉好明
IKEZAWA Eiji 池沢英二
KASE Masayuki 加瀬昌之
YANOKURA Minoru 矢野倉 実
HEMMI Masatake 逸見政武
INOUE Toshihiko 井上敏彦
MIYAZAWA Yoshitoshi 宮沢佳敏

Scientific and Engineering Personnel

Cosmic Radiation Laboratory

IMAI Takashi 今井 喬
KOHNO Tsuyoshi 河野 毅
MUNAKATA Kazuoki 宗像一起

(Visitors)
HASEBE Nobuyuki 長谷部信行 (Fac. Gen. Educ., Ehime Univ.)
MURAKAMI Hiroyuki 村上浩之 (Fac. Sci., Rikkyo Univ.)
NAGATA Katsuaki 永田勝明 (Fac. Eng., Tamagawa Univ.)
NAKAMOTO Atsusi 中本 淳 (Fac. Sci., Rikkyo Univ.)
NISHIJIMA Kyoshi 西嶋恭司 (Sci. Eng. Res. Lab., Waseda Univ.)
YANAGIMACHI Tomoki 柳町朋樹 (Fac. Sci., Rikkyo Univ.)

(Student)
KASHIWAGI Toshisuke 柏木利介 (Sci. Eng. Res. Lab., Waseda Univ.)

Cyclotron Laboratory

BE Suck Hee 裵 碩喜
FUJISAWA Takashi 藤沢高志
DATE Shin 伊達 伸
FUJITA Jiro 藤田二郎

FUJITA Shin 藤田 新
HARA Masahiro 原 雅弘
IKEGAMI Kumio 池上九三男
KAGEYAMA Tadashi 影山 正
KOHARA Shigeo 小原重夫
MORITA Kosuke 森田浩介
NAGASE Makoto 長瀬 誠
NAKAJIMA Shunji 中島諄二
OGIWARA Kiyoshi 荻原 清
SASAKI Shigeki 佐々木茂樹
SOUTOME Kouichi 早乙女光一
WADA Takeshi 和田 雄
YANO Yasushige 矢野安重
GOTO Akira 後藤 彰
HATANAKA Kichiji 畑中吉治
INAMURA Takashi 稲村 卓
KAMITSUBO Hiromichi 上坪宏道
MATSUO Masayuki 松尾正之
NAGAOKA Ryutaro 長岡隆太郎
NAKAGAWA Takahide 中川孝秀
NAKANISHI Noriyoshi 中西紀喜
SAITO Motozo 斉藤始三
SHIKATA Takashi 四方隆史
TAKEBE Hideki 武部英樹
YAMAJI Shuhei 山路修平
YOKOYAMA Ichiro 横山一郎

(Visitors)
ANAYAMA Hiroshi 穴山 汎 (Reliability Cent. for Electronic Components of Japan)
ARAI Eiichi 新井栄一 (Res. Lab. Nucl. Reactors, Tokyo Inst. Technol.)
EJIRI Hiroyasu 江尻宏泰 (Dep. Phys., Osaka Univ.)
FUJIOKA Manabu 藤岡 学 (Cyclotron Radioisot. Cent., Tohoku Univ.)
FUKUMOTO Sadayoshi 福本貞義 (KEK)
FURUNO Kohei 古野興平 (Inst. Phys. Tandem Accel. Cent., Univ. Tsukuba)
GOKA Tateo 五家建夫 (NASDA)
H. T. Duong (Lab. Aime Cotton, Orsay)
HARADA Minoru 原田 稔 (Reliability Cent. for Electronic Components of Japan)
HAYASHI Nobuyuki 林 伸行 (Electro Tech. Lab.)
HIRAO Yasuo 平尾泰男 (Natl. Inst. Radiol. Sci.)
HORIGUCHI Takayoshi 堀口隆良 (Dep. Phys., Hiroshima Univ.)
HORIUCHI Hisashi 堀内 昶 (Dep. Phys., Kyoto Univ.)
IKEDA Kiyomi 池田清美 (Dep. Phys., Niigata Univ.)
IKEGAMI Hidetsugu 池上栄胤 (RCNP, Osaka Univ.)
INOUE Makoto 井上 信 (RCNP, Osaka Univ.)
ISHIZUKA Takeo 石塚武男 (Dep. Phys., Saitama Univ.)
IWAMOTO Akira 岩本 昭 (Japan Atomic Energy Res. Inst.)
IWASHITA Yoshihisa 岩下芳久 (Inst. Chem. Res., Kyoto Univ.)
KANMURI Testuo 冠 哲夫 (Dep. Phys., Osaka Univ.)
KASAI Shunichi 河西俊一 (Japan Atomic Energy Res. Inst.)
KATAYAMA Ichiro 片山一郎 (RCNP, Osaka Univ.)
KATORI Kenji 鹿取謙二 (Dep. Phys., Osaka Univ.)
KATSURAGAWA Hidetsugu 桂川秀嗣 (Dep. Phys., Toho Univ.)
KAWAI Mitsuji 河合光路 (Dep. Phys., Kyushu Univ.)
KIKUCHI Fumio 菊地文男 (Coll. Arts Sci., Univ. Tokyo)
KISHIMOTO Teruo 岸本照夫 (Dep. Phys., Univ. Tsukuba)
KOBAYASHI Shinsaku 小林晨作 (Dep. Phys., Kyoto Univ.)
KOHMOTO Susumu 河本 進 (Univ. Electro-Commun.)
KONDO Michiya 近藤道也 (RCNP, Osaka Univ.)
KOSAKO Toshiso 小佐古敏荘 (Atomic Energy Res. Cent., Univ. Tokyo)
KOWATA Mitsuyoshi 小綿光喜 (Reliability Cent. for Electronic Components of Japan)
KUDO Hisaaki 工藤久昭 (Dep. Chem., Niigata Univ.)
KUROYANAGI Tokihiro 黒柳登喜大 (Dep. Phys., Kyushu Univ.)
MATSUKI Seishi 松木征史 (Inst. Chem. Res., Kyoto Univ.)
MINOWA Tatsuya 箕輪達哉 (Dep. Phys., Toho Univ.)
MIURA Iwao 三浦 岩 (RCNP, Osaka Univ.)
MIYATAKE Hiroari 宮武宇也 (Fac. Sci., Osaka Univ.)
MORIO Atsuo 森尾篤夫 (Reliability Cent. for Electronic Components of Japan)
MUKHOPADHYAY, N.K. (V.E.C. Cent., B.A.R.C., India)
MURAYAMA Toshiyuki 村山利幸 (Tokyo Univ. Mercantile Marine)

NAGAI Yasuki 永井泰樹 (Dep. Appl. Phys., Tokyo Inst. Technol.)
NAKAHARA Hiromichi 中原弘道 (Dep. Chem., Tokyo Metrop. Univ.)
NAKAI Koji 中井浩二 (KEK)
NAKAMURA Ichiro 中村市郎 (Dep. Phys., Saitama Univ.)
NAKAMURA Shinya 中村慎也 (Reliability Cent., Electronic Components of Japan)
NAKAMURA Takashi 中村尚司 (Cyclotron Radioisot. Cent., Tohoku Univ.)
NAKAMURA Yoshiteru 中村義輝 (Japan Atomic Energy Res. Inst.)
NARA Takayuki 奈良孝幸 (Japan Atomic Energy Res. Inst.)
NIITA Koji 仁井田浩二 (Dep. Phys., Univ. Giessen, Giessen)
NISHII Masanobu 西井正信 (Japan Atomic Energy Res. Inst.)
NOMURA Toru 野村 亨 (Inst. Nucl. Study, Univ. Tokyo)
ONISHI Naoki 大西直毅 (Dep. Phys., Coll. Gen. Educ., Univ. Tokyo)
OTA Shigemi 太田滋生 (KEK)
P. E. Hodgson (Dep. Nucl. Phys., Oxford Univ. England)
PARK Eng Soo (POSTECH, Korea)
SAKAI Hideyuki 酒井英行 (Dep. Phys., Univ. Tokyo)
SAKAMOTO Isao 坂本 勲 (Electro Tech. Lab.)
SASAGAWA Tatsuya 笹川辰弥 (Dep. Phys., Tohoku Univ.)
SASUGA Tsuneo 貴家恒男 (Japan Atomic Energy Res. Inst.)
SATO Kenichi 佐藤憲一 (Div. Phys., Tohoku Coll. Pharm.)
SHIMANO Yosuke 島野洋介 (NASDA)
SHINOZUKA Tsutomu 篠塚 勉 (Cyclotron Radioisot. Cent., Tohoku Univ.)
SUEKI Keisuke 末木啓介 (Inst. Nucl. Study, Univ. Tokyo)
SUGAI Isao 菅井 勲 (Inst. Nucl. Study, Univ. Tokyo)
SUNAGA Hiromi 須永博美 (Japan Atomic Energy Res. Inst.)
TAKEMASA Tadashi 武政尹士 (Dep. Phys., Saga Univ.)
TAMAGAKI Ryozo 玉垣良三 (Dep. Phys., Kyoto Univ.)
TANAKA Jinichi 田中仁市 (Inst. Nucl. Study, Univ. Tokyo)
TOMII Kazushi 富井和志 (Lab. Diod. Matsushita Electric Ind. Co.)
TOMIMASU Takio 富増多喜夫 (Electro Tech. Lab.)
TONG Shao-Ming 仝 暁民 (Inst. Mod. Phys., Acad. Sinica, China Univ.)
TORIYAMA Tamotsu 鳥山 保 (Dep. Appl. Phys., Tokyo Inst. Technol.)
TSUKIJI Masaru 築地 優 (NEC Corp.)
TSUNEMOTO Hiroshi 恒元 博 (Natl. Inst. Radiol. Sci.)
WAKAI Masamichi 若井正道 (Dep. Phys., Osaka Univ.)
WAKISHIMA Susumu 脇島 進 (Reliability Cent., Electronic Components of Japan)
WATANABE Hiroshi 綿鍋博志 (Electro Tech. Lab.)
YAMADA Kouichi 山田耕一 (Lab. Diod, Matsushita Electric Ind. Co.)
YAMANOUCHI Mikio 山内幹雄 (Tandem Accel. Cent., Univ. Tsukuba)
YAMAZAKI Takashi 山崎 魏 (RCNP, Osaka Univ.)
YOSHIDA Nobuaki 吉田宣章 (Dep. Phys., Univ. Tokyo)
YOSHIDA Shiro 吉田思郎 (Dep. Phys., Tohoku Univ.)
YOSHINAGA Naotaka 吉永尚孝 (Comput. Cent., Univ. Tokyo)

(Students)
AZUMA Mitsuhiro 東 光弘 (Dep. Phys., Toho Univ.)
KOBAYASHI Takayuki 小林貴之 (Fac. Sci., Tokyo Metrop. Univ.)
KOIZUMI Mitsuo 小泉光生 (Dep. Phys., Hiroshima Univ.)
KUNIHIRO Kazuaki 国弘和明 (Dep. Appl. Phys., Tokyo Inst. Technol.)
MARUYAMA Toshiki 丸山敏毅 (Dep. Phys., Kyoto Univ.)
NISHINAKA Ichiro 西中一郎 (Dep. Chem., Tokyo Metrop. Univ.)
SHIMOMURA Koichiro 下村浩一郎 (Dep. Phys., Kyoto Univ.)
YOSHIDA Atsushi 吉田 敦 (Dep. Appl. Phys., Tokyo Inst. Technol.)

Linear Accelerator Laboratory

CHIBA Toshiya 千葉利哉
FUJIMAKI Masaki 藤巻正樹
INOUE Toshihiko 井上敏彦
KUBO Toshiyuki 久保敏幸
MIYAZAWA Yoshitoshi 宮沢佳敏
TANIHATA Isao 谷畑勇夫
WADA Takahiro 和田隆宏
YOSIDA Koichi 吉田光一
CHIBA Yoshiaki 千葉好明
HEMMI Masatake 逸見政武
KASE Masayuki 加瀬昌之
KUMAGAI Hidekazu 熊谷秀和
SUZUKI Takeshi 鈴木 建
TONUMA Tadao 戸沼正雄
YANOKURA Minoru 矢野倉 実

(Visitors)
BAI Xi Xiang 白 希祥 (Inst. Atomic Energy, China)
FUJIWARA Ichiro 藤原一郎 (Inst. Atomic Energy, Kyoto Univ.)
FUJIWARA Mamoru 藤原 守 (RCNP, Osaka Univ.)
ITO Noriaki 伊藤憲昭 (Dep. Cryst. Mater., Nagoya Univ.)
KIKUCHI Jun 菊地 順 (Sci. Eng. Res. Lab., Waseda Univ.)
KIMURA Kikuo 木村喜久雄 (Fac. Sci., Kyushyu Univ.)
KOBAYASHI Toshio 小林俊雄 (KEK)
SAKAI Hideyuki 酒井英行 (Fac. Sci., Univ. Tokyo)
SHIMOURA Susumu 下浦 亨 (Fac. Sci., Univ. Tokyo)
SUDA Toshimi 須田利美 (Fac. Sci., Tohoku Univ.)
SUGAWARA Masahiko 菅原昌彦 (Fundam. Sci., Chiba Inst. Technol.)
YAMAGUCHI Hiromi 山口裕美 (Sci. Eng. Res. Lab., Waseda Univ.)

(Student)
ITO Tatsuya 伊藤達也 (Sci. Eng. Res. Lab., Waseda Univ.)

Radiation Laboratory

ASAHI Koichiro 旭 耕一郎
HASHIZUME Akira 橋爪 朗
ISHIHARA Masayasu 石原正泰
KONNO Satoshi 金野 智
OKAMURA Hiroyuki 岡村弘之
TENDO Yoshihiko 天道芳彦
GONO Yasuyuki 郷農靖之
ICHIHARA Takashi 市原 卓
IZUMO Koichi 出雲光一
NOMURA Izumi 野村和泉
TAKAHASHI Tan 高橋 旦

(Visitors)
ABE Yasuhisa 阿部恭久 (Res. Inst. Fundam. Phys., Kyoto Univ.)
ADACHI Minoru 足立 實 (Dep. Appl. Phys., Tokyo Inst. Technol.)
ANDO Yoshiaki 安藤嘉章 (Dep. Phys., Rikkyo Univ.)
BEAUMEL Didier (Inst. Phys. Nucl., Orsay, France)
CHOJNACKI Slawomir (Warsaw Univ.)
DOKE Tadayoshi 道家忠義 (Sci. Eng. Res. Lab., Waseda Univ.)
ENDO Saburo 遠藤三郎 (Fac. Eng., Sci. Univ. Tokyo)
FUCHI Yoshihide 渕 好秀 (Inst. Nucl. Study, Univ. Tokyo)
FUJIOKA Manabu 藤岡 学 (Dep. Phys., Tohoku Univ.)
FUKUDA Mitsunori 福田光順 (Fac. Sci., Osaka Univ.)
HAMA Hiroyuki 浜 広幸 (Dep. Phys., Tokyo Inst. Technol.)
HASEGAWA Takeo 長谷川武夫 (Inst. Nucl. Study, Univ. Tokyo)
HITACHI Akira 月出 章 (Sci. Eng. Res. Lab., Waseda Univ.)
ICHIMURA Munetake 市村宗武 (Coll. Arts Sci., Univ. Tokyo)
IEKI Kazuo 家城和夫 (Fac. Sci., Rikkyo Univ.)
IJIRI Kenichi 井尻憲一 (Radioisot. Cent., Univ. Tokyo)
ISHIKAWA Masanobu 石川雅紀 (Tokyo Univ. Fisheries)
JEONG Sun Chan 鄭 淳讚 (Inst. Phys., Univ. Tsukuba)

KAGEYAMA Mayumi 影山眞弓 (Hoya Corp.)
KASAGI Jirota 笠木治郎太 (Fac. Sci., Tokyo Inst. Technol.)
KASAI Kiyomi 笠井清美 (Natl. Inst. Radiol. Sci.)
KATO Norihisa 加藤哲久 (Dep. Phys., Kyushu Univ.)
KATO Seigo 加藤静吾 (Fac. Educ. Yamagata Univ.)
KATORI Kenji 鹿取謙二 (Fac. Sci., Osaka Univ.)
KAWAKAMI Hirokane 川上宏金 (Inst. Nucl. Study, Univ. Tokyo)
KAWASHIMA Hideo 川島英雄 (Inst. Nucl. Study, Univ. Tokyo)
KITAO Kensuke 喜多尾憲助 (Natl. Inst. Radiol. Sci.)
KUBONO Sigeru 久保野 茂 (Inst. Nucl. Study, Univ. Tokyo)
KUBOTA Shinzou 窪田信三 (Fac. Sci., Rikkyo Univ.)
KUSAKARI Hideshige 草刈英榮 (Fac. Educ., Chiba Univ.)
LEE Sang Mu 李 相茂 (Inst. Phys., Univ. Tsukuba)
MAEDA Kazushige 前田和茂 (Coll. Gen. Educ., Tohoku Univ.)
MASUDA Kimiaki 増田公明 (Saitama Coll. Health)
MIKOLAS David (Dep. Phys. Astron., Michigan State Univ.)
MIYATAKE Hiroari 宮武宇也 (Coll. Gen. Educ., Osaka Univ.)
MORINAGA Haruhiko 森永晴彦 (Sec. Phys. Tech. Univ. München)
MORRISSEY David (Dep. Phys. Astron., Michigan State Univ.)
MOTOBAYASHI Tohru 本林 透 (Fac. Sci., Rikkyo Univ.)
MÜLLER Alex (Inst. Phys. Nucl., Orsay, France)
MURAKAMI Takeshi 村上 健 (Dep. Phys., Tokyo Inst. Technol.)
NAGAI Yasuki 永井泰樹 (Fac. Sci., Tokyo Inst. Technol.)
NAGASHIMA Yasuo 長島泰夫 (Dep. Phys., Univ. Tsukuba)
NAKAYAMA Shintarou 中山信太郎 (Coll. Gen. Educ., Univ. Tokushima)
OHNUMA Hajime 大沼 甫 (Fac. Sci., Tokyo Inst. Technol.)
ORIHARA Hikonojo 織原彦之丞 (Cyclotron and Radioisot. Cent., Tohoku Univ.)
OSHIMA Masumi 大島眞澄 (Japan Atomic Energy Res. Inst.)
OSHIRO Takashi 尾城 隆 (Tokyo Univ. Fisheries)
OYAIZU Mitsuhiro 小柳津充広 (Inst. Nucl. Study, Univ. Tokyo)
RUAN (GEN) Jian-zhi 阮 建治 (Dep. Phys., Rikkyo Univ.)
SAKAGUCHI Harutaka 坂口治隆 (Dep. Phys., Kyoto Univ.)
SATO Hiroshi 佐藤 竑 (Seikei Univ.)
SAWAMOTO Takeyuki 澤本健之 (Hoya Corp.)
SHIBAMURA Eido 柴村英道 (Saitama Coll. Health)
SHIMIZU Hajime 清水 肇 (Fac. Educ., Yamagata Univ.)
SHIMODA Tadashi 下田 正 (Coll. Gen. Educ., Osaka Univ.)
SHIMOURA Susumu 下浦 享 (Fac. Sci., Univ. Tokyo)
SHIRATO Shoji 白土鈔二 (Dep. Phys., Rikkyo Univ.)
SUGAWARA Masahiko 菅原昌彦 (Fundam. Sci., Chiba Inst. Technol.)
TAKAHASHI Noriaki 高橋憲明 (Coll. Gen. Educ., Osaka Univ.)
TAKIGAWA Noboru 滝川 昇 (Dep. Phys., Tohoku Univ.)
TANAKA Masahiko 田中雅彦 (Inst. Nucl. Study, Univ. Tokyo)
TOKI Hiroshi 土岐 博 (Dep. Phys., Tokyo Metrop. Univ.)
XU Hushan 徐 珊瑚 (Inst. Mod. Phys., Acad. Sin. China)
YAMAYA Takashi 山屋 堯 (Dep. Phys., Tohoku Univ.)
YASUE Masaharu 安江正治 (RCNP, Osaka Univ.)
YOSHIDA Kazuo 吉田和夫 (Hoya Corp.)
YOSHIZAWA Yasukazu 吉沢康和 (Dep. Phys., Hiroshima Univ.)
YOSOI Masaru 與曽井 優 (Fac. Sci., Tokyo Inst. Technol.)

(Students)
FUJIWARA Hideaki 藤原英明 (Inst. Phys., Univ. Tsukuba)
FUNATSU Yoshinori 船津義徳 (Fac. Sci., Univ. Tokyo)
FURUTAKA Kazuyoshi 古高和禎 (Fac. Sci., Tokyo Inst. Technol.)
FUTAMI Yasuyuki 二見康之 (Inst. Phys., Univ. Tsukuba)

HATA Kazuhiro 秦　和博 (Dep. Phys., Rikkyo Univ.)
ICHINOSE Hideo 市之瀬秀夫 (Sci. Eng. Res. Lab., Waseda Univ.)
INABE Naohito 稲辺尚人 (Fac. Sci., Kyoto Univ.)
ISHIDA Nobumichi 石田伸道 (Sch. Sci. Eng., Waseda Univ.)
ITO Tatsuya 伊藤達也 (Sci. Eng. Res. Lab., Waseda Univ.)
IWASA Naohito 岩佐直仁 (Dep. Phys., Rikkyo Univ.)
KODAMA Masakado 児玉将門 (Fac. Sci., Tokyo Inst. Technol.)
KOGUCHI Masanari 高口雅成 (Dep. Appl. Phys., Tokyo Inst. Technol.)
KUGO Harumi 久郷晴美 (Inst. Phys., Univ. Tsukuba)
KUWAHARA Kōta 桑原宏太 (Sch. Sci. Eng., Waseda Univ.)
MATSUI Hiroshi 松井　博 (Sch. Sci. Eng., Waseda Univ.)
MIZOTA Takeshi 溝田武志 (Inst. Phys., Univ. Tsukuba)
NAKAGAWA Keiko 中川恵子 (Inst. Phys., Univ. Tsukuba)
NAKAMURA Takashi 中村隆司 (Fac. Sci., Univ. Tokyo)
OGIWARA Masahiro 荻原正弘 (Dep. Phys., Rikkyo Univ.)
OGIWARA Mitsuhiko 荻原光彦 (Inst. Phys., Univ. Tsukuba)
OHNO Mariko 大野真理子 (Radisot. Cent., Univ. Tokyo)
OKUMURA Susumu 奥村　進 (Inst. Phys., Univ. Tsukuba)
OKUNO Hiroki 奥野広樹 (Fac. Sci., Univ. Tokyo)
OTOBE Eiichiro 乙部英一郎 (Sch. Sci. Eng., Waseda Univ.)
PU Y. H. 蒲　越虎 (Inst. Phys., Univ. Tsukuba)
SAKURAI Mikio 桜井幹夫 (Dep. Phys., Tokyo Inst. Technol.)
SHIBUYA Shinji 渋谷真二 (Dep. Phys., Rikkyo Univ.)
TAKANASHI Hidehiko 高梨英彦 (Fac. Sci., Tokyo Inst. Technol.)
TAKEI Taro 武井太郎 (Dep. Phys., Rikkyo Univ.)
TAMURA Akitoshi 田村彰敏 (Fac. Sci., Tokyo Inst. Technol.)
TOYOKAWA Hidenori 豊川秀訓 (Fac. Sci., Tokyo Inst. Technol.)
TSUDA Shoko 津田祥子 (Radiosot. Cent., Univ. Tokyo)
UTSUMI Motoharu 内海資元 (Sci. Eng. Res. Lab., Wasada Univ.)
YASHIRO Yoshinori 矢代義徳 (Fac. Sci., Tokyo Inst. Technol.)
YOSHIDA Hiroshi 吉田浩司 (Fac. Sci., Tokyo Inst. Technol.)

Atomic Processes Laboratory

ANDO Kozo 安藤剛三
AWAYA Yohko 粟屋容子
FUKUDA Hiroshi 福田　宏
KAMBARA Tadashi 神原　正
KANAI Yasuyuki 金井保之
NISHIDA Masami 西田雅美
SHIMAMURA Isao 島村　勲
WATANABE Tsutomu 渡部　力

(Visitors)
AZUMA Toshiyuki 東　俊行 (Coll. Arts Sci., Univ. Tokyo)
DANJO Atsunori 檀上篤徳 (Dep. Phys., Niigata Univ.)
DÖRNER Reinhard (Kernphys. Inst., Frankfurt Univ.)
FUJIMA Kazumi 藤間一美 (Fac. Eng., Yamanashi Univ.)
HARA Shunsuke 原　俊介 (Inst. Phys., Univ. Tsukuba)
HINO Ken-ichi 日野健一 (Univ. Electro-Commun.)
HITACHI Akira 月出　章 (Inst. Sci. Technol., Waseda Univ.)
ICHIMIYA Ayahiko 一宮彪彦 (Dep. Eng., Nagoya Univ.)
ISHII Keishi 石井慶之 (Dep. Eng. Sci., Kyoto Univ.)
ISOZUMI Yasuhito 五十棲泰人 (Radioisot. Res. Cent., Kyoto Univ.)
ITO Shin 伊藤　真 (Radioisot. Res. Cent., Kyoto Univ.)
ITOH Yoh 伊藤　陽 (Fac. Sci., Josai Univ.)
IWATA Yasushi 岩田康嗣 (Coll. Arts Sci., Univ. Tokyo)
KARASHIMA Shosuke 唐島照介 (Dep. Electron. Eng., Tokyo Univ. Sci.)
KAWATSURA Kiyoshi 川面　澄 (Kyoto Inst. Technol.)

KOBAYASHI Nobuo 小林信夫 (Dep. Phys., Tokyo Metrop. Univ.)
KOIKE Fumihiro 小池文博 (Sch. Med., Kitasato Univ.)
KOIZUMI Tetsuo 小泉哲夫 (Dep. Phys., Rikkyo Univ.)
KOMAKI Ken-ichiro 小牧研一郎 (Coll. Arts Sci., Univ. Tokyo)
KUROKI Kenro 黒木健郎 (Natl. Res. Inst. Police Sci.)
MATSUO Takashi 松尾 崇 (Dep. Pathol., Tokyo Med. Dent. Univ.)
MATSUZAWA Michio 松澤通生 (Dep. Eng. Phys., Univ. Electro-Commun.)
OHSAKI Akihiko 大崎明彦 (Inst. Mol. Sci.)
OHTANI Shunsuke 大谷俊介 (Natl. Inst. Fusion Sci.)
OKUNO Kazuhiko 奥野和彦 (Dep. Phys., Tokyo Metrop. Univ.)
PAPP Tibor (Inst. Nucl. Res., Hungarian Acad. Sci.)
SATO Hiroshi 佐藤浩史 (Dep. Phys., Ochanomizu Univ.)
SHIBATA Hiromi 柴田裕実 (Res. Cent. Nucl. Sci. Technol., Univ. Tokyo)
SHIMA Kunihiro 島 邦博 (Tandem Accel. Cent., Univ. Tsukuba)
SHIMAKURA Noriyuki 島倉紀之 (Gen. Educ. Dep., Niigata Univ.)
SUZUKI Hiroshi 鈴木 洋 (Dep. Phys., Sophia Univ.)
TAKAGI Shoji 高木祥示 (Dep. Phys., Toho Univ.)
TAWARA Hiroyuki 俵 博之 (Natl. Inst. Fusion Sci.)
TERASAWA Mititaka 寺沢倫孝 (Himeji Inst. Technol.)
TRAUTMANN Dirk (Inst. Phys., Basel Univ.)
TSURUBUCHI Seiji 鶴淵誠二 (Fac. Techonol., Tokyo Univ. Agric. Technol.)
URAKAWA Junji 浦川順治 (Natl. Lab. High Energy Phys.)
VÉGH Laszlo (Inst. Nucl. Res., Hungarian Acad. Sci.)
WAKIYA Kazuyoshi 脇谷一義 (Dep. Phys., Sophia Univ.)
YAMAZAKI Yasunori 山崎泰規 (Coll. Arts Sci., Univ. Tokyo)
YOSHINO Masuhiro 吉野益弘 (Lab. Phys., Shibaura Inst. Technol.)

(Students)
INABA Takayuki 稲葉貴之 (Inst. Laser Sci., Univ. Electro-Commun.)
KUSHIMA Masahiro 久嶋真博 (Dep. Phys., Sophia Univ.)
SAKAUE Hiroyuki 坂上裕之 (Dep. Phys., Sophia Univ.)

Metal Physics Laboratory

ISHIDA Katsuhiko 石田勝彦
MATSUZAKI Teiichiro 松崎禎市郎
SHIOTANI Nobuhiro 塩谷亘弘
KOYAMA Akio 小山昭雄
NAGAMINE Kanetada 永嶺謙忠
YAGI Eiichi 八木栄一

(Visitors)
FUJIOKA Manabu 藤岡 学 (Cyclotron Radioisot. Cent., Tohoku Univ.)
MINAMISONO Tadanori 南園忠則 (Fac. Sci., Osaka Univ.)
MIYAKE Yasuhiro 三宅康博 (Meson Sci. Lab., Univ. Tokyo)
TANAKA Koki 田中幸基 (Nippon Steel Corp.)
TORIKAI Eiko 鳥養映子 (Fac. Eng., Yamanashi Univ.)

(Student)
ISHIKAWA Hiroshi 石川 浩 (Fac. Sci., Sci. Univ. Tokyo)

Magnetic Materials Laboratory

OKADA Takuya 岡田卓也
SAKAI Nobuhiko 坂井信彦

(Visitors)
YAMADAYA Tokio 山田谷時夫 (Fac. Lit. Sci., Yokohama City Univ.)
ASAI Kichizo 浅井吉蔵 (Fac. Technol., Univ. Electro-Commun.)

Plasma Physics Laboratory

ISHIBE Yukio 石部行雄　　OYAMA Hitoshi 大山　等
YANO Katsuki 矢野勝喜

(Visitor)
SAKAMOTO Yuichi 坂本雄一 (Electr. Eng. Dep., Toyo Univ.)

Semiconductor Laboratory

(Visitor)
AONO Keiko 青野桂子 (Coll. Lib. Arts, Kitasato Univ.)

Inorganic Chemical Physics Laboratory

AMBE Shizuko 安部静子　　KAWAI Jun 河合　潤
MAEDA Kuniko 前田邦子　　SASA Yoshihiko 佐々嘉彦
TAKAMI Michio 高見道生

(Visitors)
ISHI Keizo 石井慶造 (Cyclotron Radioisot. Cent., Tohoku Univ.)
KUSUYAMA Hiroyuki 楠山弘之 (Saitama Med. Sch.)
MUKOYAMA Takashi 向山　毅 (Inst. Chem. Res., Kyoto Univ.)
UDA Masayuki 宇田応之 (Dep. Mater. Phys., Waseda Univ.)
FUKUDA Yukio 福田行男 (Coll. Lib. Arts, Kobe Univ.)

Radiochemistry Laboratory

AMBE Fumitoshi 安部文敏　　ARATANI Michi 荒谷美智
ITOH Yoshiko 伊東芳子　　IWAMOTO Masako 岩本正子
KOBAYASHI Yoshio 小林義男　　OHKUBO Yoshitaka 大久保嘉高

(Visitors)
BABA Hiroshi 馬場　宏 (Fac. Sci., Osaka Univ.)
CHO Yang-Koo 趙　陽九 (Inst. Mater. Sci., Univ. Tsukuba)
ENDO Kazutoyo 遠藤和豊 (Fac. Sci., Tokyo Metrop. Univ.)
FUKUSHIMA Hiroto 福嶋浩人 (Japan Chemical Analysis Cent.)
FURUKAWA Michiaki 古川路明 (Fac. Sci., Nagoya Univ.)
IMAI Masato 今井正人 (Komatsu Electronic Metals Co., Ltd.)
IMURA Ryo 井村　亮 (Cent. Res. Lab., Hitachi, Ltd.)
KADOTA Yoshinori 角田佳績 (Sumitomo Metal Mining Co., Ltd.)
KATADA Motomi 片田元己 (Fac. Sci., Tokyo Metrop. Univ.)
KATO Hajime 加藤　一 (Fac. Educ., Yamanashi Univ.)
KIRITA Hiroshi 桐田博史 (Japan Chemical Analysis Center)
KOJIMA Sadao 小島貞男 (Nucl. Med. Cent., Aichi Medical Univ.)
KUBO Kenya 久保謙哉 (Fac. Sci., Univ. Tokyo)
KUBOTA Takeshi 久保田　剛 (Inst. Mater. Sci., Univ. Tsukuba)
KURIHARA Toshikazu 栗原俊一 (Inst. Mater. Sci., Univ. Tsukuba)
NONAKA Nobuhiro 野中信博 (Japan Chemical Analysis Cent.)
OKADA Shigenobu 岡田繁信 (R/D Eng., Shimadzu Corp.)
OOHIRA Shigeo 大平重男 (Nikkei Techno Res. Co., Ltd.)
SAITO Kazuo 斉藤和男 (Toshiba Corp., R&D Cent.)
SAITO Tadashi 斎藤　直 (Fac. Sci., Osaka Univ.)
SHIBATA Seiichi 柴田誠一 (Inst. Nucl. Study)
SHINOHARA Atsushi 篠原　厚 (Fac. Sci., Nagoya Univ.)

SUGAI Isao 菅井 勲 (Inst. Nucl. Study, Univ. Tokyo)
TAKAHASHI Naruto 髙橋成人 (Fac. Sci., Osaka Univ.)
TAKAI Mikio 高井幹夫 (Fac. Eng. Sci., Osaka Univ.)
TANIGAWA Shoichiro 谷川庄一郎 (Inst. Mater. Sci., Univ. Tsukuba)
TAZAKI Kazue 田崎和江 (Fac. Sci., Shimane Univ.)
TOMINAGA Takeshi 富永 健 (Fac. Sci., Univ. Tokyo)
WATANABE Kazuhiro 渡辺一裕 (Inst. Mater. Sci., Univ. Tsukuba)
WATANABE Yasuo 渡辺裕夫 (Fac. Sci., Tokyo Metrop. Univ.)

(Students)
HAYANO Syuichi 早野修一 (Fac. Sci., Osaka Univ.)
KOBAYASHI Hiroshi 小林 洋 (Fac. Sci., Osaka Univ.)
KUSAWAKE Hiroaki 艸分宏昌 (Fac. Sci., Osaka Univ.)
MINAMI Masaki 南 正樹 (Dep. Metal Eng., Shibaura Inst. Technol.)
MISHIMA Kenji 三嶋謙二 (Fac. Sci., Univ. Tokyo)
NAKADA Masami 中田正美 (Fac. Sci., Tokyo Metrop. Univ.)
NAKAJIMA Yoshiaki 中嶋善明 (Fac. Sci., Nagoya Univ.)
NARITA Midori 成田 緑 (Fac. Sci., Nagoya Univ.)
OHKUBO Masaaki 大久保将明 (Dep. Metal Eng., Shibaura Inst. Technol.)
SHINTAI Junichirou 新帯淳一朗 (Fac. Sci., Nagoya Univ.)
TACHI Kouju 館 弘樹 (Dep. Metal Eng., Shibaura Inst. Technol.)
TANIGUCHI Yujin 谷口勇仁 (Fac. Sci., Nagoya Univ.)
YANAGIDA Yasuo 柳田保雄 (Fac. Sci., Toho Univ.)
YUKAWA Naoki 湯川直樹 (Fac. Sci., Osaka Univ.)
YUYATANI Masanori 湯家谷誠則 (Dep. Metal Eng., Shibaura Inst. Technol.)

Chemical Dynamics Laboratory

KIMURA Kazuie 木村一宇

(Visitor)
ITO Yasuo 伊藤泰男 (Res. Cent. Nucl. Sci. Technol., Univ. Tokyo)

(Students)
SANO Fumihiko 佐野文彦 (Dep. Phys., Chuo Univ.)
YANAGISHITA Sensuke 柳下仙介 (Dep. Phys., Chuo Univ.)

Radiation Biology Laboratory

KANEKO Ichiro 金子一郎
KITAYAMA Shigeru 北山 滋
NAKANO Kazushiro 中野和城
YATAGAI Fumio 谷田貝文夫

(Visitors)
BAVERSTOCK Keith F. (Rasiobiol. Unit, Med. Res. Counc., U.K.)
FUKUMURA Akifumi 福村明史 (Natl. Inst. Radiol. Sci.)
HOSHINO Kazuo 星野一雄 (Natl. Inst. Radiol. Sci.)
KANAI Tatsuaki 金井達明 (Natl. Inst. Radiol. Sci.)
KAWACHI Kiyomitsu 河内清光 (Natl. Inst. Radiol. Sci.)
KAWASHIMA Katsuhiro 川島勝弘 (Natl. Inst. Radiol. Sci.)
KOBAYASHI Yasuhiko 小林泰彦 (Japan. Atomic Energy Res. Inst.)
McINTYRE Cindy L. (Radiobiol. Unit, Med. Res. Counc., U.K.)
NAKAI Hirokazu 中井弘和 (Dep. Agric., Shizuoka Univ.)
OHARA Hiroshi 大原 弘 (Natl. Inst. Radiol. Sci.)
SOGA Fuminori 曽我文宣 (Inst. Nucl. Study, Tokyo Univ.)
SUZUKI Keiji 鈴木啓司 (RI Cent., Fac. Med., Yokohama City Univ.)

TAKATUJI Toshihiro 高辻俊宏 (RI Cent., Nagasaki Univ.)
WATANABE Hiroshi 渡辺 宏 (Japan Atomic Energy Res. Inst.)
WATANABE Masami 渡辺正己 (RI Cent., Fac. Med., Yokohama City Univ.)
YAMASHITA Shoji 山下昌次 (Natl. Saitama Hospital)

(Student)
KOSAKA Toshifumi 小坂俊文 (Dep. Vet. Radiol., Nihon Univ.)

Safety Control Affairs Office

KAGAYA Satoru 加賀屋 悟
KURIHARA Osamu 栗原 修
MIYAGAWA Makoto 宮川真言
SAWA Hiroshi 澤 宏
USUBA Isao 薄葉 勲
KATOU Takeo 加藤武雄
MATSUZAWA Yasuhide 松沢安秀
SAKAMOTO Ichiro 坂本一郎
SHINOHARA Shigemi 篠原茂己

Surface Characterization Center

IWAKI Masaya 岩木正哉
SAKAIRI Hideo 坂入英雄
KOBAYASHI Takane 小林 峰

(Visitor)
FUJIHANA Takanobu 藤花隆宣 (Advanced Technology Inc.)

(Student)
KOBAYASHI Kenzo 小林健三 (Fac. Eng. Sci., Osaka Univ.)

Laser Science Research Group

NAMBA Susumu 難波 進

Synchrotron Radiation Facility Design Group

BE Suck Hee 裵 碩喜
KAMITSUBO Hiromichi 上坪宏道
OIKAWA Yosifumi 老川嘉郁
TAKEBE Hideki 武部英樹
WADA Takeshi 和田 雄
HARA Masahiro 原 雅弘
NAGAOKA Ryutaro 長岡隆太郎
SASAKI Shigeki 佐々木茂樹
TANAKA Hitoshi 田中 均

(Visitors)
DAIBO Hidemi 大保秀美 (Hitachi, Ltd.)
KUSAKA Takuya 日下卓也 (Kobe Steel, Ltd.)
LEE Young Pak 李 英白
MIYADE Hiroki 宮出宏紀 (Sumitomo Heavy Ind., Ltd.)
MIZOGAWA Tatsumi 溝川辰巳 (Fac. Sci., Saitama Univ.)
MORIMOTO Yoshihide 森本佳秀 (Kobe Steel, Ltd.)
MOTONAGA Syoshichi 元永昭七 (Science Service)
NISHIDONO Toshiro 西殿敏朗 (Ishikawajima-Harima Heavy Ind. Co., Ltd.)
OHNISHI Jun-ichi 大西純一 (Kawasaki Heavy Ind., Ltd.)
TAKESHITA Isao 竹下勇夫 (Irie Koken Co., Ltd.)
TSUMAKI Kouji 妻木孝治 (Hitachi, Ltd.)
YOKOUCHI Shigeru 横内 茂 (Osaka Vacuum, Ltd.)
YOSHIDA Katsuhisa 吉田克久 (Mitsubishi Electric Corp.)
YOSHIYUKI Takeshi 吉行 健 (Toshiba Corp.)

(Students)
HINAGO Nobuaki 日名子伸明 (Fac. Sci. Eng., Chuo Univ.)
HIRANO Yoshiki 平野芳樹 (Coll. Hum. Sci. Nihon Univ.)
MATSUZAKI Akira 松崎 章 (Fac. Sci. Eng., Chuo Univ.)
MORO Toshiya 茂呂敏也 (Coll. Hum. Sci., Nihon Univ.)

AUTHOR INDEX

RIKEN Accelerator Progress Report

理化学研究所加速器年次報告　第23巻（1989）

印　刷　平成2年（1990）3月25日
発　行　平成2年（1990）3月30日
発行者　理化学研究所
代表者　小　田　稔
〒351-01　埼玉県和光市広沢2番1号
電話（0484）62－1111
編集者　理化学研究所加速器研究施設運営委員会
印刷所　勝美印刷株式会社
〒112　東京都文京区小石川1丁目3番7号

定価 5,000円
（消費税別）

理化学研究所

埼玉県　和光市　広沢